THE UNIVERSITY OF WARWICK

University of Warwick institutional repository: http://go.warwick.ac.uk/wrap

A Thesis Submitted for the Degree of PhD at the University of Warwick

http://go.warwick.ac.uk/wrap/54993

This thesis is made available online and is protected by original copyright.

Please scroll down to view the document itself.

Please refer to the repository record for this item for information to help you to cite it. Our policy information is available from the repository home page.

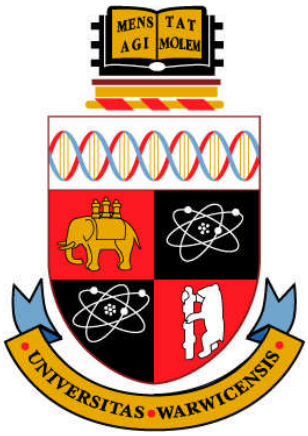

Studies of protein post-translational modifications using high resolution tandem mass spectrometry

by

Huilin Li

A thesis submitted in partial fulfillment of the requirements of the degree of Doctor of Philosophy in Chemistry

University of Warwick, Department of Chemistry

November 2012

Acknowledgements

It's a great pleasure to thank all the people who helped me during my PhD at the University of Warwick. Foremost, I would like to express my deepest gratitude to my supervisor, Prof. Peter B. O'Connor. It has been an honor to be your student and great privilege to work with you. Your enthusiasm for science is contagious. Your encouragement, patience, and support have been great motivations to push me in achieving my goals through my PhD. Your guidance and valuable insights helped me immensely towards becoming a thorough and confident scientist. Your time and effort are very much appreciated.

I am sincerely grateful to Prof. Peter J. Sadler. You have been always available for my research questions and reviewing my papers. The help from Prof. Rudolf A. Römer, Dr. Stephen A. Wells, and Dr. J. Emilio Jimenez-Roldan are greatly appreciated. I would especially like to thank Prof. Rudolf A. Römer for your time and effort to reviewing our collaborative paper and also for helping me understanding your work better. I would also like to thank Prof. Rob J. Deeth for taking your valuable time to explain me molecular modeling methods, and to allow me to access your super-fast computers.

I am also very grateful to Dr. Steve L. van Orden. Your support, enthusiasm, and knowledge helped greatly to the pulse program work that Tzu-Yung (Terry) Lin and I carried on. The support from both of you has helped me in knowing how to tune ECD experiment better and to modify all the fun pulse programs (delay-ECD, IR-ECD, DR-ECD, *et al.*)

needed for my work. I enjoyed and learned so much working with you. I am also thankful to Dr. Mark P. Barrow and Dr. Weidong Cui for your support and suggestions for tuning the FTICR MS instrument. I would also like to thank Dr. Claudia Blindauer and Dr. Kathrin Breuker for being my examiners.

I would like to acknowledge all the past and present friends and colleagues at the University of Warwick. I thank Helena Stec, Bushra Qamar, Dr. Jason R. C. Nurse, Kasra Razmkhah, Tzu-Yung Lin, Joanna Liu, Juan Wei, Yulin Qi, for your friendship and making my life at Warwick so enjoyable. I thank Dr. Yao Zhao, Jonathon R. Sneling, Dr. Hazel I. A. Phillips, Dr. Ana M. Pizarro, Dr. Anna Pashkova, Dr. David P. A. Kilgour, Qiang Zhang, and Zhijia Fang, for your help with my research. I also thank the rest of the PBO group members, Eman Allafi, Samantha Benson, Edyta Carrion, Yuko Lam, Jeffrey Li, Meng Li, Andrea Lopez-Clavijo, Pilar Perez Hurtado, Adam Mbugi, Andrew Soulby, Guang Tay, and Rebecca Wills.

I am deeply grateful to my parents and my sisters for your endless support and love through all these years. I would also acknowledge my friends back home, especially Dr. Cuihong Wan. Your friendship and support have been very important to me.

Finally, I would like to thank the Warwick Postgraduate Research Scholarship (WPRS) and the Chemistry Department for PhD studentship funding.

Declaration

I hereby declare that except where specific reference is made to other sources, the work contained in this thesis is the original work of the author. It has been composed by myself and has not been submitted, in whole or in part, for any other degree, diploma, or other qualification.

Huilin Li

November, 2012

Abstract

Electron capture dissociation (ECD) is a powerful and superior tandem mass spectrometry (MS) fragmentation technique in the study of protein post-translational modifications (PTMs) due to its unique features of preserving labile modifications and providing more detailed sequence information, which has been used to study protein platination and disulfide linked proteins. Cisplatin was found cross-linking multiple methionine (Met) pairs on calmodulin (CaM). The cross–linking of cisplatin to apo–CaM or Ca–CaM can inhibit the ability of CaM to recognize its target proteins as proved by a melittin binding assay. To further establish MS strategies to quickly assign the platinum-modification sites, a series of peptides with potential cisplatin binding sites were reacted with cisplatin and then analyzed by ECD. Radical-mediated side chain losses from the charge-reduced M+Pt species (such as $CH_3S\bullet$ or CH_3SH from Met, $SH\bullet$ from Cys, CO_2 from Glu or Asp, and $NH_2\bullet$ from amine groups) were found to be characteristic indicators for rapid and unambiguous localization of the Pt-modification sites on certain amino acid residues. Furthermore, the potential of cisplatin as a protein cross-linking reagent was further explored and demonstrated on other peptides and proteins. Many of the inherent features of cisplatin make it an interesting cross-linking reagent, such as targeting new protein functional groups (thioether and imidazole groups), its unique isotopic pattern, its inherent positive charges, its potential of binding to different functional groups, etc. However, it was found that the distance constraints obtained

from NMR structures of CaM are inconsistent with the measured distance constraints by cross–linking. Therefore, a newly developed flexibility simulation method was applied to explore whether the flexibility motions of CaM might contribute to the observed Pt-crosslinking on CaM. The flexibility analysis showed that the structural flexibility of CaM is key to cisplatin crosslinking CaM. ECD mechanism of disulfide bonds is still under debate. To further explore the ECD mechanism of sulfur–containing species, a series of disulfide (S–S), sulfur–selenium (S–Se), and diselenide (Se–Se) bond–containing peptides was studied by ECD. The results demonstrate that the radical has higher tendency to stay at selenium rather than sulfur after cleavage of Se–S bonds by ECD and suggest that direct electron capture at Se–Se and C–Se bonds is the main process during ECD of inter–chain diselenide peptides. Last but not least, a new active ion ECD (AI-ECD) method, named Shots-ECD, was developed and applied to improve Top-down ECD backbone fragmentation efficiency of disulfide-rich proteins. The results show that the Shots–ECD approach can not only cleave multiple disulfide bonds but also significantly improve the backbone cleavage efficiency. This strategy is fast, efficient, and with no need of chemical reduction of samples and instrument modification, and therefore can be a powerful approach to improve top-down ECD efficiency of not only disulfide bonded proteins but all proteins by Fourier transform ion cyclotron mass spectrometry (FTICR MS).

Table of contents

Title page……i

Acknowledgements……..ii

Declaration……...iv

Abstract……v

Table of contents……...vii

List of Tables……..xiv

List of Schemes……xvi

List of Figures……..…xvii

List of Abbreviations……...xxvi

Chapter 1 1

Introduction 1

1.1 Introduction to the study of protein post-translational modifications using mass spectrometry 1

1.2 Introduction to mass spectrometry 2

1.2.1 Major ionization techniques……3

1.2.2 Mass analyzers……..7

1.2.3 Tandem mass spectrometry methods……..22

1.2.4 12 Tesla solariX FT ICR mass spectrometer……..32

1.3 Introduction to protein platination and disulfide bound proteins 33

1.3.1 Biological importance of studying protein platination……33

1.3.2 MS studies of protein platination……..36

1.3.3 ECD applied to disulfide bonds in peptides and proteins….38

1.4 Overview of this thesis 40

Chapter 2 41

Mass spectrometry evidence for cisplatin as a protein cross-linking reagent.....41

2.1 Introduction 41

2.1.1 Techniques used for probing protein-protein interactions….41

2.1.2 The advantages of Fourier transform ion cyclotron resonance mass spectrometry (FTICR MS) in the analysis of complex samples……...42

2.1.3 Challenges in cross-linking chemistry……..42

2.1.4 The potential of cisplatin as a cross-linking reagent……..43

2.2 Experimental section.....45

2.2.1 Materials……...46

2.2.2 Reaction of peptides with Cisplatin ……46

2.2.3 Reaction of Proteins with Cisplatin and Digestion of CaM–cisplatin Adducts……46

2.2.4 FT ICR Mass Spectrometry……47

2.3 Results……..48

2.3.1 Intermolecular cross–linking of peptides……48

2.3.2 Intramolecular cross–linking of Calmodulin……55

2.3.3 Intermolecular cross–linking of protein……59

2.4 Discussion.....60

2.4.1 Chemical specificity……61

2.4.2 Compatibility with Mass Spectrometry analysis……62

2.4.3 Homobifunctional or heterobifunctional reactive groups…...64

2.4.4 Spacer arm length……...64

2.4.5 Cleavability……...66

2.5 Conclusions 67

Chapter 3 68

Use of Top-down and Bottom-up Fourier Transform Ion Cyclotron Resonance Mass Spectrometry for Mapping Calmodulin Sites Modified by Platinum Anticancer Drugs 68

3.1 Introduction 68

3.1.1 Calmodulin (CaM)……..68

3.1.2 Top–down and bottom–up mass spectrometric techniques.69

3.2 Experimental section.....72

3.2.1 Materials……...72

3.2.2 Reaction of CaM with Pt_1, Pt_2, and Pt_3……72

3.2.3 Protein Digestion……73

3.2.4 FTICR Mass Spectrometry……73

3.3 Results and discussion 74

3.3.1 FTICR MS Analyses of the interaction of platinum anti–cancer drugs with CaM……74

3.3.2 Mapping the binding sites of cisplatin (Pt_1) to CaM by top–down and bottom–up MS approaches……...77

3.3.3 Top–down MS with ECD and CAD for mapping the binding sites of [Pt(dien)Cl]Cl on CaM……84

3.4 Conclusions 90

Chapter 4 92

Protein Flexibility is Key to Cisplatin Cross-linking in Calmodulin..92

4.1 Introduction 92

4.1.1 Protein flexibility……..93

4.1.2 Protein flexibility simulation……95
4.2 Experimental section……96
4.2.1 Materials……96
4.2.2 Reaction of CaM and Ca–CaM with Cisplatin……96
4.3 Results and discussion……99
4.3.1 Analysis of the cross–linking sites of cisplatin to CaM and Ca_4–CaM by flexibility approaches……100
4.3.2 Mapping the binding sites of cisplatin to Ca_4–CaM by MS approaches……107
4.3.3 Biological insights from cross-linking experiments and flexibility analysis……110
4.3.4 Melittin–binding assay……111
4.4 Conclusions……113
Chapter 5……116
Side–Chain Losses in Electron Capture Dissociation to Improve the Identification of Pt(II)–modification Sites on Peptides and Proteins……116
5.1 Introduction……116
5.1.1 Mass Spectrometry techniques for characterizing Pt–binding sites on proteins……116
5.1.2 Side chain losses in ECD……117
5.2 Experimental section……118
5.2.1 Materials……118
5.2.2 Reaction of peptides with Cisplatin……119
5.2.3 FT ICR Mass Spectrometry……120

5.2.4 Ion Mobility Mass Spectrometry……..121
5.3 Results and discussion 121
5.3.1 Analysis of Cisplatin–Substance P Adducts Using CAD/ECD FTICR MS and IM–MS/MS (CAD)……122
5.3.2 ECD of Cisplatin–Peptides Adducts……...127
5.3.3 Intramolecular Migration of Pt(II) from Met(S) to Amine (N)……..130
5.3.4 ECD Side Chain Losses Due to Pt–binding…….132
5.3.5 Identification of the inter–chain crosslinking sites for cisplatin on insulin dimer by top–down ECD……..137
5.4 Conclusions 140
Chapter 6 142
Electron Capture Dissociation of Disulfide, Sulfur–Selenium, and Diselenide Bound Peptides.....142
6.1 Introduction 142
6.1.1 Electron capture dissociation of disulfide bonded peptides……142
6.1.2 ECD mechanisms of disulfide bonds……143
6.1.3 Study of selenium–containing compounds……143
6.2 Experimental section.....144
6.2.1 Materials……144
6.2.2 Formation of S–S, S–Se, and Se–Se bound peptides……145
6.2.3 FTICR Mass Spectrometry……..146
6.3 Results and discussion 146
6.3.1 Cleavages of S–S, S–Se, and S–Se bonds……149

6.3.2 Cleavages of C–X (X = S or Se) bonds……153

6.3.3 c/z• ions generated by cleaving both N–Cα and S–S (S–Se, or Se–Se) bonds……160

6.4 Conclusions 162

Chapter 7 164

Top-down Electron Capture Dissociation of Disulfide-Rich Proteins 164

7.1 Introduction 164

7.1.1 Bottom-up MS analysis of disulfide bound proteins……164

7.1.2 Top-down MS analysis of disulfide bound proteins……..164

7.1.3 ECD analysis of disulfide bound proteins……165

7.2 Experimental section 167

7.2.1 Materials……167

7.2.2 FTICR Mass Spectrometry……..168

7.3 Results and discussion……169

7.3.1 Top-down Shots-ECD of Insulin……169

7.3.2 Top-down ECD of Ribonuclease A (RNase A)……..180

7.4 Conclusions 184

Chapter 8 186

Conclusion and future work 186

8.1 Conclusions 186

8.2 Future work 191

Bibliography 194

Appendix A (Supporting information for Chapter 2) 224

Appendix B (Supporting Information for Chapter 3) 235

Appendix C (Supporting information for Chapter 4).....256

Appendix D (Supporting information for Chapter 5).....259

Appendix E (Supporting information for Chapter 6)……..262

Appendix F (Supporting information for Chapter 7).....269

Curriculum vitae.....274

List of Tables

Table 2.1 Amino acid sequences of the peptides and proteins studies here. Ala1 and K115 (in bold) in the sequence of calmodulin are in acetylated and tri–methylated forms, respectively……..45

Table 4.1 Predicted cross-linking sites as obtained from rigidity and flexibility analysis at energy cutoffs of -3 kcal/mol (For results from energy cutoffs of -2 kcal/mol and -1 kcal/mol, see Table C.2(A&B). The first two columns give the potential cross-linking Met residues, the third shows the sulfur-surfur distance d(1—2) obtained from the crystal structure of Ca_4–CaM (1CCL). The remaining columns show the modes in both +Ca and –Ca structures that can bring Met residues close to within 5 Å, and the corresponding d(1—2) distances, and the MS results wherever available. "-" indicates that the cross-linking of the corresponding Met pairs was not observed in MS. (kcal/mol is used as a default unit in FIRST software, which can be converted to SI unit according to 1 kcal/mol=4.2 kJ/mol)…….104

Table 5.1 Amino acid sequences of the peptides and proteins studies here. Potential Pt(II) binding sites, are highlighted in red……..…..119

Table 5.2 List of observed ECD side chain losses from charge reduced species (normal peptides and Pt–modified peptides)……...133

Table 6.1 Amino acid sequences of the peptides studied here. P1, P2, and P3 were obtained by synthesis, and rest of the S–S, Se–S, and Se–Se containing peptides obtained by reacting P1, P2, and P3 together..145

Table 6.2 Ratio of P(X•)/P(XH) (P = P1, P2, and P3; X = S, Se) species

generated during ECD of S–S, S–Se and Se–Se containing species. The ratio was calculated based on the peak area of the monoisotopic peak of each species. 2 M data sets were used deliberately to simplify the ratio calculation due to complicity of selenium isotopic distribution. Replicated errors are the standard deviation of three duplicates……152

Table 6.3 Partial peak list table of the ECD spectrum of $[P1+P1+3H]^{3+}$. For complete peak list table, see Table E.1……155

List of Schemes

Scheme 3.1 Proposed mechanism for formation of $Pt(dien)^{+\bullet}$ and $Pt(dien)(CH_3S)^{+\bullet}$ ions……..…….89

Scheme 6.1 Possible ECD fragments generated by cleaving the S–S (a) or S–CH_2 (b, c, and d) bonds of a triply–charged disulfide–linked peptide ions, $[P1+P1+3H]^{3+}$……154

Scheme 6.2 Possible S–S (a) C–S (b–e) bonds cleavage pathways of a disulfide–containing peptide. ……157

Scheme 7.1 Possible fragmentation pathways of the $[insulin+6H]^{6+}$ ion due to one or two electron(s) capture.……..174

Scheme 7.2 Possible fragmentation pathways of yielding Ac(S-S) ions by capturing two electrons……..177

List of Figures

Figure 1.1 Diagram of the principle of MALDI……5

Figure 1.2 Diagram of the principle of ESI……6

Figure 1.3 The scheme of a quadrupole device……9

Figure 1.4 Theoretical stability diagrams as a function of U and V for ions with different masses (x < y < z). By ramping the U and V values appropriately, only the peak of each individual stability diagram will be transferred……...10

Figure 1.5 Scheme of events that take place during excitation and detection in an FTICR MS. ……13

Figure 1.6 The scheme of ICR cells. (Top) cubic cell and (bottom) cylindrical cell ……...14

Figure 1.7 Ion cyclotron motion in a uniform magnetic field……15

Figure 1.8 Ion motion in a cubic Penning trap, where the arrows show the directions of ion motions, including cyclotron motion, magnetron motion, and trapping motion. ……...17

Figure 1.9 Nomenclature of peptide N- and C-terminal sequence ions used in mass spectrometry……23

Figure 1.10 The instrumental diagram of Bruker 12T SolariX FTICR MS……..32

Figure 2.1 CAD spectra of peptides–Pt adducts (a) [A + $Pt(NH_3)_2Cl$ + $2H]^{3+}$ ion at *m/z* 437.2; (b) [B + $Pt(NH_3)$ + $H]^{3+}$ ion at *m/z* 610.5. Angiotensin II and bombesin are abbreviated as A and B, separately.….49

Figure 2.2 (a) Mass spectrum of angiotensin II–bombesin–cisplatin (1:1:3)

mixture. (b) Isotopic distributions of the cross–linked products $[A + Pt(NH_3) + B + 2H]^{4+}$ and $[B + Pt + B + 2H]^{4+}$ ions. " * " represents chemical noise. Peaks are listed in Appendix I as Table S 2.1……50

Figure 2.3 (a) CAD spectrum of the cross–linked product $[A + Pt(NH_3) + B + 2H]^{4+}$ ion at *m/z* 719.34. The insert of Figure 2.3 a is the overlapping isotopic distributions of $[A + Pt + B_b_{12} + 2H]^{4+}$ (cross) and $[B + Pt + A_b_6 + 2H]^{4+}$ (circle) ions in absorption mode. (b) ECD spectrum $[A + Pt(NH_3) + B + 2H]^{4+}$ ion at *m/z* 719.34. Peak results are listed in Appendix I (Table S 2.2 (CAD) and Table S 2.3 (ECD)). (c) Fragmentation diagram of the cross–linked product A + $Pt(NH_3)$ + B……51

Figure 2.4 (a) CAD spectrum of the cross–linked product $[B + Pt + B + 2H]^{4+}$ ion at *m/z* 858.91, the insert shows the zoom spectrum from *m/z* 650 to *m/z* 950. (b) ECD spectrum of the cross–linked product $[B + Pt + B + 2H]^{4+}$ ion at *m/z* 858.9. Peak results are listed in appendix I as Table S 2.4 and S 2.5. (c) Fragmentation diagram of the cross–linked product B + Pt + B……..54

Figure 2.5 (a) Cross–linked product spectrum from the digested CaM–cisplatin (1:1) mixture. The isotopic distribution of the cross–linking product CaM(107–126) + Pt + $CaM(127–148)^{5+}$ ion (circles) is overlapped with the digested peptide $CaM(38–74)^{4+}$ ion (triangles). (b) CAD spectrum of the cross–linked product CaM(107–126) + Pt + $CaM(127–148)^{5+}$ ion at *m/z* 1018. (c) ECD spectrum of the cross–linked product CaM(107–126) + Pt + $CaM(127–148)^{6+}$ ion at *m/z* 848. (d) Fragmentation diagram of the cross–linked product CaM(107~126)+ Pt + CaM(127–148). For the full peak list, see Table S 2.6 (CAD) and Table S 2.7 (ECD) in Appendix

I……..56

Figure 2.6 Spatial distances between the thioether sulfurs of Met109, Met124, Met144 and Met145 of apo–calmodulin (1DMO).[49] The S atom of Met145 is chosen as the center, only amino acid residues within 8 Å are shown. The thioether sulfurs of methionine residues are labeled in black. The distances indicate by double arrows between the thioether sulfurs of Met109, Met124, Met144 and Met145 range from 4.5 Å to 11.3 Å……...65

Figure 3.1 Chemical structures of Pt–complexes (Pt_1, Pt_2, and Pt_3)……72

Figure 3.2 ESI–FTICR MS analyses of reaction mixtures of platinum complexes with CaM at different molar ratios. (a) CaM:Pt_1 (1:2); (b) CaM:Pt_1 (1:8); (c) CaM:Pt_3 (1:1); (d) CaM:Pt_2 (1:2); (e) CaM:Pt_2 (1:8). Figures 1a'–1e' are expansions of the corresponding parts in Figures 1a–1e. The structures of Pt(II) complexes are inserted in Figure 3.2 a, c, and d. "*" Represents chemical noise; ● CaM; ■ CaM+Pt; ★ CaM+2Pt; ◆ CaM+Pt(dien), and▲CaM+2Pt(dien)…..……74

Figure 3.3 ECD spectra of the 1:2 CaM:Pt_1 sample. (a) ECD spectra of $[CaM + 2Pt + 12H]^{16+}$ ions at *m/z* 1074, the inset is the fragmentation map from ECD spectra of CaM + 2Pt; (b) the expanded ECD spectra $[CaM + 2Pt + 12H]^{16+}$ ions. Double dots represent doubly Pt–modified fragments. Full peak list is available in Appendix B (Table B.2)……...79

Figure 3.4 CAD spectrum of the cross–linked product of [CaM(107–126) + Pt + CaM(142–CaM148) + 3H]$^{5+}$ ion at *m/z* 681. To simplify the labeling of the spectrum, CaM(107–126) is represented by X, and CaM(142–148) is represented by Y'. The insets are the CAD fragmentation map of

[CaM(107–126) + Pt + CaM(142–CaM148) + 3H]$^{5+}$ ions, and characteristic fragment ions, Y'_b_3 + Pt and X_b_3 + Pt, which show that Pt(II) cross–links Met109 and Met144 residues……..…81

Figure 3.5 Bottom–up MS/MS spectra of CaM:cisplatin (1:2). (a) ECD spectrum of [CaM(38–74) + Pt + 2H]$^{4+}$ ion at *m/z* 1066; (b) CAD spectrum of [CaM(38–74) + Pt + 2H]$^{4+}$ ion at *m/z* 1066; the observation of b_{14} + Pt^{2+} and y_5 + Pt ions suggests that Pt cross–links Met51 and Met71 or Met72. (c) CAD spectrum of [CaM(107–126) + Pt + H]$^{3+}$ ion at *m/z* 865; the observation of b_3 + Pt and y_4 + Pt suggests that Pt cross–links Met109 and Met124 (d) CAD spectrum of [CaM(127–148) + Pt + H]$^{3+}$ ion at *m/z* 895. The detection of b_4 + Pt and y_5 + Pt ions suggests that Pt cross–links E127 or D129 with Met144 and Met145……82

Figure 3.6 ECD spectrum of [CaM + 2Pt(dien) + 15H]$^{19+}$ ions at *m/z* 916 in the sample of CaM:cisplatin (1:2). The left inserts are the complimentary c/z$^{\bullet}$ ion pair, c_{82} + Pt(dien)$^{8+}$ and z_{66} + Pt(dien)$^{8+\bullet}$; the right insert is the fragmentation map of the ECD spectrum of CaM + 2Pt(dien). Single dot represent singly Pt(dien)–modified fragments; two dots represent doubly Pt(dien)–modified fragments……..…85

Figure 3.7 (a) ECD spectrum of [CaM + 5Pt(dien) + 10H]$^{20+}$ ions at *m/z* 914; the insert shows the isotopic distribution of precursor ions; (b) Complementary ion pairs, [Pt(dien)]$^{+\bullet}$ and [CaM + 4Pt(dien) + 10H]$^{18+}$ ions, [Pt(dien)(CH_3S)]$^{+\bullet}$ and [CaM + 4Pt(dien) + 10H - CH_3S]$^{18+}$ ions; (c) Isotopic distributions of Pt(dien)–modified c and z$^{\bullet}$ ions. For full peak list, see Table B.3……....86

Figure 3.8 Site–specific yields of products from backbone fragmentation

vs. backbone cleavage sites. (a) ECD of [CaM + 5Pt(dien) + 10H]$^{20+}$; (b) CAD of [CaM + 5Pt(dien) + 10H]$^{20+}$……88

Figure 4.1 NMR structure of CaM (1DMO, the first of 30 conformations) and crystal structure of Ca_4–CaM (1CCL). Calcium binding sites are in cyan, calcium ions in black, Met residues in magenta, and rest of the CaM chain in green. Sulfur atoms indicated as spheres……..…94

Figure 4.2 Rigidity dilution plots for (a) the native structure of Ca_4–CaM (1CLL), and (b) the Ca_4–CaM (1CLL) with calcium deleted. The primary sequence of the protein is represented as a line, and the secondary structure is presented by using DSSP (database of secondary structure assignments) with calcium binding sites indicated (49). A horizontal thin black line indicates a flexible region of the backbone, while a thick coloured line indicates a rigid cluster. The topmost line of the plot shows the rigidity of the structure with the inclusion of all possible hydrogen bonds; the structure is almost entirely a single rigid cluster, shown in red. When E_{cut} is decreased (left–most column, in kcal/mol), rigid clusters break up as indicated in different colors and more of the chain becomes flexible. Cutoff values used in the simulation of flexible motion (-1,-2 and -3 kcal/mol) are indicated by arrows……..……101

Figure 4.3 The C–terminal domain (residues 80–147) of Ca_4–CaM (1CLL) shows the hydrophobic protein–binding groove: (a) at the start of a flexible–motion simulation (native structure), and (b) during flexible–motion simulation along mode m_{14}–. The protein is mostly shown in cartoon view, with Met residues shown in all–atom view, and sulfurs highlighted in black. The sulfur–sulfur distance for residues 109 and 144

is shown and these two residues have clearly been brought into close proximity in mode 14–……105

Figure 4.4 (a) Native ESI spectrum of Ca–CaM:cisplatin = 1:2 reaction products; (b) Trypsin digested Ca–CaM:cisplatin = 1:2 complex, the inserts are platinum cross–linked species; (c) CAD spectrum of $[CaM(107–126) + Pt + H]^{3+}$ species. The observation of a_3 + Pt and y_4 + Pt ions indicates that cisplatin cross–links Met109 and Met124 residues……107

Figure 4.5 Native ESI spectra of protein complexes. (a) Ca–CaM:melittin = 1:1; (b) (CaM:cisplatin = 1:2)–Ca:melittin = 1:1; (c) (Ca–CaM:cisplatin = 1:2):melittin = 1:1……..…..112

Figure 5.1 MS/MS spectra of the substance P:cisplatin (1:2) sample. (a) CAD spectrum of the $[Sp + Pt(NH_3) + H]^{3+}$ ions at *m/z* 520; (b) ECD spectrum of $[Sp + Pt(NH_3) + H]^{3+}$ ions at *m/z* 520. "*" represents chemical noise……..122

Figure 5.2 A). The arrival time distribution (ATD) of three conformers of the $[Sp + Pt(NH_3) + H]^{3+}$ ions (the cross section of each conformer (a, b, and c) is listed as insets of Figure 2A; **B).** Corresponding MS/MS (CAD) ion mobility spectrum for each conformer, (a) CAD spectrum of conformer a (AT=4.22 ms); (b) CAD spectrum of conformer b (AT=5.33 ms); (c) CAD spectrum of conformer c (AT=5.83 ms). The rest of the insets are the expanded *m/z* regions from 50 to 450 and 500 to 800……125

Figure 5.3 ECD spectra of peptide-cisplatin complexes. (a) $[A+Pt(NH_3)_2Cl+2H]^{3+}$ ions at *m/z* 520 in angiotensin II:cisplatin (1:2) sample, (b) $[B+Pt(NH_3)+H]^{3+}$ ions at *m/z* 620 in bombesin:cisplatin (1:2)

sample, and (c) $[P1+Pt]^{2+}$ ions at *m/z* 728 in P1:cisplatin (1:2) sample. "*" represents noise……..….128

Figure 5.4 MS spectra of peptide–cisplatin adducts at different pH values. (a–1), (b–1), and (c–1) are the MS spectra of $Sp_{(1–7)}$–cisplatin adducts at pH 3, 7, and 10; (a–2), (b–2), and (c–2) are the MS spectra of $Sp_{(2–11)}$–cisplatin adducts at pH 3, 7, and 10; and (a–3), (b–3), and (c–3) are the MS spectra of Sp–cisplatin adducts at pH 3, 7, and 10. "*" represents noise……..131

Figure 5.5 The side chain loss region from the charge–reduced M + Pt species. (a) $[Sp + Pt + H]^{3+}$, (b) $[A + Pt]^{2+}$, (c) $[B + Pt + H]^{3+}$, and (d) $[P1 + Pt]^{2+}$. The insets show the fragment ions with the diagnostic side chain losses due to Pt–binding……134

Figure 5.6 (a) ECD spectra of the $[insulin + Pt(NH_3)_2 + insulin + 8H]^{10+}$ ion at *m/z* 1170, the insets show the details of the ECD spectrum; (b) complementary ion pairs $[I + Pt(NH_3)_2(NH_2\cdot) + 4H]^{5+\cdot}$ and $[I–NH_2\cdot + 4H]^{5+}$; (c) fragment ions ABc_{26}^{3+} and $(ABc_{29} + Pt)^{4+}$; (d) fragmentation scheme for insulin + $Pt(NH_3)_2$+insulin species (all the cleavages are mainly labeled in one insulin structure as $\{Pt(NH_3)\}^{2+}$ cross–linked two species are identical here); (e) crystal structure of a insulin dimer (4E7T).[52] The chains and amino acids are color–coded as follow: A–chains in red, B–chains in green, His in cyn, Glu in blue, and Lys in pink……..139

Figure 6.1 ECD spectra of triply–charged S–S (P1+P1), S–Se (P1+P2 and P1+P3), and Se–Se (P2+P2, P2+P3, and P3+P3) containing species. (a) $[P1+P1+3H]^{3+}$ at *m/z* 841.42281; (b) $[P1+P2+3H]^{3+}$ at *m/z* 857.73795; (c) $[P2+P2+3H]^{3+}$ at *m/z* 873.38609; (d) $[P1+P3+3H]^{3}$ at *m/z* 903.42365^{+};

(e) $[P2+P3+3H]^{3}$ at *m/z* 919.40558^{+} ; and (f) $[P3+P3+3H]^{3+}$ at *m/z* 965.09283……147

Figure 6.2 Expanded ECD spectra of the fragment species formed by cleavage of S–S, S–Se, and Se–Se bonds. The top–two rows are the simulation spectra (in red) of P1 (S·/SH), P2 (Se·/SeH), and P3 (Se·/SeH) species. Rest of the rows show the corresponding species generated during ECD experiments……148

Figure 6.3 Comparasion of ECD fragment ions generated by cleavage of (a) C–S bonds (P1+P1),(b) C–Se bond *vs* C–S bond (P1+P3), and (c) C–Se bonds (P2+P3). Experimental fragment spectra are in red and simulated isotope patterns are in black To differentiate peaks closed–by at *m/z* 1228 to 1233 Da region, the simulated spectra were color–coded ($[P1–SH+H]^{+}$ species are in black, $[P1–S+H]^{+\cdot}$ in pink, $[P1–S+2H]^{+}$ in blue, and $[P1–S+3H]^{+}$ in orange.). The inserts shows the corresponding structure of each species. The mass windows were not aligned between different fragment species……150

Figure 6.4 Comparasion of ECD fragment ions generated by cleavage of (a) C–S bonds (P1+P1),(b) C–Se bond *vs* C–S bond (P1+P3), and (c) C–Se bonds (P2+P3). Experimental fragment spectra are in red and simulated isotope patterns are in black To differentiate peaks closed–by at *m/z* 1228 to 1233 Da region, the simulated spectra were color–coded ($[P1–SH+H]^{+}$ species are in black, $[P1–S+H]^{+\cdot}$ in pink, $[P1–S+2H]^{+}$ in blue, and $[P1–S+3H]^{+}$ in orange.). The inserts shows the corresponding structure of each species. The mass windows were not aligned between different fragment species……156

Figure 6.5 Expanded ECD spectra of (a) $[P1+P1+3H]^{3+}$, (b) $[P1+P3+3H]^{3+}$, and (c) $[P2+P3+3H]^{3+}$. This spectra show the c/z·ions generated by cleaving both N-C_α and S-S, S-Se, or Se-Se bonds…….161

Figure 7.1 ECD spectra of $[Insulin+6H]^{6+}$ at *m/z* 956. The insets show the expanded spectra in mass regions from *m/z* 400 to 1100 and *m/z* 1550 to 2000……170

Figure 7.2 Fragment ions observed in the ECD spectrum of the $[I+6H]^{6+}$ ion. (a) Fragmentation diagram; (b) complementary ion pairs from the cleavage of one N-C_α bond by single electron capture; (c) complementary ion pairs from the cleavages of one N-C_α bond and one S-S bond by single electron capture; (d) complementary ion pairs from the cleavages of one N-C_α bond and one S-S bond by double electrons capture; (e) ions from insulin A-chain yielded by multiple electrons capture (n≥2); (f) A-chain and B-chain ions due to the cleavages of both inter-chain disulfide bonds; and (g) hydrogen bonding……...172

Figure 7.3 MS/MS spectra of $[Rnase\ A+13H]^{13+}$ ions at *m/z* 1053. (a) ECD; (b) IR-ECD; (c) shot-ECD; and (d) fragment ions correspond to cleavages of both N-C_α bond and disulfide bond(s) from Figure 1c. The insets are the expanded spectra to show the spectra quality and the fragmentation patterns……181

Figure 7.4 Shots-ECD spectra of the $[Rnase\ A+13H]^{13+}$ ion at different bias voltages. (a) 1.5V, (b) 3 V, (c) 5 V, (d) 10 V, and (e) 15 V. The insets show the details of each spectrum and the intensities of each spectrum are normalized to 1.0×10^9 and 5×10^8 for *m/z* 200 to 1000 and *m/z* 1250 to 1500, respectively……...183

List of Abbreviations

Å	Ångström
ACN	Acetonitrile
AI-ECD	Activated-ion ECD
Asp	Aspartic acid
CAD	Collisionally activated dissociation
CaM	Calmodulin
CD	Circular dichroism
CE	Capillary electrophoresis
CHCA	Alpha-cyano-4-hydroxycinnamic acid
CI	Chemical ionization
CPU	Central processing unit
CTR1	Copper transporter-1
Cys	Cysteine
DC	Direct current
DHB	2,5-Dihydroxybenzoic acid
DNA	Deoxyribonucleic acid
DSSP	Database of secondary structure
ECD	Electron capture dissociation
EI	Electron impact
EDD	Electron detachment dissociation
EID	Electron induced dissociation
ESI	Electrospray ionization
ETD	Electron transfer dissociation
ExD	Electron capture dissociation related
FIRST	Floppy inclusions and rigid substructure
FRODA	Framework rigidity optimized dynamic
FTICR MS	Fourier transform ion cyclotron
FWHM	Full width at half maximum
Glu	Glutamine acid

His	Histidine
ICR cell	Ion cyclotron resonance cell
IM–MS/MS	Ion mobility–mass spectrometry/mass
IR–ECD	Infrared activated ECD
IRMPD	Infrared multiple photons dissociation
ISD	In source decay
LC	Liquid chromatography
MALDI	Matrix assisted laser desorption
Met	Methionine
MS	Mass spectrometry
m/z	Mass-over-charge
MS^n	Tandem mass spectrometry
niECD	Negative ion ECD
NMR	Nuclear magnetic resonance
PIR	Protein interaction reporter
ppm	Part per million
PTMs	Post-translational modifications
R	Resolving power
RF	Radio frequency
RNase A	Ribonuclease A
RMSD	Root–mean–square deviation
SA	Sinapinic acid
SORI	Sustained off-resonance dissociation
T	Tesla
TOF	Time-of-flight
UV	Ultraviolet

Chapter 1

Introduction

1.1 Introduction to the study of protein post-translational modifications using mass spectrometry

Post-translational modifications (PTMs) are chemical modifications that are crucially important in regulating the basic biological functions and the dynamics and structures of proteins. More than 200 different types of PTM have been characterized and reported, among them, the most common and important PTMs are phosphorylation, acetylation, methylation, glycosylation, sulfation, deamidation, nitration, disulfide bond formation, as well as some other PTMs due to drug treatments, such as platination.[1] PTMs function in various ways, such as, phosphorylation can reversibly activate/inactivate enzyme activity, regulate many cellular processes including cell cycle, growth, apoptosis and signal transduction pathways; acetylation can regulate protein–deoxyribonucleic acid (DNA) interactions, and stabilize the structures of proteins; glycosylation can regulate cell-cell recognition and signaling, and affects the folding, conformation, stability, and activity of proteins; disulfide bonds can stabilize the structure of proteins.[1] Consequently, PTMs are associated with various diseases, such as cancer, diabetes, neurodegenerative diseases, and heart disease. The study of PTMs can therefore provide invaluable insight into the cellular function processes.

Mass spectrometry (MS) has been recognized as an essential tool for characterizing PTMs due to its sensitivity, selectivity, accuracy, speed, and low consumption of samples.[2-8] Modified peptides or proteins can be easily identified by MS due to the mass shift arising from the specific modification, and the modification site can be further localized by tandem MS.

This thesis focuses on protein PTMs studies by using tandem MS methods, including the electron capture dissociation (ECD) and collisionally activated dissociation (CAD), mainly ECD. This chapter includes two parts: the introduction to mass spectrometry (section 1.2) and the introduction to protein platination and disulfide proteins (section 1.3). In the first part, the components and techniques of mass spectrometry are discussed in details. In the second part, the biological importance of protein platination and disulfide bonds in proteins is described, and the applications of ECD in metal bound proteins and disulfide proteins are introduced.

1.2 Introduction to mass spectrometry

MS is a powerful analytical tool for providing molecular weight information, and for elucidating the structural details of molecules. There are three main components in a mass spectrometer, including the ionization source, the mass analyzer, and the detector. In this section, the major ionization techniques and mass analyzers will be introduced, followed by tandem fragmentation techniques.

1.2.1 Major ionization techniques

In mass spectrometers, only charged particles can be analyzed and detected; therefore, the first stage of MS is to convert sample molecules to ions in an ion source. A variety of ionization techniques has been used for mass spectrometers, among them, electron impact (EI) and chemical ionization (CI) are the most classic ionization methods.

Electron impact (EI)

Electron impact (EI) ionization is the original MS ionization method and is usually used for the ionization of volatile organic compounds, limited to volatile, low molecular weight, and thermally stable samples. In EI, the sample is first vaporized into the mass spectrometer ion source; where it collide with a beam of electrons with sufficient energy (~ 70e V) to ionize the sample molecule by detachment one electron.[9] The process is summarized as follow:

$$M + e^- \rightarrow M^{+\bullet} + 2e^- \quad (1.1)$$

The molecular ion generated, $M^{+\bullet}$, is a radical; thus is often not stable and tends to fragment. Therefore, EI mass spectra are often characterized by intense fragment ions and small molecular ion peaks.

Chemical ionization (CI)

CI involves multiple steps of ion-molecule reactions. The reagent gas molecules (such as methane, ammonia) are first ionized by EI and further undergo ion-molecule reactions with themselves and then the molecule of interest. Taking the methane as the reagent gas for an example, the processes generally occur as follow:

$$CH_4 + e^- \rightarrow CH_4^{+\bullet} + 2e^- \quad (1.2)$$

$CH_4^{+\bullet} + CH_4 \rightarrow CH_5^+ + CH_3^\bullet$ (1.3)

$M + CH_5^+ \rightarrow CH_4 + MH^+$ (1.4)

The molecular species generated in CI are not the odd-electron molecular ions ($M^{+\cdot}$) seen in EI, but the protonated even-electron molecules, MH^+. Thus, the CI molecules species are relatively more stable compared with the molecular ions in EI and are less prone to fragmentation. CI is particularly useful for providing the molecular weight information but also requires volatile and stable samples.[9]

Matrix assisted laser desorption (MALDI)

Matrix assisted laser desorption ionization (MALDI) was first invented by Karas and Hillenkamp in 1985.[10-13] In 1988, Tanaka applied a similar method to ionize large molecules, proteins and polymers, with mass over 100,000 Da,[14] Since then, MALDI has been widely applied to the analysis of biomolecules, such as peptides, proteins, DNA, and large organic molecules.[13-18] The mechanisms of MALDI are still under debate due to the complexity of the process.[19, 20] In a simplified explanation, MALDI typically involves a combination of two processes: desorption and ionization. Samples are first mixed with excess of matrix and then irradiated with UV or IR laser light. The matrix molecules heavily absorb IR or UV laser energy, and lead to the ablation of the upper layer of the matrix. Vaporized gas phase mixtures of neutral and ionized matrix molecules and neutral sample molecules are then formed, followed by proton transfer that results in the formation of ionized analytes (see Figure 1.1). Most commonly used matrix molecules for peptide and protein analysis include 2,5-dihydroxybenzoic acid (DHB), alpha-cyano-4-

hydroxycinnamic acid (CHCA), and sinapinic acid (SA). The main structure features that shared by these matrix are the aromatic structure which absorbs the laser energy, and a functional group which can donate proton, like carboxylic acid.

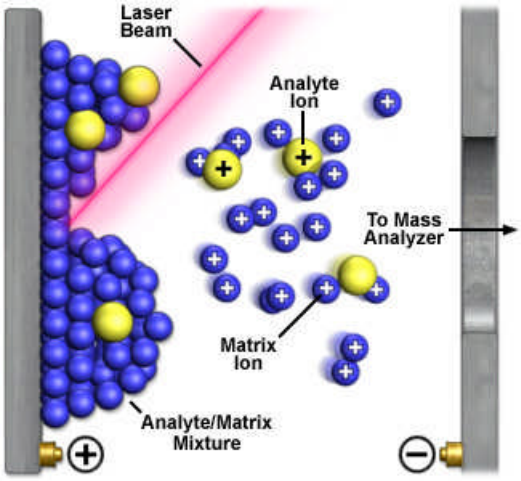

Figure 1.1 Diagram of the principle of MALDI (see http://www.magnet.fsu.edu/education/tutorials/tools/ionization_maldi.html for information, accessed 31st Dec, 2012)

MALDI is a soft ionization technique, which is particularly suitable for non-volatile samples, such as biomolecules and polymers. The ions generated in MALDI are typically singly-charged species, which simplifies the spectra interpretation. As the MALDI process is independent of the size of the compound analyzed; therefore, molecules with mass up to 300,000 Da can be detected with the hyphenation of time-of-flight mass analyzers. In addition, MALDI is also more sensitive and rapid than other laser desorption techniques, consumes fewer amounts of samples, has a better tolerance for salt adducts, and requires less sample preparation

procedure.

Electrospray ionization (ESI)

Electrospray ionization (ESI), invented by Fenn in the late 1980's,[21] along with MALDI, are the two revolutionary soft ionization techniques, which made the analysis of large biological molecules possible and contributed to the increasing understanding of the processes of life. For the recognition of their contributions, Tanaka and Fenn were rewarded the Nobel Prize in Chemistry for the inventions of MALDI and ESI techniques in 2002.

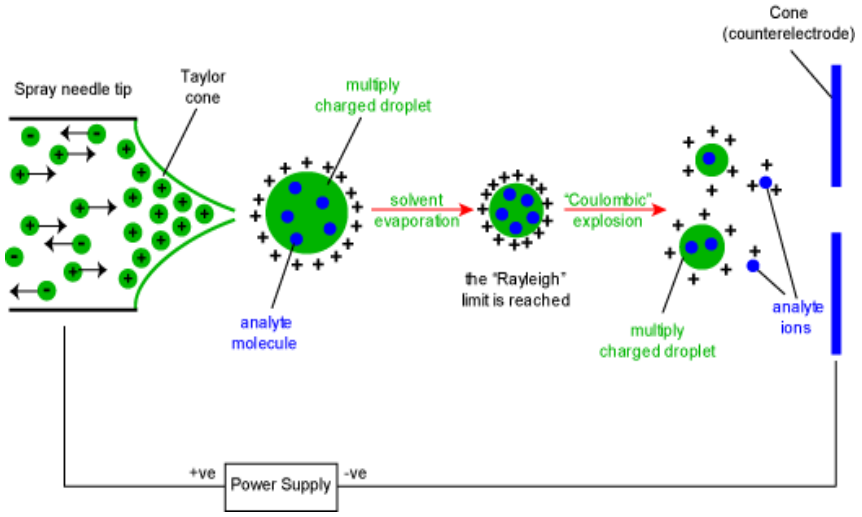

Figure 1.2 Diagram of the principle of ESI

(See http://www.chm.bris.ac.uk/ms/newversion/esi-ionisation.htm for information, accessed 31st Oct, 2012)

In ESI, the analyte is firstly dissolved in an easily evaporated solvent and then introduced into a capillary tube. As shown in Figure 1.2, a high electric potential of several kilovolts is applied to the capillary, and the resulting strong electric field between the capillary and the counter electrode induces charge accumulation at the liquid surface located at the

tip of the capillary, which produces the charged droplets. A countercurrent flow of dry gas is often used to assist the evaporation of droplets and a sheath gas is used coaxially to reduce the radial dispersion of the spray. When the “Coulombic repulsion” exceeds the surface tension, smaller sized offspring droplets are released. This process continues until the solvent is completely evaporated and the charged ions are formed.

Both positive– and negative–ion spectra can be obtained. For positive-ion mode, 50/50 H_2O/acetonitrile or H_2O/methanol is often used, 1% formic acid or acetic acid is usually added into the analyte solution to enhance protonation and increase sensitivity. For negative-ion mode, 0.1% ammonium hydroxide is suitable to add to help deprotonation and increase sensitivity.

One of the advantages of ESI is that multiply charged ions are often formed, which not only improves the sensitivity, but also allows the analysis of high molecular weight molecules. In addition, ESI is a soft ionization technique so intact molecules are observed. Overall, ESI can be used to the analysis a variety of samples, including peptides, proteins, organometallics, polymers, petroleum, organic compounds, etc.[2, 21-25]

1.2.2 Mass analyzers

Once the analyte ions are generated in the ion source, they are directed into the mass analyzer region of the mass spectrometer by electric potentials, separated, and measured by a mass analyzer according to their mass-to-charge ratios. The mass analyzer is the heart of a mass spectrometer. There are many types of mass analyzers

available, and the operating principles of several commonly used mass spectrometers, including quadrupole mass analyzers, time-of-flight (TOF) mass analyzers, and ion cyclotron resonance cell will be briefly discussed here.

The performance of a mass spectrometer can be evaluated based on the following important characteristic factors, including the mass range, the mass accuracy, the mass resolving power, the scanning speed, the sensitivity, and the transmission efficiency. Mass range is the range of mass-over-charge (*m/z*) values that can be detected by a mass spectrometer. Mass accuracy is the accuracy of *m/z* value and is usually calculated by the difference between the experimental value and the theoretical value in parts per million (ppm) units. Resolution or resolving power represents the ability of a mass spectrometer to distinguish two very close peaks in a mass spectrum. The resolving power (R) can be calculated as $R=m/\Delta m$, where m is the *m/z* value of the peak and Δm is its full width measured at half maximum (FWHM). The scanning speed is the rate at which the analyzer measures over a particular mass range. The sensitivity of a mass spectrometer indicates the lowest amount of sample that can be analyzed, which is affected by transmission efficiency. Transmission efficiency is the ratio of the actual number of ions reaching the detector to the total number of ions generated in the ion source region.

Quadrupole mass analyzer

A quadrupole mass analyzer consists of four parallel rods with each opposite pair being electronically connected. As shown in Figure 1.3, the ions enter and travel in the z direction, while oscillating in the x-y

plane. The oscillation is controlled by the radio frequency (RF) voltage (V) and a direct current (DC) voltage (U) can be applied to each pair of rods. Only ions with stable trajectories at the selected U and V values can travel through the quadrupole and be detected.

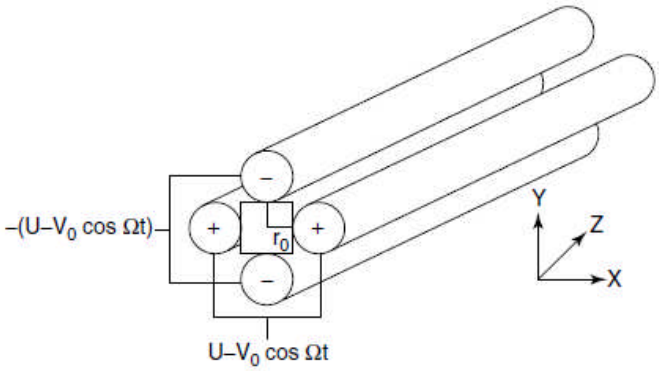

Figure 1.3 The scheme of a quadrupole device (Reproduced from Hoffmann et al. 2007)[9].

The ion motion in a quadrupole is governed by the Mathieu equation,[9] and the trajectory stability of ions can be described by the two following equations:

$$a = \frac{8eU}{mr_0^2\omega^2} \quad (1.5)$$

$$q = \frac{4eV}{mr_0^2\omega^2} \quad (1.6)$$

where a and q are related to direct DC potential U and the magnitude of radio frequency V, respectively, ω is the angular frequency and r_0 is the half distance between the two opposite rods. For each different mass, the solution to the Mathieu equation results in a different stability areas (see Figure 1.4). With specific U and V values, only ions within a narrow

m/z range can travel through the quadrupole, and the rest of the ions will have unstable trajectories and strike on the rods. Therefore, quadrupole mass analyzers can be used to isolate ions. As shown in Figure 1.4, when a constant U/V value is kept during operation, the U/V line only crosses the vertices of the stable areas; thus only the ion with specific *m/z* value is transmitted. By adjusting the U/V value, the resolution of a quadrupole mass analyzer can be varied. When the DC potential U is off, the quadrupole functions as a RF only ion guide, which allows all ions above a certain *m/z* value passing through the quadrupole.

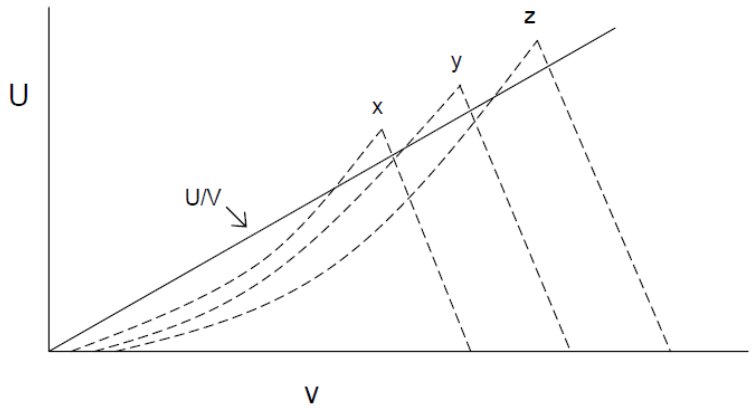

Figure 1.4 Theoretical stability diagrams as a function of U and V for ions with different masses (x < y < z). By ramping the U and V values appropriately, only the peak of each individual stability diagram will be transferred.

In practice, the upper-mass-limit of a quadrupole is around *m/z* 4000, resolution below 3000, and mass accuracy about ~100 ppm.[9] The advantages of a quadrupole mass analyzer are that they are low-cost, easy to build and operate, and have the ability for ion isolation.

Quadrupoles are often used as ions guides, ion selectors, and ion storage devices in mass spectrometers.

Time-of-Flight (TOF) mass analyzer

In a time-of-flight (TOF) MS, ions generated in an ion source are accelerated by an applied electric field and then separated in an evacuated field-free flight tube (the drift region) of the instrument based on their *m/z* values. The TOF mass analyzer measures the mass based on the flight time of an accelerated ion travelling through the drift region to a detector.[26] The flight time can be calculated based on the length of the flight tube (L) and the velocity (v) as:

$$t = \frac{L}{v} \quad (1.7)$$

the velocity can be derived from the initial kinetic energy,

$$E = \frac{mv^2}{2} = zeV \quad (1.8)$$

Then the flight time (t) can be derived from equations 1.7 and 1.8 as:

$$t = \sqrt{\frac{mL^2}{2zeV}} \quad (1.9)$$

where m and z are the mass and charge of the analyte ion, respectively, and V is the accelerating potential. It can be seen from equation 1.9 that lighter ions travel fast and reach the detector first, followed by heavier ions. Ion flight times typically lie in the range of ~ 100 μs;[9] thus the TOF analyzers are very fast. The pressure in the drift region is in the 10^{-7} torr range so that the ions are allowed to drift with a minimum number of collisions with background gases.

In reality, the initial velocities of ions with the same *m/z* generated

are slightly different, which cause peak broadening and lower the mass resolution of the TOF mass analyzer. There are several methods that have been used to correct the kinetic energy spread, including the time-lag-focusing method, the retarding field, and the reflectron.[26, 27] With the implementation of these techniques, modern TOF instruments can easily reach a resolving power of 20,000 and mass accuracy of <10 ppm.[27] In addition, TOF instruments have high sensitivities and require relatively small amount of samples, and there is no limitation for its mass range.

Fourier transform ion cyclotron resonance mass spectrometer (FTICR MS)

The principle of cyclotron resonance acceleration was discovered by Ernest O. Lawrence in 1930, and was first applied into a mass spectrometer by Sommer et al. in 1950s. Two decades later, Melvin B. Comisarow and Alan G. Marshall applied the Fourier transform method to ion cyclotron resonance (ICR) mass spectrometry and built the first FTICR MS instrument.[28] The FTICR determines the mass-to-charge ratio of ions by measuring their cyclotron frequency in a uniform magnetic field.[29, 30] As shown in Figure 1.5, ions are trapped radially in a homogeneous axial magnetic field, and trapped axially by an electric field. By applying a RF resonance excitation pulse to the two excitation plates, ions are resonantly excited to higher cyclotron radius. The coherent ion cyclotron motion of an ion package of given *m/z* induces image charge in the detection plates. The image charge is amplified, and digitized to generate the time domain transient. The transient signal can be Fourier transformed into a frequency domain spectrum, calibrated, and converted

into a mass spectrum.[29] The advantage of FTICR MS is that the excited ions can travel a distance of ~ kilometers during a detection time of a 1-s. Thus, for a typical transient length of a few second or even minutes, a resolving power over ~10^6 can be achieved.

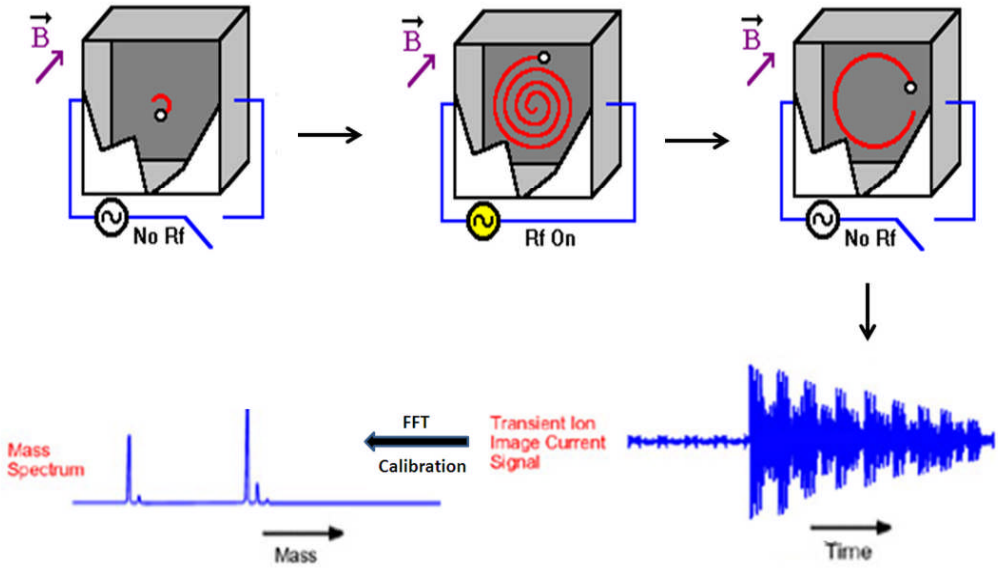

Figure 1.5 Scheme of events that take place during excitation and detection in an FTICR MS.

The main components of all FTICR MS instruments include a magnet, a mass analyzer ─ ion cyclotron resonance cell (ICR cell), ultra-high vacuum system, and data system. Among the magnets used for FTICR MS, including permanent magnets, electromagnets, and superconducting magnets, actively shielded superconducting magnets are the most commonly used ones. As the core part of a FTICR MS, the ICR cell is introduced in detail in the following section, along with ion motions in the ICR cell, excitation, and detection.

Ion cyclotron resonance (ICR) cell. There are several types of

ICR cells, including cubic cells, open cylindrical cells, cylindrical cells with end-caps, “infinity cells”, and the newly developed ParaCell.[29, 31] The cubic cell is the original one as shown on the top-left of Figure 1.6. It has the simplest configuration, with three sets of opposed plates for the purpose of excitation, detection and trapping ions. The ions are trapped in the z-direction by the two end-caps, and confined in the x-y plane by the magnetic field. The trapped ions can then be excited and detected using the other two sets of opposed plates.

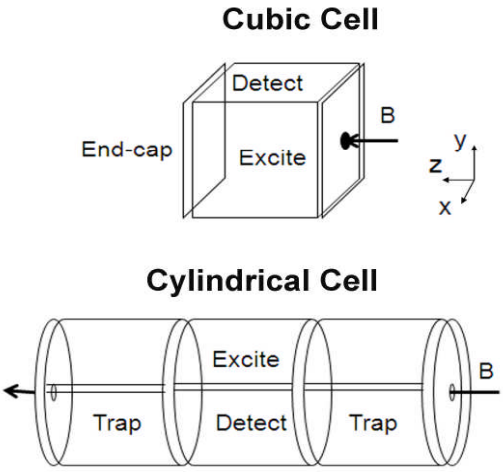

Figure 1.6 The scheme of ICR cells. (Top) cubic cell and (bottom) cylindrical cell.

The open cylindrical cell as shown in the bottom of Figure 1.6 is a cylinder that axially segmented into three parts to produce ring electrodes. The central cylinder has four plates, with two opposed ones function as excitation plates and the other two as detection plates. The two cylinders at the end are trapping plates to confine ions in the z-direction. The advantage of open cylindrical cells is the uniformed excitation field generated and easy access for ions as well as for electrons and photons.

Ion motions in the ICR cell. Ions in the ICR cell experience a complex combination motion of three types: cyclotron motion, trapping motion, and magnetron motion.[29, 30]

Ion cyclotron motion. When an ion moves perpendicular to the magnetic field, the ion will experience Lorentz force (F_1) and be deflected in a direction that is perpendicular to both its velocity and the magnetic field (Figure 1.7).

$$F_1 = q(v \times B) \quad (1.10)$$

Where *q* is the ion's charge, *v* is its velocity, and B is the magnetic field strength.

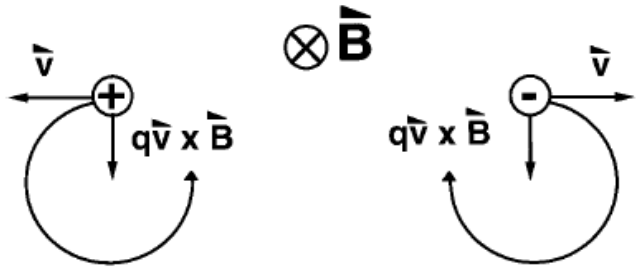

Figure 1.7 Ion cyclotron motion in a uniform magnetic field (B) (Reproduced from Marshall et al. 1998).[29]

Under the influence of the magnetic field, a stable circular orbit of radius *r* results when the inward directed centripetal "force"

$$F_2 = \frac{mv^2}{r} \quad (1.11)$$

F_2 is balanced by the inward magnetic force, namely

$$F_1 = F_2 \quad (1.12)$$

$$\frac{mv^2}{r} = q(v \times B) \quad (1.13)$$

The angular velocity ω of an ion is

$$\omega = \frac{v}{r} \quad (1.14)$$

Thus, by combining the above two equations, we have:

$$\omega_c = \frac{qB}{m} \quad (1.15)$$

The cyclotron frequency f_c equals to ω_c; therefore it can be calculated as:

$$f_c = \frac{qB}{2\pi m} \quad (1.16)$$

This equation specifies that the cyclotron frequency of an ion in a constant magnetic field is inversely proportional to its mass-to-charge ratio, and most importantly, the cyclotron frequency does not depend on the velocity or energy of the ion, which is the key feature why FTICR MS is capable to achieve such high resolving power. While, for most other types of mass spectrometers, their resolutions are limited by the energy spread. Typically, the cyclotron frequency ranges from a few kHz to a few MHz.

Trapping motion. Ions are confined radially by a magnetic field as mentioned above; however, ions are free to escape along *z*-axis. To prevent the escape of ions along the *z*-axis, a small voltage is applied to the trapping plates; an electrostatic potential well is therefore created. Ions are trapped in the well if their energy is lower than the trapping voltage, and oscillate slowly back and forth between the trapping plates. Typically, the frequency of the trapping motion is around a few kHz.

Magnetron motion. The trapping potential also produces a radial force, which acts on the ion and produces an outward-directed electric

force that opposes to the inward-directed magnetic force from the applied magnetic field. Thus, the voltage V_T on the trapping plates causes a small decrease in the cyclotron frequencies, and the effective total force experienced by the ion in the ICR cell can be calculated as:

$$Force = m\omega^2 r = qB_0\omega r - \frac{qV_{Trap}\alpha}{a^2} r \quad (1.17)$$

or $$\omega^2 - \frac{qB_0\omega}{m} + \frac{qV_{Trap}\alpha}{ma^2} = 0 \quad (1.18)$$

Solving equation (1.18) for ω, we then can obtain two natural rotational frequencies in place of the original "unperturbed" cyclotron frequency.

$$\omega_c = \frac{\omega_c}{2} + \sqrt{(\frac{\omega_c}{2})^2 - \frac{\omega_z^2}{2}} \quad (1.19)$$

$$\omega_c = \frac{\omega_c}{2} - \sqrt{(\frac{\omega_c}{2})^2 - \frac{\omega_z^2}{2}} \quad (1.20)$$

in which, $\omega_z = \sqrt{\frac{2q\alpha V_{Trap}}{ma^2}}$ (1.21), and $\omega = \frac{qB}{m}$ (1.15)

where ω_+ and ω_- are the reduced cyclotron frequency and magnetron frequency, respectively, ω_c is the unperturbed cyclotron motion, ω_z is the frequency of the trapped ions in the z-direction.

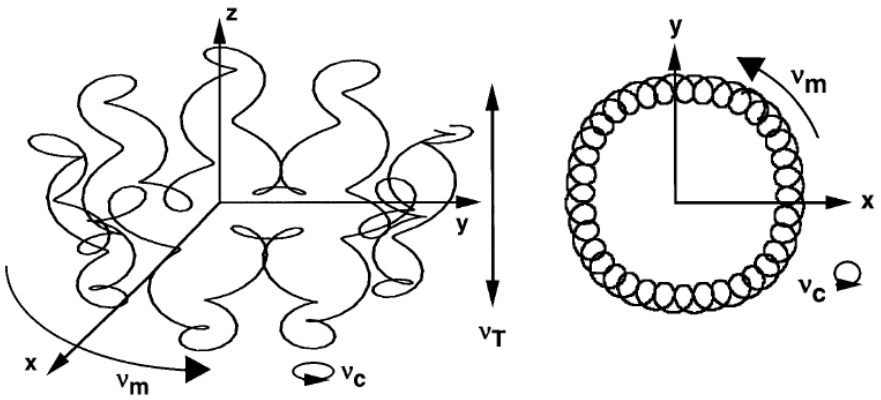

Figure 1.8 Ion motion in a cubic Penning trap, where the arrows show the directions of ion motions, including cyclotron motion, magnetron motion, and trapping motion (Reproduced from Marshall et al. 1998).[29]

Z-axis motion ω_z is proportional to V_T, so increasing the trapping potential increases ω_z and ultimately decreases ω_c. Therefore, there is a trade-off between raising the trapping plate voltages to better trap/detect the ions and perturbing the true cyclotron frequency. Figure 1.8 shows the ion motions in a Penning trap. The magnetron frequency (a few Hz) and trapping frequency (a few kHz) are usually much less than the cyclotron frequency (~ kHz to ~ MHz), and are mot determined in typical experiments.[29]

Excitation and detection. Typically, initial ion cyclotron radii are in the sub-millimeter ranges, which are too small to induce detectable image current in the detection plates. In addition, the thermal cyclotron motion of the ions is incoherent and generates zero net image current on the detection plates. Therefore, a spatially uniform rf electric field (E_0) with frequency corresponding to a particular *m/z* value is used to accelerate ions coherently to a larger cyclotron radius (see Figure 1.5), which thus induces detectable image current on the detection plates. The post-excitation radius *r* can be calculated from the following equation (1.22):

$$r = \frac{E_0 T_{Excite}}{2B} \quad (1.22)$$

or $$r = \frac{V_{p-p} T_{Excite}}{2dB} \quad (1.23)$$

where $V_{p\text{-}p}$ represents the peak-to-peak excitation voltage, T_{excite} is the excitation duration in seconds, and *d* is the distance between the two opposite detection plates in meters.

It is clear from equation 1.22 that the post-excitation ion cyclotron radius is independent of *m/z*. Thus, all ions of a certain range *m/z* can be excited to the same ICR orbital radius. A broadband exication is usually performed by frequency-sweep (chirp) excitation or stored waveform inverse Fourier transfrom (SWIFT) excitation.[29, 32] However, when using the chirp-excitation, the power that ions experience is not evenly distributed over the excitation range; therefore ions are excited to slightly different cyclotron orbital radius, typical varying 10%. In addition, the mass selectivities at the beginning and end of the frequency sweep are poor. SWIFT, on the other hand, produces the flattest excitation. The idea was proposed by Marshall et al.,[32] in which the whole process is reversed. The desired mass-domain is first defined and converted to a frequency-domain spectrum, followed by performing an inverse Fourier transform of the frequency spectrum to a time-domain excitation signal.

Resonant excitation creates spatially coherent ion packets, which induces image current on the two opposite parallel detection plates. The image current can be calculated as follow:

$$\Delta Q = -\frac{2qy}{d} \quad (1.24)$$

where *q* represents the charge of an ion and d is the distance between the two detection plates.

Thus, the ICR signal is proportional to the induced current, which inturn is proportional to the post-excitation radius. In addition, the

detected signal intensity increases linearly with ion charge, so that the ICR is more sensitive for multiply charged ions. Moreover, all ions of a certain *m/z* range can be excited to the same ICR orbital radius; thus ions of a wide *m/z* range can be detected simultaneously.[29]

Resolving power/resolution. In MS, resolution is defined as the full width of a spectra peak at half-maximum peak height, $\Delta m_{50\%}$, and the resolving power is the observed mass divided by the mass peak width at half-maximum height, namely $m/\Delta m_{50\%}$. In FTICR, the resolution can be estimated by:

$$R \sim \frac{fT}{2} \quad (1.25)$$

Where f is the cyclotron frequency and T is the transient length. Therefore, the resolution in FTICR is determined by the transient length and frequency. Although the length of the transient can last forever in theory, in reality, the transient signal decays with time because background gas in the ICR cell can lead to collisions between ions and neutral gas molecules, the coherent ion cyclotron motion of the ion package can then be destroyed and lead to signal decay. Therefore, ultra-low pressure is essential to achieve high resolution, cryogenic pumps or turbopumps are often used to achieve pressures down to ~ 10^{-10} torr.

Since $f = \frac{qB}{2\pi m}$, the mass resolving power increases linearly with the strength of magnetic field. In general, the performance of the FTICR MS instrument improves as the magnetic field strength increases; however, the costs for the magnets of high field also increase

dramatically. Currently, the magnet strengths of the commercial magnets range from 3 to 15 T. However, the FTICR instrument using 21 T superconducting magnets are under construction by the national high magnetic field laboratory at Florida University and Pacific Northwest national laboratory, respectively, aiming to achieve revolutionary capabilities in FTICR MS.

Dynamic range. The detection limit of a MS indicates the lowest amount of sample that can be analyzed. For a FTICR MS, typically ~ 100 charges of a given mass-over-charge are required to induce a detectable image current for a broadband detection. Therefore, FTICR MS is inherently less sensitive than ion-counting mass spectrometers. A lot more ions can be trapped inside the ICR cell; however, when more than ~ 100, 000 ions are presented in the cell, space charge effect needs to be considered, which can induce peak broadening or peak coalescence, and eventually leads to transient signal decay.[29] Theoretically, the dynamic range increases linearly with the magnetic field; therefore, higher magnet field strength is preferred.

Deleterious factors. Space charge and magnetron expansion are the two factors that cause the most deleterious effects on the performance of ICR instruments.[29, 30] The space charge effect is the result of Coulombic interactions between and within ion clouds in an ICR cell. It affects the instantaneous trapping field experienced by the ions, thus the duration of the observable signal and the stability of the resonant frequency. Space charge increases both the peak width and the uncertainty of the peak position, causing frequency shift and peak

coalescences, hence reducing the resolving power and the mass accuracy. Magnetron motion is associated with the geometry of the trapping potentials and its radius expands over time. This magnetron expansion results in the exposure of the ion packets to increasingly inhomogeneous trapping field, thus causing a decrease in the resolving power and the mass accuracy.

The ultrahigh resolving power (~ 500, 000) and mass accuracy (< 1 ppm) of the FTICR MS make it particularly suited for complex sample analysis, such as top-down protein analysis.[33-35] The instrument used in this thesis is a commercial 12 T Bruker solariX FTICR MS instrument; therefore the main components of this instrument will be introduced briefly in a later section.

1.2.3 Tandem mass spectrometry methods

Tandem mass spectrometry (MS^n) can provide detailed structural information for organic and biological samples by fragmenting the parent ions. Over the years, many different fragmentation techniques have been introduced, including collisionally activated dissociation (CAD),[36] also known as collision-induced dissociation (CID),[37] sustained off-resonance dissociation (SORI-CAD),[38] blackbody infrared radiative dissociation (BIRD),[39] infrared multiple photon dissociation (IRMPD), electron capture dissociation (ECD),[40] electron transfer dissociation (ETD),[41] electron detachment dissociation (EDD),[42] electron induced dissociation (EID), *etc*. Different fragmentation techniques can produce different types of fragments. The structure or sequence information can

then be deduced based on the masses of the fragments. Figure 1.9 shows the types of fragment ions of peptides or proteins that can be generated in MS/MS analyses, which was proposed by Roepstorff in 1984.[43]

Collisionally activated dissociation (CAD)

CAD or CID was first introduced by Jennings[37] and later by McLafferty,[36] and refers to the process in which inelaslic collisions between ions and neutral gas molecules, such as gases are helium, nitrogen, and argon, results in the conversion of part of the translational energy into internal energy of ions and subsequent fragmentation. The deposited vibration energy is redistributed rapidly throughout the molecule prior fragmentation; therefore, the cleaved bonds are mostly the weakest bonds. In peptides, the cleavages typically occur at the backbone amide bond, yielding b and y ions (see Figure 1.9). Preferential cleavages at the N-terminal proline and C-terminal aspartic acid have been previously reported.[44-46]

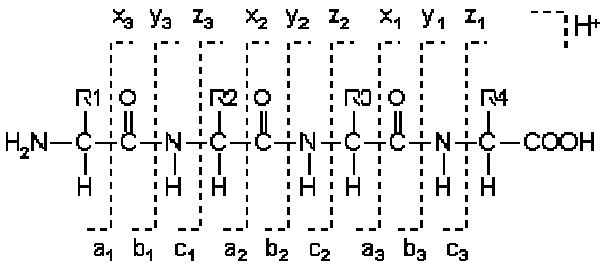

Figure 1.9 Nomenclature of peptide N- and C-terminal sequence ions used in mass spectrometry.

CAD is by far the most commonly used tandem fragmentation

technique, which has been extensively used in the structural analyses of peptides and proteins, oligosaccharide, and DNA.[44, 47-51]

Infrared multiphoton dissociation (IRMPD)

IRMPD is also based on the excitation of vibrational modes of ions, in which parent ions are irradiated with an infrared laser (CO_2 laser at 10.6 μm) and the absorption of photons leads to the fragmentation of parent ions.[52, 53] IRMPD primarily produces b and y-type fragment ions, just like CAD. However, compared to CAD, IRMPD often produces more extensive fragmentation because the initial fragment ions generated by IRMPD are also irradiated by the laser beam and fragmented.[53]

Electron capture dissociation (ECD)

The first ECD-type results were observed by Guan *et al.* in ultraviolet (UV) photodissociation of multiply charged protein cations.[54] Unusual c/z fragments and charge reduced precursor were unexpectedly observed, which indicated that the parent ion reacted with electrons. Similar results were also observed in the analysis of peptides using MALDI in source decay (ISD) dissociation.[55] It was thought that electrons were produced by the UV laser hitting the edge of the ICR cell and this assumption was further examined by modifying the ICR cell to trap ions and electrons simultaneously by Zubarev *et al*. in 1998.[40] The significant increase of the charge reduced species and c/z fragments indicates that it was the secondary electrons generated by the UV laser hitting the ICR cell and not the UV photons responsible for this effect.[56] ECD was therefore born when the UV laser was replaced by a directly heated filament.

ECD mechanisms. Several mechanisms have been proposed for ECD, including mainly the Cornell mechanism,[40, 57] the Utah-Washington mechanism,[58-63] and the Free radical cascade mechanism.[64]

The Cornell mechanism (the hot-hydrogen mechanism). Based on the earliest experimental work on ECD, McLafferty *et al.* proposed that electrons were initially captured at a positively charged site to form a hypervalent radical center and a hot H• was then released to subsequently attack (1) an S-S to cleave it to form –S• and –SH species or (2) a backbone carbonyl oxygen atom for form a –(•COH) –NH–C_α– radical center and break the N–C_α bond.[57] The preservation of labile modifications and nonselective cleavage in ECD lead to the idea that ECD is a non-ergodic process, namely, the fragmentation occurs before intramolecular vibration energy redistribution. The non-ergodic idea of ECD has since then been under hot debate. Although there are experimental results that support this idea, the theoretical calculation results obtained by Turecek suggest that N-C_α bond cleavages in peptide ketyl radicals and cation-radicals are extremely facile reactions.[65] Therefore, it might not be necessary to use non-ergodicity to explain the cleavages of strong N-C_α bonds while keeping weak bonds intact.

In the ECD study of a doubly charged peptide containing a disulfide linkage at its center $(KA_jCAc)_2$ carried out by the Marshall group,[66] intense abundance of fragments resulting from the cleavage of the disulfide bond were detected and similar fragmentation pattern was also observed when the protonated Lys termini were replaced by providing the charges with Na^+ cations. These observations made them

suspect that the hot-hydrogen mechanism might not be correct or not be the only ECD mechanism because it is hard to explain how these hot H• atoms can travel up to 32 Å $(KA_{20}CAc)_2$, j=20) to cleave the S-S bond.[66] Alternative ECD mechanisms were therefore being considered.

Utah-Washington mechanism. It was proposed by the Simons group[58, 59, 67, 68] and the Turecek group[60, 65, 69] independently that the electron initially is captured in a Rydberg orbital centered on the positive charge site, and subsequently undergoes intra-molecular electron transfer to S–S σ* or an amide π* orbital to cleave the S–S or N–C_α bond.

In addition, Simons also proposed that direct electron capture at S–S σ* or amide π* orbitals can promptly cleave the disulfide bond or form a –(•COH) –NH–C_α– radical and then cleaves the N–C_α bond.[58] Although vertical electron attachment to an S– S σ* or amide π* orbital is *ca.* 1 eV or *ca.* 2.5 eV endothermic, respectively, the *ab initio* calculation results show that the Coulomb stabilization by positively charged groups can lower the energies of these low-lying anti-bonding orbitals, so that electron attachment to these orbitals becomes exothermic. In addition, based on Simons' calculation, 90~99% of the initial electron attachment in ETD (similar in ECD) most likely occurs into a Rydberg orbital on a positive site and with 1~10% directly attached to the S–S σ* or amide π* orbital.

Free radical cascade mechanism. In the ECD study of doubly charged cyclic peptides by Leymarie *et al.*,[64] many fragments corresponding to amino acid losses and side-chain losses were observed. The observation of amino acid losses was unexpected because they

require one electron capture to cleave multiple backbone sites. The free radical cascade mechanism was therefore proposed, which suggests that ECD generates an α-carbon radical species that then migrates along the protein backbone and induces secondary fragmentation. Recently, the results from the Turecek group suggest that peptide cation radicals do go through cascade dissociations.[70, 71]

Side chain cleavages from ECD. Electron capture by multiply charged peptide and protein cations can also result in cleavages in amino acid side-chains. These side-chain losses can then be used diagnostically to identify the presence of certain amino acids in a sequence. Some of the w-ions can also be used to differentiate isomeric amino acids, such as Ile and Leu.[72-75]

Implementation of electron capture dissociation. ECD has been almost exclusively equipped in FTICR MS instruments. It is mainly because the heating of electrons can be avoided in an electromagnetic field of FTICR, allowing more accurate control of electron kinetic energy, which can give sufficient time for ions and electrons to interact. The main obstacle of implementing ECD in other RF types of instrument is mainly because the electrons are energized by the RF field and are ejected typically within a microsecond. Although the simulation results show that it is possible to use ECD in a Paul trap with the addition of a weak magnetic field, the implementation of ECD in RF ion traps remains challenging and ECD efficiency achieved is rather low.[76, 77]

In the early years of using ECD, electrons were generated by a directly heated filament. Thus the cross-section of electron beam

generated by the filament is not only small in diameter but also the electron energies have a broad distribution due to the variation of the electrical potential of the heated filament. In addition, the electron energy flux is low and a good overlap between ions and electrons is often hard to achieve. Therefore, it typically requires seconds of reaction to obtain extensive fragment ions, which in turn limits the hyphenation of ECD with separation techniques, such as liquid chromatography (LC) or capillary electrophoresis (CE).

To improve the overlap of ions and electrons, to control electron energy, to shorten the reaction time, to achieve high electron flux and high rate ECD fragmentation efficiency, and to simultaneously perform IRMPD/ECD, directly heated filaments have been replaced by various types of indirectly heated dispenser cathodes to generate wide, compressed, hollow, or cold ultra-wide electron beams.[78] Each different cathode has its own advantages and disadvantages, nevertheless, with the use of dispenser cathodes, ECD fragmentation efficiency was improved and the irradiation time was lowered to milliseconds. The hollow dispenser cathode has been standardly implemented on Bruker FTICR MS systems, allowing the combination of IRMPD and ECD in a single experimental configuration.

Although ECD has been proved as a useful fragmentation technique in many applications, the conversion efficiencies of precursor ions to product ions is often limited. The experimental factors were therefore examined by different groups to improve the efficiency.[79, 80] It was shown that the optimal irradiation period is inversely proportional to

charge state, and the reflection of electrons through the ICR cell can significantly improve ECD efficiency compared to a single pass.[79, 80] A further study by Tsybin *et al.* highlighted that the magnetron motions of ions in the ICR cell can periodically modulate ECD fragmentation efficiency due to the periodic overlap (misalignment) of ion cloud and electron beams.[81] Thus, the ECD conditions can be optimized by correctly phasing electron injection with the ion magnetron motion or by sidekick to manipulate ion magnetron motion. In addition, the overlap of ions and electrons can be improved by on- and off-resonance ion excitation prior to ion ejection.[82, 83]

Another factor limiting ECD efficiency is due to the conservation of weak noncovalent interactions, which becomes problematic because c and z• fragments can be held together through non-covalent bonding, thus preventing their separation.[84] Various activation methods have been used to remove noncovalent interactions to give greater structure fluctuations favored by ECD analyses, including IR laser radiation, collision activation, blackbody radiation, or in-beam collisions.[85-89] The combination of these activation methods with ECD has been demonstrated to yield remarkable improvement in ECD fragmentation efficiencies, which in general was referred as “activated-ion ECD” (AI-ECD).[88]

Applications of ECD. ECD has proven to be a powerful and superior tandem fragmentation technique in the study of PTMs, protein complexes, and top-down analyses due to many of its unique features.[90] First, the cleavage sites in ECD are often complementary to those

generated by conventional dissociation techniques, like CAD, which makes the combination of these two types of techniques extremely powerful in sequencing polypetides. Second, although the fragment ions are usually low-abundance, the relatively nonselective homolytic cleavages nature of ECD generally results in more detailed sequence information compared to CAD, which is particularly beneficial in top-down analyses. Last but not least, ECD has a unique feature to conserving labile bonds during fragmentation, including the labile PTMs of proteins and noncovalent interactions. Therefore, various types of PTMs have been identified by ECD, including deamidation, phosphorylation, glycosylation, sulfation, oxidation, etc.[91-96] ECD has been also applied to the studies of protein folding, and protein-protein complexes. [33, 97-103]

Electron capture dissociation related fragmentation techniques (ExD)

As mentioned above, FTICR MS has been the only type of mass spectrometer that enables the successful application of ECD and the implementation of ECD in low cost and easily operated mass spectrometers like RF traps has remained challenging. To overcome the problem of storage of thermal electrons in an RF field, anions were used as electron donors to provide electrons to multiply charged peptide cations. Electron transfer dissociation (ETD) was therefore invented and implemented in a modified 3D ion trap by Skya and Coon in 2004.[41] In a similar way, N-Cα or disulfide bonds are cleaved in ETD by interacting multiply charged ions with anions. The recombination energy in ETD is lower than in ECD because the electron binding energy barrier has to be overcome to transfer electrons to from anion to parent ions; the ETD

efficiency was therefore often lower than that in ECD. However, the implementation of ETD in low-cost, low-maintenance, and widely accessible RF ion traps greatly improved the accessibility of ECD-like dissociation to the whole proteomics field. It has been demonstrated that ETD efficiency can be improved using a supplemental collisional activation method (ETcaD) that can activate the charge reduced precursor ions and promote the backbone dissociation.[104]

The development of radical-mediated fragmentation techniques has gone beyond ECD and ETD. Electron detachment dissociation (EDD)[42] and negative ion ECD (niECD) for multiply deprotonated ions,[105] and electron induced dissociation (EID) for singly-charged ions have also been discovered.[106] In EDD, multiply deprotonated ions interact with high energy electrons (> 10 eV), resulting in the electron detachment from the precursor ions and the formation of the nitrogen centred radical anions for peptides/proteins, which can undergo C_α-C bond cleavages and side chain losses.[42] The efficiency of EDD can be improved by increasing the charge state of the precursor ions, and by adjusting the voltages on the cathode and the extraction lens. EDD is particularly useful for the analysis of peptides/proteins rich in acidic residues, e.g. Asp, Glu, DNA and RNA.[107, 108] Ni-ECD was discovered by the Håkansson group,[105] they found that peptide anions can capture electrons within a narrow energy range (3.5~6.5 eV), resulting in charge-increased radical species that then undergo dissociation similar to that in ECD/ETD. The increase of charge in ni-ECD enables its application in not only multiply-charged anions, but also singly-charged ions and this technique has been found

useful in the analysis of PTMs, such as phosphorylation, sulfonation, glycation, and disulfide linked peptides.[105] EID is another technique that can be used in the analysis of singly-charged ions. Following the irradiation of peptide ions (singly or multiply charged) with fast electrons (6~ 20 eV), the precursor ions are electronically excited and generate fragments.[106, 109]

1.2.4 12 Tesla solariX FT ICR mass spectrometer

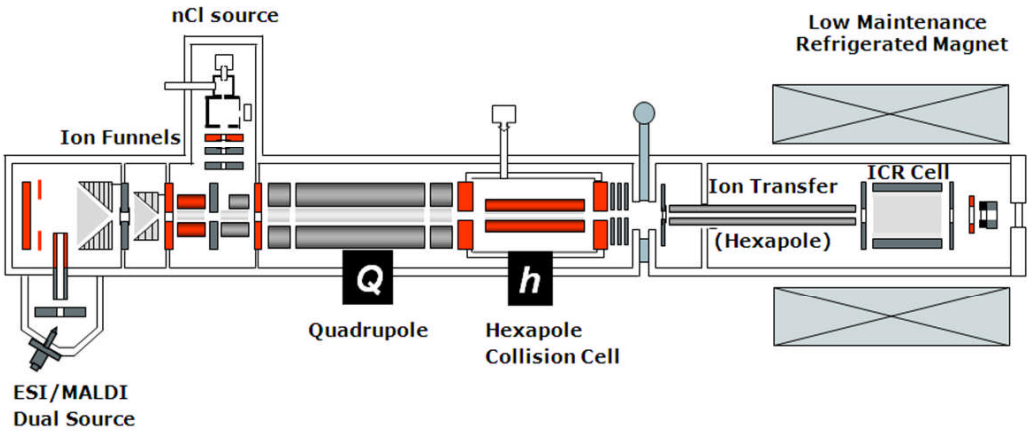

Figure 1.10 The instrumental diagram of Bruker 12T SolariX FTICR MS.

Figure 1.10 shows the diagram of the Bruker 12T SolariX FTICR MS (Bruker Daltonics, Bremen, Germany). Ions are first generated using either the ESI or MALDI source, then transferred through the heated glass capillary and directed to the ion funnel and skimmer region. The dual ion funnels can focus ions and transfer them more effectively. Ions are then focused in the source octapoles before passing through the quadrupole and hexapole collision cell (Qh front end). When performing CAD, ions can be isolated by the quadrupole, accumulated and

fragmented in the hexapole collision cell. ETD can also be performed in the hexapole collision cell, with radical anions generated by an nCI source mounted off-axis above the split octapole. Ions then fly through the transfer hexapoles (ion guide) and enter the infinity cell, where ECD and IRMPD can be performed. The hollow electron cathode is located on the other side of the infinity cell, with an extraction lens located between the ICR cell and the electron gun. The hollow electron gun design allows the on-axis introduction of an IR laser beam and performance of IRMPD and IR-ECD experiments.

Typical mass resolving power of over 500, 000 at *m/z* 400 can be routinely achieved using this 12 T solariX FTICR MS, with mass accuracy < 0.5 ppm with internal mass calibration, and < 2 ppm with external calibration.

1.3 Introduction to protein platination and disulfide bound proteins

In this thesis, the studies on PTMs are particularly focused on protein platination and disulfide linked proteins, details are introduced separately in the following sections.

1.3.1 Biological importance of studying protein platination

Since the accidental discovery of the antitumor activity of cisplatin in 1960's, platinum-based drugs have been widely used in clinical cancer treatments. During the last four decades, the research on platinum-based anticancer drugs has been mainly focused on understanding how cisplatin and its analogues induce antitumor effects, and on designing

new platinum drugs with the aim of lessening the toxicity of cisplatin, such as nephrotoxicity.[110-113] It has been found that cisplatin converts to its active form by aquation of one of the chloride leaving groups, and subsequently coordinates to DNA, forming inter- and intra-strand crosslinks, which leads to DNA-damage recognition and repair, cellular apoptosis, and cell-cycle arrest.[111]

Although cisplatin is a very effective anticancer drug, it has two major drawbacks, one is the strong toxicity to kidneys and gastrointestinal tract, and the other is that tumors usually become resistant to platinum drugs during treatment.[114, 115] Thus, it is important to research on how the tumour becomes resistant to cisplatin; new anticancer drugs with less toxicity and better selectivity can then be designed and synthesized. Intensive studies have been performed to investigate the resistance mechanisms, and several mechanisms have been proposed, including (1) insufficient amount of cisplatin reaching the target DNA, (2) increased intra-cellular trapping of cisplatin, (3) increased repair of DNA damage or increased tolerance of DNA damage, and (4) miscellaneous.[114, 115]

Cisplatin primarily binds to DNA to exert its cytotoxicity; however, it also reacts with many biologically available nucleophiles, especially sulfur- and nitrogen-containing ligands, such as methinone, cysteine and histidine. Within one day of injection of cisplatin, 65~98% of the platinum in the blood plasma is protein-bound.[116] The binding of cisplatin to proteins is implicated to be responsible for many of the severe side effects exhibited by the drug through the mechanisms (1) and (2) as mentioned above. Copper transporter-1 (CTR1), the major copper

plasma-membrane transporter, has been shown to play a critical role in cisplatin uptake.[117-120] Both copper and cisplatin can cause a rapid down-regulation of CTR1 expression in human ovarian cancer cell lines, and the loss of CTR1 can result in less platinum entering cells, and consequently lead to drug resistance.[121] In addition, there are some efflux proteins, such as multidrug resistance protein-1, copper transport proteins–ATPase, have also been shown to involve the transport of cisplatin to a certain extent.[114, 115] Moreover, increasing research has shown that the increased level of thiol-containing species is related to the drug resistance of cisplatin and its analogues. The strong binding of platinum to sulfur-containing species, such as cysteine, methionine, glutathione, and metallothioneins, can lead to drug detoxification, nephrotoxicity, and resistance.[122-128] In addition, recently it has been reported that the binding of platinum to some proteins, such as human copper chaperone Atox1 and calmodulin, can induce conformational changes of proteins, thus interfere with the normal activities of proteins.[129, 130]

The transport of cisplatin through cell membranes and possible intermediate binding to proteins remain poorly understood. Therefore, studies on the interactions of anticancer metallodrugs with proteins are attracting a growing interest because of their relevant pharmacological and toxicological consequences.

The discovery and development of new platinum-containing anticancer drugs have been focused on increasing the selectivity and lowering the toxicity of this type of antitumor drug. Pt^{IV} complexes

appeared attractive because these octahedral complexes are usually substitution-inert and require reduction to Pt^{II} species to become cytotoxic.[131, 132] A potential application of such processes is for therapeutic purposes and the development of light-sensitive Pt^{IV} pro-drugs that can be photoactivated to active antitumor agents directly at the site of the tumor. Such site-selective activation is expected to decrease the side-effects and toxicity. Hence, the clinical application of platinum antitumor agents might be expanded.

However, like cisplatin, these molecules also react with proteins, binding covalently, and little is known about the specificity or positions of this binding. It is therefore important to explore how cisplatin and its analogues react with proteins, where they bind to proteins, and what kind of effect that might have. This research can then in turn facilitate the development of new metal-based anticancer drugs with low toxicity.

1.3.2 MS studies of protein platination

Early work on studying interactions of antitumor metallodrugs with proteins has been performed using various spectroscopic techniques, including circular dichroism (CD), fluorescence, nuclear magnetic resonance (NMR) spectroscopy and X-ray crystallography. Each of these methods provides a certain level of information, but meanwhile has some drawbacks, such as, lack of sensitivity, and inability to provide binding site information.

MS has been recently shown as an extremely powerful tool to study the interactions of drugs with proteins, due to its advantage of sensitivity and ability to provide direct information on the nature of the

drug-protein adducts, even identification of binding sites.[133-136] The reactions between proteins (e.g. transferrin, cyctochrome c, ubiquitin, insulin, superoxide dismutase, hemoglobin, cytochrome c, human serum albumin) and platinum-based drugs have been studied by MS.[116, 134, 137-146] However, little attempt was made to pinpoint the binding sites for platinum binding to proteins in the early studies.

Recent progress by a combination of mass spectrometry and proteomics technologies has made the identification of binding sites much more feasible. There are basically two classes of methods to achieve this, "bottom-up" (peptide level) and "top-down" (intact protein level) approaches.[147] "Bottom up" strategies involve cleaving the protein into peptide fragments by proteolytic enzymes prior to mass spectrometry detection. By applying the bottom-up mass spectrometric approach, Allardyce *et al.* successfully identified a binding site between cisplatin and transferrin.[134] "Top-down" methods identify proteins by measuring the mass of the whole protein, then using tandem mass spectrometry, such as CAD, IRMPD, and ECD to fragment intact proteins in order to generate sequence information. Recently, Moreno-Gordaliza *et al*. were able to determine the binding sites between cisplatin and insulin by combining the top-down approach with nano-electrospray ionization mass spectrometry using a linear ion trap MS.[141] Further bottom-up MS study enabled them to identify more binding sites.[143] The combination of FTICR MS with the top-down and/or bottom-up proteomic approaches makes MS even more powerful; Hartinger *et al*. were able to identify the binding sites of three different platinum anticancer drugs on ubiquitin.[146]

In previous reports, CAD has been the main fragmentation technique used for the localization of Pt-modification sites. There are a few groups who have attempted but failed with the use of ECD for the identification of Pt-modification sites.[146, 148] It was suggested that the free electron is captured by the metal ion and thus trapped; therefore no c/z ions were observed in the ECD experiments.[146] In this thesis, ECD was successfully applied in the top-down and bottom-up analysis of Pt-modified proteins. Detailed results are given in Chapters 2, 3, and 5.

1.3.3 ECD applied to disulfide bonds in peptides and proteins

Disulfide bonds in proteins are post-translational modifications that are important for stabilizing the tertiary structures of proteins by introducing covalent constraints. For many peptides and proteins, disulfide bonds play a critical role in the folding and structural stabilization of many extracellular peptides and proteins, such as enzymes, growth factors, hormones, and toxins.[149, 150] Thus, the characterization of disulfide bonds is an important step to understand the structure of a disulfide linked protein.

Although top-down MS approach has been successfully used to sequence proteins rapidly, identify PTMs, and study protein complexes, the applications of using the top-down MS approach to sequence disulfide containing proteins remains challenging due to the fact that disulfide bonds rarely dissociate in the presence of a mobile proton using collisional activation methods.[151, 152] Therefore, recently, top-down studies of disulphide linked proteins using ECD or related electron–based dissociation techniques have drawn wide attention.

It was first reported by Zubarev that ECD preferentially cleaves disulfide bonds.[57] Later on, during the research with the use of other radical-based fragmentation techniques, such as ETD and EDD to dissociate disulfide bound protein ─ insulin, preferential cleavage of S-S bonds has been reported in both cases; therefore the sequence information obtained is often limited.[153, 154] In Chapter 7, a new AI-ECD method is applied in a top-down study of disulfide-rich proteins to enhance the backbone cleavage efficiency and sequence coverage.

The mechanism of ECD is another hot area which attracts wide attention. So far, several mechanisms have been proposed for the cleavage of disulfide bonds by ECD. One is that the electron is initially captured into a Rydberg orbital centered on a positively-charged site, and subsequently undergoes intra–molecular electron transfer to a nearby S–S σ* orbital to cleave the disulfide bond.[69] Alternatively, an electron is captured directly into the uncharged S–S σ* orbital to cleave the disulfide bonds, S• and S^- fragments to be formed through either mechanism, which subsequently converts to SH by hydrogen abstraction.[58]

Selenium and sulfur are in the same group of the periodic table and share many common physicochemical properties. Although these studies of disulfide bonds in peptides and proteins by ECD have been investigated during the past few years, little attention has been devoted to investigating of the ECD behavior of diselenide peptides or proteins. Previous theoretical calculations on the effects of electron capture on small diselenide compounds have been performed. Thus, in Chapter 6, a series of peptides with S–S, S–Se, or Se–Se bonds are studied using

ECD with FTICR MS, to examine the ECD behavior of diselenide peptides compared with previous theoretical calculations, and also to examine the differences and similarities of the ECD fragmentation patterns among disulfide (S–S), sulfur–selenium (S–Se), and diselenide (Se–Se) peptides.

1.4 Overview of this thesis

This thesis focuses on the study of protein PTMs by advanced tandem fragmentation techniques on an FTICR MS, involving both protein platination and disulphide-linked proteins, and also the mechanism of electron capture dissociation. The protein PTMs include: mass spectrometry evidence of cisplatin as a protein cross-linking reagent (Chapter 2); use of top-down and bottom-up Fourier transform ion cyclotron resonance mass spectrometry for mapping calmodulin sites modified by platinum anticancer drugs (Chapter 3); protein flexibility is key to cisplatin cross-linking in calmodulin (Chapter 4); radical-mediated side chain losses improve the determination of Pt(II)-modification sites on peptides and proteins (Chapter 5); and top-down electron capture dissociation of disulfide-rich proteins (Chapter 7). Research on the ECD mechanism includes electron capture dissociation of disulfide, sulfur-selenium, and diselenide bonds-containing peptides (Chapter 6). Chapter 8 is the conclusion and future work. This thesis demonstrates the utility of high resolution tandem mass spectrometry as a powerful method for the studying of protein PTMs.

Chapter 2

Mass spectrometry evidence for cisplatin as a protein cross-linking reagent[1]

2.1 Introduction

2.1.1 Techniques used for probing protein-protein interactions

High-throughput proteomics now enables the assignment of hundreds to thousands of proteins in a single experiment; however, the physiological function of many newly discovered proteins remains unclear. It has become evident that proteins often carry out their function as part of large complexes, and their interaction is the core of cellular function.[155] Therefore, the determination of the three dimensional structure of a protein and the identification of its interaction partners are critical next steps in understanding protein action. Many techniques have been developed to probe protein-protein interactions, such as X-ray crystallography and NMR spectroscopy, which provide high resolution structural information, but these methods require a relatively large amount of pure protein; alternatively, the chemical cross-linking approach allows low resolution structural data to be generated by covalently joining pairs of functional groups within a protein or a protein complex. The covalent bonds formed by cross-linking can stabilize or freeze labile interactions. Thus the distance constraints created between the reactive

[1]This chapter has been partially/entirely reproduced from Huilin Li, Yao Zhao, Hazel I. A. Phillips, Yulin Qi, Tzu-Yung Lin, Peter J. Sadler, and Peter B. O'Connor. Mass spectrometry evidence for cisplatin as a protein cross-linking reagent. *Anal. Chem.* 2011, 83, 5369-5376. Copyright 2011 American Chemical Society.

groups can help define 3-D structures of proteins or protein complexes.[156]

2.1.2 The advantages of Fourier transform ion cyclotron resonance mass spectrometry (FTICR MS) in the analysis of complex samples

The combination of cross-linking with MS has facilitated the investigation of protein-protein interactions due to its high sensitivity, fast speed of analysis, reliable sequence identification, and theoretically unlimited mass range.[133, 156-159] FTICR MS has been proved to be a potent tool for analyzing cross-linking reaction mixtures. The high mass accuracy of FTICR MS can greatly reduce the number of candidates for cross-linking products, and in addition, its high resolution, the ability of allowing a “gas phase” purification to accumulate low intensity cross-linking product ions, and the ability to fragment large proteins or peptides extensively are critical for the unambiguous assignment of the cross-linking products and localization of the cross-linking sites. However, the identification of the cross-linked products can be still quite difficult due to the complexity of reaction mixtures.

2.1.3 Challenges in cross-linking chemistry

The cross-linking chemistry inevitably produces a variety of products, including unmodified peptides, multiply modified peptides, dead-end, intra- and inter-peptide cross-linking products all present in the same sample, which makes the detection and identification of low-abundance cross-linked products challenging. To overcome these challenges, significant effort has been dedicated to design new cross-linkers which can enrich cross-linked products via affinity tags,[160-162] or facilitate the identification of cross-linked products by introducing mass

spectrometry-cleavable bonds[158, 159] or specific signature patterns,[162-165] such as PIR (protein interaction reporter),[159] isotope-labeled cross-linkers[163, 164] or isotope-labeled proteins.[165]

Although there is a broad range of cross-linking reagents available, they all target a few particular functional groups, generally primary amines, carboxylates, sulfhydryls, and free carbonyls (aldehyde groups generated via protein oxidation).[7] The limited choices of reactive groups have limited the application of cross-linking; moreover, some of the inherent chemical problems of existing functional groups also hinder the interpretation of cross-linking data. For example, the complexity of the reaction mixtures makes assignment difficult, and low charge states but high mass-to-charge (*m/z*) ions are often formed upon electrospray ionization when the cross-linking reagent reacts with primary amine groups of lysines and the amino terminus, which could otherwise carry a charge. Therefore, the development of MS identifiable cross-linkers which target new functional groups will be of benefit in the mapping of protein-protein interactions.

2.1.4 The potential of cisplatin as a cross-linking reagent

Cisplatin, cis-[$Pt(NH_3)_2Cl_2$], is a widely used anticancer drug which exerts its cytotoxic effect by reacting with DNA and forms 1,2-intrastrand cross-links between adjacent guanines.[166] The DNA cross-linking ability of cisplatin and its analogs have been well documented.[166-169] In addition, a new class of anticancer drugs with multinuclear platinum molecules linked by flexible arms is capable of forming long range inter- or intra-stand cross-links.[170-172] A few studies have demonstrated the ability of

platinum compounds to cross-link DNA with proteins.[173-175] However, up to 98% of the platinum in the blood plasma is protein-bound within one day of injection.[176] The binding of cisplatin to proteins is likely to be a primary cause of the side effects of such chemotherapies. However, the interactions of proteins with platinum compounds have not been extensively explored compared to DNA-Pt research.

The ability of a platinum complex to cross-link proteins has been unexpectedly observed by Guo *et al*., and their result shows that cisplatin can stabilize a multimeric complex of the human Ctr1 copper transporter by cross-linking adjacent proteins via methionine binding.[177] Recently, Hu *et al*. also found that cisplatin cross-links domains of albumin.[178] However, whether cisplatin can function as a cross-linking reagent has not been fully explored. Platinum(II) has a strong affinity for sulfur and nitrogen containing ligands, and the coordination sites are the side chains of methionine (Met), cysteine (Cys) and histidine (His), namely, thioether, sulfhydryl, and imidazole.[113] Thus, cross-linkers targeting these functional groups will broaden the application of cross-linking and contribute to the understanding of protein action. Here, the ability of cisplatin as a potential cross-linker is explored and demonstrated using standard peptides and the 16.8 kDa protein calmodulin (CaM), but was unsuccessfully tested with the 64 kDa protein hemoglobin. In addition, the features of cisplatin as a potential cross–linking reagent are discussed.

2.2 Experimental section

Table 2.1 Amino acid sequences of the peptides and proteins studies here. Ala1 and K115 (in bold) in the sequence of calmodulin are in acetylated and tri–methylated forms, respectively.

Name	**Sequence**	**Composition**	**Monoisotopic Mass (Da)**
Angiotensin II	DRVYIHPF	$C_{50}H_{71}N_{13}O_{12}$	1045.53451
Bombesin	pGlu–QRLGNQWAVGHLM–NH_2	$C_{71}H_{110}N_{24}O_{18}S$	1618.81506
Calmodulin (CaM)	ADQLTEEQIAEFKEAFSLFDKDGDGTITT KELGTVMRSLGQNPTEAELQDMINEV DADGNGTIDFPEFLTMMARKMKDTD SEEEIREAFRVFDKDGNGYISAAELRHV MTNLGEKLTDEEVDEMIREADIDGDG QVNYEEFVQMMTAK	$C_{719}H_{1128}O_{256}N_{188}S_9$	16779.85133
Hemoglobin	VLSPADKTNVKAAWGKVGAHAGEYG AEALERMFLSFPTTKTFPHFDLSHGSA QVKGHGKKVADALTNAVAHVDDMPN ALSALSDLHAHKLRVDPVNFKLLSHCLL VTLAAHLPAEFTPAVHASLDKFLASVST VLTSKYR (subunit α)	$C_{685}H_{1071}O_{194}N_{187}S_3$ (α)	15116.88510 (α)
	VHLTPEEKSAVTALWGKVNVD EVGGEALGRLLVVYPWTQRF FESFGDLSTPDAVMGNPKVKAHGKKV LGAFSDGLAHLDNLGTFATLSELHCDKL HVDPENFRLLGNVLVCVLAHHFGKEFT PPVQAAYQKVVAGVANALAHKYH (subunit β)	$C_{724}H_{1119}O_{201}N_{195}S_3$ (β)	15857.24969 (β)

2.2.1 Materials

Angiotensin II, bombesin, bovine calmodulin (CaM), trypsin, ammonium acetate (CH_3COONH_4), and ammonium bicarbonate (NH_4HCO_3) were purchased from Sigma (St. Louis, MO). HPLC grade methanol, acetic acid (HAc), and acetonitrile (ACN) were obtained from Fisher Scientific (Pittsburgh, PA). Cisplatin was synthesized and characterized by standard methods.[179] Sequences of all the peptides and proteins are shown in Table 2.1.

2.2.2 Reaction of peptides with Cisplatin

Aqueous solutions of 1000 μM angiotensin II, 1000 μM bombesin, and 500 μM cisplatin were prepared and mixed to give 200 μL of an angiotensin II:bombesin:platinum complex solution at a molar concentration of 20 μM and a molar ratio of 1:1:3. The sample was incubated at 37 °C for 24 h, the pH value was determined before and after the reaction, both were 6. The sample was diluted to 0.4 μM with 50% MeOH–1% CH_3COOH buffer immediately before mass spectrometry analysis.

2.2.3 Reaction of Proteins with Cisplatin and Digestion of CaM–cisplatin Adducts

Five hundred micromolar aqueous solutions of CaM and 500 μM cisplatin were mixed and diluted with water to give a 200 μL (40 μM) solution of protein:platinum complex at a molar ratio of 1:1. The sample was incubated at 37 °C for 24 h, and then centrifuged using Amicon filters (MW cut off = 3 kDa, Millipore, Watford, UK) at 13000 rpm (14857 x g) for 30 min at room temperature, to remove unbound platinum complex, and

washed twice with 200 μL water. Samples were then diluted to 0.4 μM immediately before for MS analysis. Aqueous solutions of hemoglobin (500 μM) and cisplatin were reacted at a molar ratio of 1:5 and treated in the same manner as above.

The CaM–platinum adducts in the 1:1 CaM–cisplatin mixture were diluted to 20 μM with 50 mM NH_4HCO_3 (pH 7.8) and then subjected to trypsin digestion at a protein to enzyme ratio of 40:1 (w/w) at 37 °C for 4 h. As a control, 20 μM free CaM was digested under the same conditions. Immediately before ESI–MS analysis, the digest solution was diluted to 0.4 μM with 50% MeOH–1% CH_3COOH buffer.

2.2.4 FT ICR Mass Spectrometry

ESI–MS was performed on a Bruker SolariX FT ICR mass spectrometer with an ESI source and a 12T actively shielded magnet. Samples are electrosprayed at 0.4 μM concentration in 50:50 MeOH:H_2O with 1% acetic acid. For collisionally activated dissociation (CAD) experiments, the parent ions were isolated using the first quadrupole (Q1), and were fragmented in the collision cell (typical collision energies 10–25 eV), and then transmitted into the ICR cell for detection. For electron capture dissociation (ECD) experiments, the parent ions were isolated in Q1 and externally accumulated in collision cell for 3–10 s. After being transferred and trapped in the Infinity ICR cell,[180] ions were irradiated with 1.5 eV electrons from a 1.7 A heated hollow cathode dispenser for 50 to 80 ms. Full spectra were internally calibrated using peptide (bombesin or digested CaM) peaks, CAD spectra were internally calibrated using known b ion masses of bombesin or y ion masses of CaM(37–74), ECD

spectra were internally calibrated using known c ion masses of bombesin or c ion masses of CaM(107–126). The assigned mass tables for each spectrum are provided in Appendix I (Tables S1~S7).

2.3 Results

2.3.1 Intermolecular cross–linking of peptides

Angiotensin II and bombesin are small peptides both with potential histidine or methionine platinum binding sites; their amino acid sequences are shown in Table 2.1. Figure 2.1 (a) and (b) are the CAD spectra of angiotensin II–cisplatin and bombesin–cisplatin adducts, respectively. As shown in Figure 2.1a, the observation of the a_1 + Pt ion suggests that platinum binds to the carboxyl group of Asp1 of angiotensin II; in addition, the detection of y_4 + Pt and internal fragments YIH + Pt, YIH + Pt-CO-NH_3 indicates that Pt(II) also binds to His6 of angiotensin. Similarly, the observation of b_3 to b_{11} ions and b_{12} + Pt ions indicates that Pt(II) coordinates to His12 of bombesin, and the $[B + Pt - CH_3SH]^{3+}$ ion implies the binding of Pt(II) to Met14.[181] Therefore, these two peptides were chosen for the cross–linking studies.

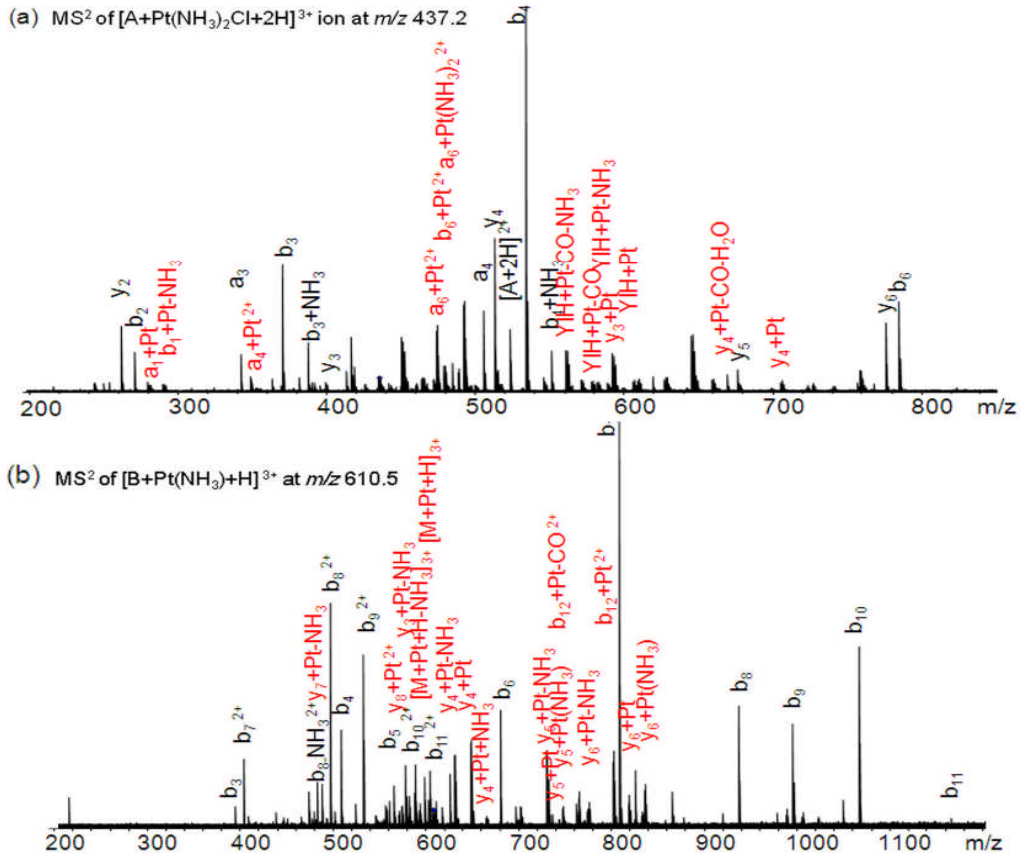

Figure 2.1 CAD spectra of peptides–Pt adducts (a) [A + $Pt(NH_3)_2Cl$ + $2H]^{3+}$ ion at *m/z* 437.2; (b) [B + $Pt(NH_3)$ + $H]^{3+}$ ion at *m/z* 610.5. Angiotensin II and bombesin are abbreviated as A and B, separately.

Platinum(II) is normally square planar with four covalent bonds. Depending on the type and number of nucleophiles available and steric accessibility of peptides or proteins, all the ligands of cisplatin can also be substituted by nucleophilic species.[125, 182, 183] Angiotensin II, bombesin, and cisplatin solution were mixed at a molar ratio of 1:1:3, incubated at 37 °C for 24 h, and diluted and subjected to MS analysis. As shown in Figure 2.2 a, in additional to the various peptide–Pt adducts, two multiply charged ions at *m/z* 719.8 (4+) and *m/z* 858.9 (4+) were detected (Figure 2.2 b).

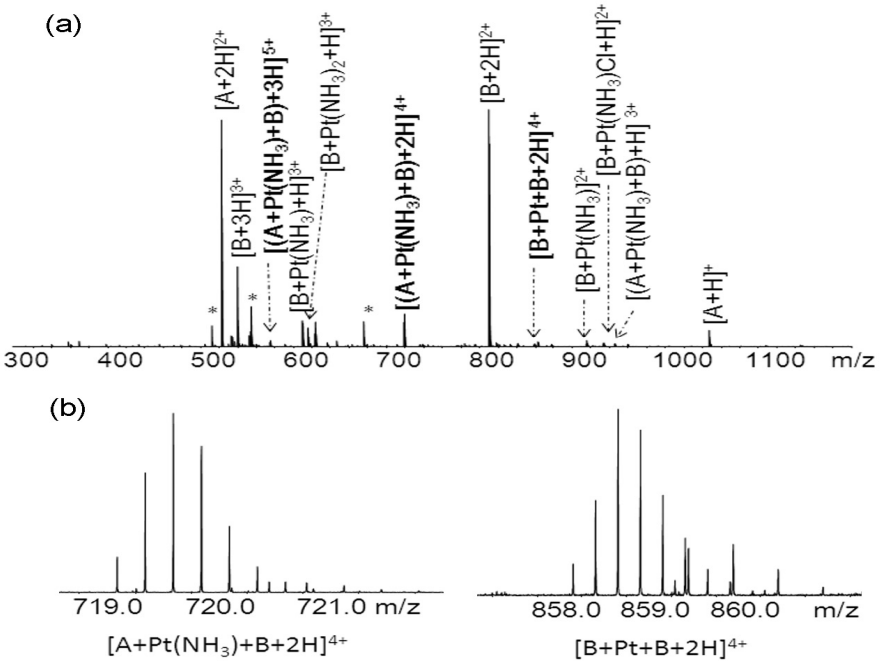

Figure 2.2 (a) Mass spectrum of angiotensin II–bombesin–cisplatin (1:1:3) mixture. (b) Isotopic distributions of the cross–linked products $[A + Pt(NH_3) + B + 2H]^{4+}$ and $[B + Pt + B + 2H]^{4+}$ ions. " * " represents chemical noise. Peaks are listed in Appendix I as Table A 2.1.

The m/z 719.8 (4+) value matches the mass of angiotensin II plus the mass of bombesin and plus $Pt(NH_3)$ (m/z 719.83924, -0.10 ppm), the m/z 858.9 (4+) value is consistent with the masses of two molecules of bombesin plus a Pt (m/z 858.90300, 0.17 ppm). To simplify the labeling of the mass spectrum of angiotensin–bombesin–cisplatin mixture, angiotensin and bombesin are abbreviated by their initials as A and B, respectively. The ions at m/z 719.8 and m/z 858.9 have isotopic distributions of that both match their theoretical isotopic distributions of $[A + Pt(NH_3) + B + 2H]^{4+}$ and $[B + Pt + B + 2H]^{4+}$ ions with mean absolute

deviation 0.37 ppm (Appendix I, Table A 2.1), which implies that platinum(II) can cross–link peptides intermolecularly.

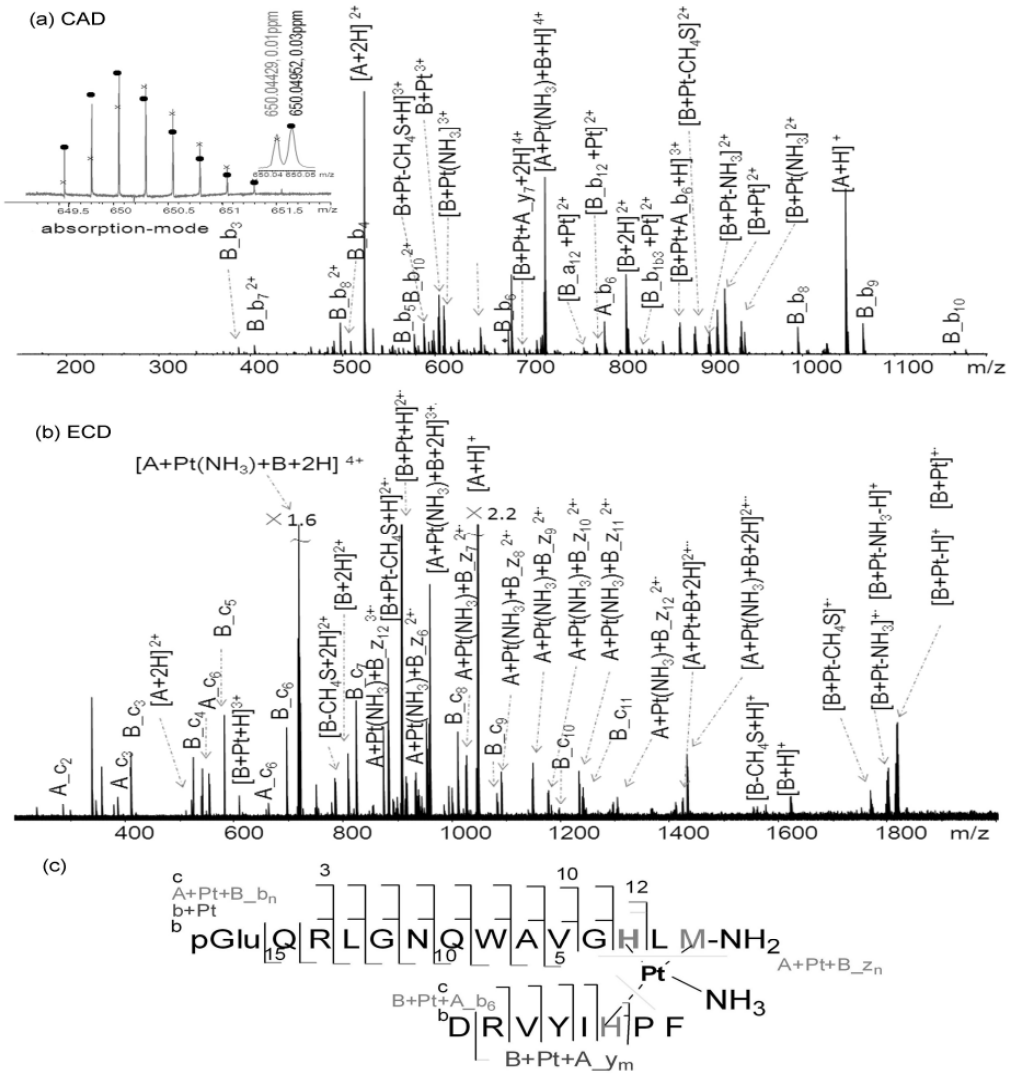

Figure 2.3 (a) CAD spectrum of the cross–linked product [A + $Pt(NH_3)$ + B + 2H] $^{4+}$ ion at *m/z* 719.34. The insert of Figure 2.3 a is the overlapping isotopic distributions of [A + Pt + B_b_{12} + 2H]$^{4+}$ (cross) and [B + Pt + A_b_6 + 2H]$^{4+}$ (circle) ions in absorption mode. (b) ECD spectrum [A + $Pt(NH_3)$ + B + 2H] $^{4+}$ ion at *m/z* 719.34. Peak results are listed in Appendix I (Table S 2.2 (CAD) and Table S 2.3 (ECD)). (c) Fragmentation diagram of the cross–linked product A + $Pt(NH_3)$ + B.

CAD and ECD experiments were both performed to locate the cross–linking sites. To label the sources of b/y and c/z ions, b/y and c/z ions from bombesin (B) are labeled as B_b_n, B_y_m, B_c_n, and B_z_m; similarly, b/y and c/z ions from angiotensin II (A) are labeled as A_b_n, A_y_m, A_c_n, and A_z_m. Figure 2.3 a shows the CAD spectrum of the $[A + Pt(NH_3) + B + 2H]^{4+}$ ion at *m/z* 719.8. Table A 2.2 in Appendix I shows the assignments of each product ion peak of $[A + Pt(NH_3) + B + 2H]^{4+}$ ion with mean absolute deviation 0.29 ppm, which yields high confidence in each product peak assignment. The detection of B_b_3 to B_b_{10} ions, $B_b_7^{2+}$ to $B_b_{11}^{2+}$ ions without platinum, and $(B_b_{12} + Pt)^{2+}$ to $(B_b_{13} + Pt)^{2+}$ ions indicates that platinum binds to His12. Also, ions at *m/z* 649.8 were found to have overlapping isotopic distributions of $[A + Pt + B_b_{12} + 2H]^{4+}$ ion and $[B + Pt + A_b_6 + 2H]^{4+}$ ion (insert of Figure 2.3 a), indicating that platinum cross–links His6 of angiotensin II and His12 of bombesin. The observation of $[B + Pt(NH_3) + A_y_7 + 2H]^{4+}$ also indicates that His6 rather than Asp1 of angiotensin II is primarily involved in the cross–linking. The mass spectrometry (MS) data ranging from *m/z* 649 to *m/z* 652 were processed with phase correction to yield the absorption mode spectrum which improves the peak shape and resolution as shown in the insert of Figure 2.3 a.[184] Platinum(II) has a total of four coordination sites; one amine (NH_3), His6 of angiotensin II and His12 of bombesin occupy three of the binding sites. Therefore, one more binding site needs to be assigned. The $[B + Pt–CH_4S]^{2+}$ ion peak was found with a deviation of -0.18 ppm (-0.16 mDa) from the calculated mass, suggesting that platinum binds to the sulfur of the Met14 of bombesin. Literature would suggest

that loss of CH_4S directly from MS/MS cleavage of the side chain of methionine is a minor fragmentation channel,[185] but it is possible that the presence of cisplatin has changed the local chemical environment to promote the reaction. In order to test whether the loss of CH_4S arises from the coordination of Met to platinum rather than direct loss of CH_4S from bombesin, different charge states of bombesin ions, the $[B + 2H]^{2+}$ ions and $[B + 3H]^{3+}$ ions were dissociated. No $[B + 2H\text{-}CH_4S]^{2+}$ ion was detected in either of the CAD spectra of the $[B + 2H]^{2+}$ ions or $[B + 3H]^{3+}$ ions (Figure A 2.1), which agrees with the hypothesis that platinum coordinates Met14(S) of bombesin (Figure 2.3 c).

Although ECD has been reported to be problematic on Pt–bound proteins,[146] an ECD experiment was still tested in an effort to further localize the cross–linking sites (Figure 2.3 b). The observation of B_c_3 to B_c_{11} ions, A_c_2 to A_c_5 ions, $A + Pt + B_z_5^{2+\cdot}$ to $A + Pt + B_z_{15}^{2+\cdot}$ ions, and the $[B - CH_4S + H]^+$ ion were all consistent with the CAD results, that is, Pt not only cross–links His6 of angiotensin II and His12 of bombesin, but also macrochelates His12 and Met14 of bombesin (Figure 2.3 c). The macrochelation of Pt with methionine (S) and histidine (N) (κ^2S_M, N_H) coordination result agrees with Gibson's and Hohage's results,[116,186] in which they showed that the macrochelates with κ^2S_M, N_H coordination modes are favorable in weakly acidic solutions ($3 \leq pH \leq 6$).

In the same sample, bombesin was also detected to cross–link with another bombesin molecule. Figure 2.4 a shows the CAD spectrum of the $[B + Pt + B + 2H]^{4+}$ ion at *m/z* 858.9. Similar diagnostic ions, like $[B_b_{12} + Pt]^{2+}$, $[B + Pt + B_b_{12}]^{2+}$, $[B + Pt + B_b_{13}]^{2+}$, and $[B + Pt - CH_4S]^{2+}$

ions, were detected, indicating that platinum cross–links two bombesin molecules by binding to the His and Met residues of bombesin.

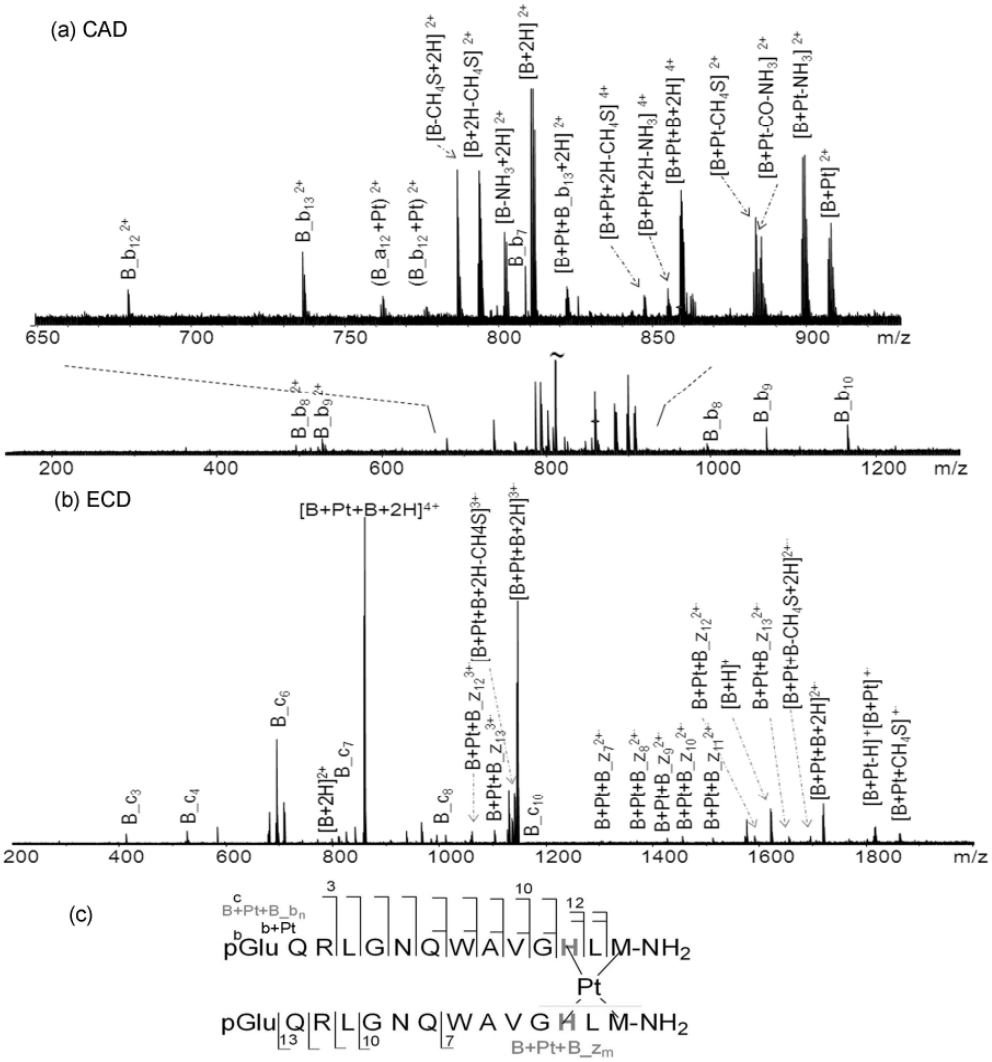

Figure 2.4 (a) CAD spectrum of the cross–linked product [B + Pt + B + 2H]$^{4+}$ ion at *m/z* 858.91, the insert shows the zoom spectrum from *m/z* 650 to *m/z* 950. (b) ECD spectrum of the cross–linked product [B + Pt + B + 2H]$^{4+}$ ion at *m/z* 858.9. Peak results are listed in appendix I as Table A 2.4 (CAD) and S 2.5 (ECD). (c) Fragmentation diagram of the cross–linked product B + Pt + B.

The ECD results are also in agreement with the CAD data, as

shown in Figure 2.4 b; the observation of B_c_3 ions to B_c_{11} ions indicates that His12 and /or Met14 are the binding sites. As platinum cross–links two peptides with the same sequence, B_c_3 ions to B_c_{11} ions can be generated from either chain, namely, the cross–linking sites are localized at His12 and Met14 sites of each chain. Compared to the CAD and ECD spectra of the $[A + Pt(NH_3) + B + 2H]^{4+}$ ion, many fewer peaks were observed in the CAD and ECD spectra of the $[B + Pt + B + 2H]^{4+}$ ion (peak lists are available in Appendix I as Table A 2.4 and Table A 2.5), which is likely to be due to the symmetric structure after platinum binding, as shown in Figure 2.4 c.

2.3.2 Intramolecular cross–linking of Calmodulin

Calmodulin (CaM) is a small 16.8 kDa acidic protein, containing 9 Met residues out of 148 amino acid residues (Table 2.1). The Met residues in CaM play an important role in its versatility, and contribute as much as 46% of the exposed surface area of the hydrophobic patches on the calmodulin surface,[187] which makes CaM an interesting target for this cross–linking study. CaM and cisplatin were incubated in a 1:1 mixture at 37 °C in water for 24 hours, and then subjected to trypsin digestion at a CaM–cisplatin to enzyme ratio of 40:1 (w/w) at 37 °C for 4 h followed by ESI–FTMS analysis. In addition to the peaks which correlate with Pt binding to the tryptic digested peptides, a peak corresponding to the platinum cross–linked tryptic digest peptides CaM(107–126) and CaM(127–148) was observed at *m/z* 1018 (5+) with a mass error of -0.08 ppm, as shown in Figure 2.5 a, which is overlapped with the 4+ charge state CaM(38–74) ion.

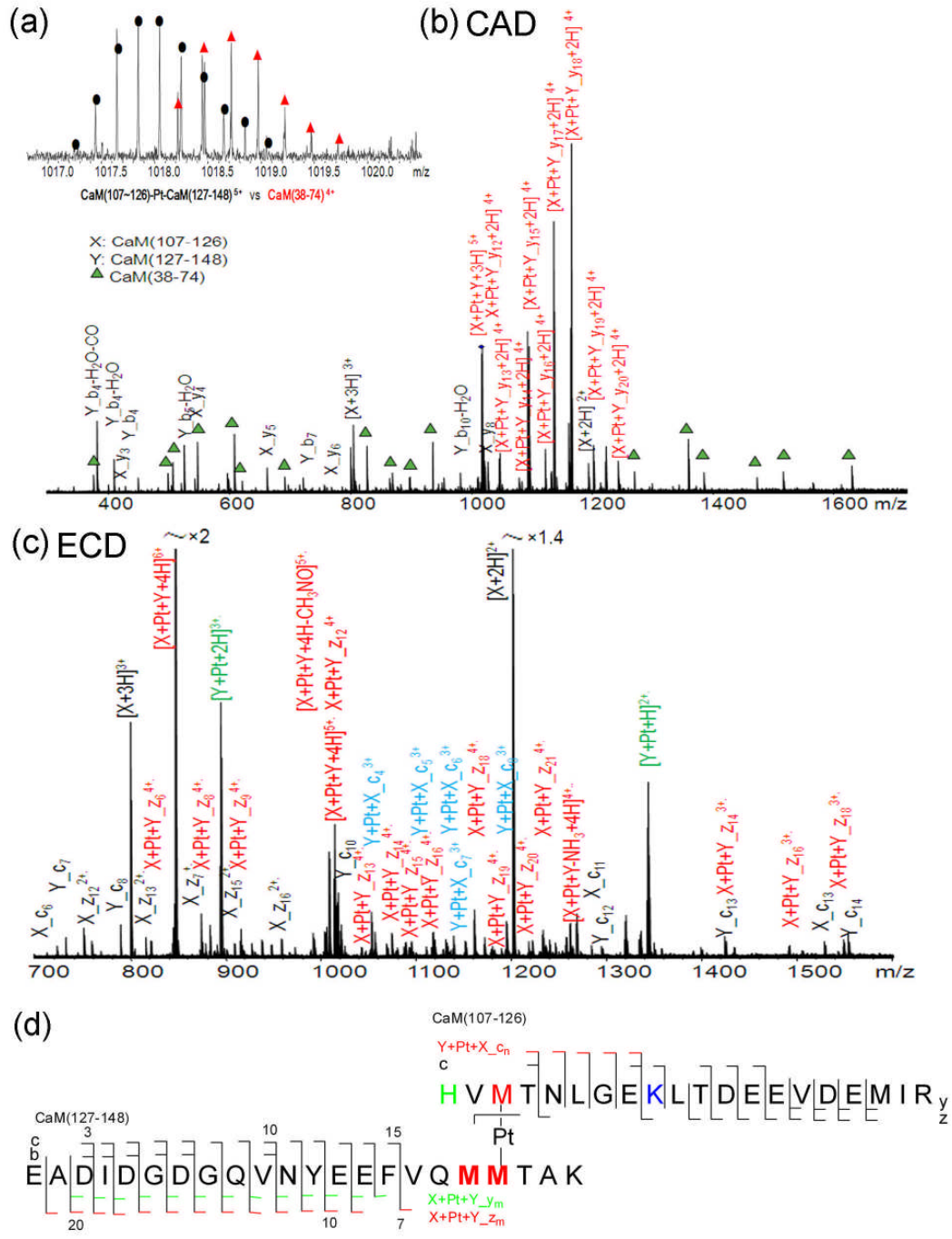

Figure 2.5 (a) Cross–linked product spectrum from the digested CaM–cisplatin (1:1) mixture. The isotopic distribution of the cross–linking product CaM(107–126) + Pt + CaM(127–148)$^{5+}$ ion (circles) is overlapped with the digested peptide CaM(38–74)$^{4+}$ ion (triangles). (b) CAD spectrum of the cross–linked product CaM(107–126) + Pt + CaM(127–148)$^{5+}$ ion at *m/z* 1018. (c) ECD spectrum of the cross–linked product CaM(107–126) +

Pt + CaM(127–148)$^{6+}$ ion at *m/z* 848. (d) Fragmentation diagram of the cross–linked product CaM(107~126)+ Pt + CaM(127–148). For the full peak list, see Table A 2.6 (CAD) and Table A 2.7 (ECD) in Appendix I.

Figure 2.5 a shows the two overlapped experimental isotopic distributions and the theoretical isotopic distributions (circles and triangles), clearly demonstrating the resolving power of the FTICR MS instrument used. Despite the fact that CaM(107–126) and CaM(127–148) are contiguous tryptic peptides within native calmodulin, these are not missed tryptic cleavages as shown in the MS/MS experiment discussed below. The [CaM(107–126) + Pt + CaM(127–148) + 3H]$^{5+}$ ion was isolated by the front-end quadrupole with an isolation window of ± 5 Da and then fragmented in the collision cell. Therefore, because of the overlap, the [CaM(38–74) + 2H]$^{4+}$ ion was also isolated and fragmented at the same time. To simplify the labeling of the product ion spectrum of the [CaM(107–126) + Pt + CaM(127–148) + 3H]$^{5+}$ ion (Figure 2.5), CaM(107–126), CaM(127–148) and CaM(38–74) are assigned as X ,Y, and Z, respectively. The observation of X_y_3 to X_y_6 ions from CaM(107–126) and Y_b_3 - H_2O to Y_b_7 - H_2O ions from CaM(127–148) show that the linkage between CaM126 and CaM127 has been cleaved during trypsin digestion, which proves the existence of cross–linking rather than platinum binding to a missed cleavage peptide and a dehydrated CaM(107–148) species. A series of [X + Pt + Y_y_{12} + 2H]$^{4+}$ to [X + Pt + Y_y_{20} + 2H]$^{4+}$ ions, further confirms that these two peptides are cross–linked by platinum, and also suggests that platinum binds to the C–

terminal Met144 or Met145 residue of CaM(127–148). In addition, the detection of a series of X_y_3 to X_y_8 ions indicates that platinum coordinates to the N–terminal Met109 site (Figure 3d). ECD experiments were performed on both the [CaM(107–126) + Pt + CaM(127–148) + 3H]$^{5+}$ ion and the [CaM(107–126) + Pt + CaM(127–148) + 4H]$^{6+}$ ion, the ECD spectrum of the [CaM(107–126) + Pt + CaM(127–148) + 4H]$^{6+}$ ion at *m/z* 848 were chosen and shown in Figure 2.5 c. The observation of Y_c_3 to Y_c_{14} ions, X + Pt + Y_z_6 ion, and X + Pt + Y_z_8 to X + Pt + Y_z_{21} ions all indicates that platinum coordinates to either/both Met144 and Met145 sites, rather than carboxyl groups (D or E) in the CaM(127–148) chain. Similarly, the detection of the Y + Pt + X_c_4 to Y + Pt + X_c_8 ion series correlates with the CAD result, that platinum binds to the Met109 site of CaM(107–126). It is generally accepted that ECD fragmentation preserves labile modification sites;[93] however, the observation of single chain ions like [X + 2H]$^{2+}$ and [X + 3H]$^{3+}$ ions (Figure 2.5 c), [A + H]$^{+}$ and [B + 2H]$^{2+}$ ions (Figure 2.3 b & Figure 2.4 b) implies that ECD may fragment the labile modification sites (Pt–N or Pt–S) in this specific Pt–bound peptide. Therefore, the origin of X_c_4 to X_c_{13} ions can either be from the cross–linked precursor ions or it can, more likely, originate from the [X + 2H]$^{2+}$ or [X + 3H]$^{3+}$ ions by secondary electron capture rather than from the precursor ions. As shown in Figure 2.5 c, for the X (CaM(107–126)) chain, intense [X + 2H]$^{2+}$ and [X + 3H]$^{3+}$ peaks were observed; for the Y (CaM(127–148)) chain, platinum-bound peaks [Y + Pt + 2H]$^{3+\cdot}$ and [Y + Pt + H]$^{2+\cdot}$ were detected, and no single Y chain ions or Y_c/z ions at the platinum bound region appeared, all these results

support the hypothesis that the X_c_4 to X_c_{13} ions were generated by secondary electron capture. Furthermore, the detection of $[X + 2H]^{2+}$, $[X + 3H]^{3+}$, $[Y + Pt + 2H]^{3+\cdot}$, and $[Y + Pt + H]^{2+\cdot}$ ions indicates that the Pt–Y chain is more strongly bound than the X–Pt chain under ECD conditions. Therefore, it is likely that platinum coordinates to the Met109 of CaM(107–126) and Met144 or Met145 of CaM(127–148) by forming stable six–membered κ^2S_M, N_M chelates on the respective residues. [188, 189]

An interesting phenomenon of cisplatin cross–links in calmodulin is that all the ligands of cisplatin are displaced, which rarely happens in cisplatin–DNA adducts.[111, 127] Similar results have also been observed in other Met–rich peptides or proteins upon reaction with cisplatin due to the trans–labilization effect. [125, 182, 183] In other words, once the displacement of chlorine by sulfur of Met or Cys residue has occurred, the Pt–NH_3 bond trans to the sulfur is significantly labilized and thus the amine group is readily substituted.

2.3.3 Intermolecular cross–linking of protein

Hemoglobin is a tetrameric heme–protein in the red cells of the blood in mammals and other animals; it contains two alpha and two beta subunits non–covalently bound, designated as $\alpha_2\beta_2$. Each subunit has multiple potential platinum binding sites, as listed in Table 2.1, the α unit has two Met, ten His, and one Cys residue; the β unit has one Met, nine His and two Cys residues. Since hemoglobin is a well understood and easy to obtain protein, it was therefore of interest to investigate whether cisplatin can cross–link α and β subunits. Although the study of cisplatin–

hemoglobin has been reported,[190] whether cisplain can cross–link hemoglobin complex subunits has not been explored.

Abundant α and β peaks along with peaks corresponding to platinum bound to either α or β subunits were detected (Figure A 2.2); however, no peaks corresponding to cisplatin cross–linking between the α and β subunits were detected.

2.4 Discussion

The cross–linking sites were identified and localized by FTICR MS because of its unsurpassed resolution and mass accuracy, and also its ability to extensively fragment large peptides by CAD and ECD fragmentation techniques. Sub–ppm mass accuracy is routinely achieved by SolariX FTICR MS (Tables S 2.1 to S 2.7) which is critical for the assignment of all the peaks as the number of peptides with the same nominal mass but different amino acid sequence increases dramatically with the number of amino acid residues in the peptides.[133] In the case of the overlapping peaks $[A + Pt + B_b_{12} + 2H]^{4+}$ at *m/z* 650.04429 and $[B + Pt + A_b_6 + 2H]^{4+}$ at *m/z* 650.04952 (the insert of Figure 2.3 a), the mass difference between these two peaks is only 5.2 mDa; therefore, the high resolution (R=200,000) and mass accuracy (0.03 ppm) of this spectrum greatly aid the assignments of these two peaks. More importantly, the assignment of these two peaks is critical for localizing the cross–linking sites.

Although the above experiments and CAD and ECD data all show that cisplatin has the potential to be a peptide and protein cross–linker, in

the development of a cross–linker, there are multiple characteristics that should be considered, such as chemical specificity, arm length, water solubility and cell membrane permeability, homobifunctional or heterobifunctional reactive groups, and cleavability.[7] In light of these considerations, the potential for cisplatin as a cross–linker is discussed below.

2.4.1 Chemical specificity

Although there are 20 different amino acids in protein structures, only a small number of protein functional groups comprise selectable targets for practical cross–linking studies. In practice, only four protein functional groups (primary amines, carboxylates, sulfhydryls, and carbonyls) account for the vast majority of cross–linking and chemical modification sites. However, there are up to nine amino acids in proteins that are readily derivatizable at their side chains, including aspartic acid, glutamic acid, lysine, arginine, cysteine, histidine, tyrosine, methionine, and tryptophan. These nine residues contain eight principal functional groups, in addition to primary amines, carboxylates, and sulfhydryls (or disulfides), thioethers, imidazoles, guanidinyl groups, phenolic and indolyl rings also have sufficient reactivity for modification reactions.[7]

Platinum(II) has a strong affinity for sulfur and nitrogen containing ligands, such as methionine, cysteine, and histidine. As shown by the data obtained here, platinum can coordinate to both histidine and methionine, providing new functional groups for cross–linking. The discovery of new cross–linkers targeting new reactive groups will facilitate the analysis of the three–dimensional structures of proteins and the

identification of interaction partners. Lysine residues are the most commonly targeted cross–linking groups, and are often located on the surface of proteins. Hence lysine cross–linking usually provides surface information on proteins. Unlike cross–linking reagents which only target hydrophilic groups, cisplatin also targets the hydrophobic residue methionine (Met). Met residues are often located in the interior of proteins; therefore, targeting Met residues potentially provides information on the core of protein complexes.

Moreover, new cross–linkers can help to overcome the inherent problems of existing reactive groups, such as primary amines.[156] Although the primary amine is by far the most commonly targeted functional group, there are several limitations. First, cross–linkers react with primary amine groups of lysine residues and the N–terminus of proteins, and trypsin cannot normally cleave C–terminal to a modified lysine residue; therefore, larger peptides are generated from such cross–linked proteins during enzymatic proteolysis due to missed cleavages. Platinum reacts with histidine, methionine, and cysteine, which can easily overcome this problem. Second, the modification of the amine group of lysine residues leads to a loss of a positively charged site. Thus, digested cross–linked peptide ions with lower charge states are created during electrospray ionization, reducing sensitivity and MS/MS performance.

2.4.2 Compatibility with Mass Spectrometry analysis

2.4.2.1 Inherent two positive charges of Pt(II)

On one hand, platinum does not result in charge loss; on the other

hand, platinum inherently has two positive charges, e.g. when the fragment $\{Pt(NH_3)_2\}^{2+}$ binds, the cross–linking products observed often have higher charge states than the peptides or proteins alone. Higher charge states not only promote the detection of cross–linking products without purification, but also result in a more comprehensive MS/MS fragmentation pattern and therefore assist in the identification of modification sites.

2.4.2.2 Unique isotopic pattern

Challenges to identify cross–linked products by mass spectrometry have arisen due to the complexity of the cross–linking reaction mixtures and low abundance of the cross–linked species. As presented in Figure 2.1, predominantly unmodified peptides, dead–end modified peptides, and a low abundance of inter–cross–linked peptides were detected. To overcome the challenges, significant effort has been made to develop new cross–linkers to facilitate the identification of cross–linked species by introducing a signature pattern in the data via isotope–labeling, such as isotope labeling the cross–linking reagents or proteins,[163-165] proteolytic digestion in ^{18}O labeling water,[162] or by enriching cross–linked products, such as affinity tags.[159-162] In many cross–linking applications, isotope labeling has greatly facilitated the identification of cross–linked products. However, frequently, isotope labeling complicates the mass spectra of products, increases the possibility of peak overlap, and lowers the possibility of cross–linked products being detected by mass spectrometry due to ion suppression effects. In addition, incomplete labeling, for example due to partial label ^{18}O exchange in proteolytic digestion

samples, distorts the natural isotopic distribution.[191] Platinum has advantages over isotope labeling because it has a normalized unique isotopic distribution (^{194}Pt (97.41%), ^{195}Pt (100%); ^{196}Pt (74.58%)), which allows for easy visual identification of cross–linked products in a spectrum without significantly complicating the spectrum or the need for intricate labeling procedures.[140] As presented in Figure 3a, the Pt–bound peptide complex has a broader and more abundant isotopic distribution compared to unlabeled peptides in the same *m/z* region (CaM(38–74)).

2.4.3 Homobifunctional or heterobifunctional reactive groups

Homobifunctional cross–linking reagents contain the same functionality at both ends; heterobifunctional cross–linkers have two different reactive groups that target different functional groups. Cisplatin has four coordinated ligands; the chloride ligands are likely to be the first leaving groups to be replaced in reaction with proteins; depending on the type and number of coordination sites available and steric accessibility, the ammine ligand(s) can also be replaced. In particular, as shown above, sulfur ligands have high *trans*–effects and can labilize *trans* NH_3 ligands, especially at a low pH value. As cisplatin can bind to Met (S), His (N), Cys (S), or carboxyl (O) groups, it gives cisplatin the flexibility to be a homobifunctional, or heterobifunctional (or even heterotetrafunctional) cross–linking reagent. However, as with other homobifunctional reagents, there is the potential for creating a wide range of non–cross linked products.

2.4.4 Spacer arm length

Cross–linkers are selected not only based on their chemical

specificities and reactivities but also their arm–lengths. The spacer arm length of the cross–linker can provide an estimate of the distance between two linked groups. In the example of cisplatin cross–linking calmodulin, the spatial distances between the thioether sulfurs of Met109, Met124, Met144 and Met145 were based on the NMR structure of apo–calmodulin, (Figure 2.6, the S atom of Met145 was chosen as the center, only amino acid residues within 8 Å are shown), and range from 4.50 Å to 11.31 Å. Based on the literature for small platinum compounds,[192] the average Pt–S bond length is 2.318 Å; thus the maximum spacer arm length of S–Pt–S is around 4.63 Å, which fits the spatial distance between Met109 and Met145 (4.54 Å). Therefore, it is likely platinum can readily *trans*–cross–link Met109 and Met145.

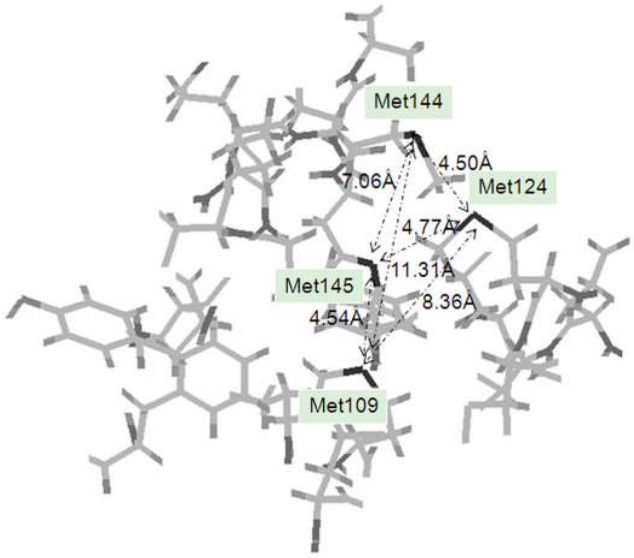

Figure 2.6 Spatial distances between the thioether sulfurs of Met109, Met124, Met144 and Met145 of apo–calmodulin (1DMO). The S atom of Met145 is chosen as the center, only amino acid residues within 8 Å are shown. The thioether sulfurs of methionine residues are labeled in black. The distances indicate by double arrows between the thioether sulfurs of

Met109, Met124, Met144 and Met145 range from 4.5 Å to 11.3 Å.

Thus, that cisplatin fails to cross–link hemoglobin subunits is a bit surprising, because according to the crystal structure of hemoglobin complex(PDB–2DN2), the distance between His122 (α)–Cys112 (β) (4.10 Å) is within platinum cross–link range.[193] Possible reasons may have to do with the steric accessibility or the chemistry of cisplatin cross–linking reactions. For example, the *trans*–labilization effect may play an important role in Pt cross–linking. Studies by Kasherman *et al*. showed that thiols (Cys) and thioethers (Met) bind to Pt(II) at similar rates, but thioethers are significantly more efficient than thiols at labilizing the amine at lower pH,[122] which might contribute to the unsuccessful Pt cross–linking of hemoglobin. Therefore, further research is still needed to explore the chemistry of cisplatin binding with proteins.

2.4.5 Cleavability

Cleavability is important in studies involving the bio–specific interactions between two molecules, which allow the verification of the cross–linking reactions through identification of the cross–linked sites. Cross–linkers can be cleaved either by chemical reactions or MS/MS fragmentation. The CAD and ECD spectra of all the Pt cross–linking products studied here have shown the cleavability of Pt–S or Pt–N bonds, which provides information on the modification sites. The effective CAD cleavability of platinum improves the information content in protein structure analysis and localization of the cross–linking sites.

2.5 Conclusions

This work effectively demonstrates the potential of cisplatin as a cross–linking reagent. The cross–linking sites were unambiguously assigned by use of high resolution FTICR MS data with sub–ppm mass accuracy; subsequent CAD and ECD FTICR MS data allowed the localization of the cross–linked sites on proteins. Cisplatin is a widely used clinical anticancer drug; it is water soluble (8 mM) and is able to penetrate membranes. Features of cisplatin, such as cross–linking DNA–DNA, DNA–protein, targeting new protein functional groups (thioether and imidazole groups), its unique isotopic pattern, and inherent two positive charges of platinum(II) make it a promising tool for cross–linking experiments in protein studies of more complicated biological systems by high resolution mass spectrometry in the future. However, the *trans*–labilizaiton effect of cisplatin and the binding of cisplatin to Cys (S) or carboxyl (O) group can complicate cross–linking results. Therefore, further efforts will have to be made in synthesizing novel cross–linkers, such as multinuclear platinum complexes, in order to understand better the chemistry of Pt cross–linking reactions.

Chapter 3

Use of Top-down and Bottom-up Fourier Transform Ion Cyclotron Resonance Mass Spectrometry for Mapping Calmodulin Sites Modified by Platinum Anticancer Drugs[2]

3.1 Introduction

Sulfur–containing biomolecules play significant roles in platinum anticancer chemotherapy because of their high affinity for platinum compounds. Studies of cisplatin drug resistance have demonstrated that a failure of a sufficient quantity of platinum to reach the target DNA can lead to resistance.[115, 123, 194, 195] Further evidence showed that increased levels of cytoplasmic sulfur–rich species, such as glutathione and metallothioneins, causes cisplatin drug resistance and leads to detoxification because platinum binds irreversibly to thiolate sulfur.[124-128]

3.1.1 Calmodulin (CaM)

CaM is a ubiquitous, calcium (Ca^{2+})–binding protein that senses changes in intracellular calcium levels to coordinate the activity of over thirty different target proteins in eukaryotic cells.[196] CaM is expressed in many cell types and can have different subcellular locations, including the cytoplasm, within organelles, or associated with the plasma or organelle membranes. CaM is a methionine–rich protein, with 9 methionine residues out of 148 amino acid residues. Upon calcium activation,

---

[2] This chapter has been partially/entirely reproduced from
Huilin Li, Tzu-Yung Lin, Steve L. Van Orden, Yao Zhao, Mark P. Barrow, Ana M. Pizarro, Yulin Qi, Peter J. Sadler, Peter B. O'Connor. Use of top-down and bottom-up Fourier transform ion cyclotron resonance mass spectrometry for mapping calmodulin sites modified by platinum anticancer drugs. *Anal. Chem.,* **2011**, 83, 9507-9515. Copyright 2011, American Chemical Society.

methionine–rich binding pockets are exposed in each of the opposing globular domains of CaM.[197] These hydrophobic binding sites facilitate CaM association with reorganizations and promote activation of a diversity of conformations depending on the target.[198] In fact Met residues contribute as much as 46% of the exposed surface area of the hydrophobic patches on the CaM surface,[199] which makes them likely targets for platinum drugs. Oxidation of methionine residues of CaM has been shown to decrease the ability of CaM to activate target enzymes.[200-204] Recent studies have suggested that cisplatin can bind strongly to CaM by forming Pt–S bonds with Met residues, which can cause inhibition of calmodulin's capacity to activate target proteins. For example, inhibition of Ca^{2+}–CaM due to direct interactions with cisplatin could play a major role in stomach distention.[205] In addition, CaM is also rich in aspartic acid (Asp) and glutamic acid (Glu) residues, nearly half of which are involved in calcium binding, and in total, one third of the CaM sequence corresponds to the potential Pt–binding sites. Thus, in view of the current widespread chemical use of platinum anticancer drugs, and the need to elucidate their mechanism of activity and their side–effects, it is of interest to investigate the interactions between CaM and cisplatin analogs more closely.

3.1.2 Top–down and bottom–up mass spectrometric techniques

Mass spectrometry is an extremely powerful tool to study the interactions of drugs with proteins, due to its advantage of sensitivity and the ability to provide direct sequence–specific information on the position and the form of the drug–protein adducts.[206] Reactions between proteins

(transferrin, cyctochrome C, ubiquitin, insulin, superoxide dismutase *etc.*) and metallodrugs have been previously studied by electrospray ionization mass spectrometry (ESI MS).[116, 134, 137, 141, 146, 181, 207] Recent progress with combination of mass spectrometry and proteomics technologies has made the identification of binding sites much more feasible. There are basically two classes of methods to achieve this, "bottom–up" (peptide level) and "top–down" (intact protein level) approaches.[93]

"Bottom–up" strategies involve cleaving the protein into peptide fragments using proteolytic enzymes prior to mass spectrometry detection. By applying the bottom–up mass spectrometric approach, Allardyce *et al*. identified that cisplatin binds to threonine 457 of transferrin.[134] However, as only some tryptic peptides are normally detected, it is possible that other cisplatin modification sites on transferrin have been missed, particularly because there are multiple potential cisplatin binding sites (44 Asp, 19 His, 8 Met, and 42 Glu residues) on transferrin.

"Top–down" methods identify proteins by measuring the mass of the whole protein, then using tandem mass spectrometry (such as collisionally activated dissociation (CAD), electron capture dissociation (ECD), or infrared multiphoton dissociation (IRMPD)) to fragment intact proteins in order to generate sequence information, so that all modifications are normally detected. Recently, Moreno–Gordaliza *et al*. were able to determine the binding sites between cisplatin and insulin by combining the top–down approach with nano–electrospray ionization mass spectrometry using a linear ion trap.[141]

The combination of Fourier transform ion cyclotron resonance mass

spectrometry (FTICR MS) with top–down and bottom–up proteomic approaches generate effective binding site information; Hartinger *et al*. identified the binding sites of three different platinum anticancer drugs with ubiquitin by top–down high resolution MS approach.[146]

Top–down analysis of proteins by ECD has developed rapidly in recent years.[33, 35, 57, 88, 100] ECD cleaves N–C_α bonds to produce mainly c and $z^\bullet$ ions, complementary to b and y ions produced in CAD by cleaving CO–NH bonds.[57] The combination of ECD and CAD has greatly improved the efficiency and sequence coverage in top–down protein analyses. However, in previous reports, the application of ECD in protein–platinum or peptide–platinum complexes for characterizing platinum binding sites is rather limited.[146, 148] Previously, ECD has been successfully applied to cisplatin cross–linked peptides and protein–CaM by Li *et al*.[208] Here, the top–down ECD mass spectrometric approach is extended to map the binding sites for platinum anti–cancer drugs on CaM.

Cisplatin and its analogues are widely used in clinical cancer treatments. The mechanisms for transport of platinum anticancer drugs through cell membranes and possible intermediate formed by binding to proteins remain poorly understood, although they may contribute to many of the drugs' side–effects.[209] The objective of this Chapter is to gain insights into the reactivity of various platinum complexes with CaM and to map the binding sites by using top–down and bottom–up high resolution MS approaches. Here, the application of top–down ECD mass spectrometry for mapping the binding sites of the platinum anticancer complexes cisplatin (Pt_1), [Pt(dien)Cl]Cl (Pt_2) and [{*cis*–

$PtCl_2(NH_3)\}_2(\mu–NH_2(CH_2)_4NH_2)]$ (Pt_3) to CaM is demonstrated.

3.2 Experimental section

3.2.1 Materials

Bovine calmodulin, trypsin (TPCK treated from bovine pancreas), ammonium acetate (CH_3COONH_4), and ammonium bicarbonate (NH_4HCO_3) were purchased from Sigma (St. Louis, MO, USA). HPLC grade methanol, acetic acid (HAc), and acetonitrile (ACN) were obtained from Fisher Scientific (Pittsburgh, PA, USA). Cisplatin (Pt_1), [(PtCl(dien))Cl] (Pt_2), and [{*cis*–$PtCl_2(NH_3)\}_2(\mu–NH_2(CH_2)_4NH_2)$] (Pt_3) were synthesized and characterized by standard methods.[179, 210, 211] The structures of compounds Pt_1, Pt_2, and Pt_3 are shown in Figure 3.1.

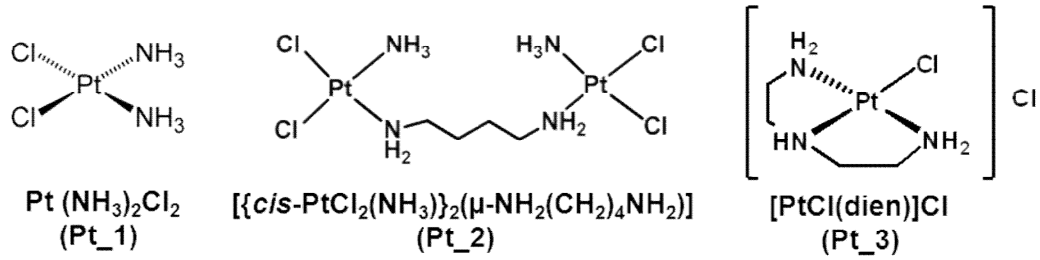

Figure 3.1 Chemical structures of Pt–complexes (Pt_1, Pt_2, and Pt_3)

3.2.2 Reaction of CaM with Pt_1, Pt_2, and Pt_3

Aqueous solutions of CaM (500 μM) and platinum complex (Pt_1, Pt_2, and Pt_3, 500 μM each) were prepared and mixed to give 200 μL (40 μM) solutions of protein:platinum complex at molar ratios of 1:1, 1:2, and 1:8. The samples were incubated at 37 °C for 24 h. To remove free platinum complexes and desalt, amicon filters (MW cut off = 3 kDa,

Millipore, Watford, UK) were used at 13000 rpm for 30 min at room temperature, and washed twice with 200 µL water. The sample was diluted to 0.4 µM with 50% MeOH–1% CH_3COOH buffer immediately before mass spectrometry analysis.

3.2.3 Protein Digestion

The CaM–platinum adducts in the 1:1, 1:2, and 1:8 molar ratios of CaM:Pt_1 or CaM:Pt_2 mixtures were diluted to 20 µM with 50 mM NH_4HCO_3 (pH 7.8) and then subjected to trypsin digestion at a protein to enzyme ratio of 40:1 (w/w) at 37 °C for 4 h. As a control, 20 µM CaM without platinum reagents was digested under the same conditions. The sample was diluted to 0.4 µM with 50% MeOH–1% CH_3COOH buffer immediately before mass spectrometry analysis.

3.2.4 FTICR Mass Spectrometry

ESI–MS was performed on a Bruker solariX FTICR mass spectrometer with an ESI source and a 12 T actively shielded magnet. Samples were electrosprayed at a flow rate of ~300 µL/hour at a concentration of 0.4 µM in 50:50 MeOH:H_2O with 1% acetic acid. For ECD experiments, the parent ions were first isolated in the first quadrupole (Q1) and externally accumulated in the collision cell for 2–20 s. After being transferred to the Infinity cell,[180] ions were irradiated with 1.5 eV electrons from a 1.7 A heated hollow cathode dispenser for 10 to 100 ms.[78] A one millisecond single frequency shot at *m/z* 100 was given at the beginning of the ECD event to improve the overlap between electron beam and the trapped ions.[82, 83] Full spectra were internally calibrated using the unmodified c-ion series of CaM.

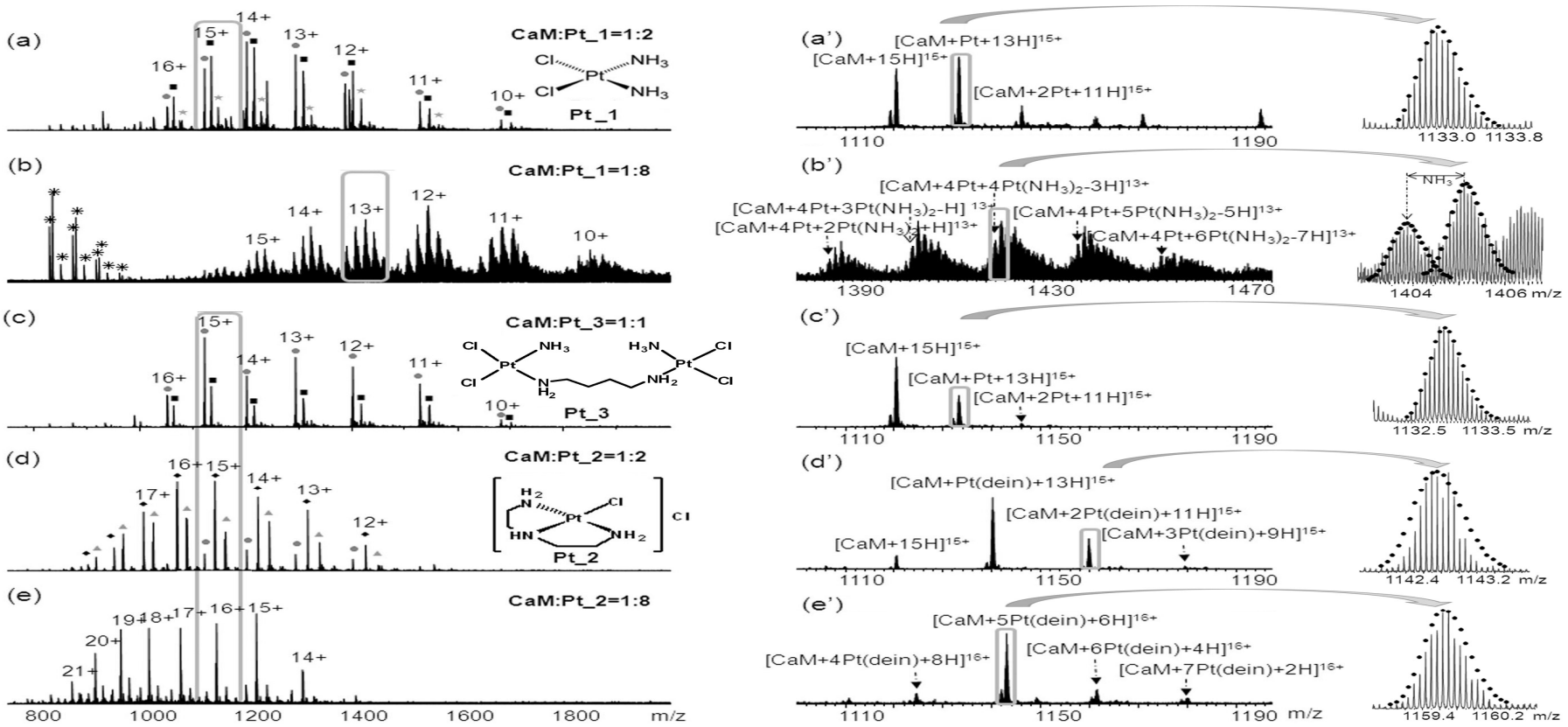

Figure 3.2 ESI–FTICR MS analyses of reaction mixtures of platinum complexes with CaM at different molar ratios. (a) CaM:Pt_1 (1:2); (b) CaM:Pt_1 (1:8); (c) CaM:Pt_3 (1:1); (d) CaM:Pt_2 (1:2); (e) CaM:Pt_2 (1:8). Figures 1a'–1e' are expansions of the corresponding parts in Figures 1a–1e. The structures of Pt(II) complexes are inserted in Figure 3.2 a, c, and d. "*" Represents chemical noise; ● CaM; ■ CaM+Pt; ★CaM+2Pt; ◆ CaM+Pt(dien), and▲CaM+2Pt(dien).

3.3 Results and discussion

3.3.1 FTICR MS Analyses of the interaction of platinum anti–cancer drugs with CaM

Figures 3.2 a–e show the mass spectra of CaM upon reaction with Pt_1, Pt_2 and the dinuclear platinum compound Pt_3 at different molar ratios. At a lower molar ratio (1:2) of CaM:Pt_1, up to two platinum molecules coordinate to CaM with all cisplatin ligands (NH_3 and Cl) displaced in CaM–Pt_1 mixtures (Figure 3.2 a&a'); increasing the molar ratio of platinum complexes in the mixtures leads to more platinum complexes coordinating to CaM (Figure 3.2 b). Taking the 13+ charge states of CaM–Pt_1 complexes (Figure 3.2 b') for example, five different groups of CaM–Pt_1 complexes were detected, varying from six up to ten cisplatin complexes bound to CaM in a variety of forms. The isotopic patterns of the $[CaM + 4Pt + nPt(NH_3)_2 + H]^{13+}$ (n=2~6) ions were compared with the theoretical isotopic patterns, which fit with mean absolute deviation within 1.5 ppm range (see the inserts of Figure 3.2 b' and Table B.1).

As previously observed, cisplatin preferentially binds to Met sites of CaM with all four cisplatin ligands displaced in low molar ratios of cisplatin–CaM mixtures;[208] herein, the maintenance of ligands, such as NH_3, indicates that cisplatin might also bind to His, Asp or Glu residues in CaM sequence when increasing the concentration of cisplatin in the cisplatin–CaM mixture. In addition, all the modified peaks shift to higher *m/z* region, namely, lower charge states, which supports the assumption

that cisplatin binds to the carboxyl groups of Asp or Glu residues because deprotonation of a carboxyl group is needed before it binds to platinum(II). Therefore, the two positive charges of platinum(II) are neutralized upon platinum coordinating to two carboxyl groups. In addition, the shifting of modified peaks to lower *m/z* region might indicate that the excessive binding of cisplatin to CaM has charged the conformation of CaM.

Similar phenomena were observed in CaM–Pt_3 mixtures (Figure 3.2 c&c'), where the bridge linking the two platinum molecules is broken and all the ligands are replaced. To address the questions as to whether the loss of all the ligands and the breakage of the bridge of Pt_3 are due to the reaction of platinum complexes to CaM or to over aggressive spray condition, the reactions were monitored and recorded at every 30 minutes. As shown in Figure B.1 a and a' (see Appendix B), after 60 minutes' reaction, both Pt_1 and Pt_3 bind to CaM in the same form, namely, CaM + Pt, CaM + $Pt(NH_3)$, CaM + $Pt(NH_3)Cl$, and CaM + $Pt(NH_3)_2Cl$; and the intensities of the CaM + Pt species keep increasing with time, which suggest that the losses of all the ligands of Pt_1 and Pt_3 are because of the binding to CaM. Similar results have also been observed in other Met–rich peptides or proteins upon reactions with cisplatin due to the *trans*–labilization effect.[122, 182, 183] In other words, once the displacement of chlorine ligand by sulfur of the Met or Cys residue has occurred, the $Pt–NH_3$ bond *trans* to the sulfur is significantly labilized and thus the amine group is readily substituted. The observation of CaM + $Pt(NH_3)Cl$ species is in agreement with the *trans*–labilization effect; in addition, this

observation also indicates that following the initial replacement of the *trans* chlorine ligand by sulfur of the Met residue, the loss of amine ligand is a reactively fast process. Therefore, the *trans*–labilization effect contributes to the release of $\{Pt(NH_3)Cl\}^+$ species from the dinuclear platinum compound Pt_3 after the displacement of chlorine by sulfur of the Met residue. A similar result was reported by Farrell and co–workers in the reaction of polynuclear platinum antitumor compounds with reduced glutathione, the final product was observed in the form of a dinuclear species $[\{trans–Pt(SG)(NH_3)_2\}_2–\mu–SG]$ with the linkage chain replaced.[212]

In contrast, as shown in Figure 3.2 d&d', Pt_2 maintains its $\{Pt(dien)\}^{2+}$ fragment and with one other coordination site binding to CaM. At a molar ratio 1:2 of CaM:Pt_2, up to three $\{Pt(dien)\}^{2+}$ species were found binding to CaM. Increasing the molar ratio to 1:8, mainly five $\{Pt(dien)\}^{2+}$ species bind to CaM, but the binding of up to seven $\{Pt(dien)\}^{2+}$ fragments to CaM was observed (Figure 3.2 e&e'). As shown in Figure 3.2 e', all the modified peaks in the sample of CaM:[PtCl(dien)]Cl (1:8) shift to lower *m/z* region (higher charge states). Although the shifting to higher charge states usually indicates that the conformation of the protein has been altered, the positive charge of the $\{Pt(dien)\}^{2+}$ fragments also contributes to the shift in charge state in the case of [PtCl(dien)]Cl binding to CaM because each $\{Pt(dien)\}^{2+}$ fragment has two positive charges and only one binding site available on Pt. Therefore, $\{Pt(dien)\}^{2+}$ contributes at least one charge upon each binding.

3.3.2 Mapping the binding sites of cisplatin (Pt_1) to CaM by top–

down and bottom–up MS approaches

For CaM:Pt_1 (1:2) sample, the CaM + 2Pt species was chosen for mapping the Pt–modification sites by performing top–down ECD experiment. Figure 3.3 shows the ECD spectra of CaM + 2Pt species. The peaks are assigned to fragments expected from the sequence of CaM with platinum modifications. In all, 86 cleavages of the total 147 available N–C_α backbone bonds were generated and assigned, representing overall backbone cleavage efficiency (fraction of inter–residue bonds cleavage) of 58%. These cleavages allow localization of the two platinum modification sites to the region of CaM(106–148). MS^3 is a reasonable option to find out the exact Pt–binding points. However, the intensities of the Pt–modified c/z· ions (as shown in Figure 3.3) are often very low, which makes getting quality data out of MS^3 very difficult.

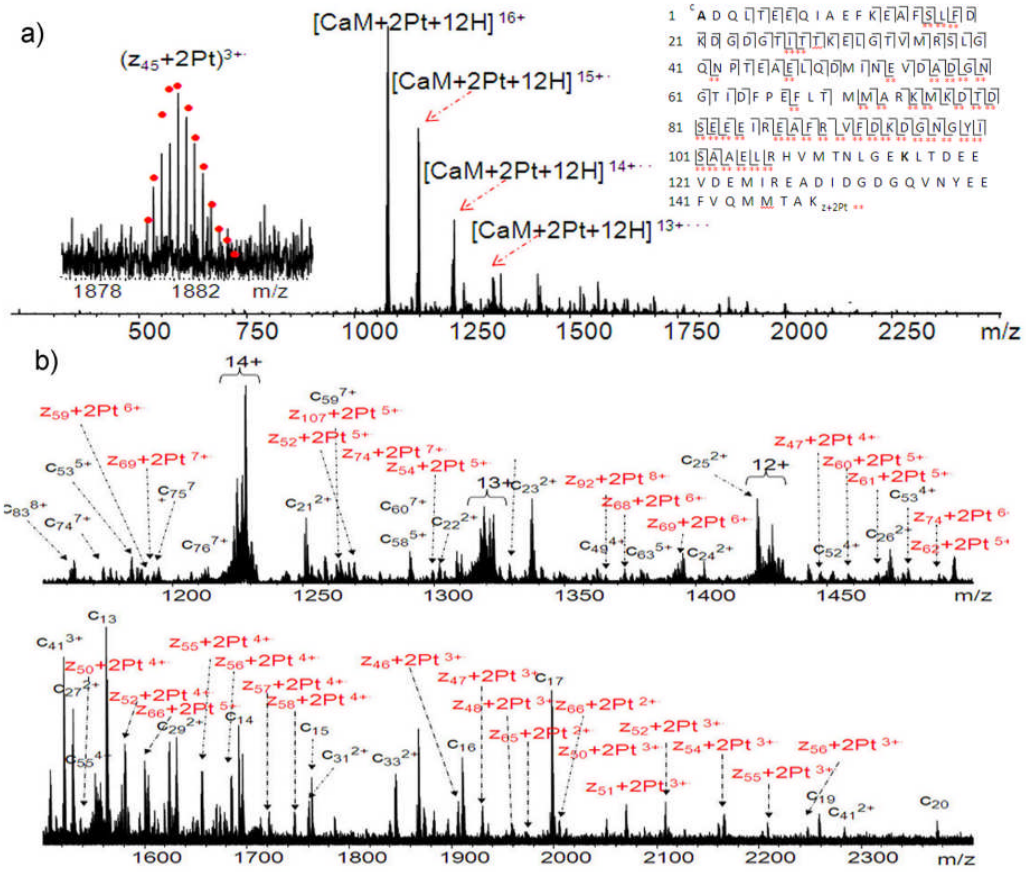

Figure 3.3 ECD spectra of the 1:2 CaM:Pt_1 sample. (a) ECD spectra of [CaM + 2Pt + 12H]$^{16+}$ ions at *m/z* 1074, the inset is the fragmentation map from ECD spectra of CaM + 2Pt; (b) the expanded ECD spectra [CaM + 2Pt + 12H]$^{16+}$ ions. Double dots represent doubly Pt–modified fragments. Full peak list is available in Appendix B (Table B.2).

To further localize the binding sites of platinum to CaM, CaM–cisplatin adducts at different molar ratios (1:1, 1:2, and 1:8) were trypsin–digested and analyzed by MS. In the 1:1 molar ratio sample of trypsin–digested CaM–cisplatin, in addition to the previously reported cross–linked species,[208] another platinum cross–linked species CaM(107–126) + Pt + CaM(142–148) as well as platinum modified CaM(38–74), CaM(107–126), and CaM(127–148) were also observed. The same Pt–modified peaks

were also observed in the CaM–cisplatin (1:2) sample; however, when the molar concentration of cisplatin is eight times higher than CaM, the intensities of all Pt–modified peaks dropped significantly, and most of them could be barely detected (Figure B.2). This result is in agreement with the MS data for 1:8 CaM–cisplatin (Figure 3.2 b'), that is, at higher molar ratio of cisplatin to CaM, multiple sites of CaM react with cisplatin giving a complicated mixture of products and significantly decreasing the intensities of each product overall. Thus, as shown in Figure 3.2 b and Figure B.2, the intensities of many of the product peaks are low or even undetectable.

Figure 3.4 shows the CAD spectrum of the cross–linked product at *m/z* 681; by matching the fragments from the precursor with digested CaM, the two platinum–cross–linking species were identified as CaM(107–126) and CaM(142–CaM148). The CaM(142–148) species, (F)VQMMTAK was unexpected in the trypsin digested samples because trypsin preferentially cleaves peptide chains mainly at the carboxyl side of the amino acids lysine or arginine, but not the carboxyl side of phenyalanine (F141). Although unusual cleavages can happen in trypsin digestion,[213] it is also possible that a small amount of chymotrypsin is active in the trypsin used.[214] In addition to the cleavage at the carboxyl side of Phe141, cleavages between Leu69 and Thr70, Met71 and Met72 were also observed (Figure B.2). To simplify the labeling of the spectrum, CaM(107–126) is represented by X, and CaM(142–148) was represented by Y'. The observation of X_b_3 + Pt and Y_b_3 + Pt ions indicates that platinum cross–links CaM at Met109 and Met144, although it does not

necessarily rule out the possibility that platinum can also bind to Met145.

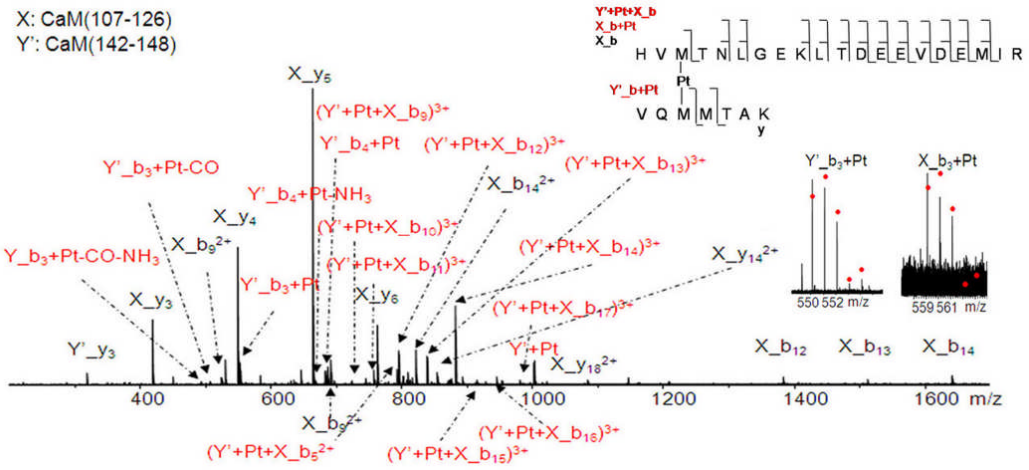

Figure 3.4 CAD spectrum of the cross–linked product of [CaM(107–126) + Pt + CaM(142–CaM148) + 3H]$^{5+}$ ion at *m/z* 681. To simplify the labeling of the spectrum, CaM(107–126) is represented by X, and CaM(142–148) is represented by Y'. The insets are the CAD fragmentation map of [CaM(107–126) + Pt + CaM(142–CaM148) + 3H]$^{5+}$ ions, and characteristic fragment ions, Y'_b_3 + Pt and X_b_3 + Pt, which show that Pt(II) cross–links Met109 and Met144 residues.

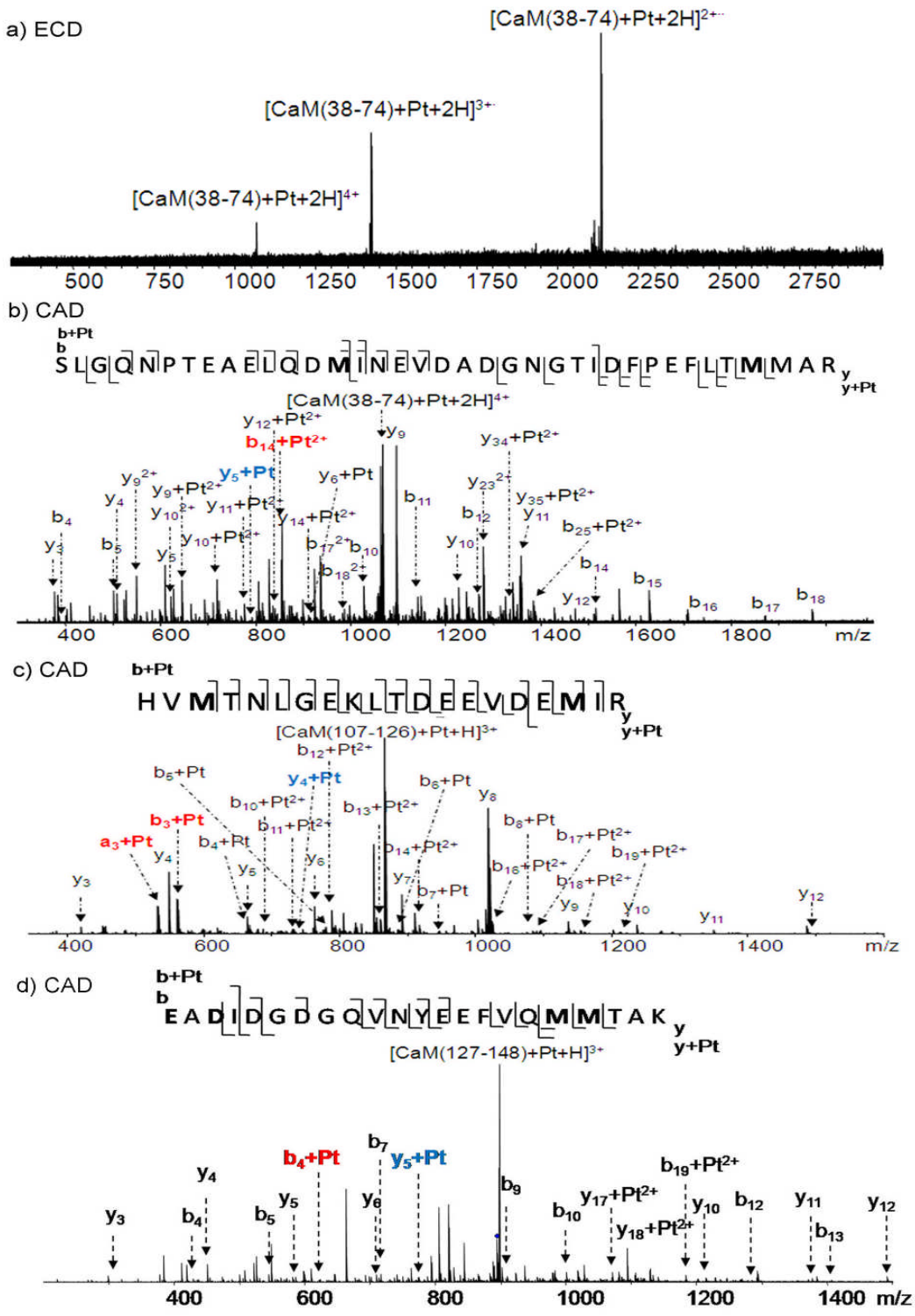

Figure 3.5 Bottom–up MS/MS spectra of CaM:cisplatin (1:2). (a) ECD spectrum of [CaM(38–74) + Pt + 2H]$^{4+}$ ion at *m/z* 1066; (b) CAD spectrum of [CaM(38–74) + Pt + 2H]$^{4+}$ ion at *m/z* 1066; the observation of b_{14} + Pt^{2+} and y_5 + Pt ions suggests that Pt cross–links Met51 and Met71 or Met72.

(c) CAD spectrum of [CaM(107–126) + Pt + H]$^{3+}$ ion at *m/z* 865; the observation of b_3 + Pt and y_4 + Pt suggests that Pt cross–links Met109 and Met124 (d) CAD spectrum of [CaM(127–148) + Pt + H]$^{3+}$ ion at *m/z* 895. The detection of b_4 + Pt and y_5 + Pt ions suggests that Pt cross–links E127 or D129 with Met144 and Met145.

To further refine other platinum binding sites on CaM, CAD and ECD experiments were performed on the platinum modified species, [CaM(38–74) + Pt + 2H]$^{4+}$ ion at *m/z* 1067, [CaM(107–126) + Pt + H]$^{3+}$ ion at *m/z* 865, and [CaM(127–148) + Pt + H]$^{3+}$ ion at *m/z* 895 (Figure 3.5). A common feature for these three cisplatin–modified species is that all the original NH_3 and Cl ligands are displaced from cisplatin, which suggests they are also platinum cross–linked species, and with at least two Met residues binding to one platinum atom in each case. In general, for the top–down analyses of the whole proteins, ECD yields more useful fragment information; for most tryptic peptides, the results were varied with CAD and ECD in some peptides (Figure 3.5), showing complementarities in that CAD worked better than ECD and *vice versa*. However, for the intra–chain Pt cross–linked peptides, clearly CAD worked better than ECD (Figure 3.5 a *vs* b). Therefore, by combination of top–down and bottom–up MS approaches, cisplatin modification sites in CaM were identified as Met51, Met71 or/and Met72, Met 109, Met124, Glu127 or Asp129, Met144, and Met145 residues (Figure 3.5); more likely, platinum cross–links Met51 and Met71/Met72 residues, Met109 and Met124 residues, Glu127/ Asp129, Met144, and Met145 residues.

Figure 3.3 a (CaM + 2Pt) presents a high quality ECD Top–down spectrum; however, no fragments were observed in the region of CaM(106–148). Further ECD experiments on CaM without platinum were performed (Figure B.3), up to 91% backbone cleavages were assigned in the full CaM sequence and nearly 30% of the total cleavages were generated in CaM(106–148) region. Therefore, by comparison, it is reasonable to conclude that the cross–linking of Pt between CaM(109) and CaM(144) contributes to repressed detections of cleavages in the region of CaM(106–148) in the top–down analyses possibly because the intramolecular cross–linking limits the flexibility of modified CaM molecules in the gas phase. It is also likely due to the same reason that only charge reduced species were observed in the ECD spectra of trypsin digested Pt–modified species (Figure 3.5 a). Therefore, the combinations of top–down and bottom–up MS approaches, and also CAD and ECD are necessary for the identification of multiple cisplatin cross–linking CaM sites.

3.3.3 Top–down MS with ECD and CAD for mapping the binding sites of [Pt(dien)Cl]Cl on CaM

The ECD spectrum of $[CaM + 2Pt(dien) + 15H]^{19+}$ ions at *m/z* 916 in the CaM:Pt_2 (1:2) sample is shown in Figure 3.6. In this spectrum, the observation of $z_{11} + 2Pt(dien)^{3+\bullet}$ indicates that there are two binding sites in the region of CaM(138–148). In addition, the detection of $c/z^{\cdot}$ complementary ion pairs, such as $c_{82} + Pt(dien)^{8+}/z_{66} + Pt(dien)^{8+\bullet}$ (see the inserts of Figure 3.6), suggests that there is one Pt(dien) binding site in the region of CaM(1–81) and the other in the region of CaM(131–

148). Therefore, there are at least two isoforms for the CaM + 2Pt(dien) species in the CaM:Pt_2 (1:2) sample.

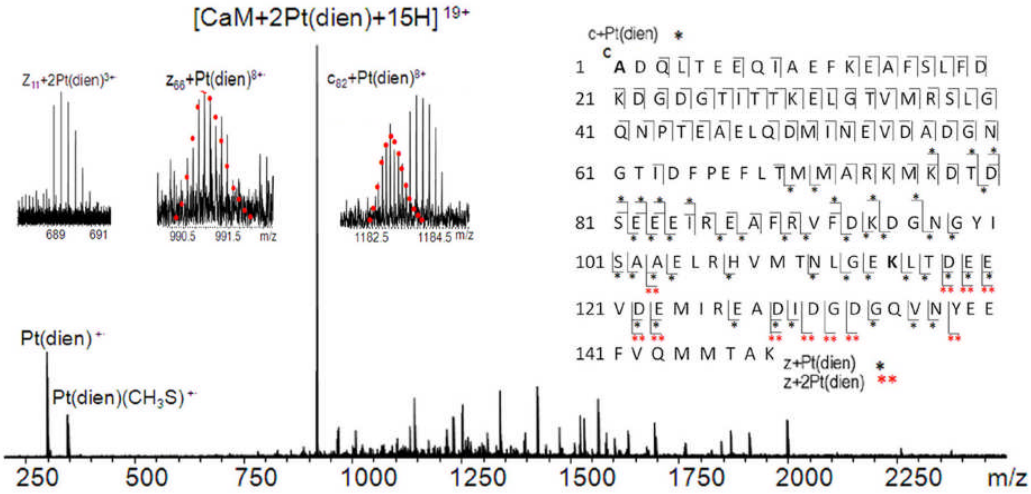

Figure 3.6 ECD spectrum of $[CaM + 2Pt(dien) + 15H]^{19+}$ ions at *m/z* 916 in the sample of CaM:cisplatin (1:2). The left inserts are the complimentary c/z$^{\bullet}$ ion pair, $c_{82} + Pt(dien)^{8+}$ and $z_{66} + Pt(dien)^{8+\bullet}$; the right insert is the fragmentation map of the ECD spectrum of CaM + 2Pt(dien). Single dot represent singly Pt(dien)–modified fragments; two dots represent doubly Pt(dien)–modified fragments.

Figure 3.7 shows the ECD spectrum of $[CaM + 5Pt(dien) + 10H]^{20+}$ ions at *m/z* 914 in the CaM:Pt_2(1:8) sample. In the low *m/z* region (Figure 3.7 b), fragment ions corresponding to $Pt(dien)^{+\bullet}$, $[Pt(dien) - 2H]^{+\bullet}$, $[Pt(dien)(CO) - H\bullet]^{+}$, and $Pt(dien)(CH_3S)^{+\bullet}$ ions were observed. Similar results have been previously observed by O'Hair and coworkers;[148] however, the CAD product ion of $[Pt^{(II)}(dien)(CH_3SH) - H]^{+}$ and ECD product ion $Pt^{(I)}(dien)(CH_3S)^{+\bullet}$ were assigned as $Pt(dien)(CH_3S)^{+}$ in both cases.

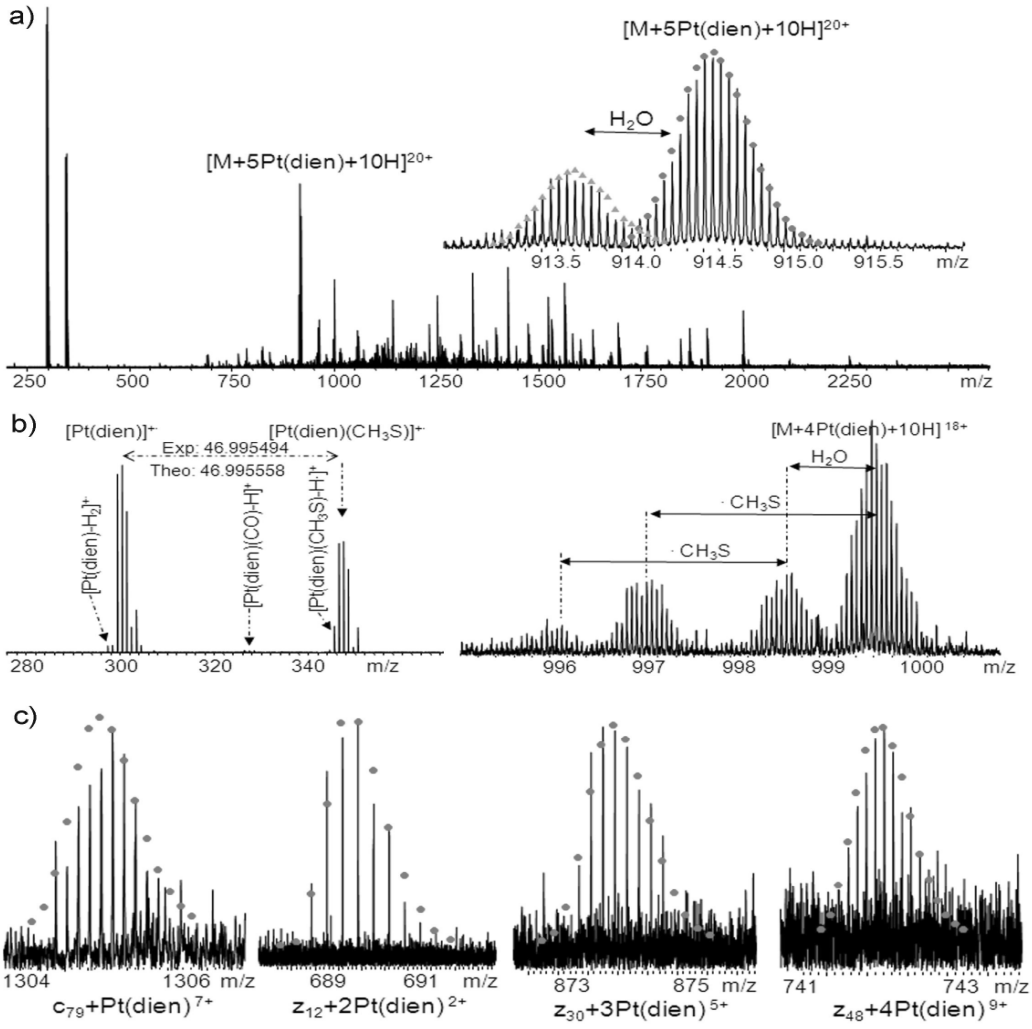

Figure 3.7 (a) ECD spectrum of [CaM + 5Pt(dien) + 10H]$^{20+}$ ions at *m/z* 914; the insert shows the isotopic distribution of precursor ions; (b) Complementary ion pairs, [Pt(dien)]$^{+\bullet}$ and [CaM + 4Pt(dien) + 10H]$^{18+}$ ions, [Pt(dien)(CH_3S)]$^{+\bullet}$ and [CaM + 4Pt(dien) + 10H - CH_3S]$^{18+}$ ions; (c) Isotopic distributions of Pt(dien)–modified c and z$^{\bullet}$ ions. For full peak list, see Table B.3.

Although the masses for [$Pt^{(II)}$(dien)(CH_3SH) - H]$^+$ and $Pt^{(I)}$(dien)(CH_3S)$^{+\bullet}$ are the same, their origins are different. The [$Pt^{(II)}$(dien)(CH_3SH) - H]$^+$ ions detected in CAD are created by even electron process rather than odd electron dissociation. However, the

generation of the $Pt^{(I)}(dien)(CH_3S)^{+\bullet}$ ions is driven by radical chemistry related to ECD as shown in Scheme 3.1 (ii). In addition, complementary ion pairs for $Pt^{(I)}(dien)^{+\bullet}$ (-0.14 ppm) and $Pt^{(I)}(dien)(CH_3S)^{+\bullet}$ (-0.03 ppm) ions, namely, $[CaM + 4Pt(dien) + 10H]^{18+}$ (-0.06 ppm) and $[CaM + 4Pt(dien) + 10H\text{-}CH_3S]^{18+}$ (0.07 ppm) ions were also detected, as shown in the right side of Figure 3.7 b, which also support the assignment as $Pt^{(I)}(dien)(CH_3S)^{+\bullet}$. In addition, the $Pt(dien)(CH_3S)^{+\bullet}$ ion indicates that Pt(dien) coordinates to the sulfur atom of Met residues; similarly, $[Pt(dien)(CO) - H\bullet]^{+}$ suggests that Pt(dien) also binds to the carboxyl group(s) of Asp or Glu residues.

As clearly demonstrated in Figure 3.8 a&b, by combination of the ECD and CAD results, the binding sites for five $\{Pt(dien)\}^{2+}$ fragments to CaM are in the regions of CaM(64–76), CaM(102–113), CaM(120–125), CaM(138–144), and Met145. In view of these multiple potential binding sites, bottom–up experiments were performed to localize them. Specific $\{Pt(dien)\}^{2+}$ binding sites were identified as Met51, Met71, Met72, His107, Met109, Met124, Met144, Met145, Glu45 or Glu47, and Asp122 or Glu123 (Figure B.4).

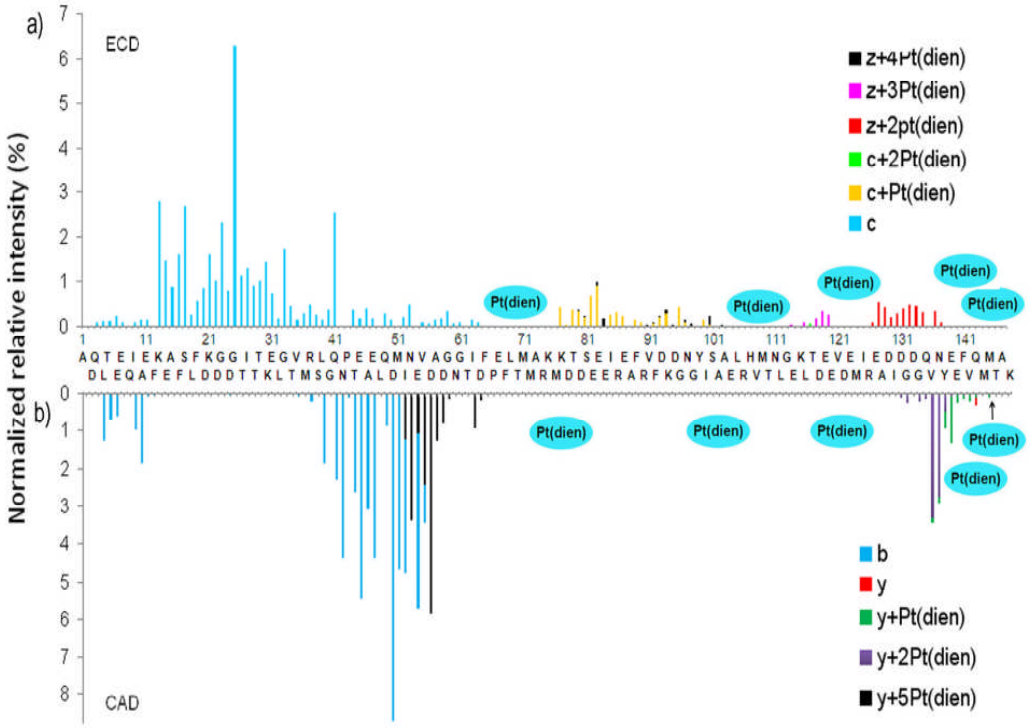

Figure 3.8 Site–specific yields of products from backbone fragmentation *vs.* backbone cleavage sites. (a) ECD of $[CaM + 5Pt(dien) + 10H]^{20+}$; (b) CAD of $[CaM + 5Pt(dien) + 10H]^{20+}$.

ECD studies of transition metal binding peptides have been previously reported by a number of groups.[215-217] Different fragmentation behaviors were observed for different transition metal ions in these complexes. For ECD of multiply–charged metal–protein ions, numerous other dissociation channels exist. As can be seen in Figure 3.7, direct electron capture by platinum(II), side–chain losses, and backbone N–C_α bond cleavage leading to $c/z^{\cdot}$ ions were all observed.

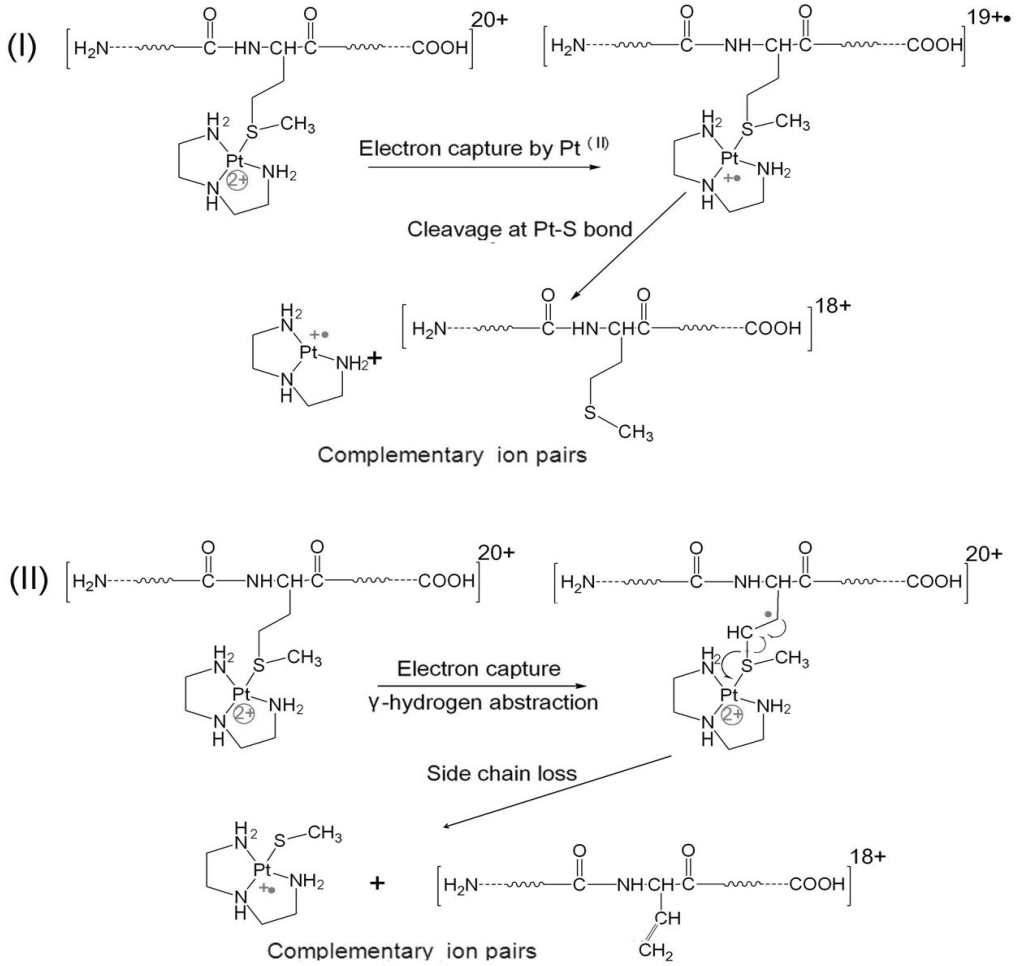

Scheme 3.1 Proposed mechanism for formation of $Pt(dien)^{+\bullet}$ and $Pt(dien)(CH_3S)^{+\bullet}$ ions.

Scheme 3.1(i) shows that direct electron capture by platinum(II) leads to the cleavage of Pt–S bonds, which is evidenced by the detection of $Pt(dien)^{+\cdot}$ ions. Scheme 3.1(ii) illustrates abstraction of the γ–hydrogen, which leads to loss of a radical side chain fragment. Because of the two inherent positive charges of platinum(II), the side chain loss of $Pt(dien)(SCH_3)^{+\bullet}$ was detected, which otherwise is neutral. The side chain losses from Met residues have been reported as $\bullet C_2H_5S$ and C_3H_8S,

the side chain loss of •SCH_3 has rarely been observed for unmodified Met residues.[218] It is likely due to the positive charge of platinum(II), therefore the side chain fragmentation pathway of Pt(II)–modified Met(S) is different. The side chain loss of Pt(dien)$(SCH_3)^{+\bullet}$ ions can be used as a signature ion which indicates the binding of platinum(II) to Met(S). Similarly, the observation of $[Pt(dien)(CO)–H\bullet]^+$ ions suggests the coordination of platinum(II) to the carboxyl group of Asp or Glu residues.

3.4 Conclusions

Top–down ECD mass spectrometry has been successfully applied to mapping the binding site of platinum complexes on CaM. Nearly 60% backbone cleavage efficiency (fraction of inter–residue bonds cleavage) was achieved in Pt–modified CaM, and over 90% backbone cleavage efficiency was achieved in CaM without Pt–modification.

Multiple electron capture pathways were observed in the platinum–modified CaM ions, such as, direct electron capture by platinum(II), side chain losses, and normal backbone N–C_α bond cleavages leads to $c/z^{\cdot}$ ions. In addition, the side–chain loss ions, Pt(dien)$(SCH_3)^{+\bullet}$ and $[Pt(dien)(CO) - H\bullet]^+$, can be used as markers to indicate the binding of Pt(dien) to Met(S), Asp(O), and Glu(O) groups.

The activity of platinum antitumor compounds is usually closely related to their binding to DNA.[219] Therefore, the loss of all the ligands of cisplatin upon binding to Met–rich calmodulin could cause cisplatin to lose much of its antitumor activity due to a failure of reaching the target DNA.[124-128] More importantly, the Met residues in calmodulin play an

important role in the function of CaM by stabilizing the open conformation of Ca^{2+}–CaM and providing a target binding interface.[198, 220] Therefore, the intramolecularly Pt–cross–linked CaM will lose its conformational flexibility to recognize calcium or target proteins, and thereby lose its function as a calcium sensor and a signal transducer. In addition, it has been widely reported that the oxidation of Met residues of CaM decreases the ability of CaM to activate target proteins.[198, 200-202] Particularly, the oxidation of Met144 and Met145 is largely responsible for the decrease in the activity of CaM to activate enzymes.[200] Therefore, the direct binding of cisplatin or its analogues to either Met144 or Met145 may also decrease the activity of CaM to recognize other target proteins.

Chapter 4

Protein Flexibility is Key to Cisplatin Cross-linking in Calmodulin[3]

4.1 Introduction

Proteins often carry out their function as part of large complexes, and their interactions are intrinsic to virtually every cellular process. Therefore, the determination of a protein's three-dimensional structure and the identification of its interaction partners are critical next steps in understanding protein action. Chemical cross-linking as a powerful tool for studying protein interactions has been used successfully for many years;[221-224] however, not until 2000, was the idea of combining cross-linking and mass spectrometry (MS) as a tool to study protein conformations and protein–protein interactions introduced by Young *et al*.[225] Since then, the developments in MS have greatly promoted the application of cross-linking in structural biology.[226, 227] Fourier transform ion cyclotron resonance mass spectrometry (FTICR MS) has been shown to be a powerful tool for analyzing cross-linking in reaction mixtures, due to its high sensitivity, high mass accuracy, high resolving power, and the availability of multiple fragmentation techniques.[131, 228-231] The combination of chemical cross-linking with FTICR MS not only yields information about protein–protein interactions but also reveals which

---

[3]This chapter has been partially/entirely reproduced from
Huilin Li, Stephen A. Wells, J. Emilio Jimenez-Roldan, Rudolf A. Römer, Yao Zhao, Peter J. Sadler, and Peter B. O'Connor. Protein flexibility is key to cisplatin cross-linking in calmodulin. *Protein Sci.* **2012.** 21, 1269-1279. Copyright 2012, Wiley.
*Flexibility simulation of CaM was done by Dr. Stephen A. Wells and rest of experimental and MS works were completed by Huilin Li.

residues within protein complexes are close to one another in space. The high mass accuracy of FTICR MS can dramatically reduce the number of candidates for cross-linking products, and in addition, its high resolution, the ability to provide a "gas phase" purification to accumulate low intensity cross-linked product ions, and the ability to fragment large proteins or peptides extensively, are critical tools that allow the unambiguous assignment of the cross-linking products and localization of the cross-linking sites. However, the identification of the cross-linked products can still be laborious and time-consuming due to the complexity of the reaction mixtures. To overcome these challenges, significant effort has been dedicated to the design of new functional cross-linkers that can enrich cross-linked products via affinity tags or facilitate the identification of cross-linked products by introducing mass spectrometry-cleavable bonds.[159, 161]

Previously, the ability of cisplatin to act as a potential protein cross-linker was explored and demonstrated using standard peptides and the 16.8 kDa protein calmodulin (CaM).[208, 232] It was found that cisplatin cross-links apo-CaM at multiple Met pairings, as follows: Met109–Met144, Met51–Met71/Met72, Met109–Met124, and Glu127/Asp129–Met144–Met145. However, the distance constraints obtained from NMR structures are inconsistent with the measured distance constraints from cross-linking (see Results and Table C.1). Our objective in this study is to resolve this inconsistency.

4.1.1 Protein flexibility

Protein structures generally are dynamic and flexible, displaying

motion on a wide range of length and time scales.[233] In carrying out its biological function, CaM displays substantial flexibility in both the nonpolar binding grooves with the α-helical linker connecting the two globular domains; this flexibility is visible in nuclear magnetic resonance (NMR) conformations of apo–CaM.[234] In addition, in a previous backbone dynamics study of calcium–saturated recombinant *Drosophila* CaM (the sequence of *Drosophila* CaM differs from the sequence of human CaM by 2 amino acids, F99–Y99 and S147–A147), Barbato *et al.* observed that a high degree of mobility exists near the middle of the central helix of CaM, and also in the loop that connects the first with the second EF–hand type calcium domain and in the loop connecting the third and fourth calcium binding domains (Figure 4.1).[235] Beck *et al.* pointed out that if a link originates from a residue localized in a flexible loop in the protein, attachments to residues scattered around the structure may be found.[155] However, it is not clear whether the cross–links found to violate the distance constraints observed in the NMR structures of CaM can be attributed to observed mobility.[235]

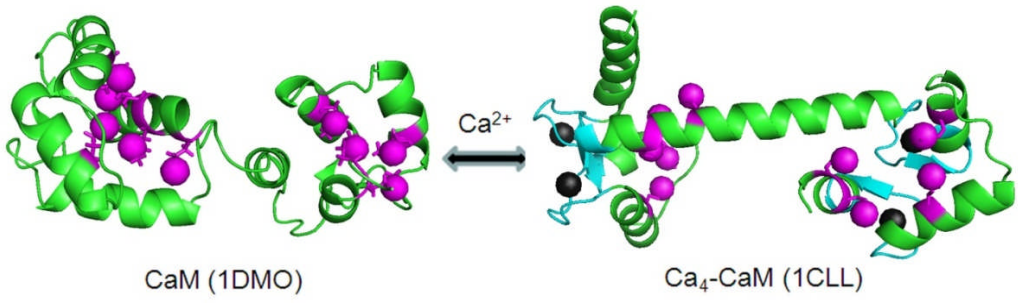

Figure 4.1 NMR structure of CaM (1DMO, the first of 30 conformations) (25) and crystal structure of Ca_4–CaM (1CCL) (26). Calcium binding sites are in cyan, calcium ions in black, Met residues in magenta, and rest of

the CaM chain in green. Sulfur atoms indicated as spheres.

4.1.2 Protein flexibility simulation

Attempts to model large–scale dynamic motion at a very high level of theory (*e.g. ab–initio* simulation) that could also describe the chemical details of the formation of Met–Pt bonds would be excessively computationally demanding. However, we expect the large–scale motion to be dominated by the intrinsic dynamics of the protein backbone,[233] and this motion can be investigated using simplified methods. In the present study, to assist in the interpretation of the experimental data, the flexible motion of CaM was modeled computationally, using a recently developed rapid method,[236] combining protein rigidity analysis,[237] geometric modelling of flexible motion[238] and elastic network modeling.[239] Coarse–grained elastic network modeling identifies low–frequency modes, which are possible directions for flexible motion. Rigidity analysis rapidly identifies rigid clusters and flexible regions which can act as "hinges". Geometric simulation using framework rigidity optimized dynamic algorithm (FRODA)[238, 240] combines the information from both analyses and moves the structure while maintaining bonding and steric constraints. The combination of all these three methods is particularly suited to modelling collective motions in a protein structure. These flexibility simulations allow us to explore large–amplitude motion along multiple normal modes in an all–atom protein structure at minimal computational expense[236] and provide valuable information on the geometry of potential platinum–binding sites. In addition, results from flexibility simulations of

Ca_4–CaM were further tested by additional MS experiments. Last but not least, based on the results of cross–linking experiments and flexibility simulations, possible mechanisms were suggested, by which the binding of anti–cancer drug cisplatin to CaM can decrease the ability of apo–CaM and Ca_4–CaM to recognize its target proteins.

4.2 Experimental section

4.2.1 Materials

Bovine calmodulin (CaM), trypsin (TPCK treated from bovine pancreas), melittin, calcium chloride ($CaCl_2$), ammonium acetate (CH_3COONH_4), and ammonium bicarbonate (NH_4HCO_3) were purchased from Sigma (St. Louis, MO, USA). HPLC grade of methanol, acetic acid (HAc), and acetonitrile (ACN) were obtained from Fisher Scientific (Pittsburgh, PA, USA). Cisplatin was synthesized and characterized by published methods.

4.2.2 Reaction of CaM and Ca–CaM with Cisplatin

In previous work, all the reactions were carried out in water.[15,22] Here, to simulate a physiological pH, all samples were reacted in 100 mM ammonium acetate (pH 6.8). Calcium–containing CaM was obtained by mixing a 500 μM apo–CaM solution with a 50 mM $CaCl_2$ solution at a 1:10 volume ratio, yielding a calcium:CaM molar ratio of 1000:1. Ca–free CaM and Ca–containing CaM solutions were then subsequently reacted with cisplatin in a 1:2 molar ratio. The samples were incubated at 37° for 24 h. To remove free platinum complexes and desalt, Amicon filters (MW cutoff = 3 kDa, Millipore, Watford, UK) were used at 13000 rpm for 30 min at

room temperature, and washed three times with 200 μL ammonium acetate (100 mM).

4.2.3 Reaction of Ca–CaM, apo–CaM–cisplatin Complexes, and Ca–CaM–cisplatin Complexes with Mellitin

Ca–CaM, apo–CaM–cisplatin complexes with calcium added subsequently, and Ca–CaM–cisplatin adducts from the above experiments were mixed with melittin (1 mM) in 100 mM ammonium acetate at a molar ratio of 1:1, to give a final concentration of 20 μM for each reaction complex. The same sample desalting procedure as described above was applied.

4.2.4 Digestion

The samples were diluted to 20 μM with 50 mM NH_4HCO_3 (pH 7.8) and then subjected to trypsin digestion at a protein to enzyme ratio of 40:1 (w/w) at 37° for 4 h. As a control, 20 μM CaM without platinum reagents was digested under the same conditions.

4.2.5 FTICR Mass Spectrometry

ESI–MS was performed on a Bruker solariX FTICR mass spectrometer with an ESI source and a 12 T actively shielded magnet. For native spray, the samples were diluted to 2 μM with 100 mM ammonium acetate (pH 6.8). For normal ESI analysis, the samples were diluted to 0.4 μM with 50% MeOH–1% CH_3COOH buffer.

4.2.6 Flexible Motion Simulations

Rapid simulations of flexible motion were carried out by using a combination of protein rigidity analysis,[237] geometric modeling of flexible motion[238] and elastic network modeling,[239] as described in detail in a

recently developed method.[236] The combined method is briefly described here: the input is an all–atom protein crystal structure. For Ca_4–CaM, the 1CLL crystal structure in the Protein Data Bank (PDB) was used,[241] with "REDUCE" (a program for adding hydrogens to a PDB molecular structure file)[242] to add hydrogens and PyMOL[243] to renumber all atoms.

Rigidity analysis is carried out in floppy inclusions and rigid substructure topography (FIRST) using the pebble–game algorithm, which matches degrees of freedom against constraints to divide a molecular framework into rigid and flexible regions.[244, 245] The constraints included are covalent bonds, hydrophobic tethers, and hydrogen bonds. Water molecules are not explicitly included but the assignment of non–covalent constraints assumes a polar solvent because of hydrophobic effects. The strength of hydrogen bonds was estimated in FIRST using a Mayo potential[246] based on donor−hydrogen−acceptor distance and angles. The set of hydrogen bonds to include in the analysis is selected using an energy cutoff value, E_{cut}. A rigidity dilution is carried out by gradually lowering E_{cut} from a value of zero (including even the weakest hydrogen bonds) to a large negative value that excludes all but the strongest hydrogen bonds.[244, 245] This provides information on the relative rigidity and flexibility of different portions of the structure, as in a recent study on the inhibition of HIV–1 protease,[247] and suggests values of E_{cut} in a physically relevant range to use in subsequent simulations of flexible motion.

Coarse–grained elastic network modeling in ElNemo[239] uses a one–site–per–residue representation of the protein structure, obtained

from the PDB structure by selecting only the Cα atom of each residue. Springs of uniform strength are placed between all pairs of sites lying within a distance cutoff, in this case of 12 Å. Diagonalisation of the resulting matrix generates a set of 3n elastic network modes (eigenvectors and frequency eigenvalues) for a protein structure of n residues; here n=144 (the terminal residues 1–3 and residue 148 were not resolved in the 1CLL crystal structure).

The FRODA implemented within FIRST, models bonding constraints in a molecular framework using a system of templates.[238, 240] Motion is generated by a small perturbation (typically of order 0.01 Å) of all atomic positions followed by reimposition of the bonding and steric constraints. To model flexible motion, an elastic network mode eigenvector was used as a systematic bias; the perturbation of the structure displaces all the atoms of a given residue in the direction of motion for that residue in the eigenvector. The process is iterated to produce a large amplitude of motion along the bias eigenvector while retaining physically reasonable bonding and steric geometry. Motions both parallel and anti–parallel to the mode eigenvector were explored by using positive (+) and negative (–) biases. A trajectory of several thousand conformations, generating motion over several *Ångström* root–mean–square deviation (RMSD), takes only a few central processing unit (CPU) minutes, allowing for the rapid exploration of many modes.[236, 248]

4.3 Results and discussion

Previously Li *et al*. reported, using a combination of top–down and

bottom–up MS methods, that cisplatin cross–links multiple Met pairs of apo–CaM, as follows: Met51–Met71/Met72, Met109–Met124, Met109–Met144, and Glu127 or Asp129–Met144–Met145. However, the spatial distances of each cross–linked pair as determined from the reported family of 30 NMR structures of apo–CaM (see Table C.1),[234] as sulfur–sulfur distances of each Met pair are as follow: Met51–Met71 (2.9 to 7.1 Å), Met51–Met72 (5.7 to 8.7 Å), Met109–Met124 (6.8 to 9.2 Å), Met109–Met144 (9.7 to 12.7 Å), and Met144–Met145 (5.2 to 9.2 Å). These values range from 2.9 to 12.7 Å; and only the spatial distances between Met51–Met71 (in 11 conformations out of 30) fit the arm length range of cisplatin (2.82 Å to 4.63 Å).

In general, protein structures are not static and rigid. The polypeptide backbones, and especially the side chains, are constantly moving due to thermal motion of the atoms.[233] In both of the calcium–free and calcium–saturated forms, CaM displays substantial flexibility in the nonpolar binding grooves and the α–helical linker connecting the two globular domains. However, it is not clear whether the inconsistency of the distance constraints between MS cross–linking data and NMR structures of apo–CaM can be explained by such dynamical phenomena. The flexible motion of CaM was therefore modeled to assist with the interpretation of the experimental data and to guide further experiment investigation.

4.3.1 Analysis of the cross–linking sites of cisplatin to CaM and Ca_4–CaM by flexibility approaches

4.3.1.1 Rigidity dilution analysis

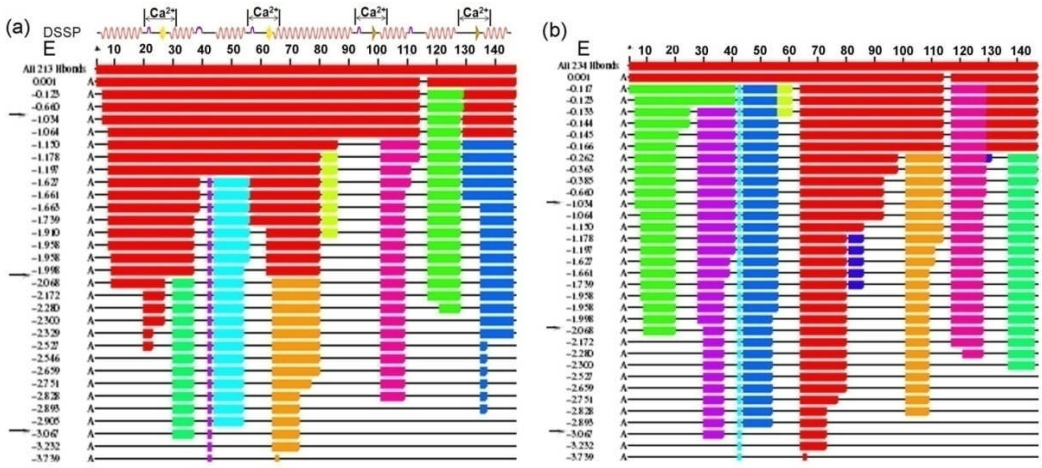

Figure 4.2 Rigidity dilution plots for (a) the native structure of Ca_4–CaM (1CLL), and (b) the Ca_4–CaM (1CLL) with calcium deleted. The primary sequence of the protein is represented as a line, and the secondary structure is presented by using DSSP (database of secondary structure assignments) with calcium binding sites indicated. A horizontal thin black line indicates a flexible region of the backbone, while a thick coloured line indicates a rigid cluster. The topmost line of the plot shows the rigidity of the structure with the inclusion of all possible hydrogen bonds; the structure is almost entirely a single rigid cluster, shown in red. When E_{cut} is decreased (left–most column, in kcal/mol), rigid clusters break up as indicated in different colors and more of the chain becomes flexible. Cutoff values used in the simulation of flexible motion (-1,-2 and -3 kcal/mol) are indicated by arrows.

Rigidity analysis is carried out in FIRST software, which accurately predicts flexible regions in proteins by analyzing the constraints on flexibility formed by the covalent and non–covalent bonds.[244, 245] Figure 4.2 shows the rigidity dilutions for the 1CLL CaM structure,[241] both in its

native state including four bound calcium ions (Figure 4.2 a), and also in an edited state with calcium ions deleted from the structure (Figure 4.2 b). In the native state, α–helical regions, for example, residues 103–111 (pink), 118–128 (green), 139–146 (blue), are generally visible as persistent rigid clusters during the dilution, and much of the N–terminal region remains a single rigid cluster to cutoff values around –2 kcal/mol (*ca.* 8.4 kJ/mol). However the central helix (residues 66–92) ceases to be a single rigid cluster at a cutoff of -1.178 kcal/mol. It appears that the capacity of the central helix to become flexible in CaM, visible in the NMR ensemble of structures 1DMO,[234] is predicted by the rigidity analysis.

Deletion of the calcium ions from the 1CLL structure (Figure 4.2 b) removes constraints from the network as protein–metal bonds are no longer present. The effects on the rigidity analysis are greatest at small values of the energy cutoff and are particularly visible in the N–terminal region. With calcium bound, residues 5–35 form as a solid robust helix structure (Figure 4.2 a); upon removal of the calcium, the same region splits into two helices connected by a flexible linker region (residues 19–30) (Figure 4.2 b). With reference to these dilution plots, flexibility simulations were carried out using three different cutoffs (-1, - 2 and - 3 kcal/mol) for both the native and calcium-deleted structures. This allowed us to explore the flexible motion of the structure both when it is largely rigid and when it is largely flexible.[234]

4.3.1.2 Elastic network mode

Coarse–grained elastic network modeling was performed to identify low–frequency modes of CaM based on its crystal structure (1CLL).

Conventionally these modes are ordered from lowest frequency to highest. Modes 1–6 represent combinations of rigid–body rotations and translations of the structure and have effectively zero frequency, so the lowest–frequency non–trivial mode is mode 7, hereinafter m_7. The motions along the 20 lowest–frequency non–trivial modes, that is, m_7–m_{26} were therefore examined. In order to distinguish between motion along the direction of a mode and motion opposite, m^+ and m^- were used, respectively. The protein displays a substantial amount of flexible motions along these modes. Some of these flexible motions bring pairs of Met residues into close proximity, potentially allowing cross–linking by cisplatin. As CaM is almost symmetric, several modes were found to occur in matched pairs, describing equivalent motions of the two globular domains.

4.3.1.3 FRODA simulation results

The FRODA software was used to determine conformational changes in CaM. Each of 20 mode eigenvectors of CaM was explored, in positive and negative directions, for each of three E_{cut} values, for the native and calcium–deleted structures, making up 240 trajectories in all. The purpose of the simulations is to explore the possible formation of platinum–binding sites, that is, locations where the side–chains of several Met residues lie close together. The conformations generated in the flexibility simulations were therefore examined and distances between the sulfur atoms of Met side–chains were extracted using a distance cutoff of 5 Å. Multiple cases were identified (Table 4.1) in which a pair of sulfur

atoms lying outside this cutoff distance in the crystal structure is brought within the cutoff by flexible motion along a mode eigenvector.

Table 4.1 Predicted cross-linking sites as obtained from rigidity and flexibility analysis at energy cutoffs of -3 kcal/mol (For results from energy cutoffs of -2 kcal/mol and -1 kcal/mol, see Table C.2(A&B). The first two columns give the potential cross-linking Met residues, the third shows the sulfur-sulfur distance d(1—2) obtained from the crystal structure of Ca_4–CaM (1CCL). The remaining columns show the modes in both +Ca and –Ca structures that can bring Met residues close to within 5 Å, and the corresponding d(1—2) distances, and the MS results wherever available. "-" indicates that the cross-linking of the corresponding Met pairs was not observed in MS. (kcal/mol is used as a default unit in FIRST software, which can be converted to SI unit according to 1 kcal/mol=4.2 kJ/mol).

Rigidity cutoff -3 kcal/mol.			+Ca structure (1CLL)			-Ca structure (calcium-deleted structure of 1CLL)		
Residue 1	Residue 2	d(1-2), (Å) native	Mode of close approach	d(1-2), (Å) simulated	MS experiment results	Mode of close approach	d(1—2), (Å) simulated	MS experiment results
36	71	10.9	m^{+}_{13}	4.9	-			-
36	72	11.6			-	m^{+}_{13}	4.3	-
51	71	9.9	m^{+}_{13}	3.8	Yes	m^{+}_{13}	3.6	Yes
51	72	12.5			-			-
109	124	5.2	Many modes	<5	Yes	Many modes	<5	Yes
109	144	12.3	m^{-}_{14}	3.7	Yes	m^{-}_{14}	3.8	Yes
109	145	10.3			-			-
124	144	9.6	m^{+}_{18},	4.1	-	m^{+}_{18}	4.6	-
124	145	11.0			-			-

In Figure 4.3, a flexible motion of the C–terminal globular domain is illustrated. The side chains of residues Met109 and Met144 are widely separated in the 1CLL crystal structure (Figure 4.3 a), but are brought together by motion along m_{14} (Figure 4.3 b), a mode that opens and closes the non–polar binding groove. This suggests that the thioether side–chains of Met109 and Met144 can coordinate to the same platinum ion when CaM binds to cisplatin. Thus, this accounts for the observation of cross–linked fragments in MS, such as CaM(107–126) + Pt + CaM(127–148).[208, 232] It is also clear that the binding of platinum to this pair of residues will effectively close the nonpolar groove and interfere with the ability of CaM to bind to protein targets, which suggests that the mechanism of action for platinum–containing drugs, such as cisplatin, could involve inhibiting the activity of CaM as discussed later.

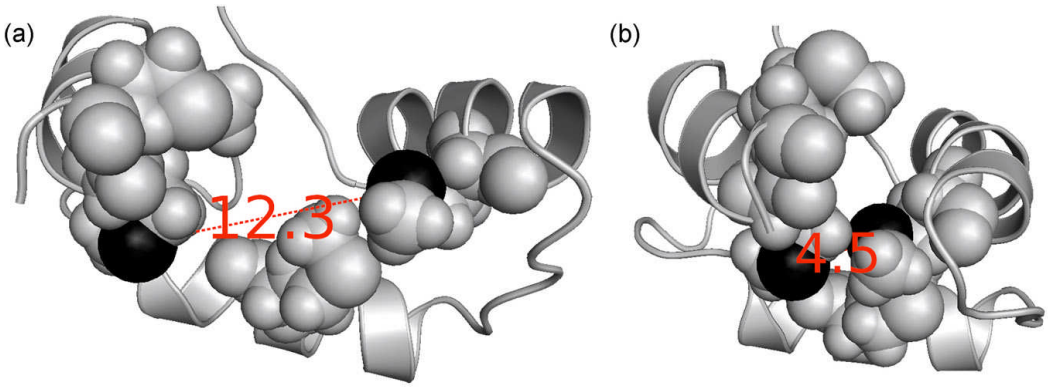

Figure 4.3 The C–terminal domain (residues 80–147) of Ca_4–CaM (1CLL) shows the hydrophobic protein–binding groove: (a) at the start of a flexible–motion simulation (native structure), and (b) during flexible–motion simulation along mode m_{14}–. The protein is mostly shown in cartoon view, with Met residues shown in all–atom view, and sulfurs

highlighted in black. The sulfur–sulfur distance for residues 109 and 144 is shown and these two residues have clearly been brought into close proximity in mode 14–.

Table 4.1 shows the results for significant pairs of Met residues in each domain, giving in each case the initial distance between the sulfur atoms, and the identity of any mode that brings the sulfur atoms within 5 Å of each other, along with the closest distance of approach in our simulations. In the N–terminal domain, the pairing of residues Met36–Met51 (Met(S)–Met(S) distance 4.97 Å) which are close in the 1CLL structure was neglected, and of residues Met71–Met72, that are adjacent in sequence. In the C–terminal domain, the pairing of residues Met144–Met145 was neglected as they are adjacent in sequence; for the pair of residues Met109–Met124, which are close in the native structure, multiple modes producing close approaches of this pair were found. Table 4.1 provides data for simulations with and without calcium in the structure at the energy cutoff of - 3 kcal/mol used in the rigidity analysis (Results obtained at energy cutoffs - 2 kcal/mol and - 1 kcal/mol are listed in Table C.2). The holo–CaM (+ Ca) structure is slightly less flexible than the apo–CaM (- Ca) structure; however, the residue pairings observed are consistent for both - Ca and + Ca CaM forms. The largest number of pairings was found at a cutoff of - 3 kcal/mol, and simulations at smaller cutoffs when the protein is more rigid have more restricted motion and produce fewer pairings (Table C.2 a&b).

4.3.2 Mapping the binding sites of cisplatin to Ca_4–CaM by MS approaches

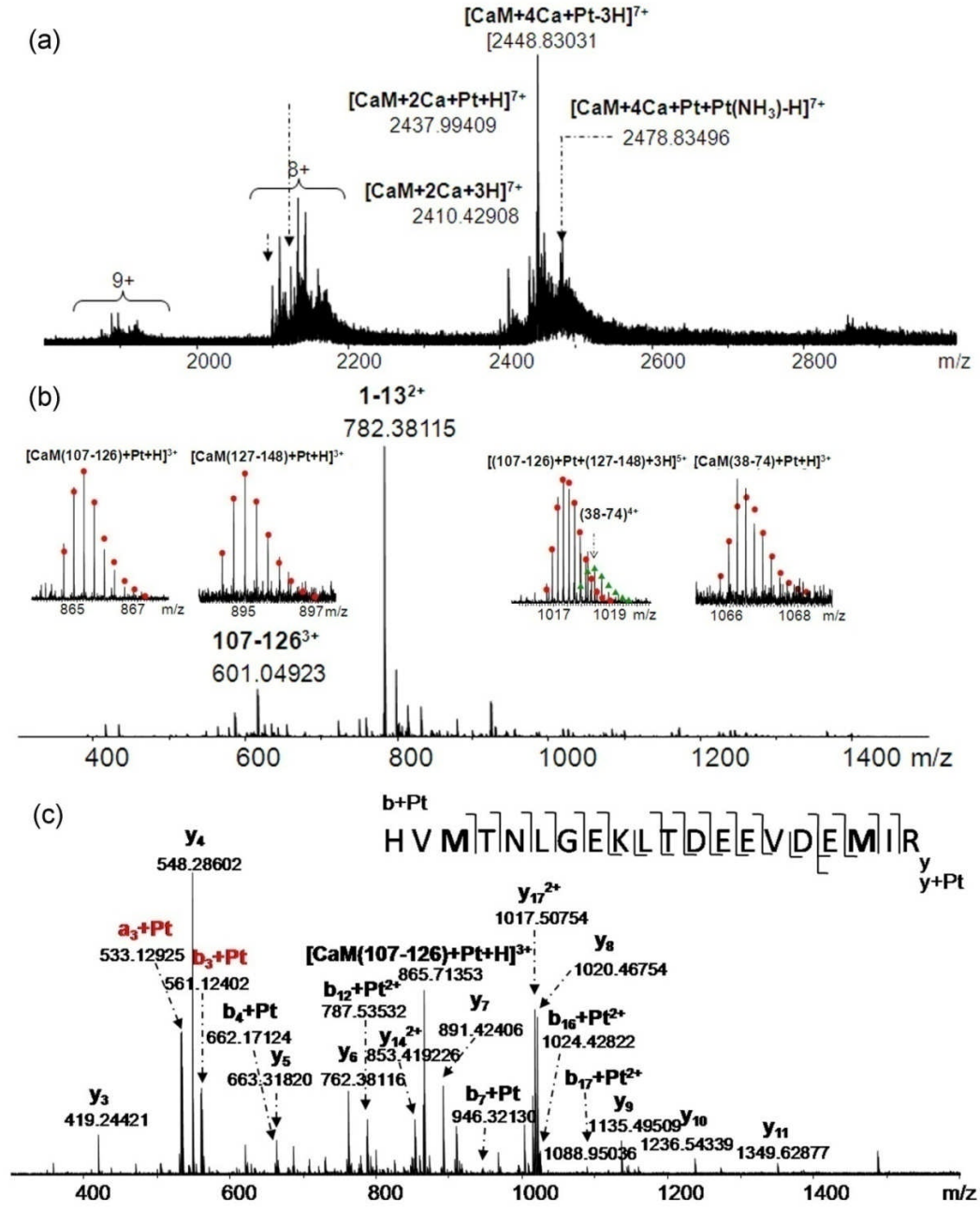

Figure 4.4 (a) Native ESI spectrum of Ca–CaM:cisplatin = 1:2 reaction products; (b) Trypsin digested Ca–CaM:cisplatin = 1:2 complex, the inserts are platinum cross–linked species; (c) CAD spectrum of [CaM(107–126) + Pt + H]$^{3+}$ species. The observation of a_3 + Pt and y_4 + Pt ions indicates that cisplatin cross–links Met109 and Met124 residues.

As shown in Table 4.1, the results obtained from flexibility analysis suggest that cisplatin can also cross–link Ca_4–CaM at multiple Met pairs. To test the predictions obtained from flexibility analysis experimentally, MS analysis of the products from reactions of cisplatin with calcium–containing CaM was carried out. Figure 4.4 a shows the mass spectrum of reaction products of calcium–containing CaM with cisplatin (Ca–CaM:cisplatin=1:2) under native spray conditions. Different calcium binding forms of CaM were observed, mainly CaM + 2Ca and CaM + 4Ca. This is accounted for by the fact that the C–terminal lobe has a 10–fold higher Ca^{2+}–binding affinity than the N–terminal lobe.[36] More importantly, calcium-bound CaM displaced all four ligands from cisplatin, giving products such as CaM + Pt + 2Ca, CaM + 4Ca + Pt, and CaM + Pt + $Pt(NH_3)$ + 2Ca, which clearly indicates that cisplatin can also cross–link calcium–bound CaM. Subsequently, the Ca–CaM:cisplatin = 1:2 reaction products were further trypsin–digested, and followed by MS analysis. Figure 4.4 b shows that spectra from the trypsin–digested Ca–CaM:cisplatin = 1:2 sample contain a number of Pt–modified species. A common feature of the species shown in the inserts of Figure 4.4 b, $[CaM(107–126) + Pt + H]^{3+}$ at *m/z* 865, $[CaM(127–148) + Pt + H]^{3+}$ at *m/z* 895, $[CaM(107–126) + Pt + CaM(127–148) + 3H]^{5+}$ at *m/z* 1018, and $[CaM(38–74) + Pt + H]^{3+}$ at *m/z* 1067, is that all the original ligands (NH_3 and Cl) of cisplatin have been displaced. This is attributable to the *trans*–labilization effect of Met sulfur.[37] The loss of two ammine ligands indicates that at least two Met residues bind to one platinum atom in each

case. Therefore, cisplatin forms both interchain cross-links CaM(107–126) and CaM(127–148) fragments, and intrachain cross-links CaM(38–74), CaM(107–126), and CaM(127–148) fragments. To further localize the cross-linking sites, the cross-linked species were fragmented by collisional activated dissociation (CAD). As an example shown in Figure 4.4 c, the observation of a_3 + Pt and y_4 + Pt ions in the CAD spectrum of [CaM(107–126) + Pt + H]$^{3+}$ species suggests that cisplatin intrachain cross–links CaM(107–126) at Met109 and Met124. Thus, cisplatin can cross–link calcium–bound CaM at the same sites as to CaM, namely, Met51–Met71/Met72, Met109–Met124, Met109–Met144, and Met144–Met145 (Table 4.1).

Since the flexibility analysis results indicate that cisplatin can also cross–link Met36 and Met72, Met124 and Met144, we then checked MS results to see whether corresponding peaks had been detected. No peaks corresponding to platinum cross–linking Met36 and Met72 were observed. Also no fragment ions indicating that cisplatin cross–links Met124 and Met144, were found in the tandem MS spectra of either CaM(107–126) + Pt + CaM(127–148) or CaM(107–126) + Pt + CaM(142–148) species. There are several reasons for a theoretically possible cross–link not being observed in MS, including its low intensity, unfavourable ionization, and unsuitable peptide length.

As Glu and Asp residues can also potentially coordinate platinum, we carried out an additional search for close approaches between the side-chain carboxylate groups of residues Glu127 and Asp129 with each other and with the Met sulfur atoms in the C-terminal domain. The side chain

carboxylate group of Glu127 is brought within 5 Å of the side chain sulphur atom of Met144 by multiple flexible modes, at all energy cutoffs studies, in both +Ca and –Ca structures. In the simulations, Glu127 was not observed to pair with Met145, and Asp129 not to pair with either Met144 or Met145. The experimental observation of Pt-crosslinked CaM(127-148) fragments can thus be explained by the formation of Glu127-Pt-Met144 cross-links as observed in the simulations. However, the formation of Asp129–Pt–Met145 cross-links in this fragment cannot be excluded. Therefore, overall, the cross-linking MS results of calcium-bound CaM are consistent with the flexibility analysis of Ca_4–CaM.

4.3.3 Biological insights from cross-linking experiments and flexibility analysis

Previously Jarve *et al.* reported that treatment of rats with the anti-cancer drug cisplatin can immunohistochemically reduce the level of the Ca_4–CaM complex.[205] In addition, an *in vitro* experiment using an analogue of CaM, Mero–CaM–1, showed that cis–diammine–diaquacisplatinum(II), a hydrolysed form of cisplatin, inhibited the CaM conformational shift through a direct interaction with the CaM molecule. The authors concluded that distention of the stomach was due to inhibition of neuronal nitric oxide synthase (NOS) activation by a direct interaction between cisplatin and the calcium binding sites of the CaM molecule. However, our previous results show that Met(S) residues are the preferential cisplatin–binding sites rather than the calcium binding sites (mainly Glu(E) and Asp(D) residues), although the binding of cisplatin to Glu and Asp residues can occur when the molar ratios of

cisplatin to CaM are high.[232] Met residues in CaM play an important role in its versatility and functions. It has been widely reported that the oxidation of Met residues (especially Met144 and Met145) of CaM decreases the ability of CaM to activate target proteins due to a large reduction in the conformational flexibility of the Met side chains.[249-251] Met residues account for nearly half the surface area of the hydrophobic patches of Ca_4–CaM, and function by providing a target-binding interface. As shown in Figure 4.1, the binding of calcium exposes the hydrophobic patches of Ca_4–CaM, which in general moves Met residues further away from each other compared to calcium–free CaM NMR structures. However, the results of the flexibility simulation suggest that the cross–linking of cisplatin to multiple Met sites on CaM will trap the binding groove in a closed state and prevent opening of the binding interface (Figure 4.3), therefore decreasing the ability of Ca_4–CaM to recognize its target proteins.

4.3.4 Melittin–binding assay

To verify the hypothesis that the cross–linking in CaM or Ca_4–CaM induced by cisplatin may decrease the ability of CaM to recognize its target proteins, reaction products of CaM and cisplatin (CaM:cisplatin = 1:2), and calcium–containing CaM with cisplatin (Ca–CaM:cisplatin = 1:2) were further reacted with melittin at a 1:1 molar ratio. Melittin is one of the most potent inhibitors of CaM activity, and has been widely used to evaluate the ability of CaM to recognize its targets.[40-42]

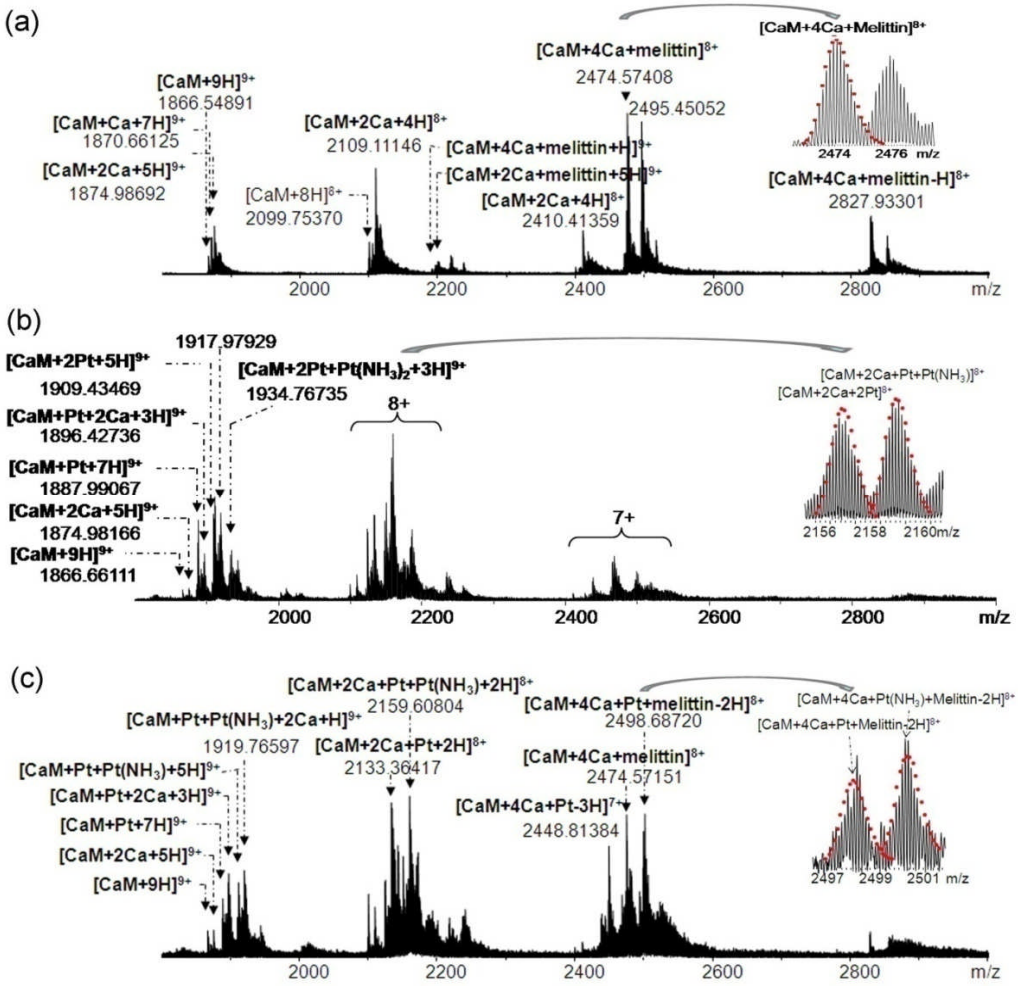

Figure 4.5 Native ESI spectra of protein complexes. (a) Ca–CaM:melittin = 1:1; (b) (CaM:cisplatin = 1:2)–Ca:melittin = 1:1; (c) (Ca–CaM:cisplatin = 1:2):melittin = 1:1.

Figure 4.5 shows MS spectra of melittin reacting with Ca–CaM, (CaM:cisplatin = 1:2)–Ca complex (calcium added to assist the recognition of melittin), and Ca–CaM:cisplatin = 1:2 complexes. As shown in Figure 4.5 a, the adduct Ca_4–CaM + melittin is the major product from the cisplatin–free CaM reaction; in addition, Ca_2–CaM also binds to melittin. On the contrary, as shown in Figure 4.5 b, once CaM has reacted with cisplatin, no peaks corresponding to Ca_4–CaM + melittin are detected when Ca^{2+} is added subsequently (with or without platinum,

or different numbers of calcium ions). The spectrum is dominated by Pt–crosslinked CaM species; in addition, no cross–linked species were detected with four calcium ions bound. In comparison, for the case of calcium–bound CaM (Figure 4.5 c), the spectrum was dominated by platinum cross–linked CaM species; however, surprisingly, a species corresponding to CaM + 4Ca + Pt + melittin was observed (see the insert of Figure 4.5 c), which suggests that calcium–binding opens up the more compact apo–CaM (calcium–free CaM) structure, as shown in Figure 4.1, increasing the exposure of hydrophobic target–binding surfaces in each of the globular domains. Therefore, even Pt–crosslinked Ca_4–CaM maintains an extended open structure, and thus maintains to a certain extent the ability to recognize its target, melittin. In contrast, the structures of calcium–free CaM are more compact, the cross–linking further closes the nonpolar groove. Therefore, addition of calcium ions after cross–linking cannot effectively change the structure of the Pt–crosslinked CaM species, and thus Pt–crosslinked CaM loses its ability to recognize its target.

4.4 Conclusions

Previously the anti–cancer drug cisplatin has been demonstrated to be a protein cross–linking reagent, cross–linking multiple sulfur atoms of multiple Met pairs on CaM. However, the distance constraints obtained from NMR structures of CaM are inconsistent with the measured distance constraints by cross–linking. Here, a flexibility analysis shows that both + Ca and – Ca CaM structures have extensive flexibility, and flexible

motions can bring sulfur atoms of Met residues in the hydrophobic patches close and within 5 Å, which provides opportunities for cisplatin to cross–link Met residues of CaM. Therefore, the simulation of flexible motion can be a very useful tool for predicting cross–linking pairs in proteins and facilitating MS data analysis. In addition, flexibility simulation also suggests a direct mechanism of action for platinum–containing drugs, such as cisplatin, to inhibit the activity of CaM. This occurs via binding of platinum to pairs of Met residues, such as Met109–Met144, which effectively traps the nonpolar groove in a closed state, and interferes with the ability of CaM to bind to protein targets. This hypothesis was further validated by a melittin binding assay, Ca_4–CaM maintains to a certain extent of its ability to recognize melittin even when cross–linked by platinum; however, calcium–free CaM, when cross–linked by cisplatin, loses its ability to recognize the target, melittin.

Collectively, these results suggest that flexibility is key to cisplatin cross–linking in CaM. The cross–linking of cisplatin to apo–CaM or Ca–CaM can inhibit the ability of CaM to recognize its target proteins. In addition, the simulation of flexible motion can be a very useful tool for predicting cross–linking pairs in proteins and facilitating MS data analysis. In the future work, it will likely be instructive to refine these simulations here to further take account the fact that protein cross–linking by cisplatin occurs in a stepwise fashion on a time scale of minutes to hours. After the initial adduct $\{Pt(NH_3)_2Cl\}^+$ is formed with the protein, the charged cisplatin residue changes the local forces, adding new attractive charge–charge and charge–dipole interactions. Thus, these simulations likely

underestimate both the reaction rate and the apparent distance over which cisplatin can crosslink proteins. Nevertheless, these cost–effective simulations can provide some structural and modal insight into the approach distances available in these proteins which helps to understand how cross–linking can occur over larger distances than initially expected. Ultimately, it is clear that such studies of platinated proteins in a proteomic context will become increasingly important in the future as more platinum and metal–based therapeutics become available.

Chapter 5

Side–Chain Losses in Electron Capture Dissociation to Improve the Identification of Pt(II)–modification Sites on Peptides and Proteins[4]

5.1 Introduction

5.1.1 Mass Spectrometry techniques for characterizing Pt–binding sites on proteins

The most frequently used tandem MS fragmentation technique for determining platinum binding sites on proteins is collision–activated dissociation (CAD), which breaks peptide C–N bonds to form N–terminal b and C–terminal y–ions.[141, 143, 146, 252] Although CAD is useful in the determination of platinum binding sites, it is still challenging to differentiate the site to which platinum binds. CAD–induced cleavage of labile post–translational modifications (PTMs), including Pt–modifications, is dependent of the collision energy used, and can lead to erroneous conclusions, especially in those situations where there are multiple potential binding sites close to each other in a sequence.

Electron capture dissociation (ECD) is a complementary fragmentation technique that produces c and z• ions upon breakage of the N–C_α bond, and often labile modifications are preserved in ECD.[40, 57] Previously it has been demonstrated that ECD can be used to localize the sites of modification by platinum on proteins and peptides.[208] The Pt–modified and unmodified c/z• ions generated by ECD are very useful for

[4] This chapter has been partially/entirely reproduced from
Huilin Li, Jonathon R. Snelling, James H. Scrivens, Peter J. Sadler, and Peter B. O'Connor. Side–Chain Losses in Electron Capture Dissociation to Improve the Identification of Pt(II)–modification Sites on Peptides and Proteins. *Anal. Chem.* **2012**. Submitted.

identifying the Pt–modification sites. As a result, Met(S), His(N), and carboxyl groups of Asp and Glu have been identified as Pt–binding sites.

However, it is important to remember that cisplatin has four ligands which can be displaced to form up to four bonds with a protein or peptide. Thus, it is still challenging to identify, unambiguously, the modification sites when there are multiple potential Pt–binding sites presented in one sequence, especially when those potential Pt–binding sites are adjacent or close to each other. Additionally, positional isomers are often formed during the reaction of Pt(II) complex with proteins. Therefore, without any prior separation, the precursor ion isolated for fragmentation is often a mixture of ions with exactly the same mass but different structures (including positional and conformational isomers), which can significantly complicate the tandem spectra and data interpretation. It is relatively easy to identify the Pt–modification sites at each end of the sequence according to Pt–modified c/z• ion information, but the sites in the middle of the sequence are often difficult to assign accurately. Determining the precise location of the Pt–binding position can be crucial due to the fact that Met(S), His(N), Cys(S), and carboxyl groups of Asp and Glu residues are often involved in the binding of metal ions *e.g.* Zn^{2+}, Cd^{2+}, Cu^{2+}, Ca^{2+}, in proteins, such as metallothioneins, superoxide dismutase, calmodulin, and cytochromes.[253]

5.1.2 Side chain losses in ECD

Previously it has been observed that when platinum binds to a Met residue of a peptide or protein sequence, there is a signature side chain loss of CH_3SH in ECD.[208] Therefore, the side chain loss of CH_3SH can

be used as an indicator for Pt–modification at Met residues. Here, to explore further the possibility of using the neutral side chain losses in ECD as signatures to improve the localization of Pt–modification sites on peptides and proteins, a detailed study of the binding of cisplatin to peptides with various types of potential Pt–binding sites (Met(S), His(N), Cys(S), Asp(O), Glu(O), disulfide bonds, Arg(N), and Lys(N)) is presented using ECD in a Fourier transform ion cyclotron resonance mass spectrometer (FTICR MS). In addition, as an alternative approach, travelling wave ion mobility mass spectrometry combined with CAD is also applied to separate and localize Pt–modification sites. It has already been demonstrated that ion mobility can distinguish between isomeric compounds with identical mass–to–charge ratios, including small molecules, peptides, and proteins, which cannot be separated from each other using mass spectrometry alone.[254-258]

Furthermore, the data analysis approach established here was further tested in the analyses of top–down ECD data of a Pt–crosslinked insulin dimer to locate the cross–linking sites.

5.2 Experimental section

5.2.1 Materials

Substance P (Sp), substance P fragment 1–7 (Sp_{1-7}), substance P fragment 2–11(Sp_{2-11}), angiotensin II (A), bombesin (B), Arg^8–vasopressin, Lys^8–vasopressin, insulin from bovine pancreas, and ammonium hydroxide solution (NH_4OH) were purchased from Sigma (St. Louis, MO). Peptides (P1) (KMGIHACVEFK) was synthesized by GL Biochem

(Shanghai, China) Ltd. HPLC grade of acetic acid (HAc), and acetonitrile (ACN), were obtained from Fisher Scientific (Pittsburgh, PA). Cisplatin was synthesized and characterized by standard methods.[122]

Table 5.1 Amino acid sequences of the peptides and proteins studies here. Potential Pt(II) binding sites, are highlighted in red.

Name	Sequence	Composition	Monoisotopic Mass (Da)
Substance P (SP)	RPKPQQFFGLM-NH_2	$C_{63}H_{98}N_{18}O_{13}S$	1346.72815
Substance P(1-7) (SP_{1-7})	RPKPQQF	$C_{41}H_{65}N_{13}O_{10}$	899.49773
Substance P(2-11) (SP_{2-11})	PKPQQFFGLM-NH_2	$C_{57}H_{86}N_{14}O_{12}S$	1190.62703
Angiotensin II (A)	DRVYIHPF	$C_{50}H_{71}N_{13}O_{12}$	1045.53451
Bombesin (B)	pGlu-QRLGNQWAVGHLM-NH_2	$C_{71}H_{110}N_{24}O_{18}S$	1618.81506
Lys^8-vasopressin	CYFQNCPKG-NH_2 [Disulfide Bridge: 1-6]	$C_{46}H_{65}N_{13}O_{12}S_2$	1055.43171
Arg^8-vasopressin	CYFQNCPRG-NH_2 [Disulfide Bridge: 1-6]	$C_{46}H_{65}N_{15}O_{12}S_2$	1083.43785
P1	KMGIHACVEFK	$C_{56}H_{91}N_{15}O_{14}S_2$	1261.63113
Insulin		$C_{254}H_{377}N_{65}O_{75}S_2$	5601.71259

5.2.2 Reaction of peptides with Cisplatin

Aqueous solutions of each peptide (1mM) and cisplatin (0.5 mM) were prepared and mixed to give a peptide:cisplatin mixture at a molar

ratio of 1:2 and then diluted to a final peptide concentration of 20 μM. The mixtures were incubated at 37 °C for 24 h and then diluted to 0.4 μM with 50% ACN–1% CH_3COOH for MS analysis. For reactions at different pH values (3, 7, and 10), the pH values of peptide:cisplatin mixtures were adjusted by adding CH3COOH or NH_4OH. Insulin (0.2 mM) was reacted with cisplatin at a molar ratio of 1:8 to a final protein concentration of 20 μM, and then incubated at 37 °C for 24 h before MS analysis.

5.2.3 FT ICR Mass Spectrometry

ESI–MS was performed on a Bruker SolariX FT ICR mass spectrometer with an ESI source and a 12 T actively shielded magnet. Samples were electrosprayed at 0.4 μM concentration in 50:50 ACN:H_2O with 1% acetic acid. For collisionally activated dissociation (CAD) experiments, the parent ions were isolated using the quadrupole, and were fragmented in the collision cell, and then transmitted into the ICR for detection. For electron capture dissociation (ECD) experiments, the parent ions were isolated in quadrupole and externally accumulated in the collision cell for 3 – 20 s. After being transferred and trapped in the Infinity ICR cell, ions were irradiated with 1.5 eV electrons from a 1.7 A heated hollow cathode dispenser for 10 to 120 ms. One millisecond single frequency shot at *m/z* 100 was given at the beginning of the ECD event to activate ions and improve the overlap between electrons and ions. Spectra using 4 M data sets were recorded from *m/z* 150 to 3000 Da.

5.2.4 Ion Mobility Mass Spectrometry

Ion mobility–mass spectrometry/mass spectrometry (IM–MS/MS) experiments were performed by means of a hybrid quadrupole–travelling wave ion mobility–orthogonal acceleration time–of–flight (oa–TOF) mass spectrometer (Synapt G2, Waters, Manchester, UK). The time–of–flight analyzer was mass calibrated using sodium iodide (NaI) for ESI experiments. Samples were electrosprayed at 0.4 μM concentration in 50:50 ACN:H_2O with 1% acetic acid. Data were acquired using the sensitivity mode of the instrument (resolution 20,000 FWHM). As described elsewhere,[259] the Synapt G2 Tri–wave region comprises three travelling–wave (T–Wave)–enabled stacked–ring ion guides: trap cell, ion mobility cell and transfer cell. Separation in the ion mobility cell was carried out using a T–Wave height of 40 volts and a velocity of 1200 m/s in full scan mode. During MS/MS acquisition all CAD experiments took place in the transfer cell, after precursor ion separation in the mobility cell. The collision voltage within the transfer cell was optimized to 30 volts. Data acquisition and processing were carried out using MassLynx (v4.1) software (Waters, Manchester, UK).

5.3 Results and discussion

CAD and ECD experiments on a 12 T Bruker solariX FTICR MS instrument and IM–MS/MS (CAD) experiments on a Waters Synapt G2 were performed separately for Pt(II) adducts of substance P (for sequence see Table 5.1) to explore the identification of conformational isomers.

5.3.1 Analysis of Cisplatin–Substance P Adducts Using CAD/ECD FTICR MS and IM–MS/MS (CAD)

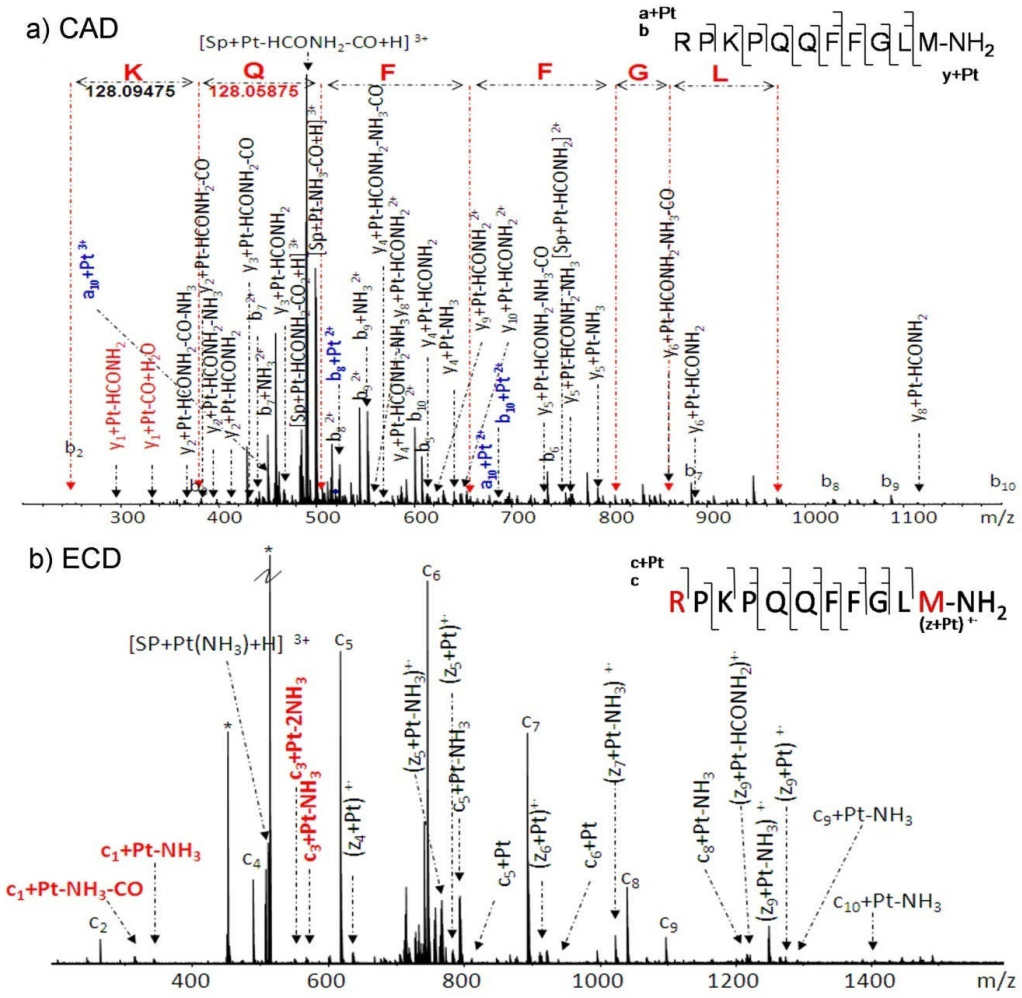

Figure 5.1 MS/MS spectra of the substance P:cisplatin (1:2) sample. (a) CAD spectrum of the $[Sp + Pt(NH_3) + H]^{3+}$ ions at *m/z* 520; (b) ECD spectrum of $[Sp + Pt(NH_3) + H]^{3+}$ ions at *m/z* 520. "*" represents chemical noise.

A CAD experiment on the platinum(II) adducts of substance P (Sp), $[Sp + Pt(NH_3) + H]^{3+}$ ions at *m/z* 519.9, was first performed in a FTICR MS instrument. As shown in Figure 5.1a, a series of ions corresponding to y_n + Pt accompanied by neutral losses were detected. The detection of

y_1 + Pt – $HCONH_2$ peak indicates that cisplatin binds to the C–terminal Met amide residue. In addition, $(b_8 + Pt)^{2+}$ and $(a_{10} + Pt)^{2+}$ ions were also observed, which suggests that platinum can also bind to some other amino acid sites in the sequence, other than the Met residue, although the observation of b_2 to b_{10} ions without Pt–modification does not provide additional information.

An interesting feature which reflects the conformation of substance P was observed in the CAD spectrum of the $[Sp + Pt(NH_3) + H]^{3+}$ ion (the same feature as in the CAD spectra of $[Sp + 3H]^{3+}$ and $[Sp + 2H]^{2+}$ ions). As shown on top of Figure 5.1a, the observation of b_2, b_3 and a series of b ions (b_5 – PQ to b_{10} – PQ) with the loss of PQ residues in the middle of the sequence. It is known that b–ions tend to form cyclic structures and a cyclic structure of b–ions from substance P has been previously reported,[260-262] in which the observation of series of cm–Lys fragmentations in ECD of several b–ions from Substance P suggested that the macro–cyclic structure may also be formed by connecting the C–terminal carbonyl group and the ε–amino group of the lysine side chain. However, losing PQ residues and forming a series of b–ions without scrambling the sequence from such a macro–cyclic structure is unlikely. The results observed here suggest that there might be certain interaction between the ε–amino group of the Lys3 side chain to the carboxyl group of Glu6, which could also explain the observation of $c_4^{\bullet}$ and $c_5^{\bullet}$ ions in the ECD spectrum of Sp.[86] Due to the intramolecular interaction of Lys3 and Glu6 residues, $c/z^{\bullet}$ ion pairs are held together by hydrogen bonding and thus lead to intra–complex hydrogen radical transfer and formation of $c^{\bullet}/z$

ions.

Figure 5.1b shows the ECD spectrum of the $[Sp + Pt(NH_3) + H]^{3+}$ ion at m/z 519.9. The observation of the $[Sp + Pt + H - CH_3S]^{2+\cdot}$ ion and a series of $z_m^{\cdot}$ + Pt – NH_3 ions (m= 4~7, 9) is consistent with the CAD results, that is, Pt binds to the C–terminal Met site. Unexpectedly, a group of ions corresponding to a_1 + Pt, b_1 + Pt, b_3 + Pt – NH_3, and b_3 + Pt ions were observed, which indicates that platinum also coordinates to the amine group of residue Arg1 or the N–terminal amine group.

As suggested from the CAD data for the $[Sp + Pt(NH_3) + H]^{3+}$ ions, substance P likely has multiple conformations in the gas phase. Pt–modified and unmodified substance P species were therefore analyzed by IM–MS/MS (CAD). The arrival time distribution (ATD) for substance P indicated the presence of conformers. Two conformers for the doubly–charged Sp ions were observed; however there was no significant difference between these two conformers in terms of product ion CAD spectra due to the close size of the cross sections of the two conformers. Figure 5.2A shows the arrival time distribution (ATD) of the $[Sp + Pt(NH_3) + H]^{3+}$ ions. Three conformers (a), (b), and (c) were observed. To further localize the Pt–modification sites, each of the three conformers was further dissociated in the transfer region after the T–wave ion mobility separation and the corresponding CAD spectrum of each conformer is shown in Figure 5.2B.

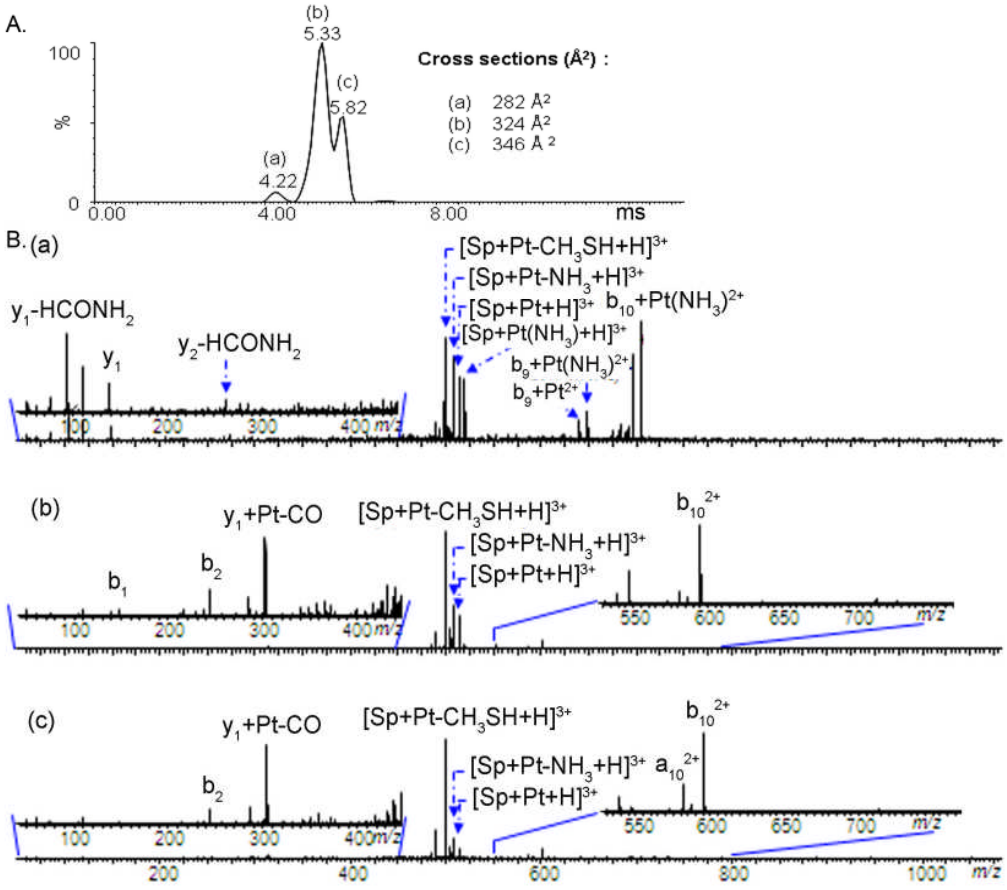

Figure 5.2 A). The arrival time distribution (ATD) of three conformers of the $[Sp + Pt(NH_3) + H]^{3+}$ ions (the cross section of each conformer (a, b, and c) is listed as insets of Figure 2A; **B).** Corresponding MS/MS (CAD) ion mobility spectrum for each conformer, (a) CAD spectrum of conformer a (AT=4.22 ms); (b) CAD spectrum of conformer b (AT=5.33 ms); (c) CAD spectrum of conformer c (AT=5.83 ms). The rest of the insets are the expanded *m/z* regions from 50 to 450 and 500 to 800.

It is clear that for conformer (a) (see Figure 5.2B_a), Pt binds to both the Met(S) residue and an amine group (Arg, Lys, or the N–terminus) as suggested by the observation of $b_9 + Pt^{2+}$ and $[Sp + Pt – CH_3SH + H]^{3+}$ ions. The result is in line with the ATD observation (see Figure 5.2A, the arrival time for the conformer (a) (4.22 ms) is shorter than other

conformers), that a cyclized [Sp + Pt(NH_3) + H]$^{3+}$ ion has a smaller cross section (282 Å) and travels faster compared to its linear form. For conformers (b) and (c) (Figure 5.2B_b and 5.2B_c), Pt(II) coordinates to Met11 in each case and no further binding site information was obtained. One difference between conformers (b) and (c) is that the third conformer (c) is more prone to further dissociation as observed in the corresponding MS/MS spectra. The cross section differences between conformers (b) and (c) can be either due to Pt(NH_3)$^+$ binding to different Sp conformers or the other two binding sites (except amine and thioether groups) for Pt(II) on Sp are different.

The separation of three different conformers of the [Sp + Pt(NH_3) + H]$^{3+}$ species (Figure 5.2) greatly simplified the data analysis for the mixture of conformers (Figure 5.1a). However, in terms of obtaining detectable binding information, the use of CAD fragmentation coupled to ion mobility instrument is not ideal, as can be seen from Figure 5.2B; the fragments obtained are rather limited. In addition, labile modifications can be lost depending on the collision energy used; therefore, the exact binding sites are often not observed (see Figure 5.1a and Figure 5.2). On the other hand, although the ions sampled for the ECD experiment on the FTICR are conformational mixtures, more Pt–binding information was obtained; the Pt–binding sites at the N–terminus were further localized to amine groups of either Arg1 or the N–terminal NH_2 (Figure 5.1b). In addition, the observation of the [Sp + Pt + H – CH_3S•]$^{2+\cdot}$ ion indicates that the radical–mediated side–chain loss of CH_3S• may be used as an indicator of platinum binding to a Met residue. Thus, a series of peptides

with potential Pt–binding sites were reacted with cisplatin to explore the possibility of using ECD side chain losses to obtain more Pt–binding information.

5.3.2 ECD of Cisplatin–Peptides Adducts

5.3.2.1 Interaction of Cisplatin with His–containing Peptides—Angiotensin II (A) and Bombesin (B)

ECD spectrum of angiotensin II:cisplatin (1:2) adducts, the [A + $Pt(NH_3)_2Cl$ + H]$^{3+}$ ion at *m/z* 437 is shown in Figure 5.3a. Observation of z_3 + Pt indicates that platinum binds to the His(N) residue at either N atom, and b_2 + Pt suggests that platinum also coordinates to either the carboxyl group of Asp1 or the amine group of Arg2, or the N–terminal NH_2. ECD spectrum of the bombesin:cisplatin (1:2) adduct, the [B + $Pt(NH_3)$ + H]$^{3+}$ ion, at *m/z* 610.6, is shown in Figure 5.3b. A series of c ions from c_3 to c_9 and c_{11}, c_{12} + Pt^{2+}, and c_{12} + Pt – NH_3 indicates the binding of platinum to His12 and the product ions of [B + Pt – CH_3SH + H]$^{2+\cdot}$ show coordination of Pt to Met14. In addition, the observation of c_3 + Pt – NH_3 suggests that platinum also coordinates to the amine group of Arg3 or the N–terminal NH_2.

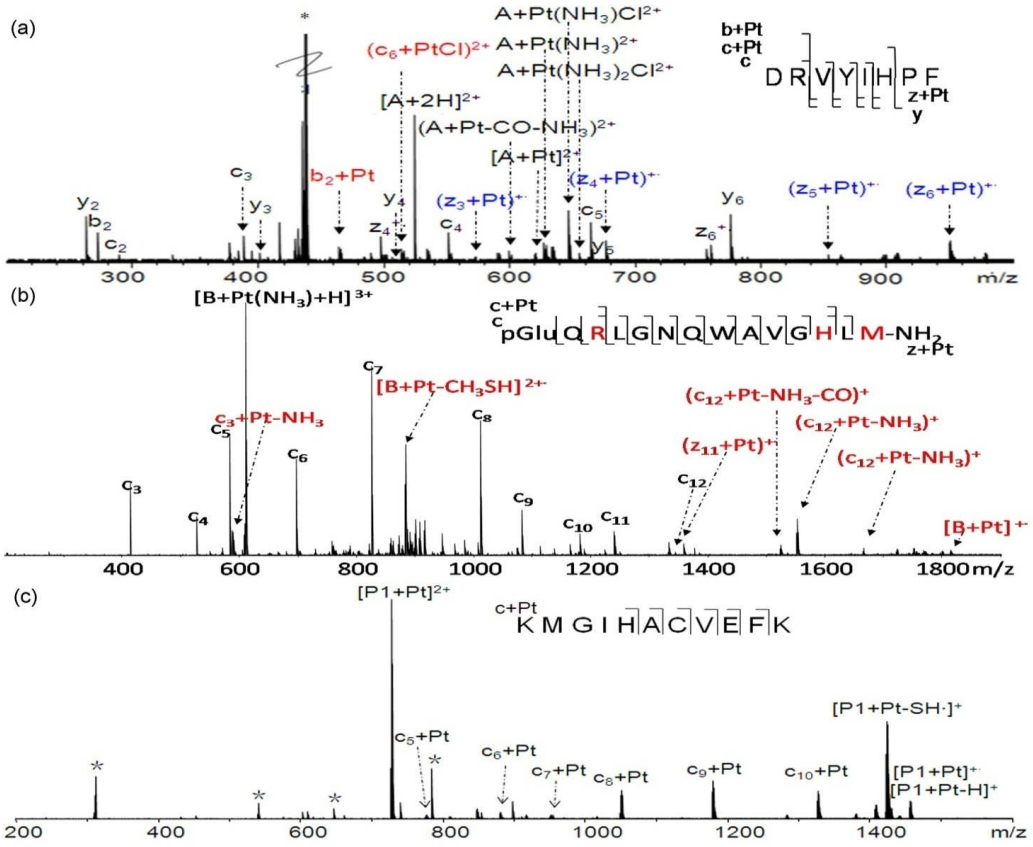

Figure 5.3 ECD spectra of peptide-cisplatin complexes. (a) $[A+Pt(NH_3)_2Cl+2H]^{3+}$ ions at *m/z* 520 in angiotensin II:cisplatin (1:2) sample, (b) $[B+Pt(NH_3)+H]^{3+}$ ions at *m/z* 620 in bombesin:cisplatin (1:2) sample, and (c) $[P1+Pt]^{2+}$ ions at *m/z* 728 in P1:cisplatin (1:2) sample. "*" represents noise.

5.3.2.2 Reaction of Cisplatin with Peptides containing Disulfide Bonds

Arg^8–vasopressin and Lys^8–vasopressin are disulfide–containing peptides and share similar sequences. No species corresponding to cisplatin binding to either Arg^8–vasopressin or Lys^8–vasopressin was observed, even when the reactions were further extended to 72 h, although it has been previously reported that disulfide bonds can be

cleaved by reacting with a platinum(II) complex [Pt(Met)Cl_2],[20–21, 263] Noting the fact that the rate of reaction of [Pt(Met)Cl_2] towards the disulfide peptide GSSG is 100–fold faster than cisplatin, thus the result obtained here is not surprising. [263] In addition, Morenao–Gordaliza and coauthors propose that the reactivity of cysteines participating in disulfide bonds is comparable to N–donors, including the N–terminus and His. [20–21] Their observation of Pt binding to cysteine disulfide sulfurs is more likely due to the reaction conditions used.

5.3.2.3 Reaction of Cisplatin to a Peptide (P1) with Potential Multiple binding Sites

Peptide 1 (KMGIHACVEFK) is a small peptide which was synthesized to study the binding of cisplatin to several potential sites, including Cys(S), His(N), Glu(O), and amine groups of N–terminus and Lys(N). the ECD spectrum of $[P1 + Pt]^{2+}$ at *m/z* 728 (Figure 5.3c), shows that all four of the original ligands of cisplatin have been displaced; however, the observation of c_5 + Pt to c_{10} + Pt fragment ions only localizes the Pt to the first five amino acids.

Interestingly, platinum(II) was found to bind to amine groups of either the N–terminus or Arg in both Pt–modified substance P and bombesin (Met–containing peptides) species, but not in Arg^8–vasopressin and Lys^8–vasopressin (no Met residues). It has been previously reported that methinione sulfur is often a kinetically preferred Pt(II) binding site.[264] At pH>6, the initial sulfur coordination is followed by a pH–dependent migration of the platinum from sulfur to the amine group.[265-267] To examine the conditions under which platinum can bind to the amine

groups of Arg or Lys; further experiments were carried out at different pH values and monitored by MS.

5.3.3 Intramolecular Migration of Pt(II) from Met(S) to Amine (N)

Peptides Sp_{1-7}, Sp_{2-11}, and Sp were reacted with cisplatin at pH values of 3, 7, and 10. For Sp_{1-7}, a peptide with amine groups (Arg, Lys, and N–terminus) but without a Met residue, no coordination of platinum was observed at pH range of 3–10 (Figure 5.4 (a–1), (b–1), and (c–1)). However, non–covalent interactions between Sp_{1-7} and cisplatin and its hydrolysis products were detected, such as Sp_{1-7} + $Pt(NH_3)_2(H_2O)(CH_3COO)$ and Sp_{1-7} + $Pt(NH_3)_2Cl_2$ at pH3, Sp_{1-7} + $Pt(NH_3)_2(H_2O)_2$ and Sp_{1-7} + $Pt(NH_3)_2Cl_2$ at pH 7, and Sp_{1-7} + $Pt(NH_3)_4$ at pH 10. The coordination of cisplatin to the Met–containing peptides Sp_{2-11}, and Sp was observed at both pH 3 and 7, but not at pH 10 (Figure 5.4). ECD experiments on Sp_{2-11} + $Pt(NH_3)_2Cl$ and Sp + $Pt(NH_3)$ at pH 3 and 7 were further carried out and are shown in the supporting information as Figures D.1 and D.2. The observation of c_5 + Pt – H in ECD of Sp_{2-11} + $Pt(NH_3)_2Cl$ suggests that platinum can bind to the amine group of Lys or the N–terminus; similarly, the observation of a_1 + Pt and b_1 + Pt fragments in ECD of Sp + $Pt(NH_3)$ species suggests that platinum can bind to the amine of the Arg residue or the N–terminus. More importantly, the lack of binding in the absence of methionine suggests that binding of Pt to Lys or Arg may arise from the intramolecular migration of Pt(II) from Met(S) to amine groups.

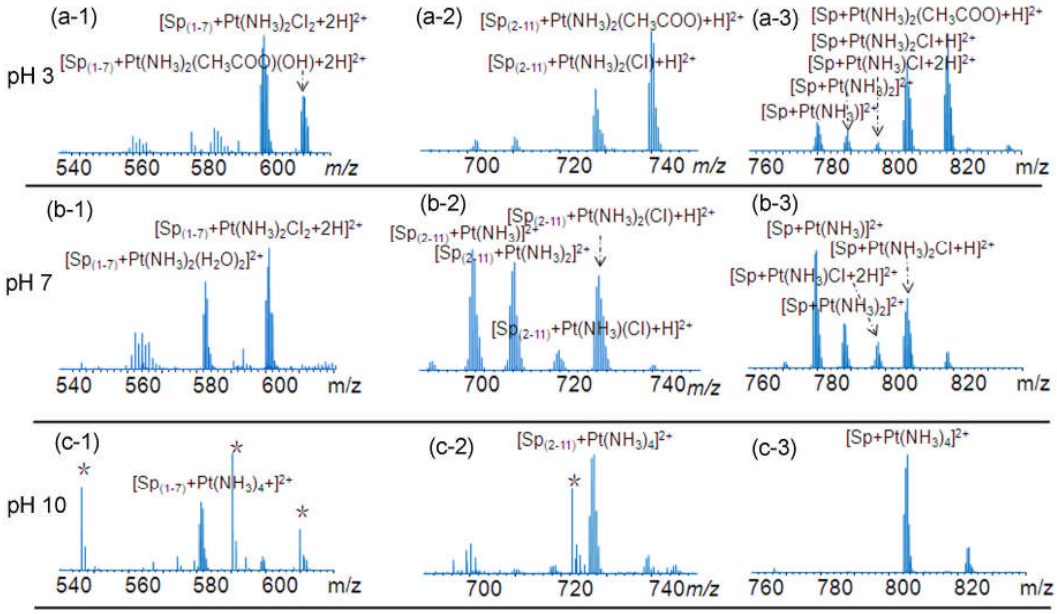

Figure 5.4 MS spectra of peptide–cisplatin adducts at different pH values. (a–1), (b–1), and (c–1) are the MS spectra of $Sp_{(1–7)}$–cisplatin adducts at pH 3, 7, and 10; (a–2), (b–2), and (c–2) are the MS spectra of $Sp_{(2–11)}$–cisplatin adducts at pH 3, 7, and 10; and (a–3), (b–3), and (c–3) are the MS spectra of Sp–cisplatin adducts at pH 3, 7, and 10. "*" represents noise.

These results are not entirely in line with previously published results, in which it was suggested that the migration of the platinum moiety from sulfur to the amine group occurs under basic conditions rather than under acidic conditions as observed here.[265-267] The differences of experimental conditions, including the use of ammonium hydroxide solution (NH_4OH) to adjust the pH to basic values, thus many contribute to the lack of observation of Pt–peptide coordination complexes under basic conditions. Cisplatin undergoes hydrolysis and reacts with NH_3 groups under basic conditions; therefore, the formation of

$[Pt(NH_3)_4]^{2+}$ species hinders the further reaction of $[Pt(NH_3)_4]^{2+}$ with peptides because the Pt–NH_3 bonds are stable towards displacement compared to Pt–Cl bonds (Figure 5.4c). Thus, particular attention needs to be given to the chemicals used to adjust pH values when using cisplatin as a cross–linking reagent. The observation of Pt–N bound species under acidic conditions indicates that the migration of platinum from sulfur to nitrogen can occur at least in the pH range of 3 to 10. The reason that it has not been previously reported might be due to the lower sensitivity of nuclear magnetic resonance (NMR) used in the previous studies compared to the MS methods used here.[265-267]

5.3.4 ECD Side Chain Losses Due to Pt–binding

The ECD side chain losses in peptides have been previously used to improve peptide sequencing.[72, 75, 218, 268, 269] For Pt–modified peptides, it has been observed that when platinum binds to the side chain of Met, it gives a signature side chain loss of CH_3SH in ECD. Here, to explore the possibility of using side chain losses to further localize the Pt–modification sites, the regions corresponding to ECD side chain losses are shown in Figure 5.5. In addition, the side chain loss information due to Pt–binding from the charge reduced M + Pt species in comparison with side chain losses of unmodified peptides obtained from the literature are summarized in Table 5.2.[72, 75, 218, 268, 269]

Table 5.2 List of observed ECD side chain losses from charge reduced species (normal peptides[a] and Pt–modified peptides[b])

	Normal peptides		Pt–modified peptides	
Amino Acid	Chemical Formula	Exact Mass	Chemical Formula	Exact Mass
Arg	$C_4H_{11}N_3$	101.09530	NH_2•	16.01926
	CH_3N_2	43.02962		
Lys	C_3H_8N	58.06567	NH_2•	16.01926
	C_4H_9N	71.07350		
Cys	C_2H_4NO	58.02929	SH•	32.98044
	$C_2H_4NO + NH_3$	75.05584		
	$C_2H_4NOS + NH_3$	107.02791		
	C_2H_5NO	59.03711		
	C_2H_4NOS	90.00136		
Met	C_2H_5S	61.01120	CH_3•	15.02403
			CH_3S•	46.99664
	$C_3H_6S + NH_3$	91.04557	CH_3SH	48.00337
Asp	$C_2H_4O_2$	60.02113	CO_2[c]	43.98983
	$CHO_2 + NH_3$	62.02420		
Glu	$C_2H_4O_2$	60.02113	CO_2[c]	43.98983
	$C_2H_3O_2 + NH_3$	76.03985		
	$C_3H_4O_2 + NH_3$	89.04768		
His	$C_4H_4N_2$	80.03745	—	—
	$C_3H_3N_2$	67.02962		

[a]Results obtained from literature. [b] To simplify the interpretation of spectra, the side chain losses were calculated based on the *m/z* of the charge–reduced M + Pt species in the spectra regardless of the original form of the Pt–peptide complex. [c]The loss of CO_2 has been previously observed

in ECD spectra of deamidated samples also from z• ions. Cautions still need to be given when using loss of CO_2 as an indicator of Pt(II) binding to carboxyl groups of Asp or Glu. However, if the Pt–complex bound to CO or CO_2 was observed at low *m/z* region,[23] it will confirm the binding of Pt to carboxyl groups.

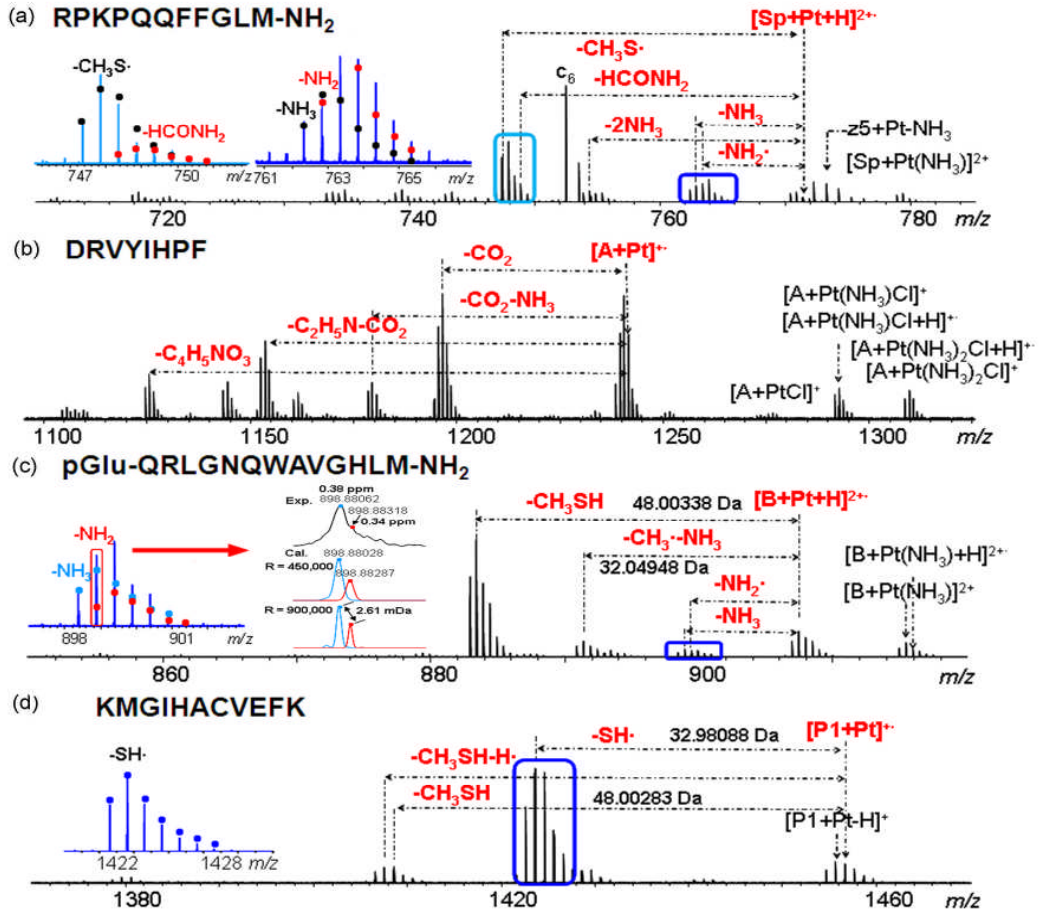

Figure 5.5 The side chain loss region from the charge–reduced M + Pt species. (a) $[Sp + Pt + H]^{3+}$, (b) $[A + Pt]^{2+}$, (c) $[B + Pt + H]^{3+}$, and (d) $[P1 + Pt]^{2+}$. The insets show the fragment ions with the diagnostic side chain losses due to Pt–binding.

To simplify the interpretation of spectra, the side chain losses were

calculated based on the *m/z* of the charge–reduced M + Pt species in the spectra regardless of the original form of the Pt–peptide complex. All the side chain losses were calculated based on the *m/z* of the $[Sp + Pt + H]^{2+\bullet}$ species. Taking Figure 5.5a for example, side chain losses of NH_3, $NH_2\bullet$, $HCONH_2$, and $CH_3S\bullet$ were observed and the detailed spectra of fragments with side chain losses are shown on the left–hand side of Figure 5.5a. Fragments at *m/z* 748 are a mixture of two groups of isotopic ions, $[Sp + Pt + H - CH_3S\bullet]^{2+}$ and $[Sp + Pt + H–HCONH_2]^{2+\bullet}$, and fragments at *m/z* 763 are a mixture of isotopic ions of $[Sp + Pt + H - NH_2\bullet]^{2+}$ and $[Sp + Pt + H - NH_3]^{2+\bullet}$. Similarly, side chain losses of CO_2 and other neutral losses along with CO_2 were observed in the ECD spectra of $[A + Pt(NH_3)_2Cl + H]^{2+}$ (Figure 5.5b); side chain losses of NH_3, $NH_2\bullet$, and $CH_3S\bullet$ in the ECD of $[B + Pt(NH_3) + H]^{3+}$ (Figure 5.5c), and neutral losses of $SH\bullet$ and CH_3SH in the ECD of $[P1 + Pt]^{2+}$ (Figure 5.5d).

Peak overlapping was commonly observed in all the spectra as shown in the insets of Figure 5.5. Taking the inset of Figure 5.5c for an example, for the peaks observed at *m/z* region of 898 to 901, it is apparent that they are overlapping peaks of two groups of ions, assigned as $[B + Pt + H - NH_3]^{2+\cdot}$ and $[B + Pt + H - NH_2\cdot]^{2+\cdot}$. The theoretical mass difference between the isotopic peak A + 1 of $[B + Pt + H - NH_3]^{2+\cdot}$ (898.88028) and the isotopic peak A of $[B + Pt + H - NH_2\cdot]^{2+\cdot}$ (898.88287) is 2.61 mDa. In theory, it would need nearly a 1 M resolution to resolve these two peaks. Based on the observation from the inset spectrum, the peak height ratio between $[B + Pt + H - NH_3]^{2+\cdot}$ (A + 1) and $[B + Pt + H - NH_2\cdot]^{2+\cdot}$ (A) is about 2:1; the theoretical peaks were therefore simulated to

show how much resolution would be needed to separate these two peaks with a peak height ratio of 2:1. As can be seen from the inset of Figure 5.5c, resolution of 0.9 M is needed to fully resolve these two peaks and they can be partially separated under the resolution of 0.45 M. On top of the theoretical simulations, it shows the experimental spectrum of peaks at *m/z* 898.88. The peak at m/z 898.88062 can be assigned confidently as $[B + Pt + H - NH_3]^{2+\cdot}$ (A + 1) with a sub–ppm mass accuracy (0.4 ppm). Although the mass accuracy for the peak assigned as $[B + Pt + H - NH_2\cdot]^{2+\cdot}$ (A) is also within sub–ppm range (0.34 ppm), the peak intensity is rather low and can be seen as an artifact under certain circumstances. Attempt to further improve the resolution was made; however wasn't successful due to the transient damping. The signal damping is likely because in the infinity cell, the electric field that ions experience is inhomogeneous, which causes the peak coalescence of these two closely spaced masses.[270, 271]

The observation of neutral losses of SH• and CH_3SH in the ECD of $[P1 + Pt]^{2+}$ is consistent with the displacement of the original two NH_3 ligands from cisplatin due to the *trans*–labilization effect.[4] By comparing the ECD side chain losses observed from Pt–modified peptides with those reported from normal peptides, as listed in Table 5.2, it can be seen that radical–mediated side chain losses in Pt–modified peptides are different from the side chain losses from unmodified peptides. Although the mechanism of the side chain losses in ECD of the Pt–modified peptides is not yet clear, the side chain losses of CH_3SH and CH_3S• from Met residue, NH_2• from amine groups, CO_2 from Asp or Glu residue, and

SH• from Cys residue are unique from the ECD side chain losses of unmodified peptides, and thus can be used as signatures to locate the Pt–modification sites rapidly.

5.3.5 Identification of the inter–chain crosslinking sites for cisplatin on insulin dimer by top–down ECD

To further test the methodology and the data interpretation approach proposed above, insulin was chosen for cisplatin modification. Insulin is a small protein with two peptide chains (A and B) linked by two inter–chain disulfide bonds, containing also an intra A–chain disulfide bond. Previously, the interaction of cisplatin with insulin has been studied using a top–down CAD mass spectrometric approach by Moreno–Gordaliza *et al.*[141, 143] However, due to the limitation of the resolution on the Linear Ion Trap (LIT) instrument used, a cisplatin inter–chain cross–linked insulin species, insulin + $Pt(NH_3)_2$ + insulin, was not reported. Therefore, this system was used for testing the top–down ECD approach and data analysis strategy for identification of inter–chain cross–linking sites of cisplatin on a protein with multiple potential Pt–binding sites (6 Cys, 2 His, 4 Glu, 1 Arg, 1 Lys, and the N–terminus).

In solution without the presence of metal ions, insulin exists as a mixture of monomer, dimer, hexamer, and higher order aggregates.[272] To investigate whether the observed species, insulin + $Pt(NH_3)_2$ + insulin, consists of $Pt(NH_3)_2^{2+}$ binding to a single insulin of the insulin dimer rather than cross–linking the two insulin molecules, the sample was diluted with 50% acetonitrile and 1% CH_3COOH to destabilize any noncovalent interactions. In addition, in–source–dissociation (ISD) voltages up to 70

V were applied because noncovalent interactions are prone to dissociation under collision activation condition. No signal intensity decrease in the insulin + $Pt(NH_3)_2$ + insulin species was observed as compared to the intensity of insulin + $Pt(NH_3)_2$ + insulin ions under conditions with and without ISD (see Figure D.3a and 3b), which suggests that insulin + $Pt(NH_3)_2$ + insulin is a covalently cross–linked product. It is notable that the intensity of insulin + $Pt(NH_3)_2$ + insulin ions is 100 times lower than the most intense peak in the spectrum, so hexapole accumulation was used in FTICR MS to significantly improve the quality of the tandem fragmentation spectra of this low intensity species.

Figure D.3c shows the CAD spectrum of [insulin + $Pt(NH_3)_2$ + insulin + 7H]$^{9+}$ species at *m/z* 1300. The main fragment peaks observed are the charge separated species [I + Pt + 3H]$^{5+}$ and [I + 4H]$^{4+}$, so no detailed cisplatin binding site information was obtained. In contrast, as shown in Figure 5.6a, the ECD spectrum of the [Insulin + $Pt(NH_3)_2$ + Insulin + 8H]$^{10+}$ species at *m/z* 1170 is more informative, but also harder to interpret. However, by using the data analysis method established above, a complementary ion pair which contains the Pt–binding information can be easily found as shown in Figure 5.6b. The observation of the [I + $Pt(NH_3)_2(NH_2)$ + 4H]$^{5+\cdot}$ and [I + 4H – NH_2]$^{4+}$ species indicates that one of the $\{Pt(NH_3)_2\}^+$ cross–linking sites is an amine group, which significantly localize one of the cross–linking sites to an amine group of Arg, Lys or the N–terminus. Hence, one of the cross–linking sites can be readily identified as Lys29 in B chain with the observations of ABc_{19}^{3+} to ABc_{26}^{3+} series and $(ABc_{29} + Pt)^{3+}$ ions (see the right–hand

spectra of Figure 5.6c).

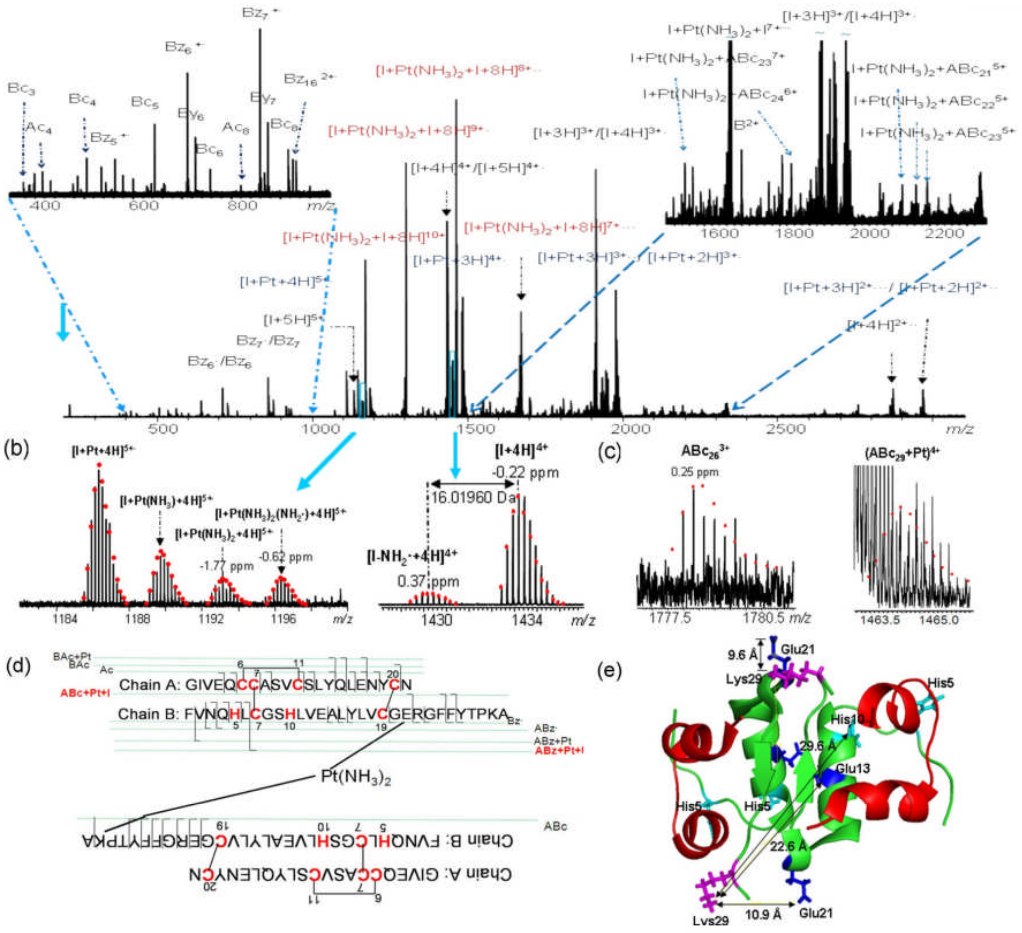

Figure 5.6 (a) ECD spectra of the [insulin + $Pt(NH_3)_2$ + insulin + 8H]$^{10+}$ ion at *m/z* 1170, the insets show the details of the ECD spectrum; (b) complementary ion pairs [I + $Pt(NH_3)_2(NH_2\cdot)$ + 4H]$^{5+\cdot}$ and [I–$NH_2\cdot$ + 4H]$^{5+}$; (c) fragment ions $ABc_{26}{}^{3+}$ and $(ABc_{29} + Pt)^{4+}$; (d) fragmentation scheme for insulin + $Pt(NH_3)_2$+insulin species (all the cleavages are mainly labeled in one insulin structure as $\{Pt(NH_3)\}^{2+}$ cross–linked two species are identical here); (e) crystal structure of a insulin dimer (4E7T).[52] The chains and amino acids are color–coded as follow: A–chains in red, B–chains in green, His in cyn, Glu in blue, and Lys in pink.

Figure 5.6d presents the observed fragmentation diagram for the

insulin + $Pt(NH_3)_2$ + insulin species. The observation of fragments ABc_{21} + Pt + I and ABz_{24} + Pt + I can further narrow the other cross–linking site down to a His10, Glu13, or Glu21 or in B–chain; however, no further information of radical–mediated side chain loss was observed in the ECD spectrum of the cross–linked species. The absence of further ECD side chain loss information can be due to either of the following reasons: (1) Pt(II) binds to another amine group, thus yielding the same fragment as observed; (2) Pt(II) binds to a His residue, which gives no characteristic ECD side chain loss as shown in Table 5.2; or (3) Pt(II) might bind to any possible residue but no observable fragments were detected due to low signal–to–noise level.

To aid location of the other Pt–binding site, the crystal structure of an insulin dimer was examined as shown in Figure 5.6e.[273] The distances between the amine–N of Lys29 and the carboxyl–O of Glu13 or Glu21 range from 9.6 to 23.2 Å, and the distances between the amine–N of Lys29 and imidazo–N of His10 are over 29.6 Å. Although the distance between Lys29 and Glu21 (9.6 Å) is still out of the Pt–crosslinking range, it is clear that both the side chains of Lys29 and Glu21 are flexible, and the flexible motion could bring them within the crosslinking arm length of Pt.[130, 155] Therefore, it is still likely that $\{Pt(NH_3)_2\}^{2+}$ can cross–link Lys29 and Glu21 from different insulin B–chains.

5.4 Conclusions

This work demonstrates that radical–mediated side–chain losses from the charge–reduced M + Pt species (such as $CH_3S\bullet$ or CH_3SH from

Met, SH• from Cys, CO_2 from Glu or Asp, and NH_2• from amine groups, see Figure 5.5 and Table 5.2) can be characteristic indicators for rapid and unambiguous localization of the Pt–modification sites on certain amino acid residues. This approach therefore improves data interpretation and produces a more comprehensive picture of Pt–modifications. Although FTICR MS is powerful for analyzing complex biological samples, the ions sampled for fragmentation are often isomers; thus, the hyphenation of ion mobility spectrometry to a FTICR MS instrument might be the best approach to analyze complicated biological samples. In this way sample analysis could not only benefit from the separation of isomers in gas phase from ion mobility but also the superior resolving power, mass accuracy, and comprehensive fragmentation information from FTICR MS equipped with multiple fragmentation techniques (such as, CAD, ECD, ETD).

Chapter 6

Electron Capture Dissociation of Disulfide, Sulfur–Selenium, and Diselenide Bound Peptides[5]

6.1 Introduction

6.1.1 Electron capture dissociation of disulfide bonded peptides

Electron capture dissociation (ECD) was first introduced in 1998 by Zubarev *et al.* for the study of peptides and proteins.[40] It has been shown that ECD preferentially cleaves disulfide[57] and N–C_α bonds, preserves labile post–translation modifications, and gives high peptide sequence coverage compared with collisional activation methods,[93] which has made ECD a powerful and widely used tandem mass spectrometry technique for the study of peptides and proteins over the last decade.[35, 93, 94, 274, 275] Formation of a disulfide bond is a post–translation modification (PTM), which is critical to protein folding and structure stability. Characterization of disulfide–containing proteins remains challenging due to the fact that disulfide bonds rarely dissociate in the presence of a mobile proton using collisional activation methods.[276] Therefore, recently, studies of proteins or peptides containing disulfide bonds using ECD or related electron–based dissociation techniques have drawn wide attention.[153, 218, 277-281]

---

[5]This chapter has been partially/entirely reproduced from
Huilin Li, and Peter B. O'Connor. Electron Capture Dissociation of Disulfide, Sulfur–Selenium, and Diselenide Bound Peptides. *J. Am. Soc. Mass Spectrom.* **2012.** 23, 2001-2010. Copyright 2012, Springer.

6.1.2 ECD mechanisms of disulfide bond cleavage

Several mechanisms have been suggested for the cleavage of disulfide bonds by ECD. One is that the electron is initially captured into a Rydberg orbital centered on a positively charged site, and subsequently undergoes intra–molecular electron transfer to a nearby S–S σ* orbital to cleave the disulfide bond. Alternatively, electron is captured directly into the uncharged S–S σ* orbital to cleave the disulfide bonds, S• and S^- fragments to be formed through either mechanism, which subsequently convert to SH by hydrogen abstraction.[57-59, 63, 68, 282]

6.1.3 Study of selenium–containing compounds

Selenium and sulfur are in the same column at the element periodic table and share many common physicochemical properties. In proteins, selenium is mainly presented in the form of selenocysteine (Sec) and selenomethionine and plays a crucial role in biological systems, such as, elimination of peroxides and other oxidant agents, inflammation protection, and cancer prevention.[4, 283-285] The substitution of Cys by Sec has been carried out in a variety of systems. It was found that the substitution of Cys by Sec is much conserved, and only minor structural distortion and biological activity variations happened in all cases.[286-289] Therefore, due to the importance of disulfide bridges for protein structures and activity, the study of the reductive cleavage of diselenide (Se–Se) bonds has started to attract attention.[290, 291]

Although the studies of disulfide bound peptides or proteins by ECD have been investigated in the past few years,[153, 218, 277-281] little attention has been devoted to investigate the ECD behavior of diselenide

peptides or proteins. Previous studies have been mainly focused on using theoretical calculations to study the effects of electron capture on small diselenide compounds (XSeSeX'), such as $CH_3SeSeCH_3$, $CH_3SeSeOH$, CH3SeSeF, and such.[292-295] So, it is interesting to examine the ECD behavior of diselenide peptides compared with previous theoretical calculations, and also to examine the differences and similarities of the ECD fragmentation patterns among disulfide (S–S), sulfur–selenium (S–Se), and diselenide (Se–Se) peptides. Thus, in this study, a series of free cysteine and selenocysteine–containing peptides were reacted to form S–S, S–Se, and Se–Se bonds, and then studied using electron capture dissociation (ECD) with Fourier transform ion cyclotron mass spectrometry (FTICR MS).

6.2 Experimental section

6.2.1 Materials

Peptide P1 (K M G I H A C V E F K) was initially synthesized by GL Biochem Ltd (Shanghai, China) for the study of interaction with cisplatin for a different project. Here P1, as a peptide containing a free cysteine residue, was used for the study of disulfide bonds. Therefore, a selenocysteine–containing peptide, P2 (K G M I H A C(Se) V F E K), with a similar sequence as P1 was synthesized accordingly by the same company. Peptide P3 is a by–product of P2 synthesis, and its sequence was identified as K G M I H HA C(Se) V F E K by CAD and ECD sequencing. HPLC grade acetic acid (HAc) and methanol (MeOH) were

obtained from Fisher Scientific (Pittsburgh, PA, USA).

6.2.2 Formation of S–S, S–Se, and Se–Se bound peptides

Aqueous solutions of 1 mM P1 and 1 mM P2 (contains P3) were prepared. P1 and P2 solutions were mixed together at a molar ratio of 1:1 and further diluted to a concentration of 200 μM each. To form S–S, S–Se, and Se–Se bound peptides, 200 μM P1, 200 μM P2, and 200 μM P1:P2 (1:1) mixture were incubated separately at 37°C for 24 h (Table 6.1).

Table 6.1 Amino acid sequences of the peptides studied here. P1, P2, and P3 were obtained by synthesis, and rest of the S–S, Se–S, and Se–Se containing peptides obtained by reacting P1, P2, and P3 together.

Name	Sequence	Composition	Monoisotopic Mass (Da)
P1	K M G I H A C V E F K	$C_{56}H_{91}N_{15}O_{14}S_2$	1261.63113
P2	K G M I H A C(Se) V F E K	$C_{56}H_{91}N_{15}O_{14}SSe$	1309.57558
P3	K G M I H H A C(Se) V F E K	$C_{62}H_{98}O_{15}N_{18}SSe$	1446.63450
P1+P1	K M G I H A C V E F K K M G I H A C V E F K	$C_{112}H_{180}N_{30}O_{28}S_4$	2521.24662
P1+P2	K M G I H A C V E F K K G M I H A C(Se) V F E K	$C_{112}H_{180}N_{30}O_{28}S_3Se$	2563.19702
P2+P2	K G M I H A C(Se) V F E K K G M I H A C(Se) V F E K	$C_{112}H_{180}N_{30}O_{28}S_2Se_2$	2607.14417
P1+P3	K M G I H A C V E F K K G M I H H A C(Se) V F E K	$C_{118}H_{187}O_{29}N_{33}S_3Se$	2706.24998
P2+P3	K G M I H A C(Se) V F E K K G M I H H A C(Se) V F E K	$C_{118}H_{187}O_{29}N_{33}S_2Se_2$	2754.19443
P3+P3	K G M I H H A C(Se) V F E K K G M I H H A C(Se) V F E K	$C_{124}H_{194}O_{30}N_{36}S_2Se_2$	2891.25334

6.2.3 FTICR Mass Spectrometry

ESI–MS was performed on a Bruker solariX FTICR mass spectrometer with an ESI source and a 12 T actively shielded magnet. For MS experiments, P1, P2, and P1:P2 = 1:1 reaction products were mixed together at a molar ratio of 2:1:1 and diluted to yield a final concentration of 2 μM in 50:50 MeOH:H_2O with 1% acetic acid. Samples were then electrosprayed at a flow rate of 240 μL/h. For ECD experiments, the parent ions were first isolated in the first quadrupole and externally accumulated in the collision cell for 5 s. After being transferred to the ICR cell, ions were irradiated with 1.5 eV electrons from a 1.7 A heated hollow cathode dispenser for 80 ms. Each ECD experiment was repeated three times under the same condition, and 100 scans were averaged for each spectrum. For the need of higher resolution (over 250,000) to separate fragment peaks within ~5 mDa at *m/z* 1230 region, 4 M data sets were recorded from *m/z* 500 to 3000. Otherwise, 4 M data sets spectra were recorded from *m/z* 150 to 3000.

6.3 Results and discussion

Free selenium containing (P2 and P3) peptides are very reactive, and once dissolved, diselenide bonds are formed rapidly. In contrast, the formation of disulfide bonds between free cysteine containing peptides is relatively slow. After 24 h incubation of P1, P2, and P1:P2 = 1:1 at 37 °C, the reacted products were mixed and further diluted for MS analysis. As shown in Figure 6.1, a series of S–S, S–Se, and Se–Se species were formed during the incubation, including P1 + P1, P1 + P2, P2 + P2, P1 +

P3, P2 + P3, and P3 + P3 species. ECD experiments were performed on each triply–charged species, namely, P1 + P1 at *m/z* 841.42281, P1 + P2 at *m/z* 857.73795, P2 + P2 at *m/z* 873.38609, P1 + P3 at *m/z* 903.42365, P2+P3 at *m/z* 919.40558, and P3 + P3 at *m/z* 965.09283.

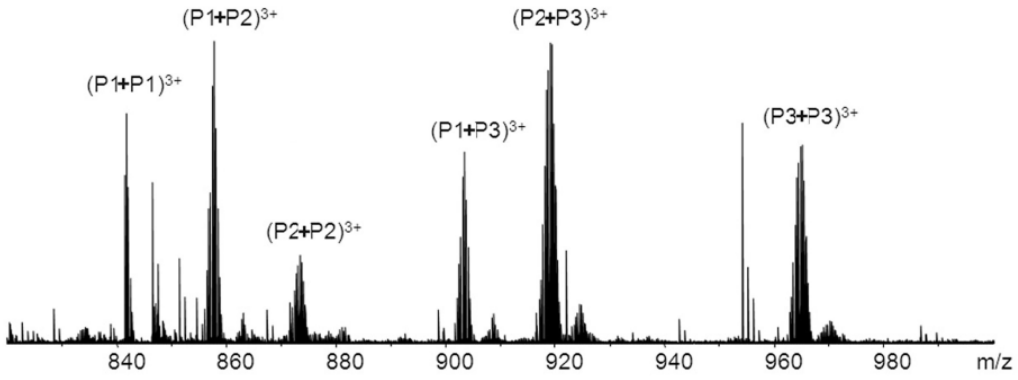

Figure 6.1 Full spectrum of P1, P2, and P1:P2=1:1 reaction product mixture.

To simplify the labelling of the fragment ions of ECD spectra, P1, P2, and P3 here represent half of the structures of S–S, S–Se, or Se–Se bonds–connected species. In elemental composition forms, P1 ($C_{56}H_{90}N_{15}O_{14}S_2$), P2 ($C_{56}H_{90}N_{15}O_{14}SSe$), and P3 ($C_{62}H_{97}O_{15}N_{18}SSe$), are 1.00782 Da lower compared with the corresponding free cysteine or free selenocysteine–containing peptides. Taking ECD spectrum of a disulfide bond–containing species (R_1 + R_2) for example, the cleavage of disulfide bonds by an electron generates R_1(S•) and R_2(SH). For P1 + P1, R_1 and R_2 are of the same, so P1 (S•) represents R_1(S•) and P1 (SH) represents R_2(SH), which differ by exactly 1.00727 Da.

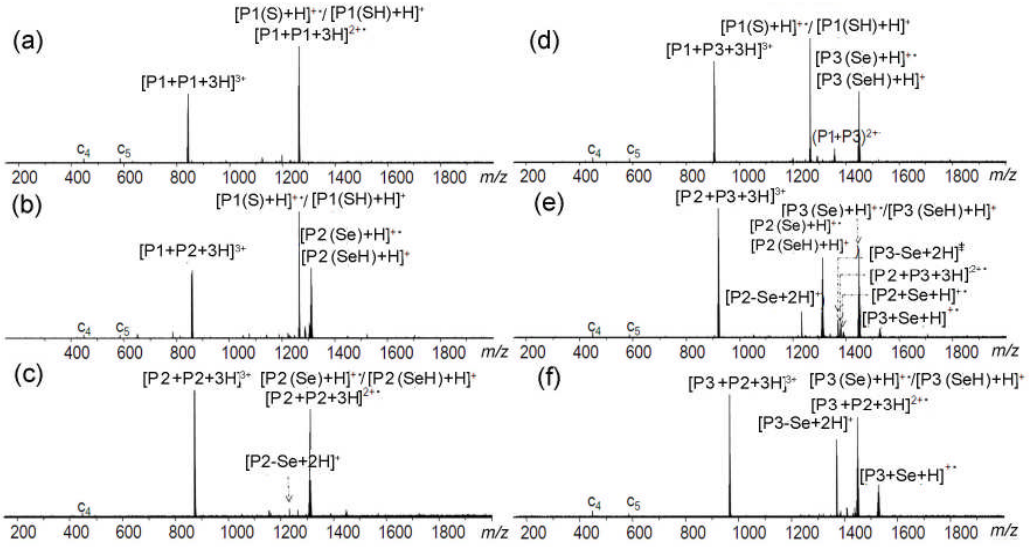

Figure 6.2 ECD spectra of triply–charged S–S (P1+P1), S–Se (P1+P2 and P1+P3), and Se–Se (P2+P2, P2+P3, and P3+P3) containing species. (a) $[P1+P1+3H]^{3+}$ at *m/z* 841.42281; [#] (b) $[P1+P2+3H]^{3+}$ at *m/z* 857.73795; (c) $[P2+P2+3H]^{3+}$ at *m/z* 873.38609; (d) $[P1+P3+3H]^{3}$ at *m/z* 903.42365^{+}; (e) $[P2+P3+3H]^{3}$ at *m/z* 919.40558^{+}; and (f) $[P3+P3+3H]^{3+}$ at *m/z* 965.09283.

Figure 6.2 shows the ECD spectra of S–S (P1 + P1), S–Se (P1 + P2, P1 + P3), and Se–Se (P2 + P2, P2 + P3, and P3 + P3) bonded peptides. The observed fragments can be mainly categorized into four classes based on cleavage sites. The first class includes normal c/z• cleavages without involving the cleavage of S–S, S–Se, or Se–Se bonds. The second class originates from the cleavage of S–S, S–Se, or Se–Se bonds. The third class is the result of cleavage of C–S or C–Se bonds,

[#] As the two chains of the disulfide–linked peptide P1 + P1 are identical, the charge reduced species $[P1 + P1 + 3H]^{2+\cdot}$ at *m/z* 1262.13450, the fragment ions $[P1(S)H]^{+\cdot}$ at *m/z* 1261.63059, and $[P1(SH+H]^{+}$ at *m/z* 1262.63841 are overlapped in the same *m/z* region (See Figure 6.2a). The same phenomena were observed for the P2+P2 and P3+P3 species as shown in Figure 6.2c and f.

and the fourth class involves the cleavages of both N–C_α and S–S, S–Se, or Se–Se bonds. To focus on the cleavages involving disulfide, sulfur–selenium, and diselenide bonds, the first class, normal c/z• cleavages, which do not involve the S–S, S–Se, or Se–Se bonds cleavages, are not discussed further.

6.3.1 Cleavages of S–S, S–Se, and S–Se bonds

Figure 6.2 shows that the fragmentation pattern is dominated by the cleavages of S–S and S–Se bonds for P1 + P1 (Figure 6.2a), P1 + P2 (Figure 6.2b), P1 + P3 (Figure 6.2d), and P2 + P2 (Figure 6.2c) species. In contrast, for P2 + P3 (Figure 6.2e) and P3 + P3 (Figure 6.2f) species, the cleavages of C–Se bonds competed with the dissociation of S–S and S–Se bonds. The cleavage of disulfide bonds by electron capture would generate P_1(S•) / P_2(SH) or P_2(S•) / P_1(SH) species (see Scheme 6.1a, where P_1 = P_2); similar fragmentation patterns also apply to S–Se and Se–Se species. The spectral details of the fragments originated from the cleavage of S–S, S–Se, and Se–Se bonds are shown in Figure 6.3. As expected, the ions detected were a mixture of both P(S•) and P(SH) forms for P1–containing species (see Scheme 6.1 a & 6.2 a), and P(Se•) and P(SeH) forms for P2 and P3 containing species (P represents a one chain of a inter–chain disulfide–linked peptide; the sequences of P1, P2, and P3 are shown in Table 6.1).

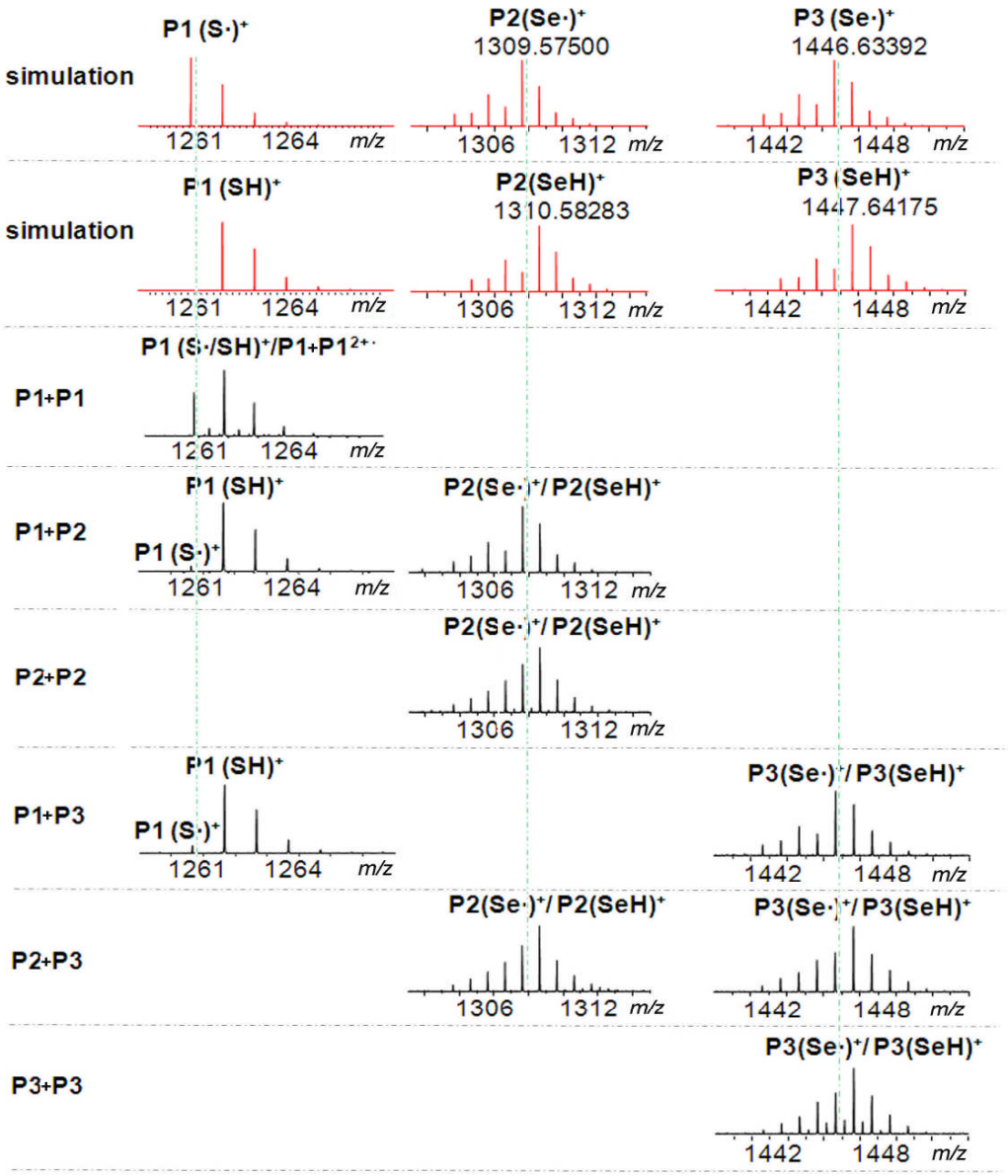

Figure 6.3 Expanded ECD spectra of the fragment species formed by cleavage of S–S, S–Se, and Se–Se bonds. The top–two rows are the simulation spectra (in red) of P1 (S·/SH), P2 (Se·/SeH), and P3 (Se·/SeH) species. Rest of the rows show the corresponding species generated during ECD experiments.

The charge–reduced molecular ion regions from Figure 6.2 a–f are expanded in Figure 6.3. By comparing the experimental spectrum (in black) with the simulated isotope distribution spectrum (in red) of each

fragment, it can be noticed that for ECD of S–Se bound peptides (P1 + P2 and P1 + P3), the peak intensities of P(S•) species is apparently much lower than its corresponding P(SH) species, and the peak intensities corresponding to P(Se•) are accordingly higher than its P(SeH) species. Taking P1 + P2 for an example, the cleavage of S–Se bonded peptides can give two pairs of complementary ions, namely, P1(S•)/P2(SeH) and P1(SH)/P2(Se•). Thus, the ratio of P1(S•)/P1(SH) can be used to estimate the ratio of each fragmentation pathway; thereby, providing preferential S–Se bond cleavage pathway information, namely, either P1(S•)/P2(SeH) or P1(SH)/P2(Se•). Table 6.2 shows the ratios of P(X•)/P(XH) (P = P1, P2, and P3; X = S, Se) calculated based on the area of the monoisotopic peak. The cleavage of the disulfide bond of P1–P1 gave a P1(S•)/P1(SH) ratio of 1.02 ± 0.05, which is expected because the two chains connected by disulfide bonds are of the same sequence. In contrast, the ratios of P1 (S•/SH) for S–Se linked peptides (P1 + P2 and P1 + P3), are 0.07 ± 0.00 and 0.10 ± 0.01, respectively, which indicates that the radical has a higher tendency to reside at the Se atoms when S–Se bonds cleave. This result is surprising because the electronegativities value of S and Se are almost identical, with S of 2.58 and Se of 2.55 in Pauling units,[296] and the electron affinities of S(2.07 eV) and Se (2.02 eV) are also around the same.[297] Thus, the electronegativities or electron affinities of S and Se alone should not have caused such a significant bias in fragmentation behaviour. Therefore, some other factors must contribute to drive the radical to the Se atoms during the ECD process.

Table 6.2 Ratio of P(X•)/P(XH) (P = P1, P2, and P3; X = S, Se) species generated during ECD of S–S, S–Se and Se–Se containing species. The ratio was calculated based on the peak area of the monoisotopic peak of each species.* 2 M data sets were used deliberately to simplify the ratio calculation due to complicity of selenium isotopic distribution. Replicated errors are the standard deviation of three duplicates.

Precursor ions	***m/z* (Da)**	**Ratio of P1(S·)/P1(SH)**	**Ratio of P2(Se·)/P2(SeH)**	**Ratio of P3(Se·)/P3(SeH)**
P1+P1	841.42281	1.02 ± 0.05	—	—
P1+P2	857.73795	0.07 ± 0.00		—
P2+P2	873.38609	—	1.93 ± 0.36	—
P1+P3	903.42365	0.10 ± 0.01		—
P2+P3	919.40558	—	1.16 ± 0.21	0.87 ± 0.16
P3+P3	965.09283	—	—	0.82 ± 0.36

Previously, Dumont *et al.*[292] used *ab initio* calculations to investigate the gas–phase electron addition on selenium–containing organic compounds, dimethyldisulfide, dimethylseleneylsulfide, and dimethyldiselenide. It is found that selenium strongly enhances the electron affinity, with an increase of adiabatic electron affinity by about 0.20 eV by replacing a sulfur with a selenium. The formed radical

*For P1+P2 and P1+P3, the ratios of P2(Se•)/P2(SeH) and P3(Se•)/P3(SeH) were also calculated to determine the preference of the radical to residue on the Se atom. Although the ratios of P2(Se•)/P2(SeH) indicate that the radical prefers to residing at the Se atom, the data was not shown in Table 2 because the errors for these ratios are rather large. It is likely because the area of the P2(Se•) (A+1) peak has a significant contribution to the overlapping peak of P2(SeH) (A). Therefore, the area of the P2(Se•) (A+1) peak overshadows the area of the P2(SeH) (A) peak, which leads to big errors.

anionic intermediates are stable against dissociation. Their calculations could explain the experimental results observed here. For ECD of diselenide bound peptides, the ratios of P (Se•/SeH) for P2 + P3 and P3 + P3 range from 0.82 ± 0.36 to 1.16 ± 0.21 (see Table 6.2), which suggests that there is no specific force pulling the electron towards a certain selenium although sequence differences might have some contributions. However, the value of P2 (Se•/SeH) ratio for P2 + P2 diselenide–containing molecule is anomalous at 1.93 ± 0.36, indicating that other effects, perhaps conformational, are also contributing. One possible option is that P_2(SeH) may have an additional low energy fragmentation pathway which could deplete its abundance.

6.3.2 Cleavages of C–X (X = S or Se) bonds

Scheme 6.1(b, c, and d) shows the possible fragments generated by cleavages of C–S bonds during ECD. Taking the triply charged disulfide peptide (P1 + P1) for an example, theoretically, the cleavage of C–S bonds by ECD may generate the following three types of complementary pair ions, namely, $[P1–SH + H]^+$ / $[P1 + S + 3H]^{+\bullet}$ (Scheme 6.1b), $[P1–S + H]^{+\bullet}$ / $[P1 + SH + H]^+$ (Scheme 6.1c), and $[P1 – S + 2H]^+$ / $[P1 + S\bullet + H]^{+\bullet}$ (Scheme 6.1d). Similar nominations also apply to S–Se and Se–Se bound species. Although the cleavages displayed in Scheme 6.1 might not necessarily go through the proposed processes or always give detectable complementary ions.

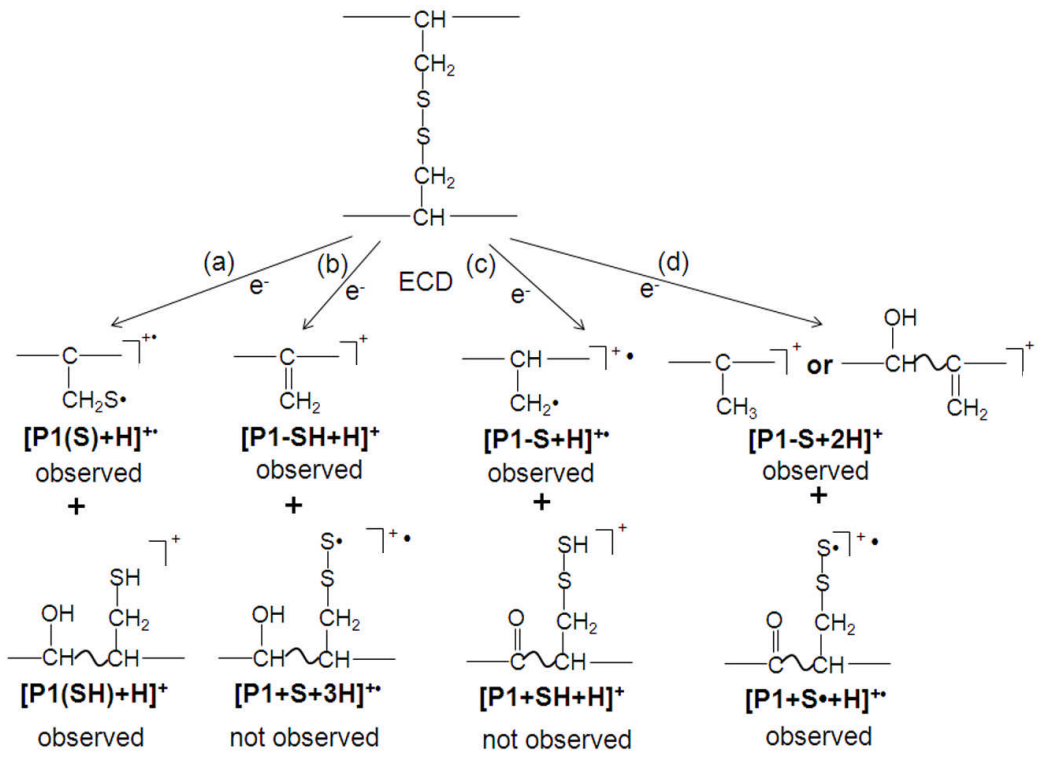

Scheme 6.1 Possible ECD fragments generated by cleaving the S–S (a) or S–CH_2 (b, c, and d) bonds of a triply–charged disulfide–linked peptide ions, $[P1+P1+3H]^{3+}$.

Figure 6.4a shows the ECD fragment ions spectra corresponding to the cleavage of a C–S bond of the triply–charged disulfide peptide ions, $[P1 + P1 + 3H]^{3+}$. Interestingly, in the *m/z* region of 1228 to 1232 Da, fragments corresponding to $[P1 – SH + H]^{+}$ (–SH) at *m/z* 1228.65234, $[P1 – S + H]^{+\bullet}$ (–S) at *m/z* 1229.66047, and $[P1 – S + 2H]^{+}$ (–S + H) at *m/z* 1230.66772 ions, were all detected (A proposed corresponding structure of each species is shown as the insert of Figure 6.4a). As presented in the left–hand of Figure 6.4a, the isotope species of all three of $[P1 – S + H]^{+\bullet}$ (in black), $[P1 – SH + H]^{+}$ (in pink), and $[P1 – S + 2H]^{+\bullet}$ (in cyan) ions were resolved using a high resolution 12–Tesla FTICR MS instrument. As listed in Table 6.3, the theoretical mass differences between the A + 2

isotopic peak of $[P1 – SH + H]^+$ and the A + 1 isotopic peak of $[P1 –S + H]^{+\cdot}$, and between the A +1 isotopic peak of $[P1 – S + H]^{+\cdot}$ and the A isotopic peak of $[P1 – S + 2H]^+$ are 4.51 and 4.45 mDa, respectively. Thus, a minimum resolving power of 250,000 is needed to separate all three of these peaks at half height. A 5.5 s transient was obtained and yielded a resolving power over 280,000 from *m/z* 1228 to 1232 Da. An overall mean absolute deviation (MAD) less than 0.80 ppm across the whole mass over charge region was achieved, as shown in Table E.1 (full peak list table) and a MAD of 1.14 ppm was obtained at *m/z* 1228 to 1232 Da region as listed in Table 6.3, which suggest that the peak assignments are valid.

Table 6.3 Partial peak list table of the ECD spectrum of $[P1+P1+3H]^{3+}$. For complete peak list table, see Table E.1.

Assignments	Isotopic number	Experimental *m/z* (Da)	Theoretical *m/z* (Da)	Mass error (ppm)
1+	A	1228.58695		
$[P1–SH+H]^+$	A	1228.65234	1228.65069	1.34
1+	A+1	1229.59002		
$[P1–SH+H]^+$	A+1	1229.65528	1229.65406	0.99
$[P1–S+H]^{+\cdot}$	A	1229.66047	1229.65851	1.59
1+	A+2	1230.59302		
$[P1–SH+H]^+$	A+2	1230.65809	1230.65738	0.58
$[P1–S+H]^{+\cdot}$	A+1	1230.66275	1230.66189	0.70
$[P1–S+2H]^+$	A	1230.66772	1230.66634	1.12
$[P1–S+H]^{+\cdot}$	A+2	1231.664	1231.66520	–0.97
$[P1–S+2H]^+$	A+1	1231.6714	1231.66971	1.37
$[P1–S+2H]^+$	A+2	1232.67502	1232.67303	1.61
Mean absolute deviation (ppm)				1.14

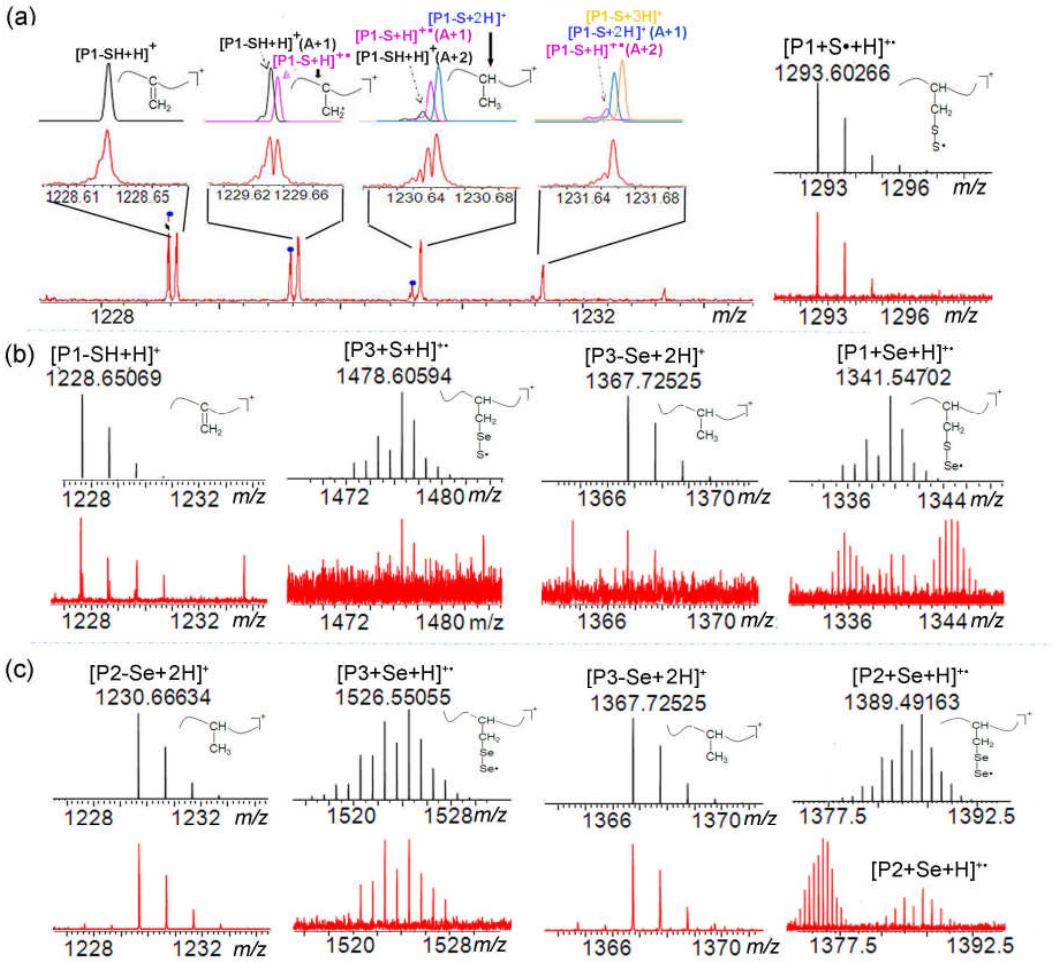

Figure 6.4 Comparasion of ECD fragment ions generated by cleavage of (a) C–S bonds (P1+P1),(b) C–Se bond *vs* C–S bond (P1+P3), and (c) C–Se bonds (P2+P3). Experimental fragment spectra are in red and simulated isotope patterns are in black To differentiate peaks closed–by at *m/z* 1228 to 1233 Da region, the simulated spectra were color–coded ($[P1–SH+H]^+$ species are in black, $[P1–S+H]^{+\cdot}$ in pink, $[P1–S+2H]^+$ in blue, and $[P1–S+3H]^+$ in orange.). The inserts shows the corresponding structure of each species. The mass windows were not aligned between different fragment species.

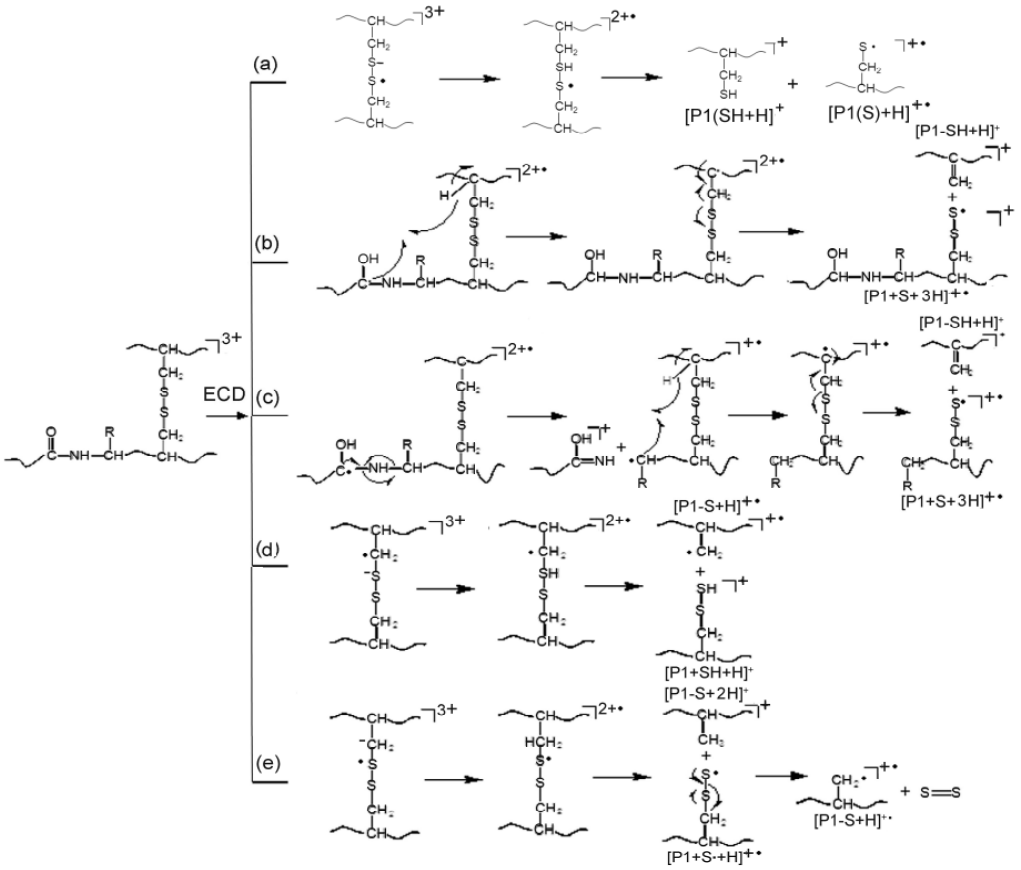

Scheme 6.2 Possible S–S (a) C–S (b–e) bonds cleavage pathways of a disulfide–containing peptide.

The right–hand spectra of Figure 6.4a show the corresponding complementary–ion regions of the above species. In comparison with the simulated isotope distribution spectra, the ions at *m/z* 1293.60407 can be assigned as $[P1 + S + H]^{+\bullet}$ species, which is complementary to the $[P1 – S + 2H]^{+}$ species. Previously, the generation of $[P1 – SH + H]^{+}$ ions by cleaving the C–S bonds of disulfide–containing species has been reported,[218, 280, 281] which can be initiated from the C_α position, either by radical migrations (Scheme 6.2b),[64] or by cleaving the N–Cα bond first, following by the radical migration to C_α position as shown in Scheme 6.2c.[218] For the first proposed fragmentation pathway as shown in

Scheme 6.2b, the complementary ion $[P1 + S + 3H]^{+\bullet}$ should be observed. However, neither the $[P1 + S + 3H]^{+\bullet}$ species nor the further fragments $[P1 – S + 3H]^{+\cdot}$ (simulated isotope pattern is in orange as shown in Figure 6.4a) by losing S═S, were detected. Therefore, the generation of the $[P1 – SH + H]^{+}$ species is more likely through the second proposed pathway (Scheme 6.2c).

The observation of the $[P1 – SH + H]^{+}$(– SH, – 32.97990 Da) species is not surprising. However, the $[P1 – S + H]^{+\bullet}$(–S, 31.97207 Da) and $[P1 – S + 2H]^{+}$(–S+H, –30.96424 Da) fragments haven't been previously reported, possibly because of the low–resolution of the instruments used.[218, 280, 281] Alternatively, it is also possible that the processes to generate $[P1 – S + H]^{+\bullet}$ and $[P1 – S + 2H]^{+}$ ions are unfavorable, although the peak intensities shown in Figure 6.4 a argue against this hypothesis. Theoretically, the generation of both $[P1 – S + H]^{+\bullet}$ and $[P1 – S + 2H]^{+}$ fragments can both occur through homolytic cleavage of a C–S bond and lead to fragment pairs of $[P1 – S + H]^{+\cdot}$/$[P1 + SH + H]^{+}$ and $[P1 – S + 2H]^{+}$/$[P1 + S + H]^{+\cdot}$ (Scheme 6.2d and 6.2e), although, it has been previously suggested that the later process is impossible or unfavorable because the β–carbon position is not predicted to have a high hydrogen atom affinity.[218] The electron transmission spectroscopy (ETS) results show that the C–S σ* orbital lies vertically < 3.75 eV above its corresponding neutral;[298] therefore, Sawicka and co–authors suggested that C–S bonds can be cleaved by direct electron attachment if a positive charge site is close to the C–S σ bond within ~3.8 Å.[5817]

Figure 6.4b shows the fragment ions spectra that correspond to the cleavage of the C–S and C–Se bonds of a triply–charged S–Se bonded peptide ion, $[P1 + P3 + 3H]^{3+}$. The scission of the C–S bond of S–Se peptides, such as $[P1 + P3 + 3H]^{3+}$, gave similar fragments at the *m/z* 1228 to 1232 region to those obtained in the ECD of the disulfide containing species, $[P1 + P1 + 3H]^{3+}$. However, the cleavage of C–Se bond yielded a complementary fragment pair of $[P3 – Se + 2H]^{+}$ and $[P1 + Se + H]^{+\bullet}$. Regardless of the backbone sequences of P1 and P3, plausibly proposed structures of $[P1 – SH + H]^{+}$ and $[P3 – Se + 2H]^{+}$ are different as shown in the insets of Figure 6.4. Thus, the cleavages of C–S and C–Se bonds are likely occurring via different fragmentation pathways. Nevertheless, the intensities of fragments from cleaving C–S bonds of the S–Se peptide (P1+P3) is rather low, which indicates that neither C–S or C–Se bond cleavage is a favourable process for ECD of S–Se containing peptides.

In contrast to the ECD result of a S–S bound peptide ion,$[P1 + P1 + 3H]^{3+}$ (Figure 6.4a), Figure 6.4c shows ECD of a triply–charged Se–Se bonded peptide ion, $[P2 + P3 + 3H]^{3+}$ and presents a very different C–Se bond cleavage pattern. The cleavages of C–Se bonds gave two pairs of complementary ions, namely, $[P2 – Se + 2H]^{+}/[P3 + Se + H]^{+\cdot}$ and $[P3 – Se + 2H]^{+}/[P2 + Se + H]^{+\cdot}$. For complementary pairs generated from the same fragmentation pathway, the intensities of the two complementary pairs should be around the same. Based on the total intensities of all the isotopic peaks of each species, the intensity ratios of $[P2 – Se + 2H]^{+}$:$[P3 + Se + H]^{+\cdot}$ and $[P3 – Se + 2H]^{+}$:$[P2 + Se + H]^{+\cdot}$ were therefore calculated

as 0.99 ± 0.02 and 1.21 ± 0.06, respectively. Thus, it is more likely that the cleavage of C–Se bonds is through a direct electron capture into an orbital of the C–Se bond as suggested in Scheme 6.2e. Although there is a slight possibility that $[P2 – Se + H]^{+\cdot}$ ions can abstract a hydrogen from elsewhere to form a $[P2 – Se + 2H]^{+}$ species, the intensities of $[P2 – SeH + H]^{+}$ and $[P2 – Se + H]^{+\cdot}$ indicate that this process cannot be a dominant process. In addition, the complementary pair species, $[P3 + Se + H]^{+\cdot}$ and $[P2 + Se + H]^{+\cdot}$would not be observed based on this hypothesis, but were both detected here.

As can be seen from Figure 6.2e and 6.2f, the cleavages of C–Se bonds are comparable with the cleavages of Se–Se bonds for P2 + P3 and P3 + P3 species. However, the cleavage of C–Se bonds is a minor pathway compared to the cleavage of Se–Se bond for P2 + P2. Gamez *et al.*[293, 294, 299] previously have done extensive *ab initio* calculations to study the ECD behaviours of Se–Se bond compounds. They also discovered that Se–Se bond cleavage is not always the most favourable process in electron attachment to diselenides, the effects of asymmetry and the electronegativity of the substituents attached to the Se–Se bond have strong impact on the ECD cleavage of diselenide compounds, as observed here.

6.3.3 c/z• ions generated by cleaving both N–Cα and S–S (S–Se, or Se–Se) bonds

The last category of fragments ions was generated by cleaving both N–C_α and S–S, S–Se, or Se–Se bonds. The ECD spectra of $[P1 + P1 + 3H]^{3+}$, $[P1 + P3 + 3H]^{3+}$, and $[P2 + P3 + 3H]^{3+}$ from *m/z* 840 to 1120

are shown in Figure 6.5. It can be seen from the inserts of Figure 6.5a that c ions generated from P1 chain are a mixture of c(S) and c(SH) species; in contrast, the c ions generated from P2 and P3 chains (Se–containing species) are only c(Se) species (see the inset of Figure 6.5c). The c(SH) species should result from double electron capture dissociation. C(S) and z (S·) ions can both be generated from P1(S·) species by cleaving N–Cα bonds and forming cyclized c(S) and z(S·) species. However, it is not clear whether cyclized c(Se) and z(Se·) ions can be generated by the same fragmentation pathway as Se strongly enhances the electron affinity and radicals tend to remain on Se atoms.

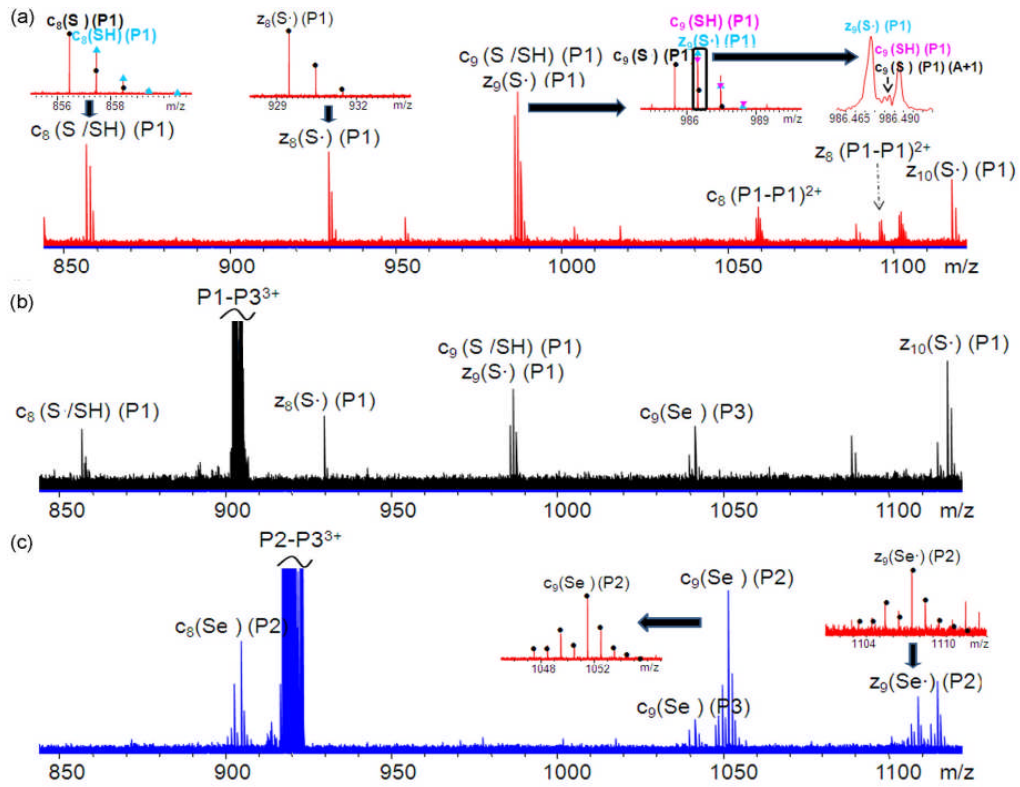

Figure 6.5 Expanded ECD spectra of (a) $[P1+P1+3H]^{3+}$, (b) $[P1+P3+3H]^{3+}$, and (c) $[P2+P3+3H]^{3+}$. This spectra show the c/z·ions generated by cleaving both N-C_α and S-S, S-Se, or Se-Se bonds.

ECD experiments were also performed on doubly–charged ions to further explore the fragment pathway of ions generated by cleaving both N–C_α and S–S, S–Se, or Se–Se bonds. However, the results are less informative and mainly the charge reduced species were observed, which might be mainly because the electron capture cross section is dependent on the ionic charge squared (z^2), thus leading to lower fragmentation efficiency.[35] Similar results were also observed in electron transfer dissociation (ETD) experiment of a large scale of peptides ranging from ~ 1000 to 5000 by Good *et al*,[300] in which they found that there is a linear decrease in fragmentation efficiency as a function of increasing precursor *m/z*.

6.4 Conclusions

A series of disulfide (S–S), sulfur–selenium (S–Se), and diselenide (Se–Se) bond–containing peptides was studied by ECD. The results demonstrate that the radical has higher tendency to stay at selenium compared to sulfur after the cleavage of Se–S bonds by ECD. In addition, the cleavage pathways of C–S bonds of a disulfide peptide and C–Se bonds of a diselenide peptide are different. In the former, the cleavage of C–S bonds gave fragments by losing SH (–33), S (–32), and (– S + H) (–31) small neutral losses. In the later, the cleavage of C–Se bonds mainly gave fragments by neutral loss of (– Se + H) and the radical tended to reside at the selenium of its corresponding complementary pair. The results suggest that direct electron capture at Se–Se and C–Se bonds is the main process during ECD of inter–chain diselenide peptides, and

possibly in ECD of inter–chain disulfide peptides as well.

Chapter 7

Top-down Electron Capture Dissociation of Disulfide-Rich Proteins

7.1 Introduction

7.1.1 Bottom-up MS analysis of disulfide bound proteins

Disulfide bonds in proteins are post-translational modifications that are important for stabilizing the tertiary structures of proteins by introducing covalent constraints. For many peptides and proteins, disulfide bonds are crucial for their proper biological function.[301] Thus, the characterization of disulfide bonds is an important step to understand the structure of a protein. The strategies of sequencing disulfide-linked proteins usually involve enzyme digestion and chemical reduction and alkylation, followed by mass spectrometry analysis. Although this so-called "bottom-up" MS approach has been proven useful and widely used for the sequencing of disulfide linked proteins, there are some inherent limitations. First of all, the sample preparation procedures consume time and sample. Second, in a bottom-up approach, only a sub-fraction of the digested peptides can be detected, many are lost, and even fewer provide useful fragmentation information; therefore, the sequence information is incomplete.[302]

7.1.2 Top-down MS analysis of disulfide bound proteins

As an alternative strategy, top-down MS approach enables the identification and characterization of intact proteins by directly introducing

protein ions into the gas phase and subsequently being analyzed by MS^n in the mass spectrometer.[303] One of the great advantages of the top-down approach is that fragmentation on an intact protein rather than at the peptides level in principle enables the examination of the entire sequence and direct characterization of the protein and PTMs.[303, 304] In addition, no extensive sample preparation (such as digestion or chemical modification) is needed, although sample clean-up stage can be more intensive. The top-down MS approach has been successfully used to rapidly sequence proteins, identify PTMs,[40, 107, 274, 305-310] and study protein complexes,[33, 101, 311] with the remarkable record of characterizing a protein over 200 kDa.[310] However, the application of using top-down MS approach to sequence disulfide bound proteins remains challenging due to the low fragmentation efficiency.[57, 151-153, 312]

7.1.3 ECD analysis of disulfide bound proteins

Collisionally activated dissociation (CAD) and Electron capture dissociation (ECD) are the most commonly used tandem MS fragmentation techniques in top-down analysis. However, the sequence information obtained during fragmentation of disulfide bonded proteins can be rather limited, because multiple backbone bonds must be cleaved to yield product ions within the disulfide loop. ECD is well-known for its abilities on top-down sequencing of intact proteins.[33, 88, 101, 274] It was first proposed and demonstrated by Zubarev *et al*. that ECD preferentially cleaved disulfide bonds.[57] Insulin, a small protein with two peptide chains (A and B) linked by two inter-chain disulfide bonds, containing a third intra-chain disulfide bond, as a perfect example has been extensively

studied by different radical-based fragmentation techniques beyond ECD, such as ETD, and electron detached dissociation (EDD).[153, 154] Preferential cleavages of S-S bonds have been observed in all cases; therefore the sequences information obtained is often limited. Only recently, Huang *et al*. were able to demonstrate that up to 70% backbone fragment efficiency can be achieved by ECD.[313]

As a general approach, activation of ions by collisional activation, thermal heating, and infrared activation, in-beam collision before, during, or after ECD events have been shown to improve the ECD fragmentation efficiency of proteins.[88, 314-317] The added energy helps to remove the intra-molecular noncovalent bonds and results in more extended structures, which are favorable for ECD analysis. However, interestingly, some contradictive results have been recently reported by Breuker *et al*.[318] In their research, a few disulfide-bonded proteins, including ecotin, aprotinin, and trypsin inhibitor, were studied by ECD. Interestingly, no c and z• fragment ions from the regions of the proteins bridged by disulfide bonds were observed even under activation conditions (such as, using collisional activation and infrared activation).[318] In one way or another, insufficient sequence information is typically obtained in the ECD analyses of disulfide-linked proteins.

Alternatively, Zhang *et al.* were able to improve the backbone fragmentation efficiency of disulfide bound proteins by 3 to 13 fold by reducing the disulfide bonds using an online electrochemistry strategy prior to top-down ECD of proteins.[95] In the research by Loo *et al.*, supercharging has been shown to improve the backbone cleavage

efficiency of disulfide bonded proteins by increasing the charge on the protein ions.[319]

Here we demonstrate a simple approach to tackle this challenging problem by simultaneously giving a one millisecond single frequency excitation pulse at the beginning of the ECD events to activate the ions. We discovered that this activation approach not only improves the overlapping of ions and electrons but also activates ions and leads to more comprehensive fragmentation. One may expect that this method is the same as the strategy to improve the overlapping of ions and electrons by sustained off-resonance excitation (SORI)[83] (usually a few kHz off compared to the cyclotron frequency of the precursor ions); however, the frequencies used here to activate ions are at ~ MHz range (frequencies in the range from a few hundred kHz to MHz have been examined to activate ions as discussed below). In addition, in a typical SORI experiment, the excitation pulse length is in a few hundred milliseconds to a few second ranges, which is significantly longer than the excitation duration used in Shot-ECD (1 ms).

7.2 Experimental section

7.2.1 Materials

Bovine insulin and bovine ribonuclease A (RNase A) were purchased from Sigma (St. Louis, MO, USA). HPLC grade methanol, acetic acid (HAc), and acetonitrile (ACN) were obtained from Fisher Scientific (Pittsburgh, PA, USA).

7.2.2 FTICR Mass Spectrometry

ESI-MS was performed on a Bruker solariX FTICR mass spectrometer with an ESI source and a 12 Tesla actively shielded magnet. Samples were electrosprayed at a flow rate of ~150 μL/hour at a concentration of 1μM in 50:50 MeOH:H_2O with 1% acetic acid. For ECD experiments, the parent ions were first isolated in the first quadrupole and externally accumulated in the collision cell for 1-5 s. After being transferred to the ICR cell, ions were irradiated with 1.5 eV electrons from a 1.7 A heated hollow cathode dispenser[78] for 10 to 50 ms. A 1 ms single frequency excitation pulse at *m/z* 100 (frequency ~ 1.8 MHz) with a clean-up shots power of 5%~10% (17.5~35 V_{pp}) was generated simultaneous to the beginning of the ECD event to improve the overlap between electron beam and the trapped ions. For IR-ECD experiments, a vertically mounted 75 W, 10.6 μM CO_2 laser (Synrad, Mukilteo, WA) was used. A 420 ms IR activation pulse with laser power of 7.5 W was given prior to the ECD event. To improve the overlap of ions and photons as well as ions and electrons, different trapping voltages (TP) were used for IR (TP=1.0 V) and ECD (TP=0.5 V) events with 10 ms delay in between IR and ECD events, during which the trapping voltages were ramped down from 1.0 V to 0.5 V (Based on the experimental observation on this instrument that the better overlap of ions and photons can be achieved when using higher trapping voltages, and lower trapping voltages are preferred for a slightly better overlap of ions and electrons with ECD and for preventing fast signal decay. A detailed modification of pulse program is provided in the appendix F. The same TP value of 0.5 V was

maintained for the excitation and detection events. Full spectra were internally calibrated using the singly-charged c ions of insulin or Rnase A.

7.3 Results and discussion

Previously we have observed that the backbone cleavage efficiency of peptides can be significantly improved by giving a millisecond single frequency excitation pulse at low m/z simultaneously to the beginning of the ECD events,[208, 232] this method has therefore been used for ECD analysis of various modified- and unmodified- peptides and proteins.[34, 35] To differentiate this method from normal ECD and IR-ECD, it is referred as Shots-ECD (modified pulse program is given in the supporting information). Here, Shots-ECD was further applied in the top-down analysis of the disulfide-rich proteins, insulin and ribonuclease A (Rnase A). In addition, normal ECD, infrared activated ECD (IR–ECD), along with Shots–ECD were performed to compare the fragment efficiencies of different methods in Rnase A as discussed below.

7.3.1 Top-down Shots-ECD of Insulin

Insulin is a small protein with two peptide chains (A and B chains) linked by two inter-chain disulfide bonds, containing a third intra-chain disulfide bond in the A-chain. Insulin has been extensively studied previously, by different electron-based fragmentation techniques, such as ECD, ETD, and EDD. A maximum backbone cleavage efficiency of ~ 70% was achieved by Huang *et al*. using ECD.[313]

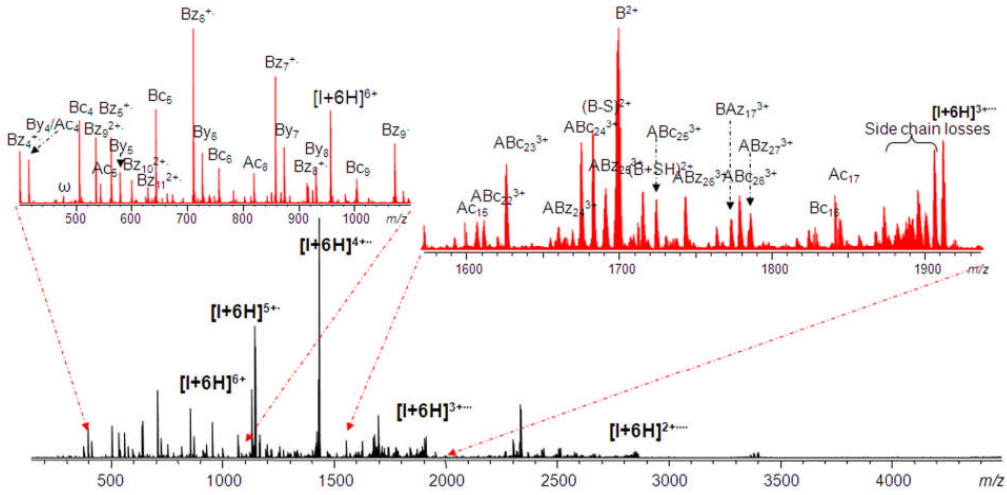

Figure 7.1 ECD spectra of $[Insulin+6H]^{6+}$ at *m/z* 956. The insets show the expanded spectra in mass regions from *m/z* 400 to 1100 and *m/z* 1550 to 2000.

Figure 7.1 shows the Shots-ECD spectrum of the $[I+6H]^{6+}$ ions at *m/z* 956.4, and a detailed fragmentation scheme is provided in Figure 7.2a. It can be seen from the insets of Figure 7.1 and the fragmentation scheme of Figure 7.2a that multiple groups of complementary fragment pairs resulting from the cleavages of multiple bonds including multiple disulfide bond(s) were observed. To simplify the labeling of fragment ions, Insulin A-chain is referred as A and B-chain as B, and ABc(n) or ABz(m) represents c- or z- ion from insulin B-chain with insulin A-chain attached by disulfide linkage(s). Some of the typical complementary pairs are shown in Figure 7.2, such as $Ac_{18}(SH)^{+}$ and $BAz_3^{3+\bullet}$, $Bc_9(S\bullet)^{+}$ and $ABz_{21}(SH)^{3+\bullet}$ generated by cleaving of one backbone (either A-chain or B-chain) N-C_α bond and one disulfide bond (Figure 7.2d); A^{+} at *m/z* 2335 and B^{3+} at *m/z* 1334 originated from the cleavages of the two inter-chain disulfide bonds (Figure7. 2f). Overall, with the use of Shots–ECD, all

three disulfide bonds of insulin were cleaved and nearly 100% backbone cleavage efficiency was achieved with the exception of proline residues due to its ring structure.[40] In addition, the observation of multiple groups of complementary ion-pairs (c/z•) in the Shots-ECD experiments of insulin, therefore provides us the opportunity to assign the charge carrier sites and to explore the fragmentation pathways of disulfide-rich proteins.

7.3.1.1 Charge carrier sites

The observation of Ac_4^+, Az_3^+(cyclic), Bc_2^+, $Bz_4^{+\bullet}$, and $Bz_9^{2+\bullet}$ suggest that the N-terminus of both A– and B–chains, Asn21(A), Arg22(B), Lys29(B) are the five out of the total six of charge carrier sites.

7.3.1.2 Fragment ions generated by single, double, or multiple electron capture

The term “complementary fragments” has been previously defined as a pair of fragments formed by cleaving between the same pair of amino acids, and the masses of the two fragments sum up to the mass of the molecular ion, namely, $c+z\bullet = M_m+H\bullet$ in ECD.[316] This definition of “complementary fragments” refers to the cleavage of one N-C_α bond by one electron capture. However, as discussed later, the fragments observed for ECD of disulfide proteins (cleavages of both disulfide and N-C_α bonds) often originate from multiple electron capture ($n\geq 2$). Here, to simplify the calculation of the mass of the molecule and to determine the numbers of electrons captured that lead to fragmentation, hydrogen numbers were tracked for each complementary pair. In addition, to guarantee that the two fragments of each complementary pairs are from the same fragmentation pathway(s), the total number of charges (q) from

both c and z• ions and electrons (e) ($n=n_{q(c)}+n_{q(z•)}+n_e$) for each complementary pair was also calculated.

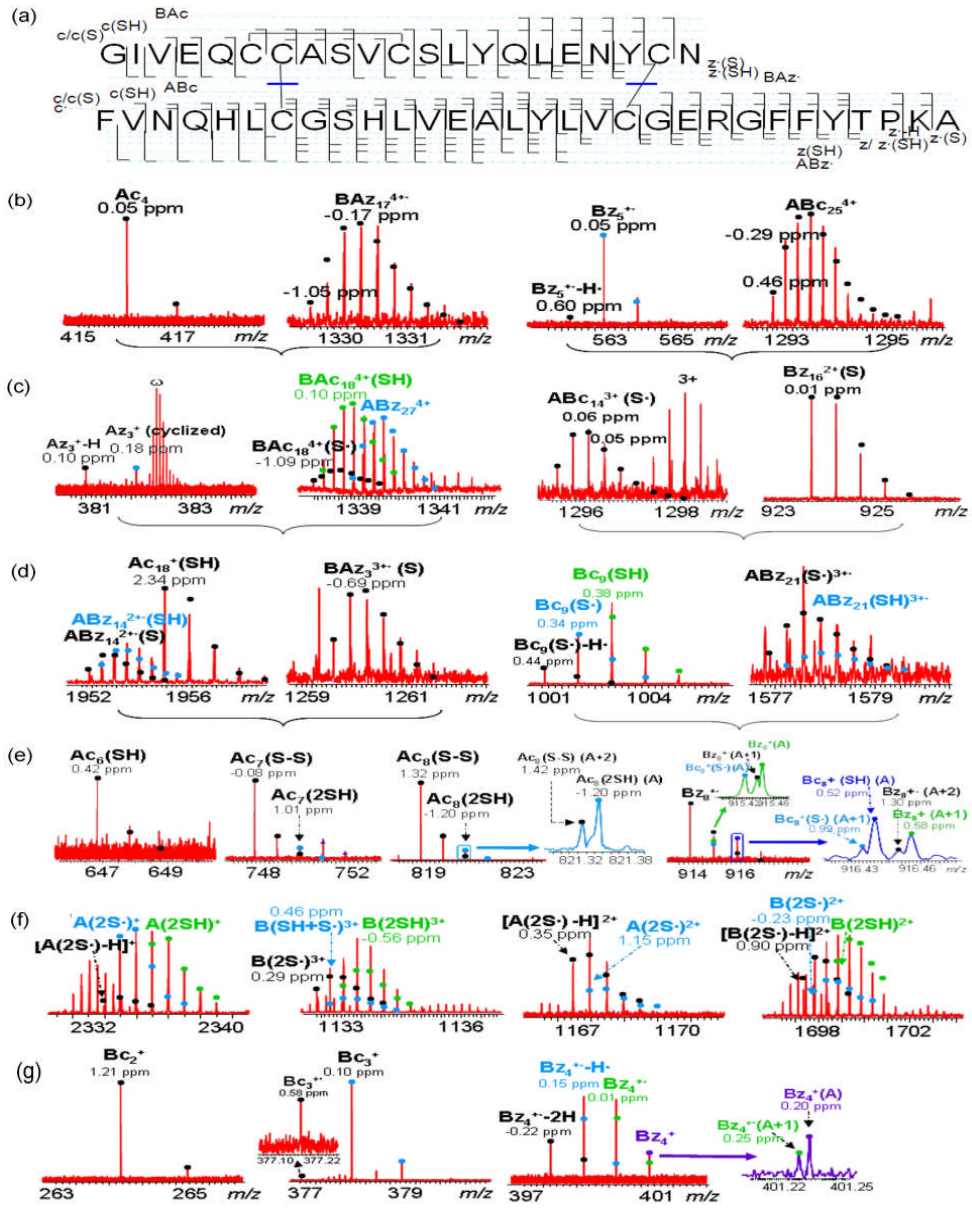

Figure 7.2 Fragment ions observed in the ECD spectrum of the $[I+6H]^{6+}$ ion. (a) Fragmentation diagram; (b) complementary ion pairs from the cleavage of one N-C_α bond by single electron capture; (c) complementary ion pairs from the cleavages of one N-C_α bond and one S-S bond by single electron capture; (d) complementary ion pairs from the cleavages

of one N-C_α bond and one S-S bond by double electrons capture; (e) ions from insulin A-chain yielded by multiple electrons capture (n≥2) ; (f) A-chain and B-chain ions due to the cleavages of both inter-chain disulfide bonds; and (g) hydrogen bonding.

Taking the ECD results of the $[I+6H]^{6+}$ ions of insulin (total numbers of hydrogen: H_m=377) for an example, in the case of fragment pairs originated from a single electron capture dissociation, total hydrogen number should equal to 378 ($H_c+H_{z\bullet}$=378), and the total number of charges and electrons should equal to 6 ($n=n_{q(c)}+n_{q(z\bullet)}+n_e$=6, n_e=1), such as $Ac_4^{+}/BAz_{17}^{4+\bullet}$ (Hc+Hz•=263+115=378, n=1+4+1=6) and $Bz_5^{+\bullet}/ABc25^{4+}$ (Hc+Hz•=378, n=4+1+1=6) as shown in Figure 7.2b. Similarly, for complementary pairs generated by double electron capture dissociation, $H_c+H_{z\bullet}$=379 and $n=n_{q(c)}+n_{q(z\bullet)}+n_e$=6 ($n_e$ = 2).

Some of the complementary fragments observed in the ECD spectrum of the $[I+6H]^{6+}$ ions are presented in Figure 7.2 b-d and f as examples, which were divided into different categories according to the number of electrons being captured. The first category shown in Figure 7.2b, are fragment pairs originating from single electron capture by cleavage of either (1) a single N-Cα bond, such as $Ac_4/BAz_{17}^{4+\bullet}$ (Hc+Hz•=263+115=378, n=1+4+1=6) and $ABc_{25}^{4+}/Bz_5^{+\bullet}$ (Hc+Hz•=378, n=4+1+1=6), or (2) both an N–C_α and a disulfide bond, such as, Az^{3+} (cyclized z-ion)/$BAc(S\bullet)^{4+}$ (Figure 7.2c). Taking insulin as an example, possible fragmentation pathways of the $[I+6H]^{6+}$ ion due to single or double electron(s) capture dissociation are summarized in Scheme 7.1.

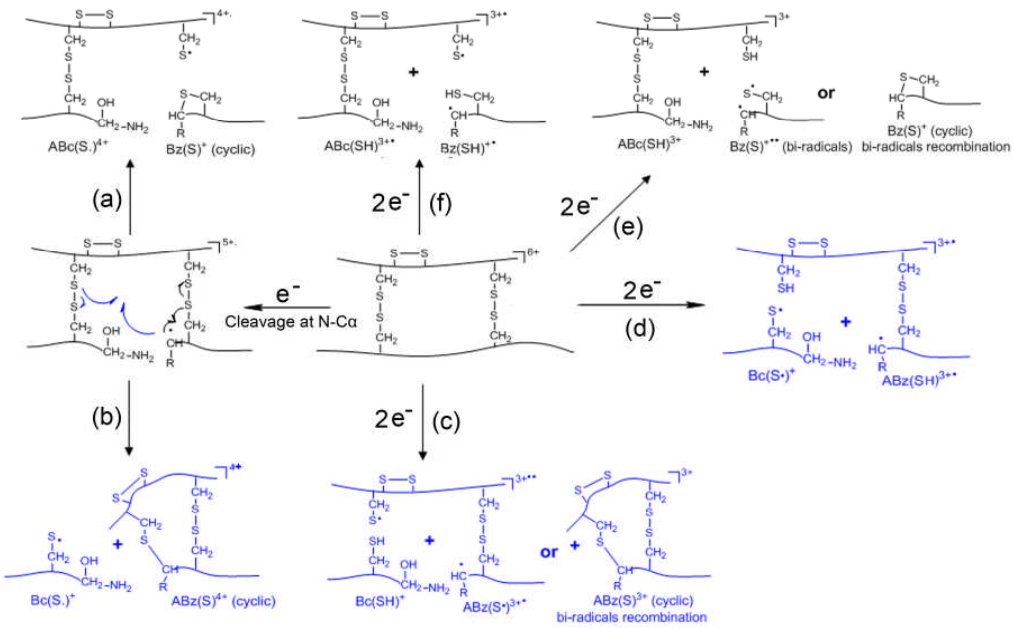

Scheme 7.1 Possible fragmentation pathways of the $[insulin+6H]^{6+}$ ion due to one or two electron(s) capture.

As shown in Scheme 1a and 1b, initial electron capture at or transfer to amide π* orbital forms a –(·CO-)–NH–C_α– radical anion and then cleaves its N–C_α bond to form c and z· ions.[320] The radical at z· ions can migrate to either inter–chain disulfide bonds (Cys7(A)—Cys7(B) or Cys20(A)—Cys17(B)), cleave the disulfide bonds, and form complementary pairs of either $ABc(S\cdot)^{4+}$/cyclic z^+ (Scheme 1a) or $Bc(S\cdot)^+$/cyclic ABz^{4+} (Scheme 7.1b). The cleavage sites are only drawn in B–chain of insulin for demonstration, the same process can also happen in A–chain as observed, such as Az^{3+} (cyclized z-ion)/$BAc(S\bullet)^{4+}$ (Figure 7.2c). It has been previously reported that a single electron transfer reaction can cleave both one S–S bond and one N–C_α bond,[152, 281] and the formation of cyclic z-ions has been observed by Cole *et al.*[281] on ETD of intra–chain disulfide peptides. Here, the observation of

complementary pairs (in both mass and charge), such as $AB_{18}c^{4+}$(S·)/cyclic z_3^{+}(SH) and Bc_9(S·)+/cyclic $ABz_{21}^{4+\cdot}$(S) (Figure 7.2c), suggests that single electron capture can dissociate both N-C_α and S-S bonds in ECD of the $[I+6H]^{6+}$ ion as proposed in Scheme 7.1a&b. In addition, initial electron capture into an S–S δ* orbital can also happen, promptly cleave the disulfide bond, and form -S· and -SH through hydrogen abstraction from elsewhere. Previously Lee *et al*.[280] proposed that the radical at -S· can abstract a hydrogen from either α- or β- carbon; then a radical site generated at the α-carbon can lead to b·/y ions (Scheme S-1a), while the β-carbon radical yields a/x· ions (Scheme S-1b) or c·/z ions (Scheme S-1c). Although By_4 to By_{11} ion series were detected, no complementary b·/y, or a/x· ion pairs were observed in ECD of the $[I+6H]^{6+}$ ion. In the case of c·/z ion pairs as proposed in Scheme S-1c, it is not clear whether this pathway happened or at what extent as the masses of $Bc(SH)^{+\cdot}$ and $ABz(SH)^{4+}$ are exactly the same as $Bc(S\cdot)^{+}$/cyclic $ABz(S)^{4+\cdot}$ (Scheme 7.1a), respectively.

Scheme 7.1c-f proposed the fragmentation pathways induced by double electron capture dissociation. The fragment ion structures are given without detailed pathways because it is not known whether the capture of two electrons lead to the fragmentation of N-C_α or S-S bond one after another or simultaneously, nor which happens first. As shown in Scheme 7.1 c&d, when one of the two electrons targets the Cys7(A)-Cys7(B) bond, the fragments yielded can be either $Bc(SH)^{+}$/$ABz(S\cdot)^{3+\cdot}$ (Scheme 7.1c) or $Bc(S\cdot)^{+}$/$ABz(SH)^{3+\cdot}$ (Scheme 7.1 d) ion pairs; likewise, the cleavages of Cys20(A)—Cys17(B) and one N-C_α

bond of B-chain would induce fragments of $ABc(SH)^{3+}/z(S\cdot)^{+\cdot}$ as bi-radical species (Scheme 7.1e) or $ABc(SH)^{3+}$/cyclized z^{+}(two radicals are recombined and formed a cyclic structure)[321] and $ABc(S\cdot)^{3+}/z(SH)^{+\cdot}$ (Scheme 7.1f). Figure 7.2d shows some of the complementary ion pairs observed with the cleavage of both N-C_α and S-S bonds by capturing two electrons, such as $Ac_{18}(SH)^{+}/BAz^{3+\cdot}(S\cdot)$, $Bc_9(S\cdot)+/ABz_{21}(SH)^{3+\cdot}$, and $Bc_9(SH)^{+}/ABz_{21}(S\cdot)^{3+\cdot}$. The results indicate that the ECD fragmentation of the $[I+6H]^{6+}$ ions (Figure 7.1) possibly go through the proposed pathways (Scheme 7.1 c&d). Previously, in SORI-CID of the bi-radical lacticin 481 species (a small peptide with three lanthionine bridges), Kleinnijenhuis *et al.* observed that the recombination of the two radical sites is the dominant process.[321] However, it is not clear whether the species observed here, such as $BAz^{3+\cdot}(S\cdot)$ and $ABz_{21}(S\cdot)^{3+\cdot}$, are bi-radical species or species with two unpaired radicals recombined. The masses are the same and the fragment ion abundances are too low for MS^3.

Figure 7.2e shows the c-ion fragments from A-chain sequenced by cleaving an N-C_α and one S-S bond by multiple electron capture (n=2, 3). Fragment ion Ac_6 is mainly in $Ac_6(SH)^{+}$ form due to the cleavages of one N–C_α bond and one S–S bond by two different electrons. The observation of fragment ions of Ac_7 and Ac_8 is interesting because they both must derive from the cleavage of three bonds, including two nearby disulfide bonds and one N–C_α bond. In addition, two forms of fragments Ac(S–S) or A(2×S•) and Ac(2×SH) were observed for both Ac_7 and Ac_8 (see the inset of Figure 7.2d, in blue) and they are different by 2 Da. In

theory, for the cleavage of a disulfide linked peptide or protein (R_1S-SR_2) in ECD, the ratio of R_1S•/R_1SH or R_2S•/R_2SH should be approximately 1:1. However, surprisingly, the intensities of Ac_7(S-S) and Ac_8(S-S) are around 10 times higher than their corresponding Ac(2×SH) peaks, which indicates that there are other fragmentation pathway(s) contributing to the generation of Ac_7(S-S) and Ac_8(S-S) ions. Considering the fragmentation pathways for Ac(S-S) and Ac(2×SH) species, they can both be generated by the capture of three electrons. In that case, Ac_7(S-S) and Ac_8(S-S) are both bi-radical species, which might not be stable. Considering Cys6(S•) and Cys7(S•) are adjacent, it is likely that the two radicals recombined and formed stable c-ions with a new disulfide bond. In addition, there are two possible pathways that can lead to Ac_7(S-S) and Ac_8(S-S) ions by capturing two electrons as shown in Scheme 7.2. In each possible pathway, the obtained c-ion has a newly formed disulfide bond, which could possibly explain why the intensities of Ac_7(S-S) and Ac_8(S-S) are much higher than their corresponding Ac(2×SH) peaks.

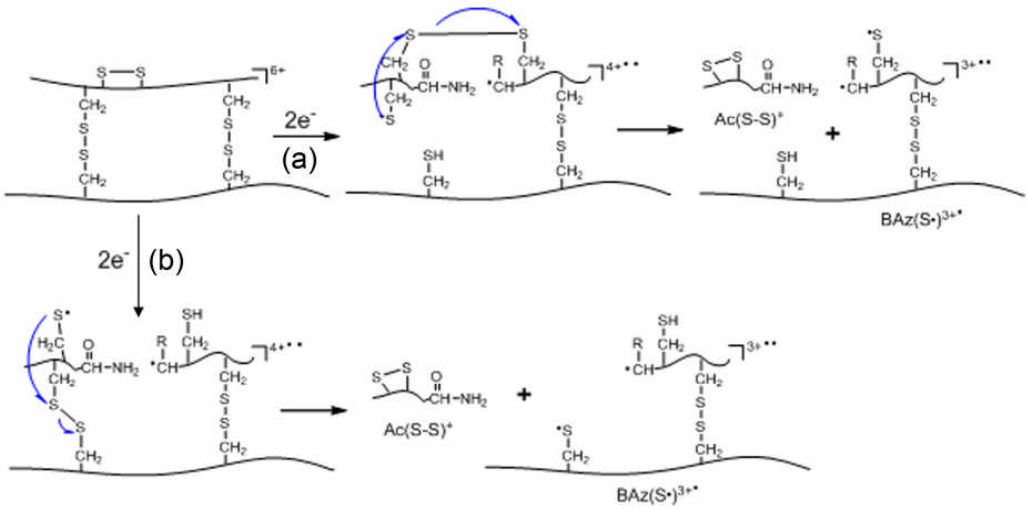

Scheme 7.2 Possible fragmentation pathways of yielding Ac(S-S) ions by

capturing two electrons.

Top-down ECD spectra are often complicated to interpret due to the overlap of fragment peaks, which is particularly evidenced in the ECD spectrum of the disulfide-rich protein—insulin (Figure 7.1 and 7.2). As an example, shown in the left-hand of Figure 7.2e, the ions centered at *m/z* 916 are overlapping peaks of four species, including, $Bc_8(S\cdot)^+$ (A+1), $Bc_8(SH)^+$ (A), $Bz_8(A+2)^{+\cdot}$, and $Bz_8^+(A+1)$. The peak overlap is primarily because when one disulfide bond is cleaved, the hydrogen can attach to either sulfur of one disulfide. Thus the fragments, such as $Bc_8(S\cdot)^+$ and $Bc_8(SH)^+$, are 1.00728 Da apart, depending on the charge states of ions, which cause the overlapping of isotopic peaks of different groups of ions.

Since more than one electron is often needed to cleave both disulfide and N-C_α bonds in disulfide bound proteins to generate detectable backbone fragments, it is not surprising that in the previous ETD study of insulin by Liu *et al.*, neither separation of the two constituent chains of insulin (+6) nor cleavages within the loop defined by the disulfide bridges were observed under normal ETD conditions, and only up to 38.8% backbone cleavage efficiency was achieved by ETD with simultaneous ion trap collisional activation of the first generation charge-reduced product during the ion/ion reaction period.[22]

7.3.1.3 Hydrogen abstraction

The cleavage of the two inter-chain disulfide bonds of insulin was also observed as expected (see Figure 7.2f); however, it is surprising to

observe the $[A(2\times S\bullet)+H\text{-}H]^+$, $[A(2\times S\bullet)+2H\text{-}H]^{2+}$, and $[B(2\times S\bullet)+2H\text{-}H]^{2+}$ species. Taking the $[B(2\times S\bullet)+2H\text{-}H]^{2+}$ species for an example, the results suggest that one of the hydrogens on the B-chain was abstracted by A-chain when the two inter-chain disulfide bonds were cleaved, and likewise for the generation of $[A(2\times S\bullet)+H\text{-}H]^+$, $[A(2\times S\bullet)+2H\text{-}H]^{2+}$ species. Therefore, this observation indicates that, for both A- and B-chains, one of the hydrogen atoms abstracted by the $-S^-$ anion ions is not from the charge carrier site but elsewhere within the insulin sequence. The whole spectrum (Figure 7.1) was examined to track possible sites of hydrogen abstracted, and the observation of Az_3^+-H• (Figure 7.2c) and $Bz_4^{+\bullet}$-H• (Figure 7.2g) ions suggests that the abstraction of hydrogens both came from the C-terminal region of A– and B–chains of insulin, respectively. Previously, the hydrogen loss from z• ions has been reported by Savitski *et al.*, in which they observed that amino acids Ser, Thr, and Trp in certain position of the peptide's sequence promote the H• loss from z• ions.[322] However, it is not known where exactly the hydrogen is from; possibilities include C_α, C_β, or from the hydroxyl groups of Tyr of Az_3 or Thr of Bz_4. Therefore, an attempt to further locate the abstracted hydrogens by reacting hydroxyl groups with acetic anhydride was carried out. However, as shown in the appendix Figure F.1, the charge state of insulin shifts from mainly +6 to +4 after the reaction, which suggests that two of the charge carrier sites, the $-NH_2$ groups, also reacted with acetic anhydride as a side reaction. Thus, the ECD reaction was severely suppressed. Similar results were also observed in the ETD study of triply fixed-charge disulfide peptides by McLuckey *et al.*,[278] in which they postulated that an

amide-hydrogen might be a possible source for hydrogen abstraction.

7.3.1.4 Hydrogen transfer from c to z• ions

As mentioned above, the observation of the z_8^+ ion (Figure 7.2b) suggests the existence of hydrogen bonding in the gas-phase structure of the $[I+6H]^{6+}$ ion of insulin. The detection of Bc_2^+, Bc_3^+, $Bc_3^{+\bullet}$ (c_3-H•), $Bz_4^{+\bullet}$, and Bz_4^+($z_4^{+\bullet}$+H•) ions further localize the hydrogen bond interactions to the side chains of Asn3(B) and Thr27(B), which is also evidenced by the observation of c_n•/z_m^+ ions in the middle of the B-chain (n=3~18, m=4~23). Most likely, the hydrogen bonding to the side chains of Asn3(B) and Thr27(B) residues hold the c/z• pairs together, which leads to the transfer of H• from c ions to z• ions.[84, 323]

7.3.2 Top-down ECD of Ribonuclease A (RNase A)

7.3.2.1 ECD, IR-ECD, *vs* shots-ECD

RNase A is a ~13.7 kDa protein with 124 residues and four disulfide bonds (Cys26–Cys84, Cys58–110, Cys40–95, and Cys65–72). In previous reports of sequencing RNase A by using top-down ECD, no backbone fragment ions were observed for intact RNase A, and up to 47% backbone cleavage efficiency was achieved for a fully disulfide reduced RNase A.[324] Here RNase A was chosen as an example to further test the method. In comparison, normal ECD, infrared activated ECD (IR–ECD), and Shots–ECD were performed to compare the fragment efficiencies of different methods as shown in Figure 7.3.

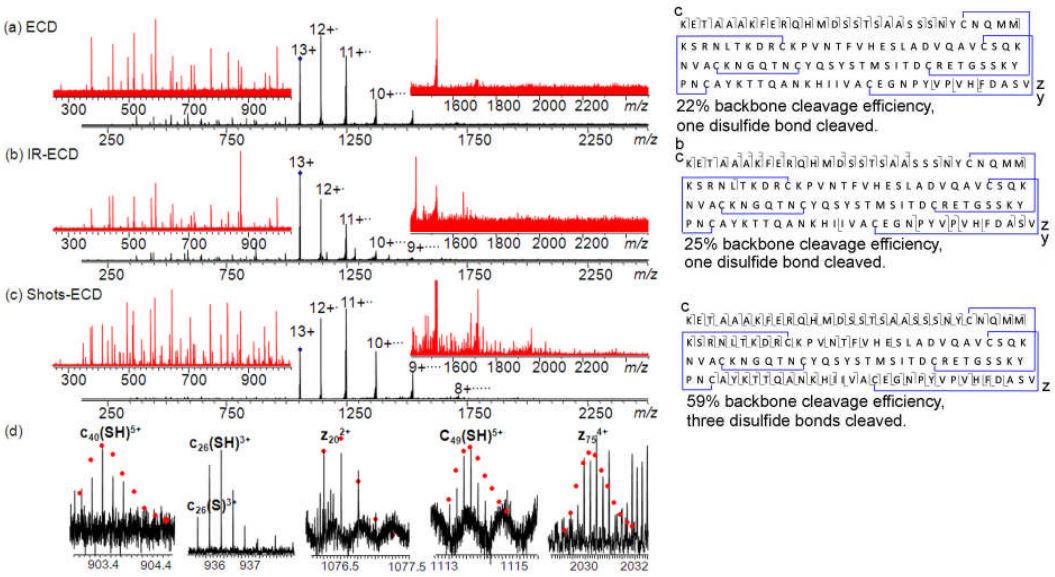

Figure 7.3 MS/MS spectra of $[Rnase\ A+13H]^{13+}$ ions at *m/z* 1053. (a) ECD; (b) IR-ECD; (c) shot-ECD; and (d) fragment ions correspond to cleavages of both N-C_α bond and disulfide bond(s) from Figure 7.1c. The insets are the expanded spectra to show the spectra quality and the fragmentation patterns.

Figure 7.3a shows the normal ECD spectra of RNase A and it can be seen that fragments obtained are mainly c ions outside of the disulfide-linked regions, and only 22% backbone cleavage efficiency was achieved (see the left-hand of Figure 7.3a). In addition, one tiny peak corresponding to c_{30}^{3+} was observed, which originates from the cleavage of the disulfide bond Cys26–Cys84 and one N-Cα bond. This result primarily agrees with the ECD data of other disulfide bonded proteins obtained by Breuker *et al*.[318] To further improve the ECD fragmentation efficiency, IR (420ms, 2.5 W) heating prior to ECD was used to activate ions and the IR-ECD spectra are shown in Figure 7.3b. A slight increase (3%) in backbone cleavage efficiency was gained with one additional c-

ion (c_{35}) from the Cys26-Cys84 bridged region and one additional z•-ion (z_{18}) from the Cys58-Cys110 linked region (see insets of Figure 7.3b). Further increasing the IR laser power to 15% leads to more b/y but not c/z• fragments (see appendix, Figure F.2), which indicates that ions and photons were well overlapped and 10% of laser power is sufficient to activate ions but not cause significant amount of b/y fragment generation. In contrast, when a one millisecond single-frequency activation clean-up power was simultaneously given (at *m/z* 100 Da with 5% clean-up shots power) at the beginning of the ECD event, a significant improvement in fragmentation efficiency was achieved as presented in Figure 7.3c&d. Compared to ECD and IR-ECD, Shots-ECD generates many more fragment ions, as shown in the insets of Figure 7.3c. Overall, eleven more backbone cleavages were detected outside the disulfide-bridged regions; moreover, the cleavages of three out of four disulfide bonds along with 35 new backbone cleavages within the disulfide-bridged regions were observed. Some of the examples of ions generated by cleaving both disulfide and N-C_α bonds are presented in Figure 7.3d, such as c_{26}^{3+} (Cys26–Cys84 cleaved), c_{40}^{5+} and c_{49}^{5+} (both Cys26–Cys84 and Cys40–95 cleaved), z_{20}^{2+} (Cys58–110 cleaved), and z_{75}^{4+} (both Cys26–Cys84 and Cys40–95 cleaved).

7.3.2.2 Effect of bias voltages on backbone cleavage efficiency of Rnase A

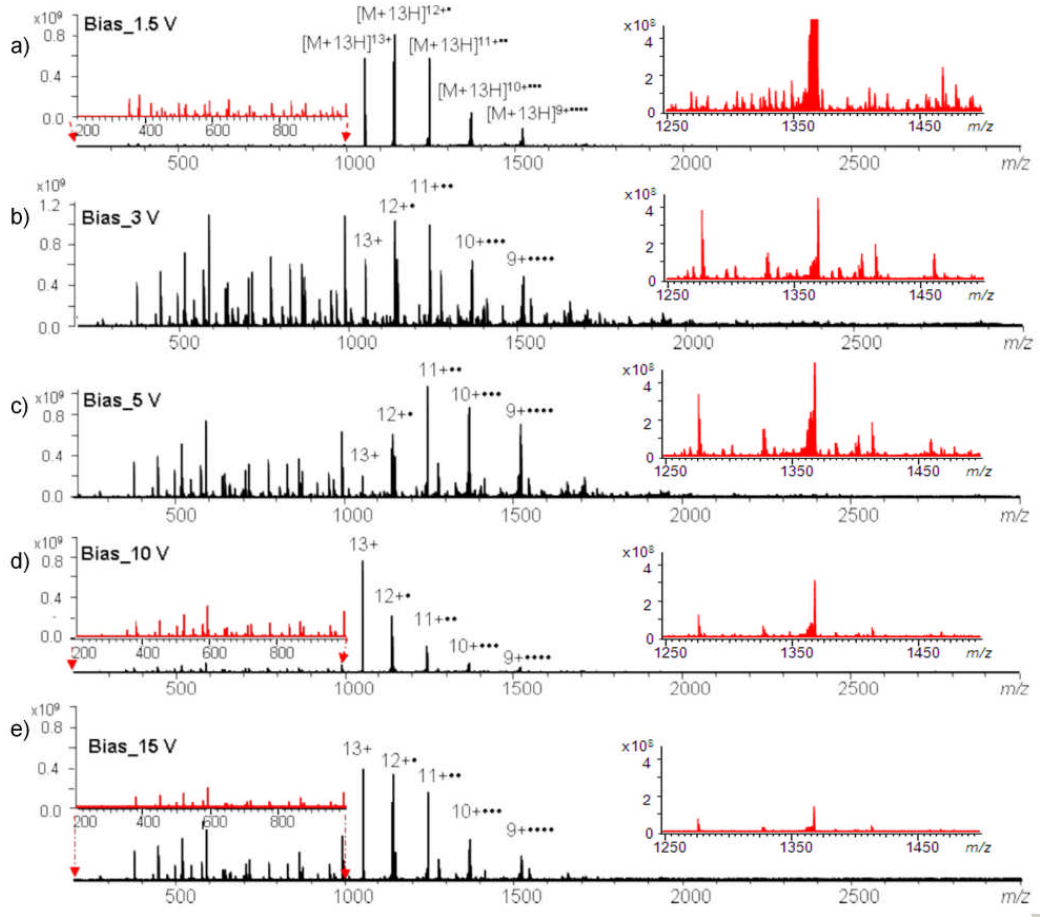

Figure 7.4 Shots-ECD spectra of the [Rnase A+13H]$^{13+}$ ion at different bias voltages. (a) 1.5V, (b) 3 V, (c) 5 V, (d) 10 V, and (e) 15 V. The insets show the details of each spectrum and the intensities of each spectrum are normalized to 1.0×10^{9} and 5×10^{8} for *m/z* 200 to 1000 and *m/z* 1250 to 1500, respectively.

Different electron gun bias voltages were applied to the hollow cathode used for generating electrons to examine the effect of bias voltages on radical-mediated fragmentation of the disulfide-rich protein, Rnase A. Figure 7.4 shows the shots-ECD spectra of the [Rnase A+13H]$^{13+}$ ion at different bias voltages, 1.5 V, 3 V, 5 V, 10 V, and 15 V (Figure 7.4a~e). The intensity (y-axis) of the *m/z* 200~1000 region of

each spectrum was normalized to 1×10^9 (arbitrary units) to compare the data quality of each method. The highest overall intensities of ions at low *m/z* region (*m/z* 200 to 1000) were achieved at a bias voltage of 3 V (inset of Figure 7.4b) and the peak intensities decrease when higher bias voltages were used (Figure 7.4c~e). Although the intensity of each individual fragment ion observed in the *m/z* 200~1000 region varies when using different bias voltages, there are no significant differences in terms of the presence of these ions. In contrast, the presence of the fragment ions in the high *m/z* region varies dramatically at different bias voltages. Taking the fragments in the *m/z* 1250~1500 region for an example, it is clear that more fragment ions were observed at the bias voltage of 1.5 V and the numbers and the intensities of fragment ions decreased as the bias voltage being increased. The peaks that likely disappear while using higher bias voltages are mostly z•-ions, which is likely because z-ions are radical species and prone to undergo secondary fragmentation especially when excessive energy is deposited into them.[64]

7.4 Conclusions

As demonstrated in the ECD study of disulfide bonded proteins, the Shots-ECD method can significantly improve backbone fragmentation efficiency of proteins. This strategy is fast, efficient, and with no need of chemical reduction of samples and instrument modification, and therefore can be a powerful approach to improve top-down ECD efficiency of not only disulfide bonded proteins but all proteins by FTICR MS. Although

capture of one electron can cleave one N–C_α bond and one S–S bond of a disulfide linked protein, multiple electron capture is often needed to generate more comprehensive sequence information for disulfide-rich proteins. Thus, activating charge reduced species (the ones capture multiple electrons ($n \geq 2$) should provide more information for disulfide bonded proteins.

Although it is not clear why such a short (1 ms) activation can make such a huge difference, there are a few things that are clear: first, the excitation frequency used at ~ 1.8 MHz range is far away from the frequency of the precursor or fragment ions. Second, in the comparison experiment of IR-ECD and Shots-ECD, more c/z fragment ions but not b/y ions were observed, which indicates that the mechanism of ions being activated in Shots-ECD is different from IR heating. Third, the cleanup shots power works at ~15%, further increasing the power leads to the loss of ions. Last but not least, different shot-excitation frequencies have been used to activate ions; excitation pulse at higher frequencies usually works better, and the performance appears to vary with the molecular ions. Further experiments are currently underway and will be reported separately.

Chapter 8

Conclusion and future work

8.1 Conclusions

Cisplatin along with other platinum-based drugs are the most widely used anticancer agents. However drug resistance has been a major problem for the successful chemotherapeutic treatment of cancer. Protein platination is implicated to be responsible for many of the severe side effects, which is a modification obtained during the treatment of cancer with Pt-based drugs due to the binding of platinum to proteins. The mode of transport of cisplatin and its analogs through the cell membranes and possible intermediate binding to proteins remain largely unknown. Therefore, it is important to study the reaction of Pt-based drugs with proteins and to build analytical methodologies, with the ultimate goal of building some reaction and analysis rules for doing bulk proteomics to determine where these drugs bind in vivo and how this correlates with chemotherapy side-effects. This thesis focuses on the application of tandem fragmentation techniques, mainly electron capture dissociation (ECD), to characterize the reaction products and Pt-modification sites, and to understand possible side effects of platination on proteins.

Sulfur–containing biomolecules play significant roles in platinum anticancer chemotherapy because of their high affinity for platinum compounds. CaM is a methionine (Met)–rich protein, with 8 out of 9 Met

residues locating on the hydrophobic areas that facilitate CaM association and activation of a diversity protein targets. CaM was therefore chosen to study its interaction with cisplatin and its analogues using high resolution tandem mass spectrometry (MS). It was first time that ECD has been successfully applied in top-down MS analysis of Pt-modified proteins. Unlike previous suggestions that metals are electron traps, which terminate the normal ECD fragmentation pathways, multiple electron capture pathways were observed in the platinum–modified CaM ions, such as, direct electron capture by platinum(II), side chain losses, and normal backbone N–C_α bond cleavages leading to c/$z^{\cdot}$ ions. With the combination of top-down and bottom-up MS approaches, the binding forms of Pt-based drugs to CaM and the Pt-modification sites on CaM were characterized. It was found that cisplatin cross-links multiple Met pairs on CaM, which leads to the assumption that these intramolecular Pt–crosslinkings on CaM might induce loss of CaM conformational flexibility to recognize calcium or target proteins, and thereby loss of its function as a calcium sensor and a signal transducer. This hypothesis was further tested by a melittin binding assay. The results show that Ca_4–CaM maintains to a certain extent its ability to recognize melittin even when cross–linked by platinum; however, calcium–free CaM, when cross–linked by cisplatin, loses its ability to recognize the target, melittin. Thus, the cross–linking of cisplatin to apo–CaM or Ca–CaM can inhibit the ability of CaM to recognize its target proteins.

Further, the results from cross-linking of platinum on CaM suggests the possibility of using cisplatin as a protein cross–linking reagent. The

cross-linking ability of cisplatin was further explored and demonstrated on other peptides and proteins. However, it is not just Pt-crosslinking but many of the inherent features of platinum(II) which make cisplatin an interesting cross-linking reagent, such as targeting new protein functional groups (thioether and imidazole groups), its unique isotopic pattern, its inherent positive charge, its potential of binding to different functional groups.

One problem encountered when re-examining the Pt-crosslinking results on CaM is that the distance constraints obtained from NMR structures of CaM are inconsistent with the measured distance constraints by cross–linking. Therefore, a combined flexibility simulation method was applied to explore whether the flexibility motions of CaM might contribute to the observation Pt-crosslinking on CaM. The flexibility analysis showed that both + Ca and – Ca CaM structures have extensive flexibility, and flexible motions can bring sulfur atoms of Met residues in the hydrophobic patches close and within 5 Å, which provides opportunities for cisplatin to cross–link Met residues of CaM. The simulation analysis is consistent with the MS results. Therefore, the simulation of flexible motion can be a very useful tool for predicting cross–linking pairs in proteins and facilitating MS data analysis. In addition, flexibility simulation also suggests that the crosslinking of cisplatin on CaM can inhibit the activity of CaM, as observed in the mellitin binding essay.

As mentioned above, based on fragment information obtained in CAD and ECD experiments, including the Pt-modified b/y and c/z ions

and unmodified b/y and c/z ions, the Pt-modification sites have been successfully localized. However, there are situations that still make the unambiguous identification of Pt-modification sites challenging, such as (1) cisplatin has four ligands which can be displaced to form up to four bonds with a protein or peptide. (2) There are often multiple potential Pt–binding sites presented in one sequence, sometimes those potential Pt–binding sites are adjacent or close to each other. (3) Positional isomers are often formed during the reaction of Pt(II) complexes with proteins. Therefore, without any prior separation, the precursor ion isolated for fragmentation is often a mixture of ions with exactly the same mass but different structures, which can significantly complicate the tandem spectra and data interpretation. (4) CAD-induced cleavage of PTMs, including Pt-modifications, depends on the collision energy used, thus can lead to erroneous conclusions, especially in those situations where there are multiple potential binding sites close to each other in a sequence. Previously it was observed that when platinum binds to a Met residue of a peptide or protein sequence, there is a signature side chain loss of CH_3SH in ECD. Therefore, to further explore the possibility of using radical-mediated side chain loss to assist the assignment the platinum-modification sites, a series of peptides with potential cisplatin binding sites (Met(S), His(N), Cys(S), disulfide, carboxyl groups of Asp and Glu, and amine groups of Arg and Lys, were reacted with cisplatin, then analyzed by ECD in FTICR MS. The results demonstrate that radical–mediated side–chain losses from the charge–reduced (M + Pt) species (such as $CH_3S\bullet$ or CH_3SH from Met, $SH\bullet$ from Cys, CO_2 from Glu or Asp,

and NH_2• from amine groups, can be used as characteristic indicators for rapid and unambiguous localization of the Pt–modification sites to certain amino acid residues. The method was further successfully applied to interpret the top-down ECD spectrum of an inter-chain Pt-crosslinked insulin dimer, insulin+Pt(NH_3)$_2$+insulin (>10 kDa). It was believed that radical-mediated side chain losses can be used to improve data interpretation and produce a more comprehensive picture of Pt–modifications on proteins.

Disulfide bonds are PTM that are important for stabilizing the tertiary structures of proteins. The characterization of disulfide bonds is important to understand the structure of a protein. The sequence information obtained during CAD fragmentation of disulfide linked proteins is often rather limited, because multiple backbone bonds must be cleaved to yield product ions within the disulfide loop. Therefore, much more effort has been paid to apply ECD in the characterization of disulfide-linked peptides and proteins, and to understand the ECD mechanisms of disulfide-containing species.

Selenium and sulfur share many common physicochemical properties. To further explore the ECD mechanisms of sulfur– or selenium–containing species, a series of disulfide (S–S), sulfur–selenium (S–Se), and diselenide (Se–Se) bond–containing peptides was studied by ECD. Although the electron affinities of S atom (2.07 eV) and Se atom (2.02 eV) are very close, they have very different reactivity towards electrons. The results demonstrate that the radical has higher tendency to stay at selenium compared to sulfur after the cleavage of Se–S bonds

by ECD. In addition, the cleavage pathways of C–S bonds of a disulfide peptide and C–Se bonds of a diselenide peptide are different, and the results suggest that direct electron capture at Se–Se and C–Se bonds is the main process during ECD of inter–chain diselenide peptides. This research leads to a better understanding of the ECD mechanisms.

Although, top-down MS approach has been successfully used to sequence proteins rapidly, with the remarkable record of characterizing a protein over 200 kDa, the application of top-down MS approach to sequence disulfide-containing proteins remains challenging due to the lower fragmentation efficiency. Here, a new AI-ECD method, named Shots-ECD was applied, to improve the backbone fragmentation efficiency of disulfide-rich proteins. The results show that the Shots–ECD approach can not only cleave multiple disulfide bonds but also significantly improve the backbone cleavage efficiency. This strategy is fast, efficient, and with no need of chemical reduction of samples and instrument modification, and therefore can be a powerful approach to improve top-down ECD efficiency of not only disulfide bonded proteins but all proteins by FTICR MS. In addition, the observation of multiple groups of complementary ion-pairs (c/z•) in the Shots-ECD experiments of insulin makes the exploration of the fragmentation pathways of disulfide-rich proteins possible.

8.2 Future work

Pt(IV) complexes have become attractive due to their potential anticancer activity and the inert nature of platinum(IV). Platinum(IV)

requires reduction to Pt(II) species to become cytotoxic. [131, 132] Recently, Sadler's group has been developing light-sensitive Pt(IV) pro-drugs that can be photoactivated to active antitumor agents directly at the site of the tumor.[131, 229, 230] This therefore decreases the side-effects and toxicity. Similar to cisplatin, these molecules also react with proteins and little is known about the specificity or sites of this binding. Some preliminary research has been performed, and it is interesting to notice that Pt(IV) complexes preferentially interact with Met residues of peptides with all its original ligands intact, namely noncovalent interaction. In addition, many more new Pt-species will be generated during the reduction of Pt(IV) to Pt(II), and the system can be significantly complicated; thus it is necessary to study the interaction of Pt(IV) complexes to peptides or proteins in simple systems before performing large scale proteomic analysis.

Pt-drug resistance is a complex and multifactorial problem due to changes of multiple biological pathways, which involves a large number of proteins. Thus global quantitative proteomics screens are essential to identify the protein targets that are differentially expressed in drug resistant cell lines. The identification of proteins involved in Pt-drug resistance in cells would be useful in completing our understanding of Pt-complex interaction. Previously, the bottom-up MS approach in combination with other methods has been applied to proteomic of screening proteins that involve in cisplatin drug resistance, which allows high throughput protein identification, but prevent the interrogation of the complete sequence of the protein. [226, 228] A top-down MS approach, as an

alternative, can provide entire sequence information and the PTM sites. Although top-down MS analysis of intact proteins remains challenging due to the sample complexity, the lack of sensitivity, and the relatively low backbone cleavage efficiency, it has been successfully applied in many proteomics studies. [325, 326]

By covalently binding to the reactive groups of proteins, cross-linking reagents create the distance constraints that can help define 3-D structures of proteins or protein complexes. For protein-protein complex studies, a cross-linker with a short spacer arm (4-8 Å) is often used first to determine the degree of cross-linking. The space arm length of cisplatin is about 2.8 to 4.6 Å, which fits in this range. However, different spacer arm lengths are often required because steric effects dictate the distance between potential reaction sites for cross-linking, and a cross-linker with a longer spacer arm is favored for intermolecular cross-linking study. One way of increasing the arm length of Pt-based cross-linking reagents is to synthesize dinuclear-platinum complexes. By varying the lengths of the linker region between the two Pt-complexes, different arm lengths can be obtained. Previously, the cross-linking ability of a dinuclear Pt-complex, [{*cis*–$PtCl_2(NH_3)$}$_2$(μ–$NH_2(CH_2)_4NH_2$)], has been tested on calmodulin. Unfortunately, due to the *trans*-labilization effect, all four of the original ligands of each of the platinum are displaced. However, one can resolve this problem by replacing the chloride group that *trans* to the linker with other ligands that cannot be easily displaced, such as ammine groups. In addition, further research on finding the optimal crosslinker-to-protein molar ratios and the reaction time is also needed. With the combination

of flexibility simulation and Pt-based cross-linkers, it is possible to develop a general approach for probing of protein interactions and protein flexibility.

Furthermore, although the possibility of using radical-mediated side chain losses to quickly localize Pt-modification sites has been explored, it is not clear how these side chains bound to platinum disappeared during ECD, but platinum still binds to the peptide sequence. Ab initio calculations provide useful approach to tackle this puzzle, and to further explore the ECD mechanism of metal-bound peptides.[63, 67, 217]

Bibliography

1. Mann, M.; Jensen, O. N., Proteomic analysis of post-translational modifications. *Nature Biotechnology* **2003,** *21*, 255-261.

2. Baumann, M.; Meri, S., Techniques for studying protein heterogeneity and post-translational modifications. *Expert Review of Proteomics* **2004,** *1*, 207-217.

3. Sickmann, A.; Mreyen, M.; Meyer, H. E., Identification of modified proteins by mass spectrometry. *IUBMB Life* **2002,** *54*, 51-57.

4. Patterson, S. D., Protein identification and characterization by mass spectrometry. In *Current Protocols in Molecular Biology*, John Wiley & Sons, Inc.: 2001.

5. Lin, D.; Tabb, D. L.; Yates, J. R., Large-scale protein identification using mass spectrometry. *Bba-Proteins Proteom* **2003,** *1646*, 1-10.

6. Sickmann, A.; Mreyen, M.; Meyer, H., Mass spectrometry — a key technology in proteom research proteomics of microorganisms. Hecker, M., et al., Eds. Springer Berlin / Heidelberg: 2003; Vol. 83, pp 141-176.

7. Stone, K. L.; Crawford, M.; McMurray, W.; Williams, N.; Williams, K. R., Identification of proteins based on MS/MS spectra and location of posttranslational modifications peptide characterization and application protocols. Fields, G. B., Ed. Humana Press: 2007; Vol. 386, pp 57-77.

8. Nørregaard Jensen, O., Modification-specific proteomics:

characterization of post-translational modifications by mass spectrometry. *Current Opinion in Chemical Biology* **2004,** *8*, 33-41.

9. Hoffmann, E. D.; Stroobant, V., Mass spectrometry: principles and applications. 3rd Edition. *John Wiley & Sons, Ltd.* **2007**.

10. Karas, M.; Bachmann, D.; Hillenkamp, F., Influence of the wavelength in high-irradiance ultraviolet laser desorption mass spectrometry of organic molecules. *Analytical Chemistry* **1985,** *57*, 2935-2939.

11. Karas, M.; Bachmann, D.; Bahr, U.; Hillenkamp, F., Matrix-assisted ultraviolet laser desorption of non-volatile compounds. *International Journal of Mass Spectrometry and Ion Processes* **1987,** *78*, 53-68.

12. Karas, M.; Hillenkamp, F., Laser desorption ionization of proteins with molecular masses exceeding 10,000 daltons. *Analytical Chemistry* **1988,** *60*, 2299-2301.

13. Karas, M.; Bahr, U., Laser desorption ionization mass spectrometry of large biomolecules. *TrAC Trends in Analytical Chemistry* **1990,** *9*, 321-325.

14. Tanaka, K.; Waki, H.; Ido, Y.; Akita, S.; Yoshida, Y.; Yoshida, T.; Matsuo, T., Protein and polymer analyses up to m/z 100 000 by laser ionization time-of-flight mass spectrometry. *Rapid Communications in Mass Spectrometry* **1988,** *2*, 151-153.

15. Dettmer, K.; Aronov, P. A.; Hammock, B. D., Mass spectrometry-based metabolomics. *Mass Spectrometry Reviews* **2007,** *26*, 51-78.

16. Zhao, Y.; Kent, S. B. H.; Chait, B. T., Rapid, sensitive structure analysis of oligosaccharides. *Proceedings of the National Academy of Sciences of the United States of America* **1997,** *94*, 1629-1633.

17. Jurinke, C.; Oeth, P.; van den Boom, D., MALDI-TOF mass spectrometry. *Molecular Biotechnology* **2004,** *26*, 147-163.

18. Kirpekar, F.; Nordhoff, E.; Larsen, L. K.; Kristiansen, K.; Roepstorff, P.; Hillenkamp, F., DNA sequence analysis by MALDI mass spectrometry. *Nucleic Acids Research* **1998,** *26*, 2554-2559.

19. Zenobi, R.; Knochenmuss, R., Ion formation in MALDI mass spectrometry. *Mass Spectrometry Reviews* **1998,** *17*, 337-366.

20. Karas, M.; Krüger, R., Ion formation in MALDI: the cluster ionization mechanism. *Chemical Reviews* **2003,** *103*, 427-440.

21. Fenn, J.; Mann, M.; Meng, C.; Wong, S.; Whitehouse, C., Electrospray ionization for mass spectrometry of large biomolecules. *Science* **1989,** *246*, 64-71.

22. Chowdhury, S. K. K., V.; Chait, B. T., An electrospray-ionization mass spectrometer with new features. *Rapid Communications in Mass Spectrometry* **1990,** *4*, 81-87.

23. Nielen, M. W. F.; Buijtenhuijs, F. A., Polymer analysis by liquid chromatography/electrospray ionization time-of-flight mass spectrometry. *Analytical Chemistry* **1999,** *71*, 1809-1814.

24. Colton, R.; Traeger, J. C., The application of electrospray mass spectrometry to ionic inorganic and organometallic systems. *Inorganica Chimica Acta* **1992,** *201*, 153-155.

25. Loo, J. A., Electrospray ionization mass spectrometry: a technology for studying noncovalent macromolecular complexes. *International Journal of Mass Spectrometry* **2000,** *200*, 175-186.

26. Guilhaus, M., Principles and instrumentation in time-of-flight mass spectrometry: physical and instrumental concepts. *Journal of Mass Spectrometry* **1995,** *30*, 1519-1532.

27. Chernushevich, I. V.; Loboda, A. V.; Thomson, B. A., An introduction to quadrupole–time-of-flight mass spectrometry. *Journal of Mass Spectrometry* **2001,** *36*, 849-865.

28. Comisarow, M. B.; Marshall, A. G., Fourier transform ion cyclotron resonance spectroscopy. *Chemical Physics Letters* **1974,** *25*, 282-283.

29. Marshall, A. G.; Hendrickson, C. L.; Jackson, G. S., Fourier transform ion cyclotron resonance mass spectrometry: A primer. *Mass Spectrometry Reviews* **1998,** *17*, 1-35.

30. Amster, I. J., Fourier transform mass spectrometry. *Journal of Mass Spectrometry* **1996,** *31*, 1325-1337.

31. Nikolaev, E.; Boldin, I.; Jertz, R.; Baykut, G., Initial experimental characterization of a new ultra-high resolution FTICR cell with dynamic harmonization. *Journal of the American Society for Mass Spectrometry* **2011,** *22*, 1125-1133.

32. Marshall, A. G.; Wang, T. C. L.; Ricca, T. L., Tailored excitation for Fourier transform ion cyclotron mass spectrometry. *Journal of the American Chemical Society* **1985,** *107*, 7893-7897.

33. Xie, Y.; Zhang, J.; Yin, S.; Loo, J. A., Top-down ESI-ECD-FT-ICR mass spectrometry localizes noncovalent protein-ligand binding sites. *Journal of the American Chemical Society* **2006,** *128*, 14432-14433.

34. Horn, D. M.; Zubarev, R. A.; McLafferty, F. W., Automated de novo sequencing of proteins by tandem high-resolution mass spectrometry. *Proceedings of the National Academy of Sciences of the United States of America* **2000,** *97*, 10313-10317.

35. Zubarev, R. A.; Horn, D. M.; Fridriksson, E. K.; Kelleher, N. L.; Kruger, N. A.; Lewis, M. A.; Carpenter, B. K.; McLafferty, F. W., Electron capture dissociation for structural characterization of multiply charged protein cations. *Analytical Chemistry* **2000,** *72*, 563-573.

36. McLafferty, F. W.; Bente, P. F.; Kornfeld, R.; Tsai, S.-C.; Howe, I., Metastable ion characteristics. XXII. Collisional activation spectra of organic ions. *Journal of the American Chemical Society* **1973,** *95*, 2120-2129.

37. Jennings, K. R., Collision-induced decompositions of aromatic molecular ions. *International Journal of Mass Spectrometry and Ion Physics* **1968,** *1*, 227-235.

38. Gauthier, J. W.; Trautman, T. R.; Jacobson, D. B., Sustained off-resonance irradiation for collision-activated dissociation involving Fourier transform mass spectrometry. Collision-activated dissociation technique that emulates infrared multiphoton dissociation. *Analytica Chimica Acta* **1991,** *246*, 211-225.

39. Schnier, P. D.; Price, W. D.; Jockusch, R. A.; Williams, E. R., Blackbody infrared radiative dissociation of bradykinin and its analogues: energetics, dynamics, and evidence for salt-bridge structures in the gas phase. *Journal of the American Chemical Society* **1996,** *118*, 7178-7189.

40. Zubarev, R. A.; Kelleher, N. L.; McLafferty, F. W., Electron capture dissociation of multiply charged protein cations. A nonergodic process. *Journal of the American Chemical Society* **1998,** *120*, 3265-3266.

41. Syka, J. E. P.; Coon, J. J.; Schroeder, M. J.; Shabanowitz, J.; Hunt, D. F., Peptide and protein sequence analysis by electron transfer dissociation mass spectrometry. *Proceedings of the National Academy of Sciences of the United States of America* **2004,** *101*, 9528-9533.

42. Budnik, B. A.; Haselmann, K. F.; Zubarev, R. A., Electron detachment dissociation of peptide di-anions: an electron–hole recombination phenomenon. *Chemical Physics Letters* **2001,** *342*, 299-302.

43. Roepstorff, P.; Fohlman, J., Proposal for a common nomenclature for sequence ions in mass spectra of peptides. *Biomedical mass spectrometry* **1984,** *11*, 601.

44. Qin, J.; Chait, B. T., Collision-induced dissociation of singly charged peptide ions in a matrix-assisted laser desorption ionization ion trap mass spectrometer. *International Journal of Mass Spectrometry* **1999,** *190–191*, 313-320.

45. Breci, L. A.; Tabb, D. L.; Yates, J. R.; Wysocki, V. H., Cleavage N-terminal to proline: analysis of a database of peptide tandem mass spectra. *Analytical Chemistry* **2003,** *75*, 1963-1971.

46. Jockusch, R. A.; Schnier, P. D.; Price, W. D.; Strittmatter, E. F.; Demirev, P. A.; Williams, E. R., Effects of charge state on fragmentation pathways, dynamics, and activation energies of ubiquitin ions measured by blackbody infrared radiative dissociation. *Analytical Chemistry* **1997,** *69*, 1119-1126.

47. Feng, R.; Konishi, Y., Collisionally-activated dissociation of multiply charged 150-kDa antibody ions. *Analytical Chemistry* **1993,** *65*, 645-649.

48. Gabelica, V.; De Pauw, E., Comparison of the collision-induced dissociation of duplex DNA at different collision regimes: Evidence for a multistep dissociation mechanism. *Journal of the American Society for Mass Spectrometry* **2002,** *13*, 91-98.

49. Duffin, K. L.; Welply, J. K.; Huang, E.; Henion, J. D., Characterization of N-linked oligosaccharides by electrospray and tandem mass spectrometry. *Analytical Chemistry* **1992,** *64*, 1440-1448.

50. Reinhold, V. N.; Reinhold, B. B.; Costello, C. E., Carbohydrate molecular weight profiling, sequence, linkage, and branching data: ES-MS and CID. *Analytical Chemistry* **1995,** *67*, 1772-1784.

51. Domon, B.; Costello, C. E., Structure elucidation of glycosphingolipids and gangliosides using high-performance tandem mass spectrometry. *Biochemistry* **1988,** *27*, 1534-1543.

52. Baykut, G.; Watson, C. H.; Weller, R. R.; Eyler, J. R., Infrared multiphoton dissociation of some oxygen-containing hydrocarbon ions: Differentiation of isomeric ion structures in the gas-phase. *Journal of the American Chemical Society* **1985,** *107*, 8036–8042.

53. Little, D. P.; Speir, J. P.; Senko, M. W.; O'Connor, P. B.; McLafferty, F. W., Infrared multiphoton dissociation of large multiply charged ions for biomolecule sequencing. *Analytical Chemistry* **1994,** *66*, 2809-2815.

54. Guan, Z.; Kelleher, N. L.; O'Connor, P. B.; Aaserud, D. J.; Little, D. P.; McLafferty, F. W., 193 nm photodissociation of larger multiply-charged biomolecules. *International Journal of Mass Spectrometry and Ion Processes* **1996,** *157–158*, 357-364.

55. Reiber, D. C.; Brown, R. S.; Weinberger, S.; Kenny, J.; Bailey, J., Unknown peptide sequencing using matrix-assisted laser desorption/ionization and in-source decay. *Analytical Chemistry* **1998,** *70*, 1214-1222.

56. Zubarev, R. A.; Haselmann, K. F.; Budnik, B.; Kjeldsen, F.; Jensen, F., Towards an understanding of the mechanism of electron-capture dissociation: a historical perspective and modern ideas. *ChemInform* **2003,** *34*, 337-349.

57. Zubarev, R. A.; Kruger, N. A.; Fridriksson, E. K.; Lewis, M. A.; Horn, D. M.; Carpenter, B. K.; McLafferty, F. W., Electron capture

dissociation of gaseous multiply-charged proteins is favored at disulfide bonds and other sites of high hydrogen atom affinity. *Journal of the American Chemical Society* **1999,** *121*, 2857-2862.

58. Sawicka, A.; Skurski, P.; Hudgins, R. R.; Simons, J., Model calculations relevant to disulfide bond cleavage via electron capture influenced by positively charged groups. *The Journal of Physical Chemistry B* **2003,** *107*, 13505-13511.

59. Anusiewicz, W. B.-K., J. Simons, J., Coulomb-assisted dissociative electron attachment: application to a model peptide. *The Journal of Physical Chemistry A* **2005,** *109*, 5801-5813.

60. Turecek, F.; Chen, X.; Hao, C., Where does the electron go? Electron distribution and reactivity of peptide cation radicals formed by electron transfer in the gas phase. *Journal of the American Chemical Society* **2008,** *130*, 8818-8833.

61. Chamot-Rooke, J.; van der Rest, G.; Dalleu, A.; Bay, S.; Lemoine, J., The combination of electron capture dissociation and fixed charge derivatization increases sequence coverage for O-glycosylated and O-phosphorylated peptides. *Journal of the American Society for Mass Spectrometry* **2007,** *18*, 1405-1413.

62. Sohn, C. H.; Chung, C. K.; Yin, S.; Ramachandran, P.; Loo, J. A.; Beauchamp, J. L., Probing the mechanism of electron capture and electron transfer dissociation using tags with variable electron affinity. *Journal of the American Chemical Society* **2009,** *131*, 5444-5459.

63. Simons, J., Mechanisms for S–S and N–Cα bond cleavage in peptide ECD and ETD mass spectrometry. *Chemical Physics Letters* **2010,** *484*, 81-95.

64. Leymarie, N.; Costello, C. E.; O'Connor, P. B., Electron capture dissociation initiates a free radical reaction cascade. *Journal of the American Chemical Society* **2003,** *125*, 8949-8958.

65. Turečček, F., NCα bond dissociation energies and kinetics in amide and peptide radicals. Is the dissociation a Non-ergodic process? *Journal of the American Chemical Society* **2003,** *125*, 5954-5963.

66. Hudgins, R. R.; Håkansson, K.; Quinn, J. P.; Hendrickson, C. L.; Marshall, A. G., Electron capture dissociation of peptides and proteins does not require a hydrogen atom mechanism. *Proceedings of the 50th ASMS Conference on Mass Spectrometry and Allied Topics, Orlando, Florida.* **2002**.

67. Skurski, P.; Sobczyk, M.; Jakowski, J.; Simons, J., Possible mechanisms for protecting NCα bonds in helical peptides from electron-capture (or transfer) dissociation. *International Journal of Mass Spectrometry* **2007,** *265*, 197-212.

68. Sobczyk, M.; Neff, D.; Simons, J., Theoretical study of through-space and through-bond electron transfer within positively charged peptides in the gas phase. *International Journal of Mass Spectrometry* **2008,** *269*, 149-164.

69. Syrstad, E.; Turecček, F., Toward a general mechanism of electron capture dissociation. *Journal of the American Society for Mass Spectrometry* **2005,** *16*, 208-224.

70. Chung, T.; Hui, R.; Ledvina, A.; Coon, J.; Tureček, F., Cascade dissociations of peptide cation-radicals. Part 1. Scope and effects of amino acid residues in penta-, nona-, and decapeptides. *Journal of the American Society for Mass Spectrometry* **2012,** *23*, 1336-1350.

71. Ledvina, A.; Chung, T.; Hui, R.; Coon, J.; Tureček, F., Cascade dissociations of peptide cation-radicals. Part 2. Infrared multiphoton dissociation and mechanistic studies of z-ions from pentapeptides. *Journal of the American Society for Mass Spectrometry* **2012,** *23*, 1351-1363.

72. Savitski, M. M.; Nielsen, M. L.; Zubarev, R. A., Side-chain losses in electron capture dissociation to improve peptide identification. *Analytical Chemistry* **2007,** *79*, 2296-2302.

73. Cooper, H. J.; Hudgins, R. R.; Håkansson, K.; Marshall, A. G., Characterization of amino acid side chain losses in electron capture dissociation. *Journal of the American Society for Mass Spectrometry* **2002,** *13*, 241-249.

74. Xia, Q.; Lee, M. V.; Rose, C. M.; Marsh, A. J.; Hubler, S. L.; Wenger, C. D.; Coon, J. J., Characterization and diagnostic value of amino acid side chain neutral losses following electron-transfer dissociation. *Journal of the American Society for Mass Spectrometry* **2011,** *22*, 255-264.

75. Fung, Y. M. E.; Chan, T. W. D., Experimental and theoretical investigations of the loss of amino acid side chains in electron capture dissociation of model peptides. *Journal of the American Society for Mass Spectrometry* **2005,** *16*, 1523-1535.

76. Baba, T.; Hashimoto, Y.; Hasegawa, H.; Hirabayashi, A.; Waki, I., Electron capture dissociation in a radio frequency ion trap. *Analytical Chemistry* **2004,** *76*, 4263-4266.

77. Silivra, O.; Kjeldsen, F.; Ivonin, I.; Zubarev, R., Electron capture dissociation of polypeptides in a three-dimensional quadrupole ion trap: Implementation and first results. *Journal of the American Society for Mass Spectrometry* **2005,** *16*, 22-27.

78. Tsybin, Y.; Quinn, J.; Tsybin, O.; Hendrickson, C.; Marshall, A., Electron capture dissociation implementation progress in fourier

transform ion cyclotron resonance mass spectrometry. *Journal of the American Society for Mass Spectrometry* **2008,** *19*, 762-771.

79. Tsybin, Y. O.; Witt, M.; Baykut, G.; Håkansson, P., Electron capture dissociation Fourier transform ion cyclotron resonance mass spectrometry in the electron energy range 0–50 eV. *Rapid Communications in Mass Spectrometry* **2004,** *18*, 1607-1613.

80. McFarland, M. A.; Chalmers, M. J.; Quinn, J. P.; Hendrickson, C. L.; Marshall, A. G., Evaluation and optimization of electron capture dissociation efficiency in Fourier transform ion cyclotron resonance mass spectrometry. *Journal of the American Society for Mass Spectrometry* **2005,** *16*, 1060-1066.

81. Tsybin, Y. O.; Hendrickson, C. L.; Beu, S. C.; Marshall, A. G., Impact of ion magnetron motion on electron capture dissociation Fourier transform ion cyclotron resonance mass spectrometry. *International Journal of Mass Spectrometry* **2006,** *255–256*, 144-149.

82. Mormann, M.; Peter-Katalinić, J., Improvement of electron capture efficiency by resonant excitation. *Rapid Communications in Mass Spectrometry* **2003,** *17*, 2208-2214.

83. Gorshkov, M. V.; Masselon, C. D.; Nikolaev, E. N.; Udseth, H. R.; Paša-Tolić, L.; Smith, R. D., Considerations for electron capture dissociation efficiency in FTICR mass spectrometry. *International Journal of Mass Spectrometry* **2004,** *234*, 131-136.

84. O'Connor, P.; Lin, C.; Cournoyer, J.; Pittman, J.; Belyayev, M.; Budnik, B., Long-lived electron capture dissociation product ions experience radical migration via hydrogen abstraction. *Journal of the American Society for Mass Spectrometry* **2006,** *17*, 576-585.

85. Tsybin, Y. O.; Witt, M.; Baykut, G.; Kjeldsen, F.; Håkansson, P., Combined infrared multiphoton dissociation and electron capture dissociation with a hollow electron beam in Fourier transform ion cyclotron resonance mass spectrometry. *Rapid Communications in Mass Spectrometry* **2003,** *17*, 1759-1768.

86. Lin, C.; Cournoyer, J.; O'Connor, P., probing the gas-phase folding kinetics of peptide ions by IR activated DR-ECD. *Journal of the American Society for Mass Spectrometry* **2008,** *19*, 780-789.

87. Tsybin, Y. O.; He, H.; Emmett, M. R.; Hendrickson, C. L.; Marshall, A. G., Ion activation in electron capture dissociation to distinguish between N-terminal and C-terminal product Ions. *Analytical Chemistry* **2007,** *79*, 7596-7602.

88. Horn, D. M.; Ge, Y.; McLafferty, F. W., Activated ion electron capture dissociation for mass spectral sequencing of larger (42 kDa) proteins. *Analytical Chemistry* **2000,** *72*, 4778-4784.

89. Laskin, J.; Futrell, J. H., Activation of large Ions in FT-ICR mass spectrometry. *Mass Spectrometry Reviews* **2005,** *24*, 135-167.

90. Cooper, H. J.; Håkansson, K.; Marshall, A. G., The role of electron capture dissociation in biomolecular analysis. *Mass Spectrometry Reviews* **2005,** *24*, 201-222.

91. Sweet, S. M. M.; Cooper, H. J., Electron capture dissociation in the analysis of protein phosphorylation. *Expert Review of Proteomics* **2007,** *4*, 149-159.

92. Kelleher, N. L.; Zubarev, R. A.; Bush, K.; Furie, B.; Furie, B. C.; McLafferty, F. W.; Walsh, C. T., Localization of Labile Posttranslational Modifications by Electron Capture Dissociation: The Case of γ-Carboxyglutamic Acid. *Analytical Chemistry* **1999,** *71*, 4250-4253.

93. Kelleher, N. L.; Zubarev, R. A.; Bush, K.; Furie, B.; Furie, B. C.; McLafferty, F. W.; Walsh, C. T., Localization of labile posttranslational modifications by electron capture dissociation: the case of γ-carboxyglutamic acid. *Analytical Chemistry* **1999,** *71*, 4250-4253.

94. Cournoyer, J. J.; Lin, C.; O'Connor, P. B., Detecting deamidation products in proteins by electron capture dissociation. *Analytical Chemistry* **2005,** *78*, 1264-1271.

95. Zhang, Y.; Cui, W.; Zhang, H.; Dewald, H. D.; Chen, H., Electrochemistry-assisted top-down characterization of disulfide-containing proteins. *Analytical Chemistry* **2012,** *84*, 3838-3842.

96. Diedrich, J. K.; Julian, R. R., Facile identification of phosphorylation sites in peptides by radical directed dissociation. *Analytical Chemistry* **2011,** *83*, 6818-6826.

97. Breuker, K.; McLafferty, F. W., Native electron capture dissociation for the structural characterization of noncovalent interactions in native cytochrome c. *Angewandte Chemie International Edition* **2003,** *42*, 4900-4904.

98. Skinner, O.; McLafferty, F.; Breuker, K., How ubiquitin unfolds after transfer into the gas phase. *Journal of the American Society for Mass Spectrometry* **2012,** *23*, 1011-1014.

99. Breuker, K.; McLafferty, F. W., The thermal unfolding of native cytochrome c in the transition from solution to gas phase probed by native electron capture dissociation. *Angewandte Chemie International Edition* **2005,** *44*, 4911-4914.

100. Breuker, K.; McLafferty, F. W., Stepwise evolution of protein native structure with electrospray into the gas phase, 10−12 to 102 s. *Proceedings of the National Academy of Sciences of the United States of America* **2008,** *105*, 18145-18152.

101. Zhang, H.; Cui, W.; Wen, J.; Blankenship, R.; Gross, M., Native electrospray and electron-capture dissociation in FTICR mass spectrometry provide top-down sequencing of a protein component in an intact protein assembly. *Journal of the American Society for Mass Spectrometry* **2010,** *21*, 1966-1968.

102. Marty, M. T.; Zhang, H.; Cui, W.; Blankenship, R. E.; Gross, M. L.; Sligar, S. G., Native mass spectrometry characterization of intact nanodisc lipoprotein complexes. *Analytical Chemistry* **2012**.

103. Zhang, H.; Cui, W.; Wen, J.; Blankenship, R. E.; Gross, M. L., Native electrospray and electron-capture dissociation FTICR mass spectrometry for top-down studies of protein assemblies. *Analytical Chemistry* **2011,** *83*, 5598-5606.

104. Swaney, D. L.; McAlister, G. C.; Wirtala, M.; Schwartz, J. C.; Syka, J. E. P.; Coon, J. J., Supplemental activation method for high-efficiency electron-transfer dissociation of doubly protonated peptide precursors. *Analytical Chemistry* **2006,** *79*, 477-485.

105. Yoo, H. J.; Wang, N.; Zhuang, S.; Song, H.; Håkansson, K., Negative-ion electron capture dissociation: radical-driven fragmentation of charge-increased gaseous peptide anions. *Journal of the American Chemical Society* **2011,** *133*, 16790-16793.

106. Budnik, B. A.; Haselmann, K. F.; Elkin, Y. N.; Gorbach, V. I.; Zubarev, R. A., Applications of electron−ion dissociation reactions for analysis of polycationic chitooligosaccharides in Fourier transform mass spectrometry. *Analytical Chemistry* **2003,** *75*, 5994-6001.

107. Ganisl, B.; Valovka, T.; Hartl, M.; Taucher, M.; Bister, K.; Breuker, K., Electron detachment dissociation for top-down mass spectrometry of acidic proteins. *Chemistry – A European Journal* **2011,** *17*, 4460-4469.

108. Yang, J.; Mo, J.; Adamson, J. T.; Håkansson, K., Characterization of oligodeoxynucleotides by electron detachment dissociation Fourier transform ion cyclotron resonance mass spectrometry. *Analytical Chemistry* **2005,** *77*, 1876-1882.

109. Wolff, J.; Laremore, T.; Aslam, H.; Linhardt, R.; Amster, I., Electron-induced dissociation of glycosaminoglycan tetrasaccharides. *Journal of the American Society for Mass Spectrometry* **2008,** *19*, 1449-1458.

110. Fuertes, M. A.; Alonso, C.; Pérez, J. M., Biochemical Modulation of Cisplatin Mechanisms of Action: Enhancement of Antitumor Activity and Circumvention of Drug Resistance. *Chemical Reviews* **2003,** *103*, 645-662.

111. Jamieson, E. R.; Lippard, S. J., Structure, recognition, and processing of cisplatin−DNA adducts. *Chemical Reviews* **1999,** *99*, 2467-

2498.

112. Wong, E.; Giandomenico, C. M., Current status of platinum-based antitumor drugs. *Chemical Reviews* **1999,** *99*, 2451-2466.

113. Reedijk, J., Why does cisplatin reach guanine-N7 with competing S-donor ligands available in the cell? *Chemical Reviews* **1999,** *99*, 2499-2510.

114. Wang, D.; Lippard, S. J., Cellular processing of platinum anticancer drugs. *Nature Reviews Drug Discovery* **2005,** *4*, 307-320.

115. Kelland, L., The resurgence of platinum-based cancer chemotherapy. *Nature Review Cancer* **2007,** *7*, 573-584.

116. Gibson, D.; Costello, C. E., A mass spectral study of the binding of the anticancer drug cisplatin to ubiquitin. *European Journal of Mass Spectrometry* **1999,** *5*, 501-510.

117. Lin, X.; Okuda, T.; Holzer, A.; Howell, S. B., The copper transporter CTR1 regulates cisplatin uptake in Saccharomyces cerevisiae. *Molecular Pharmacology* **2002,** *62*, 1154-1159.

118. Holzer, A. K.; Howell, S. B., The internalization and degradation of human copper transporter 1 following cisplatin exposure. *Cancer Research* **2006,** *66*, 10944-10952.

119. Pabla, N.; Murphy, R. F.; Liu, K.; Dong, Z., The copper transporter Ctr1 contributes to cisplatin uptake by renal tubular cells during cisplatin nephrotoxicity. *American Journal of Physiology - Renal Physiology* **2009,** *296*, F505-F511.

120. Wang, X.; Du, X.; Li, H.; Chan, D. S.-B.; Sun, H., The effect of the extracellular eomain of human copper transporter (hCTR1) on cisplatin activation. *Angewandte Chemie International Edition* **2011,** *50*, 2706-2711.

121. Du, X.; Wang, X.; Li, H.; Sun, H., Comparison between copper and cisplatin transport mediated by human copper transporter 1 (hCTR1). *Metallomics* **2012,** *4*, 679-685.

122. Kasherman, Y.; Sturup, S.; Gibson, D., Trans labilization of am(m)ine ligands from platinum(II) complexes by cancer cell extracts. *Journal of Biological Inorganic Chemistry* **2009,** *14*, 387-399.

123. Wang, X.; Guo, Z., The role of sulfur in platinum anticancer chemotherapy. *Anti-cancer agents in medicinal chemistry* **2007,** *7*, 19-34.

124. Karotki, A. V.; Vašák, M., Interaction of metallothionein-2 with platinum-modified 5′-guanosine monophosphate and DNA. *Biochemistry* **2008,** *47*, 10961-10969.

125. Knipp, M.; Karotki, A. V.; Chesnov, S.; Natile, G.; Sadler, P. J.; Brabec, V.; Vašák, M., Reaction of Zn_7Metallothionein with cis- and trans-[Pt(N-donor)$_2$Cl$_2$] anticancer complexes: trans-PtII complexes retain their N-Donor ligands. *Journal of Medicinal Chemistry* **2007,** *50*, 4075-4086.

126. Kröning, R.; Lichtenstein, A. K.; Nagami, G. T., Sulfur-containing amino acids decrease cisplatin cytotoxicity and uptake in renal tubule epithelial cell lines. *Cancer Chemotherapy and Pharmacology* **2000,** *45*, 43-49.

127. Lau, J. K.-C.; Deubel, D. V., Loss of ammine from platinum(II) complexes: implications for cisplatin inactivation, storage, and resistance. *Chemistry – A European Journal* **2005,** *11*, 2849-2855.

128. Arnesano, F.; Boccarelli, A.; Cornacchia, D.; Nushi, F.; Sasanelli, R.; Coluccia, M.; Natile, G., Mechanistic Insight into the Inhibition of Matrix Metalloproteinases by Platinum Substrates†. *Journal of Medicinal Chemistry* **2009,** *52*, 7847-7855.

129. Palm, M. E.; Weise, C. F.; Lundin, C.; Wingsle, G.; Nygren, Y.; Björn, E.; Naredi, P.; Wolf-Watz, M.; Wittung-Stafshede, P., Cisplatin binds human copper chaperone Atox1 and promotes unfolding in vitro. *Proceedings of the National Academy of Sciences of the United States of America of the United States of America* **2011,** *108*, 6951-6956.

130. Li, H.; Wells, S. A.; Jimenez-Roldan, J. E.; Römer, R. A.; Zhao, Y.; Sadler, P. J.; O'Connor, P. B., Protein flexibility is key to cisplatin crosslinking in calmodulin. *Protein Science* **2012,** *21*, 1269-1279.

131. Phillips, H. I. A.; Ronconi, L.; Sadler, P. J., Photoinduced reactions of cis,trans,cis-[PtIV(N_3)$_2$(OH)$_2$(NH_3)$_2$] with 1-methylimidazole. *Chemistry – A European Journal* **2009,** *15*, 1588-1596.

132. Westendorf, A. F.; Woods, J. A.; Korpis, K.; Farrer, N. J.; Salassa, L.; Robinson, K.; Appleyard, V.; Murray, K.; Grünert, R.; Thompson, A. M.; Sadler, P. J.; Bednarski, P. J., Trans,trans,trans-[PtIV(N_3)$_2$(OH)$_2$(py)(NH_3)]: a light activated antitumor platinum complex that kills human cancer cells by an apoptosis independent mechanism. *Molecular Cancer Therapeutics* **2012,** *11*, 1894-904.

133. Novak, P.; Haskins, W. E.; Ayson, M. J.; Jacobsen, R. B.; Schoeniger, J. S.; Leavell, M. D.; Young, M. M.; Kruppa, G. H., Unambiguous assignment of intramolecular chemical cross-links in modified mammalian membrane proteins by Fourier transform-tandem mass spectrometry. *Analytical Chemistry* **2005,** *77*, 5101-5106.

134. Allardyce, C. S.; Dyson, P. J.; Coffey, J.; Johnson, N., Determination of drug binding sites to proteins by electrospray ionisation mass spectrometry: the interaction of cisplatin with transferrin. *Rapid Communications in Mass Spectrometry* **2002,** *16*, 933-935.

135. Müller, M. Q.; de Koning, L. J.; Schmidt, A.; Ihling, C.; Syha, Y.; Rau, O.; Mechtler, K.; Schubert-Zsilavecz, M.; Sinz, A., An innovative method to study target protein−drug interactions by mass spectrometry. *Journal of Medicinal Chemistry* **2009,** *52*, 2875-2879.

136. Archakov, A. I.; Govorun, V. M.; Dubanov, A. V.; Ivanov, Y. D.; Veselovsky, A. V.; Lewi, P.; Janssen, P., Protein-protein interactions as a target for drugs in proteomics. *PROTEOMICS* **2003,** *3*, 380-391.

137. Zhao, T.; King, F., Direct determination of the primary binding site of cisplatin on cytochrome C by mass spectrometry. *Journal of the American Society for Mass Spectrometry* **2009,** *20*, 1141-1147.

138. Zhang, N.; Du, Y.; Cui, M.; Xing, J.; Liu, Z.; Liu, S., Probing the interaction of cisplatin with cytochrome c by electrospray ionization Fourier transform ion cyclotron resonance mass spectrometry. *Analytical Chemistry* **2012,** *84*, 6206-6212.

139. Zhao, T.; King, F., Mass-spectrometric characterization of cisplatin binding sites on native and denatured ubiquitin. *Journal of Biological Inorganic Chemistry* **2011,** *16*, 633-639.

140. Williams, J.; Phillips, H.; Campuzano, I.; Sadler, P., Shape changes induced by N-terminal platination of ubiquitin by cisplatin. *Journal of the American Society for Mass Spectrometry* **2010,** *21*, 1097-1106.

141. Moreno-Gordaliza, E. a.; Cañas, B.; Palacios, M. a. A.; Gómez-Gómez, M. M., Top-down mass spectrometric approach for the full characterization of insulin−cisplatin adducts. *Analytical Chemistry* **2009,** *81*, 3507-3516.

142. Møller, C.; Sprenger, R.; Stürup, S.; Højrup, P., Determination of the binding sites for oxaliplatin on insulin using mass spectrometry-based approaches. *Analytical and Bioanalytical Chemistry* **2011,** *401*, 1623-1633.

143. Moreno-Gordaliza, E.; Canas, B.; Palacios, M. A.; Gomez-Gomez, M. M., Novel insights into the bottom-up mass spectrometry proteomics approach for the characterization of Pt-binding proteins: The insulin-cisplatin case study. *Analyst* **2010,** *135*, 1288-1298.

144. Weidt, S. K.; Mackay, C. L.; Langridge-Smith, P. R. R.; Sadler, P. J., Platination of superoxide dismutase with cisplatin: tracking the ammonia ligands using Fourier transform ion cyclotron resonance mass spectrometry (FT-ICR MS). *Chemical Communications* **2007**, 1719-1721.

145. Casini, A.; Gabbiani, C.; Michelucci, E.; Pieraccini, G.; Moneti, G.; Dyson, P.; Messori, L., Exploring metallodrug–protein interactions by mass spectrometry: comparisons between platinum coordination complexes and an organometallic ruthenium compound. *Journal of*

Biological Inorganic Chemistry **2009,** *14*, 761-770.

146. Hartinger, C. G.; Tsybin, Y. O.; Fuchser, J.; Dyson, P. J., Characterization of platinum anticancer drug protein-binding sites using a top-down mass spectrometric approach. *Inorganic Chemistry* **2007,** *47*, 17-19.

147. Doerr, A., Top-down mass spectrometry. *Nature Methods* **2008,** *5*, 24-24.

148. Feketeová, L.; Ryzhov, V.; O'Hair, R. A. J., Comparison of collision- versus electron-induced dissociation of Pt(II) ternary complexes of histidine- and methionine-containing peptides. *Rapid Communications in Mass Spectrometry* **2009,** *23*, 3133-3143.

149. Mamathambika, B. S.; Bardwell, J. C., Disulfide-linked protein folding pathways. *Annual Review of Cell and Developmental Biology* **2008,** *24*, 211-235.

150. Fass, D., Disulfide bonding in protein biophysics. *Annual Review of Biophysics* **2012,** *41*, 63-79.

151. Chen, J.; Shiyanov, P.; Zhang, L.; Schlager, J. J.; Green-Church, K. B., Top-down characterization of a native highly intralinked protein: concurrent cleavages of disulfide and protein backbone bonds. *Analytical Chemistry* **2010,** *82*, 6079-6089.

152. Mentinova, M.; Han, H.; McLuckey, S. A., Dissociation of disulfide-intact somatostatin ions: the roles of ion type and dissociation method. *Rapid Communications in Mass Spectrometry* **2009,** *23*, 2647-2655.

153. Kalli, A.; Håkansson, K., Preferential cleavage of SS and CS bonds in electron detachment dissociation and infrared multiphoton dissociation of disulfide-linked peptide anions. *International Journal of Mass Spectrometry* **2007,** *263*, 71-81.

154. Liu, J.; Gunawardena, H. P.; Huang, T.-Y.; McLuckey, S. A., Charge-dependent dissociation of insulin cations via ion/ion electron transfer. *International Journal of Mass Spectrometry* **2008,** *276*, 160-170.

155. Back, J. W.; de Jong, L.; Muijsers, A. O.; de Koster, C. G., Chemical cross-linking and mass spectrometry for protein structural modeling. *Journal of Molecular Biology* **2003,** *331*, 303-313.

156. Sinz, A., Chemical cross-linking and mass spectrometry to map three-dimensional protein structures and protein–protein interactions. *Mass Spectrometry Reviews* **2006,** *25*, 663-682.

157. Sinz, A., Chemical cross-linking and FTICR mass spectrometry for protein structure characterization. *Analytical and Bioanalytical Chemistry* **2005,** *381*, 44-47.

158. Yang, L.; Tang, X.; Weisbrod, C. R.; Munske, G. R.; Eng, J. K.; von Haller, P. D.; Kaiser, N. K.; Bruce, J. E., A photocleavable and mass spectrometry identifiable cross-linker for protein interaction studies. *Analytical Chemistry* **2010,** *82*, 3556-3566.

159. Tang, X.; Bruce, J. E., A new cross-linking strategy: protein interaction reporter (PIR) technology for protein-protein interaction studies. *Molecular BioSystems* **2010,** *6*, 939-947.

160. Alloza, I.; Martens, E.; Hawthorne, S.; Vandenbroeck, K., Cross-linking approach to affinity capture of protein complexes from chaotrope-solubilized cell lysates. *Analytical Biochemistry* **2004,** *324*, 137-142.

161. Tagwerker, C.; Flick, K.; Cui, M.; Guerrero, C.; Dou, Y.; Auer, B.; Baldi, P.; Huang, L.; Kaiser, P., A tandem affinity tag for two-step purification under fully denaturing conditions. *Molecular & Cellular Proteomics* **2006,** *5*, 737-748.

162. Chu, F.; Mahrus, S.; Craik, C. S.; Burlingame, A. L., Isotope-coded and affinity-tagged cross-linking (ICATXL): an efficient strategy to probe protein interaction surfaces. *Journal of the American Chemical Society* **2006,** *128*, 10362-10363.

163. Ihling, C.; Schmidt, A.; Kalkhof, S.; Schulz, D.; Stingl, C.; Mechtler, K.; Haack, M.; Beck-Sickinger, A.; Cooper, D.; Sinz, A., Isotope-labeled cross-linkers and fourier transform ion cyclotron resonance mass spectrometry for structural analysis of a protein/peptide complex. *Journal of the American Society for Mass Spectrometry* **2006,** *17*, 1100-1113.

164. Petrotchenko, E. V.; Olkhovik, V. K.; Borchers, C. H., Isotopically coded cleavable cross-linker for studying protein-protein interaction and protein complexes. *Molecular & Cellular Proteomics* **2005,** *4*, 1167-1179.

165. Taverner, T.; Hall, N. E.; O'Hair, R. A. J.; Simpson, R. J., Characterization of an antagonist interleukin-6 dimer by stable isotope labeling, cross-linking, and mass spectrometry. *Journal of Biological Chemistry* **2002,** *277*, 46487-46492.

166. Burstyn, J. N.; Heiger-Bernays, W. J.; Cohen, S. M.; Lippard, S. J., Formation of cis-diamminedichloroplatinum(II) 1,2-intrastrand cross-links on DNA is flanking-sequence independent. *Nucleic Acids Research* **2000,** *28*, 4237-4243.

167. Malinge, J.-M.; Giraud-Panis, M.-J.; Leng, M., Interstrand cross-links of cisplatin induce striking distortions in DNA. *Journal of Inorganic Biochemistry* **1999,** *77*, 23-29.

168. Wozniak, K.; Blasiak, J., Recognition and repair of DNA-cisplatin adducts. *Acta Biochimica Polonica* **2002,** *49*, 583-596.

169. Boulikas, T.; Pantos, A.; Bellis, E.; Christofis, P., Designing platinum compounds in cancer: structures and mechanisms. *Cancer*

Therapy **2007,** *5*, 537-583.

170. Qu, Y.; Scarsdale, N.; Tran, M.-C.; Farrell, N., Cooperative effects in long-range 1,4 DNA-DNA interstrand cross-links formed by polynuclear platinum complexes: an unexpected orientation of adenine bases outside the binding sites. *Journal of Biological Inorganic Chemistry* **2003,** *8*, 19-28.

171. Zehnulova, J.; Kasparkova, J.; Farrell, N.; Brabec, V., Conformation, recognition by high mobility group domain proteins, and nucleotide excision repair of DNA intrastrand cross-links of novel antitumor trinuclear platinum complex BBR3464. *Journal of Biological Chemistry* **2001,** *276*, 22191-22199.

172. Hegmans, A.; Berners-Price, S. J.; Davies, M. S.; Thomas, D. S.; Humphreys, A. S.; Farrell, N., Long range 1,4 and 1,6-interstrand cross-links formed by a trinuclear platinum complex. Minor groove preassociation affects kinetics and mechanism of cross-link formation as well as adduct structure. *Journal of the American Chemical Society* **2004,** *126*, 2166-2180.

173. Van Houten, B.; Illenye, S.; Qu, Y.; Farrell, N., Homodinuclear (Pt,Pt) and heterodinuclear (Ru,Pt) metal compounds as DNA-protein cross-linking agents: Potential suicide DNA lesions. *Biochemistry* **1993,** *32*, 11794-11801.

174. Chválová, K.; Brabec, V.; Kašpárková, J., Mechanism of the formation of DNA–protein cross-links by antitumor cisplatin. *Nucleic Acids Research* **2007,** *35*, 1812-1821.

175. Kloster, M.; Kostrhunova, H.; Zaludova, R.; Malina, J.; Kasparkova, J.; Brabec, V.; Farrell, N., Trifunctional dinuclear platinum complexes as DNA−protein cross-linking agents. *Biochemistry* **2004,** *43*, 7776-7786.

176. DeConti, R. C.; Toftness, B. R.; Lange, R. C.; Creasey, W. A., Clinical and pharmacological studies with cis-diamminedichloroplatinum(II). *Cancer Research* **1973,** *33*, 1310-1315.

177. Guo, Y.; Smith, K.; Petris, M. J., Cisplatin stabilizes a multimeric complex of the human Ctr1 copper transporter. *Journal of Biological Chemistry* **2004,** *279*, 46393-46399.

178. Hu, W.; Luo, Q.; Wu, K.; Li, X.; Wang, F.; Chen, Y.; Ma, X.; Wang, J.; Liu, J.; Xiong, S.; Sadler, P. J., The anticancer drug cisplatin can cross-link the interdomain zinc site on human albumin. *Chemical Communications* **2011,** *47*, 6006-6008.

179. Dhara, S. C., A rapid method for the synthesis of cis-$[Pt(NH_3)_2Cl_2]$. *Indian Journal of Chemistry* **1970,** *8*, 193-194.

180. Caravatti, P.; Allemann, M., The 'infinity cell': A new trapped-ion cell with radiofrequency covered trapping electrodes for fourier transform ion cyclotron resonance mass spectrometry. *Organic Mass Spectrometry*

1991, *26*, 514-518.

181. Will, J.; Sheldrick, W.; Wolters, D., Characterisation of cisplatin coordination sites in cellular Escherichia coli DNA-binding proteins by combined biphasic liquid chromatography and ESI tandem mass spectrometry. *Journal of Biological Inorganic Chemistry* **2008,** *13*, 421-434.

182. Wu, Z.; Liu, Q.; Liang, X.; Yang, X.; Wang, N.; Wang, X.; Sun, H.; Lu, Y.; Guo, Z., Reactivity of platinum-based antitumor drugs towards a Met- and His-rich 20mer peptide corresponding to the N-terminal domain of human copper transporter 1. *Journal of Biological Inorganic Chemistry* **2009,** *14*, 1313-1323.

183. Crider, S. E.; Holbrook, R. J.; Franz, K. J., Coordination of platinum therapeutic agents to met-rich motifs of human copper transport protein1. *Metallomics* **2010,** *2*, 74-83.

184. Qi, Y.; Thompson, C.; Van Orden, S.; O'Connor, P., Phase correction of Fourier transform ion cyclotron resonance mass spectra using MatLab. *Journal of the American Society for Mass Spectrometry* **2011,** *22*, 138-147.

185. O'Hair, R. A. J.; Reid, G. E., Neighboring group versus cis-elimination mechanisms for side chain loss from protonated methionine, methionine sulfoxide and their peptides. *European Journal of Mass Spectrometry* **1999,** *5*, 325-334.

186. Hohage, O.; Sheldrick, W. S., Cisplatin mediates selective downstream hydrolytic cleavage of Met-(Gly)n-His segments in methionine- and histidine-containing peptides: The role of ammine loss trans to the initial Pt-S(Met) anchor in facilitating amide hydrolysis. *Journal of Inorganic Biochemistry* **2006,** *100*, 1506-1513.

187. O'Neil, K. T.; DeGrado, W. F., How calmodulin binds its targets: sequence independent recognition of amphiphilic alpha-helices. **1990,** *15*, 59-64.

188. Hahn, M.; Kleine, M.; Sheldrick, W., Interaction of cisplatin with methionine- and histidine-containing peptides: competition between backbone binding, macrochelation and peptide cleavage. *Journal of Biological Inorganic Chemistry* **2001,** *6*, 556-566.

189. Manka, S.; Becker, F.; Hohage, O.; Sheldrick, W. S., Cisplatin-mediated selective hydrolytic cleavage of methionine-containing peptides with neighboring serine or histidine residues. *Journal of Inorganic Biochemistry* **2004,** *98*, 1947-1956.

190. Mandal, R.; Kalke, R.; Li, X.-F., Mass spectrometric studies of cisplatin-induced changes of hemoglobin. *Rapid Communications in Mass Spectrometry* **2003,** *17*, 2748-2754.

191. Li, X.; Cournoyer, J.; Lin, C.; O'Connor, P., Use of ^{18}O labels to monitor deamidation during protein and peptide sample processing. *Journal of the American Society for Mass Spectrometry* **2008,** *19*, 855-864.

192. Ienco, A.; Caporali, M.; Zanobini, F.; Mealli, C., Is 2.07 Å a record for the shortest Pt−S sistance? Revision of two reported X-ray structures. *Inorganic Chemistry* **2009,** *48*, 3840-3847.

193. Park, S.-Y.; Yokoyama, T.; Shibayama, N.; Shiro, Y.; Tame, J. R. H., 1.25 Å resolution crystal structures of human haemoglobin in the oxy, deoxy and carbonmonoxy forms. *Journal of Molecular Biology* **2006,** *360*, 690-701.

194. Cohen, S. M.; Lippard, S. J., Cisplatin: From DNA damage to cancer chemotherapy. In *Progress in Nucleic Acid Research and Molecular Biology*, Academic Press: 2001; Vol. 67, pp 93-130.

195. Borst, P.; Rottenberg, S.; Jonkers, J., How do real tumors become resistant to cisplatin? *Cell Cycle* **2008,** *7*, 1353-1359.

196. Crivici, A.; Ikura, M., Molecular and structural basis of target recognition by calmodulin. *Annual Review of Biophysics and Biomolecular Structure* **1995,** *24*, 85-116.

197. Nelson, M. R.; Chazin, W. J., An interaction-based analysis of calcium-induced conformational changes in Ca^{2+} sensor proteins. *Protein Science* **1998,** *7*, 270-282.

198. Vetter, S. W.; Leclerc, E., Novel aspects of calmodulin target recognition and activation. *European Journal of Biochemistry* **2003,** *270*, 404-414.

199. O'Neil, K. T.; DeGrado, W. F., How calmodulin binds its targets: sequence independent recognition of amphiphilic alpha-helices. *Trends in biochemical sciences* **1990,** *15*, 59-64.

200. Bartlett, R. K.; Bieber Urbauer, R. J.; Anbanandam, A.; Smallwood, H. S.; Urbauer, J. L.; Squier, T. C., Oxidation of Met144 and Met145 in calmodulin blocks calmodulin dependent activation of the plasma membrane Ca-ATPase. *Biochemistry* **2003,** *42*, 3231-3238.

201. Vougier, S.; Mary, J.; Dautin, N.; Vinh, J.; Friguet, B.; Ladant, D., Essential role of methionine residues in calmodulin binding to bordetella pertussis adenylate cyclase, as probed by selective oxidation and repair by the peptide methionine sulfoxide reductases. *The Journal of Biological Chemistry* **2004,** *279*, 30210-30218.

202. Yao, Y.; Yin, D.; Jas, G. S.; Kuczera, K.; Williams, T. D.; Schöneich, C.; Squier, T. C., Oxidative modification of a carboxyl-terminal vicinal methionine in calmodulin by hydrogen peroxide inhibits calmodulin-dependent activation of the plasma membrane ca-ATPase.

Biochemistry **1996,** *35*, 2767-2787.

203. Gao, J.; Yin, D. H.; Yao, Y.; Sun, H.; Qin, Z.; Schöneich, C.; Williams, T. D.; Squier, T. C., Loss of conformational stability in calmodulin upon methionine oxidation. *Biophysical Journal* **1998,** *74*, 1115-1134.

204. Bigelow, D. J.; Squier, T. C., Redox modulation of cellular signaling and metabolism through reversible oxidation of methionine sensors in calcium regulatory proteins. *Biochimica et Biophysica Acta (BBA) - Proteins and Proteomics* **2005,** *1703*, 121-134.

205. Jarve, R. K.; Aggarwal, S. K., Cisplatin-induced inhibition of the calcium-calmodulin complex, neuronal nitric oxide synthase activation and their role in stomach distention. *Cancer chemotherapy and pharmacology* **1997,** *39*, 341-348.

206. Carr, S. A.; Annan, R. S., Overview of peptide and protein analysis by mass spectrometry. In *Current Protocols in Molecular Biology*, John Wiley & Sons, Inc.: 2001; Vol. 62, pp 16.1.1–16.1.30.

207. Mandal, R.; Sawyer, M. B.; Li, X.-F., Mass spectrometry study of hemoglobin-oxaliplatin complexes in colorectal cancer patients and potential association with chemotherapeutic responses. *Rapid Communications in Mass Spectrometry* **2006,** *20*, 2533-2538.

208. Li, H.; Zhao, Y.; Phillips, H. I. A.; Qi, Y.; Lin, T.-Y.; Sadler, P. J.; O'Connor, P. B., Mass spectrometry evidence for cisplatin as a protein cross-linking reagent. *Analytical Chemistry* **2011,** *83*, 5369-5376.

209. Timerbaev, A. R.; Hartinger, C. G.; Aleksenko, S. S.; Keppler, B. K., Interactions of antitumor metallodrugs with serum proteins: advances in characterization using modern analytical methodology. *Chemical Reviews* **2006,** *106*, 2224-2248.

210. Annibale, G.; Brandolisio, M.; Pitteri, B., New routes for the synthesis of chloro(diethylenetriamine)platinum(II)chloride and chloro(2,2':6',2''-terpyridine)platinum(II) chloride dihydrate. *Polyhedron* **1995,** *14*, 451-453.

211. Farrell, N. Q., Yun, Chemistry of bis(platinum) complexes. Formation of trans derivatives from tetraamine complexes. *Inorganic Chemistry* **1989,** *28*, 3416-3420.

212. Oehlsen, M. E.; Qu, Y.; Farrell, N., Reaction of polynuclear platinum antitumor compounds with reduced glutathione studied by multinuclear (1H, 1H−15N gradient heteronuclear single-quantum coherence, and 195Pt) NMR spectroscopy. *Inorganic Chemistry* **2003,** *42*, 5498-5506.

213. Rodriguez, J.; Gupta, N.; Smith, R. D.; Pevzner, P. A., Does trypsin cut before proline? *Journal of Proteome Research* **2007,** *7*, 300-

305.

214. Carpenter, F. H., Treatment of trypsin with TPCK. In *Methods in Enzymology*, Hirs, C. H. W., Ed. Academic Press: 1967; Vol. 11, p 237.

215. Kleinnijenhuis, A. J.; Mihalca, R.; Heeren, R. M. A.; Heck, A. J. R., Atypical behavior in the electron capture induced dissociation of biologically relevant transition metal ion complexes of the peptide hormone oxytocin. *International Journal of Mass Spectrometry* **2006,** *253*, 217-224.

216. Liu, H.; Håkansson, K., Divalent metal ion-peptide interactions probed by electron capture dissociation of trications. *Journal of The American Society for Mass Spectrometry* **2006,** *17*, 1731-1741.

217. Tureček, F.; Jones, J. W.; Holm, A. I. S.; Panja, S.; Nielsen, S. B.; Hvelplund, P., Transition metals as electron traps. I. Structures, energetics, electron capture, and electron-transfer-induced dissociations of ternary copper–peptide complexes in the gas phase. *Journal of Mass Spectrometry* **2009,** *44*, 707-724.

218. Moore, B. N.; Ly, T.; Julian, R. R., Radical conversion and migration in electron capture dissociation. *Journal of the American Chemical Society* **2011,** *133*, 6997-7006.

219. Fuertes, M. A.; Alonso, C.; Pérez, J. M., Biochemical modulation of cisplatin mechanisms of action: enhancement of antitumor activity and circumvention of drug resistance. *Chemical Reviews* **2003,** *103*, 645-662.

220. Balog, E. M.; Norton, L. E.; Thomas, D. D.; Fruen, B. R., Role of calmodulin methionine residues in mediating productive association with cardiac ryanodine receptors. *American Journal of Physiology - Heart and Circulatory Physiology* **2006,** *290*, H794-H799.

221. Cho, Y.-E.; Singh, T. S. K.; Lee, H.-C.; Moon, P.-G.; Lee, J.-E.; Lee, M.-H.; Choi, E.-C.; Chen, Y.-J.; Kim, S.-H.; Baek, M.-C., In-depth Identification of Pathways Related to Cisplatin-induced Hepatotoxicity through an Integrative Method Based on an Informatics-assisted Label-free Protein Quantitation and Microarray Gene Expression Approach. *Molecular & Cellular Proteomics* **2012,** *11*.

222. Chappell, N. P.; Teng, P.-n.; Hood, B. L.; Wang, G.; Darcy, K. M.; Hamilton, C. A.; Maxwell, G. L.; Conrads, T. P., Mitochondrial Proteomic Analysis of Cisplatin Resistance in Ovarian Cancer. *Journal of Proteome Research* **2012,** *11*, 4605-4614.

223. Chavez, J. D.; Hoopmann, M. R.; Weisbrod, C. R.; Takara, K.; Bruce, J. E., Quantitative Proteomic and Interaction Network Analysis of Cisplatin Resistance in HeLa Cells. *PLoS ONE* **2011,** *6*, e19892.

224. Martelli, L.; Di Mario, F.; Ragazzi, E.; Apostoli, P.; Leone, R.; Perego, P.; Fumagalli, G., Different accumulation of cisplatin, oxaliplatin

and JM216 in sensitive and cisplatin-resistant human cervical tumour cells. *Biochemical Pharmacology* **2006,** *72*, 693-700.

225. Le Moguen, K.; Lincet, H.; Deslandes, E.; Hubert-Roux, M.; Lange, C.; Poulain, L.; Gauduchon, P.; Baudin, B., Comparative proteomic analysis of cisplatin sensitive IGROV1 ovarian carcinoma cell line and its resistant counterpart IGROV1-R10. *PROTEOMICS* **2006,** *6*, 5183-5192.

226. Hasinoff, B. B.; Wu, X.; Krokhin, O. V.; Ens, W.; Standing, K. G.; Nitiss, J. L.; Sivaram, T.; Giorgianni, A.; Yang, S.; Jiang, Y.; Yalowich, J. C., Biochemical and Proteomics Approaches to Characterize Topoisomerase IIα Cysteines and DNA as Targets Responsible for Cisplatin-Induced Inhibition of Topoisomerase IIα. *Molecular Pharmacology* **2005,** *67*, 937-947.

227. Gatti, L.; Beretta, G. L.; Carenini, N.; Corna, E.; Zunino, F.; Perego, P., Gene expression profiles in the cellular response to a multinuclear platinum complexe. *Cellular and Molecular Life Sciences* **2004,** *61*, 973-981.

228. Castagna, A.; Antonioli, P.; Astner, H.; Hamdan, M.; Righetti, S. C.; Perego, P.; Zunino, F.; Righetti, P. G., A proteomic approach to cisplatin resistance in the cervix squamous cell carcinoma cell line A431. *PROTEOMICS* **2004,** *4*, 3246-3267.

229. Ihling, C.; Schmidt, A.; Kalkhof, S.; Schulz, D. M.; Stingl, C.; Mechtler, K.; Haack, M.; Beck-Sickinger, A. G.; Cooper, D. M. F.; Sinz, A., Isotope-labeled cross-linkers and Fourier transform ion cyclotron resonance mass spectrometry for structural analysis of a protein/peptide complex. *Journal of the American Society for Mass Spectrometry* **2006,** *17*, 1100-1113.

230. Farrer, N. J.; Woods, J. A.; Munk, V. P.; Mackay, F. S.; Sadler, P. J., Photocytotoxic trans-Diam(m)ine Platinum(IV) Diazido Complexes More Potent than Their cis Isomers. *Chemical Research in Toxicology* **2009,** *23*, 413-421.

231. Kelleher, N. L., Peer Reviewed: Top-Down Proteomics. *Analytical Chemistry* **2004,** *76*, 196 A-203 A.

232. Li, H.; Lin, T.-Y.; Van Orden, S. L.; Zhao, Y.; Barrow, M. P.; Pizarro, A. M.; Qi, Y.; Sadler, P. J.; O'Connor, P. B., Use of top-down and bottom-up Fourier transform ion cyclotron resonance mass spectrometry for mapping calmodulin sites modified by platinum anticancer drugs. *Analytical Chemistry* **2011,** *83*, 9507-9515.

233. Henzler-Wildman, K.; Kern, D., Dynamic personalities of proteins. *Nature* **2007,** *450*, 964-972.

234. Zhang, M.; Tanaka, T.; Ikura, M., Calcium-induced conformational transition revealed by the solution structure of apo calmodulin. *Nature*

Structural & Molecular Biology **1995,** *2*, 758-767.

235. Barbato, G.; Ikura, M.; Kay, L. E.; Pastor, R. W.; Bax, A., Backbone dynamics of calmodulin studied by 15N relaxation using inverse detected two-dimensional NMR spectroscopy: the central helix is flexible. *Biochemistry* **1992,** *31*, 5269-5278.

236. Jimenez-Roldan, J. E.; Freedman, R. B.; Roemer, R. A.; Wells, S. A., Rapid simulation of protein motion: merging flexibility, rigidity and normal mode analysis. *Physical Biology* **2012,** *9*, 016008.

237. Jacobs, D. J.; Rader, A. J.; Kuhn, L. A.; Thorpe, M. F., Protein flexibility predictions using graph theory. *Proteins: Structure, Function, and Bioinformatics* **2001,** *44*, 150-165.

238. Wells, S. A.; Menor, S.; Hespenheide, B.; Thorpe, M. F., Constrained geometric simulation of diffusive motion in proteins. *Physical Biology* **2005,** *2*, S127-S136.

239. Suhre, K.; Yves-Henri., S., ElNémo: a normal mode web server for protein movement analysis and the generation of templates for molecular replacement. *Nucleic Acids Research Supplement* **2004,** *1*, W610–W614.

240. Jolley, C. C.; Wells , S. A.; Hespenheide, B. M.; Thorpe, M. F.; Fromme, P., Docking of photosystem I subunit C using a constrained geometric simulation. *Journal of the American Chemical Society* **2006,** *128*, 8803-8812.

241. Chattopadhyaya, R.; Meador, W. E.; Means, A. R.; Quiocho, F. A., Calmodulin structure refined at 1.7 Å resolution. *Journal of Molecular Biology* **1992,** *228*, 1177-1192.

242. Word, J. M.; Lovell, S. C.; Richardson, J. S.; Richardson, D. C., Asparagine and glutamine: using hydrogen atom contacts in the choice of side-chain amide orientation. *Journal of Molecular Biology* **1999,** *285*, 1735-1747.

243. The PyMOL Molecular Graphics System", *Publisher is Schrodinger LLC, URL is www.pymol.org*.

244. Hespenheide, B. M.; Rader, A. J.; Thorpe, M. F.; Kuhn, L. A., Identifying protein folding cores from the evolution of flexible regions during unfolding. *Journal of Molecular Graphics & Modelling* **2002,** *21*, 195-207.

245. Wells, S. A.; Jimenez-Roldan, J. E.; Roemer, R. A., Comparative analysis of rigidity across protein families. *Physical Biology* **2009,** *6*, 1-11.

246. Dahiyat, B. I.; Benjamin Gordon, D.; Mayo, S. L., Automated design of the surface positions of protein helices. *Protein Science* **1997,** *6*, 1333-1337.

247. Heal, J. W.; Jimenez-Roldan, J. E.; Wells, S. A.; Freedman, R. B.; Römer, R. A., Inhibition of HIV-1 protease: the rigidity perspective. *Bioinformatics* **2012,** *28*, 350-357.

248. Jimenez-Roldan, J. E.; Wells, S. A.; Freedman, R. B.; Roemer, R. A., Integration of FIRST, FRODA and NMM in a coarse grained method to study protein disulphide Isomerase conformational change. *Conference on Condensed Matter and Materials Physics (CMMP10)* **2011,** *286*.

249. Snijder, J.; Rose, R. J.; Raijmakers, R.; Heck, A. J. R., Site-specific methionine oxidation in calmodulin affects structural integrity and interaction with Ca^{2+}/calmodulin dependent protein kinase II. *Journal of Structural Biology* **2011,** *174*, 187-195.

250. Pan, J. X.; Konermann, L., Calcium-induced structural transitions of the calmodulin-melittin system studied by electrospray mass spectrometry: conformational subpopulations and metal-unsaturated intermediates. *Biochemistry* **2010,** *49*, 3477-3486.

251. Kataoka, M.; Head, J. F.; Seaton, B. A.; Engelman, D. M., Melittin binding causes a large calcium-dependent conformational change in calmodulin. *Proceedings of the National Academy of Sciences of the United States of America* **1989,** *86*, 6944-8.

252. Benkestock, K.; Edlund, P.-O.; Roeraade, J., Electrospray ionization mass spectrometry as a tool for determination of drug binding sites to human serum albumin by noncovalent interaction. *Rapid Communications in Mass Spectrometry* **2005,** *19*, 1637-1643.

253. Permyakov., E. A., Metalloproteomics *Hoboken, NJ: Wiley-Interscience* **2009**.

254. Wu, C.; Siems, W. F.; Klasmeier, J.; Hill, H. H., Separation of isomeric peptides using electrospray ionization/high-resolution ion mobility spectrometry. *Analytical Chemistry* **1999,** *72*, 391-395.

255. Srebalus, B.; Hilderbrand, A. E.; Valentine, S. J.; Clemmer, D. E., Resolving isomeric peptide mixtures: a combined HPLC/ion mobility-TOFMS analysis of a 4000-component combinatorial library. *Analytical Chemistry* **2002,** *74*, 26-36.

256. Hilton, G. R.; Jackson, A. T.; Thalassinos, K.; Scrivens, J. H., Structural analysis of synthetic polymer mixtures using ion mobility and tandem mass spectrometry. *Analytical Chemistry* **2008,** *80*, 9720-9725.

257. Williams, J. P.; Bugarcic, T.; Habtemariam, A.; Giles, K.; Campuzano, I.; Rodger, P. M.; Sadler, P. J., Isomer separation and gas-phase configurations of organoruthenium anticancer complexes: ion mobility mass spectrometry and modeling. *Journal of the American Society for Mass Spectrometry* **2009,** *20*, 1119-1122.

258. Cuyckens, F.; Wassvik, C.; Mortishire-Smith, R. J.; Tresadern, G.; Campuzano, I.; Claereboudt, J., Product ion mobility as a promising tool for assignment of positional isomers of drug metabolites. *Rapid Communications in Mass Spectrometry* **2011,** *25*, 3497-3503.

259. Giles, K.; Williams, J. P.; Campuzano, I., Enhancements in travelling wave ion mobility resolution. *Rapid Communications in Mass Spectrometry* **2011,** *25*, 1559-1566.

260. Harrison, A. G., Cyclization of peptide b9 ions. *Journal of the American Society for Mass Spectrometry* **2009,** *20*, 2248-2253.

261. Atik, A.; Yalcin, T., A systematic study of acidic peptides for b-type sequence scrambling. *Journal of the American Society for Mass Spectrometry* **2011,** *22*, 38-48.

262. Li, X.; Huang, Y.; O'Connor, P.; Lin, C., Structural heterogeneity of doubly-charged peptide b-Ions. *Journal of the American Society for Mass Spectrometry* **2011,** *22*, 245-254.

263. Wei, H.; Wang, X.; Liu, Q.; Mei, Y.; Lu, Y.; Guo, Z., Disulfide bond cleavage induced by a platinum(II) methionine complex. *Inorganic Chemistry* **2005,** *44*, 6077-6081.

264. Appleton, T. G.; Connor, J. W.; Hall, J. R.; , *Journal of the Chemical Society, Chemical Communications* **1988,** *27*, 130.

265. Chen, Y.; Guo, Z.; del Socorro Murdoch, P.; Zang, E.; Sadler, P. J., Interconversion between S- and N-bound L-methionine adducts of Pt(dien)2+ (dien = diethylenetriamine) via dien ring-opened intermediates. *Journal of the Chemical Society, Dalton Transactions* **1998**, 1503-1508.

266. Lempers, E. L. M.; Reedijk, J., Characterization of products from chloro(diethylenetriamine)platinum(1+) chloride and S-adenosyl-L-homocysteine. Evidence for a pH-dependent migration of the platinum moiety from the sulfur atom to the amine group and vice versa. *Inorganic Chemistry* **1990,** *29*, 1880-1884.

267. Frohling, C. D. W.; Sheldrick, W. S., Intramolecular migration of $[Pt(dien)]^{2+}$ (dien = 1,5-diamino-3-azapentane) from sulfur to imidazole-N1 in histidylmethionine (his-metH). *Chemical Communications* **1997**, 1737-1738.

268. Fälth, M.; Savitski, M. M.; Nielsen, M. L.; Kjeldsen, F.; Andren, P. E.; Zubarev, R. A., Analytical utility of small neutral losses from reduced species in electron capture dissociation studied using SwedECD database. *Analytical Chemistry* **2008,** *80*, 8089-8094.

269. Sun, Q.; Nelson, H.; Ly, T.; Stoltz, B. M.; Julian, R. R., Side chain chemistry mediates backbone fragmentation in hydrogen deficient peptide radicals. *Journal of Proteome Research* **2008,** *8*, 958-966.

270. Huang, J.; Tiedemann, P. W.; Land, D. P.; McIver, R. T.; Hemminger, J. C., Dynamics of ion coupling in an FTMS ion trap and resulting effects on mass spectra, including isotope ratios. *International Journal of Mass Spectrometry and Ion Processes* **1994,** *134*, 11-21.

271. Peurrung, A. J.; Kouzes, R. T., Analysis of space-charge effects in cyclotron resonance mass spectrometry as coupled gyrator phenomena. *International Journal of Mass Spectrometry and Ion Processes* **1995,** *145*, 139-153.

272. Blundell, T.; Dodson, G.; Hodgkin, D.; Mercola, D., Insulin: the structure in the crystal and its reflection in chemistry and biology. *Advances in Protein Chemistry* **1972,** *26*, 279-402.

273. Harris, P., Frankaer, C.G., Knudsen, M.V., The structure of T6 bovine insulin. *To be submitted* **2012,** *DOI:10.2210/pdb4e7t/pdb*

274. Ge, Y.; Lawhorn, B. G.; ElNaggar, M.; Strauss, E.; Park, J.-H.; Begley, T. P.; McLafferty, F. W., Top down characterization of larger proteins (45 kDa) by electron capture dissociation mass spectrometry. *Journal of the American Chemical Society* **2002,** *124*, 672-678.

275. Pan, J.; Han, J.; Borchers, C. H.; Konermann, L., Hydrogen/deuterium exchange mass spectrometry with top-down electron capture dissociation for characterizing structural transitions of a 17 kDa protein. *Journal of the American Chemical Society* **2009,** *131*, 12801-12808.

276. Lioe, H.; Duan, M.; O'Hair, R. A. J., Can metal ions be used as gas-phase disulfide bond cleavage reagents? A survey of coinage metal complexes of model peptides containing an intermolecular disulfide bond. *Rapid Communications in Mass Spectrometry* **2007,** *21*, 2727-2733.

277. Chrisman, P.; Pitteri, S.; Hogan, J.; McLuckey, S., $SO^{2-\cdot}$ electron transfer ion/ion reactions with disulfide linked polypeptide ions. *Journal of The American Society for Mass Spectrometry* **2005,** *16*, 1020-1030.

278. Gunawardena, H. P.; Gorenstein, L.; Erickson, D. E.; Xia, Y.; McLuckey, S. A., Electron transfer dissociation of multiply protonated and fixed charge disulfide linked polypeptides. *International Journal of Mass Spectrometry* **2007,** *265*, 130-138.

279. Agarwal, A.; Diedrich, J. K.; Julian, R. R., Direct elucidation of disulfide bond partners using ultraviolet photodissociation mass spectrometry. *Analytical Chemistry* **2011,** *83*, 6455-6458.

280. Lee, M.; Lee, Y.; Kang, M.; Park, H.; Seong, Y.; June Sung, B.; Moon, B.; Bin Oh, H., Disulfide bond cleavage in TEMPO-free radical initiated peptide sequencing mass spectrometry. *Journal of Mass Spectrometry* **2011,** *46*, 830-839.

281. Cole, S.; Ma, X.; Zhang, X.; Xia, Y., Electron transfer dissociation

(ETD) of peptides containing intrachain disulfide bonds. *Journal of the American Society for Mass Spectrometry* **2012,** *23*, 310-320.

282. Sobczyk, M.; Simons, J., Distance dependence of through-bond electron transfer rates in electron-capture and electron-transfer dissociation. *International Journal of Mass Spectrometry* **2006,** *253*, 274-280.

283. Rayman, M. P., The importance of selenium to human health. *The Lancet* **2000,** *356*, 233-241.

284. Chen, J.; Berry, M. J., Selenium and selenoproteins in the brain and brain diseases. *Journal of Neurochemistry* **2003,** *86*, 1-12.

285. Schomburg, L.; Schweizer, U.; Köhrle, J., Selenium and selenoproteins in mammals: extraordinary, essential, enigmatic. *Cellular and Molecular Life Sciences* **2004,** *61*, 1988-1995.

286. Metanis, N.; Keinan, E.; Dawson, P. E., Synthetic seleno-glutaredoxin 3 analogues are highly reducing oxidoreductases with enhanced catalytic efficiency. *Journal of the American Chemical Society* **2006,** *128*, 16684-16691.

287. Hondal, R. J.; Nilsson, B. L.; Raines, R. T., Selenocysteine in native chemical ligation and expressed protein ligation. *Journal of the American Chemical Society* **2001,** *123*, 5140-5141.

288. Aldag, C.; Gromov, I. A.; García-Rubio, I.; von Koenig, K.; Schlichting, I.; Jaun, B.; Hilvert, D., Probing the role of the proximal heme ligand in cytochrome P450cam by recombinant incorporation of selenocysteine. *Proceedings of the National Academy of Sciences of the United States of America* **2009,** *106*, 5481-5486.

289. Cohen, S.; Kumar, D.; Shaik, S., In silico design of a mutant of cytochrome P450 containing selenocysteine. *Journal of the American Chemical Society* **2006,** *128*, 2649-2653.

290. Movassagh, B.; Shamsipoor, M.; Joshaghani, M., Reductive cleavage of the Se—Se bond in the presence of a $Zn/AlCl_3$ system: synthesis of selenol esters. *ChemInform* **2004,** *35*, 148-149.

291. Russavskaya, N.; Levanova, E.; Sukhomazova, E.; Grabel'nykh, V.; Klyba, L.; Zhanchipova, E.; Albanov, A.; Korchervin, N., Synthesis and oxidative cleavage of poly(trimethylene diselenides). *Russian Journal of General Chemistry* **2006,** *76*, 229-234.

292. Dumont, É.; Loos, P.-F.; Laurent, A. D.; Assfeld, X., Electronic effects and ring strain influences on the electron uptake by selenium-containing bonds. *International Journal of Quantum Chemistry* **2010,** *110*, 513-523.

293. Gámez, J. A.; Yáñez, M., Electron attachment to diselenides

revisited: Se–Se bond cleavage is neither adiabatic nor the most favorable process. *Journal of Chemical Theory and Computation* **2011,** *7*, 1726-1735.

294. Gámez, J. A.; Yáñez, M., Asymmetry and electronegativity in the electron capture activation of the Se−Se Bond: σ*(Se−Se) vs σ*(Se−X). *Journal of Chemical Theory and Computation* **2010,** *6*, 3102-3112.

295. Meija, J.; Beck, T. L.; Caruso, J. A., Interpretation of alkyl diselenide and selenosulfenate mass spectra. *Journal of the American Society for Mass Spectrometry* **2004,** *15*, 1325-1332.

296. Pauling, L., The natuer of the chemical bond. IV. The energy of single bonds and the relative electronegativity of atoms. *Journal of the American Chemical Society* **1932,** *54*, 3570-3582.

297. IUPAC. Compendium of Chemical Terminology, 2nd edn. (the "Gold Book"). Compiled by McNaught, A.D., Wilkinson, A.: Blackwell. Scientific Publications (1997). XML on-line corrected version: http://goldbook.iupac.org9 2006- created by Nic, M.,Jirat, J., Kosata, B.: updates compiled by Jenkins, A.

298. Dezarnaud–Dandine, C. B., F.; Tronc, M.; Jones, D.; Modelli, A., δ* Resonances in electron transmission (ETS) and x–ray absorption (XAS) spectroscopies of dimethyl(poly)sulphides $(CH_3)_2S$ x(x = 1, 2, 3). *Journal of Physics B: Atomic, Molecular and Optical Physics* **1998,** *31*, L497–L501.

299. Gamez, J. A.; Yanez, M., Is Se-Se bond cleavage the most favourable process in electron attachment to diselenides? The importance of asymmetry. *Chemical Communications* **2011,** *47*, 3939-3941.

300. Good, D. M.; Wirtala, M.; McAlister, G. C.; Coon, J. J., Performance characteristics of electron transfer dissociation mass spectrometry. *Molecular & Cellular Proteomics* **2007,** *6*, 1942-1951.

301. Bulaj, G., Formation of disulfide bonds in proteins and peptides. *Biotechnology Advances* **2005,** *23*, 87-92.

302. Chait, B. T., Mass spectrometry: bottom-up or top-down? *Science* **2006,** *314*, 65-66.

303. Reid, G. E.; McLuckey, S. A., 'Top down' protein characterization via tandem mass spectrometry. *Journal of Mass Spectrometry* **2002,** *37*, 663-675.

304. McLafferty, F. W.; Breuker, K.; Jin, M.; Han, X.; Infusini, G.; Jiang, H.; Kong, X.; Begley, T. P., Top-down MS, a powerful complement to the high capabilities of proteolysis proteomics. *FEBS Journal* **2007,** *274*, 6256-6268.

305. Zabrouskov, V.; Giacomelli, L.; van Wijk, K. J.; McLafferty, F. W., A new approach for plant proteomics. *Molecular & Cellular Proteomics* **2003,** *2*, 1253-1260.

306. Siuti, N.; Kelleher, N. L., Decoding protein modifications using top-down mass spectrometry. *Nature Methods* **2007,** *4*, 817-821.

307. Mazur, M. T.; Cardasis, H. L.; Spellman, D. S.; Liaw, A.; Yates, N. A.; Hendrickson, R. C., Quantitative analysis of intact apolipoproteins in human HDL by top-down differential mass spectrometry. *Proceedings of the National Academy of Sciences of the United States of America* **2010**.

308. Tipton, J. D.; Tran, J. C.; Catherman, A. D.; Ahlf, D. R.; Durbin, K. R.; Kelleher, N. L., Analysis of intact protein isoforms by mass spectrometry. *Journal of Biological Chemistry* **2011,** *286*, 25451-25458.

309. Tran, J. C.; Zamdborg, L.; Ahlf, D. R.; Lee, J. E.; Catherman, A. D.; Durbin, K. R.; Tipton, J. D.; Vellaichamy, A.; Kellie, J. F.; Li, M.; Wu, C.; Sweet, S. M. M.; Early, B. P.; Siuti, N.; LeDuc, R. D.; Compton, P. D.; Thomas, P. M.; Kelleher, N. L., Mapping intact protein isoforms in discovery mode using top-down proteomics. *Nature* **2011,** *480*, 254-258.

310. Han, X.; Jin, M.; Breuker, K.; McLafferty, F. W., Extending top-down mass spectrometry to proteins with masses greater than 200 kilodaltons. *Science* **2006,** *314*, 109-112.

311. Yin, S.; Loo, J. A., Top-down mass spectrometry of supercharged native protein–ligand complexes. *International Journal of Mass Spectrometry* **2011,** *300*, 118-122.

312. Thakur, S.; Balaram, P., Fragmentation of peptide disulfides under conditions of negative ion mass spectrometry: Studies of oxidized glutathione and contryphan. *Journal of The American Society for Mass Spectrometry* **2008,** *19*, 358-366.

313. Huang, Y.; Cui, W.; Remple, D.; L., G. M., Investigating insulin oligomers by native spray H/D exchange and top-down mass spectrometry. *59th ASMS Conference on Mass Spectrometry and Allied Topics. Denver, CO* **2011**.

314. OH, H.; McLafferty, F. W., A variety of activation methods employed in "activated-ion" electron capture dissociation mass spectrometry : A test against Bovine ubiquitin 7+ ons. *Bulletin of the Korean Chemical Society* **2006,** *27*, 389-394.

315. Mikhailov, V. A.; Cooper, H. J., Activated ion electron capture dissociation (AI ECD) of proteins: synchronization of infrared and electron irradiation with ion magnetron motion. *Journal of the American Society for Mass Spectrometry* **2009,** *20*, 763-771.

316. Oh, H.; Breuker, K.; Sze, S. K.; Ge, Y.; Carpenter, B. K.; McLafferty, F. W., Secondary and tertiary structures of gaseous protein

ions characterized by electron capture dissociation mass spectrometry and photofragment spectroscopy. *Proceedings of the National Academy of Sciences of the United States of America* **2002,** *99*, 15863-15868.

317. Shi, S. D. H.; Hemling, M. E.; Carr, S. A.; Horn, D. M.; Lindh, I.; McLafferty, F. W., Phosphopeptide/phosphoprotein mapping by electron capture dissociation mass spectrometry. *Analytical Chemistry* **2000,** *73*, 19-22.

318. Breuker, K.; Ganisl, B., Disulfide vs. backbone bond cleavage in electron capture dissociation of proteins. *10th European FTMS Worshop, Coventry, UK* **2012**.

319. Zhang, J.; Loo, J. A., Mapping protein disulfide bonds by top-down ESI-MS/MS and supercharging. *60th ASMS Conference on Mass Spectrometry and Allied Topics. Vancouver, Canada* **2012**.

320. Anusiewicz, I.; Berdys-Kochanska, J.; Simons, J., Electron attachment step in electron capture dissociation (ECD) and electron transfer dissociation (ETD). *The Journal of Physical Chemistry A* **2005,** *109*, 5801-5813.

321. Kleinnijenhuis, A.; Heck, A.; Duursma, M.; Heeren, R., Does double electron capture lead to the formation of biradicals? An ECD-SORI-CID study on lacticin 481. *Journal of The American Society for Mass Spectrometry* **2005,** *16*, 1595-1601.

322. Savitski, M. M.; Kjeldsen, F.; Nielsen, M. L.; Zubarev, R. A., Hydrogen rearrangement to and from radical z fragments in electron capture dissociation of peptides. *Journal of The American Society for Mass Spectrometry* **2007,** *18*, 113-120.

323. Lin, C.; Cournoyer, J. J.; O'Connor, P. B., Use of a double resonance electron capture dissociation experiment to probe fragment intermediate lifetimes. *Journal of The American Society for Mass Spectrometry* **2006,** *17*, 1605-1615.

324. Zabrouskov, V.; Han, X.; Welker, E.; Zhai, H.; Lin, C.; van Wijk, K. J.; Scheraga, H. A.; McLafferty, F. W., Stepwise deamidation of ribonuclease A at five sites determined by top down mass spectrometry. *Biochemistry* **2005,** *45*, 987-992.

325. Zhang, H.; Ge, Y., Comprehensive Analysis of Protein Modifications by Top-Down Mass Spectrometry. *Circulation: Cardiovascular Genetics* **2011,** *4*, 711.

326. Forbes, A. J.; Patrie, S. M.; Taylor, G. K.; Kim, Y.-B.; Jiang, L.; Kelleher, N. L., Targeted analysis and discovery of posttranslational modifications in proteins from methanogenic archaea by top-down MS. *Proceedings of the National Academy of Sciences of the United States of Americ* **2004,** *101*, 2678-2683.

Appendix A (Supporting information for Chapter 2)

Figure A.1 Zoom CAD-MS^2 spectra of (a) bombesin triply charged ion at *m/z* 540; (b) bombesin doubly-charged ion at *m/z* 810; (c) $[A+Pt(NH_3)+B+2H]^{4+}$ ion at *m/z* 719. The fragment ions of $[B+2H-CH_4S]^{2+}$, $[B+2H]^{2+}$, and $[B+Pt-CH_4S]^{2+}$ are highlighted in grey. These spectra show that Pt binds to the thioether sulfur of the N-terminal Met14 site.

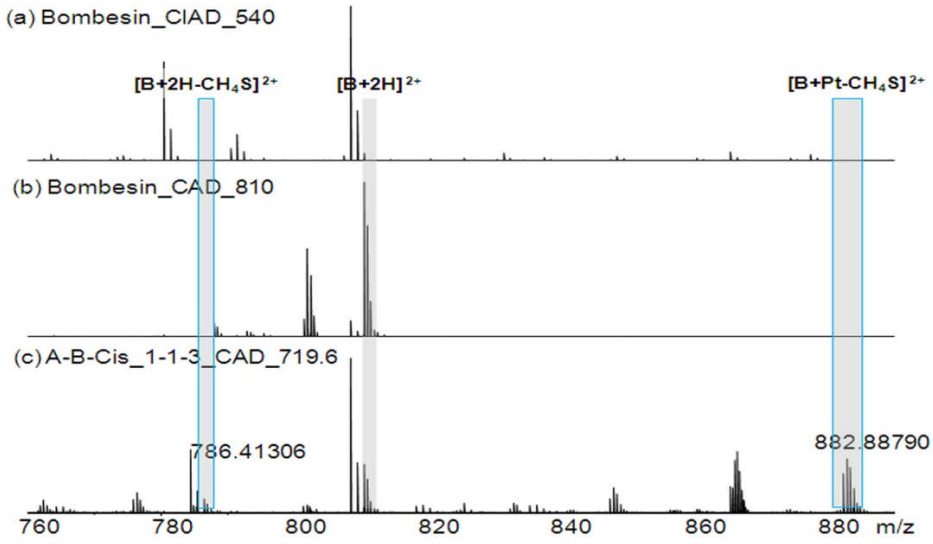

Figure A.2 Mass spectra of (a) hemoglobin-cisplatin (1:5) mixture; (b) hemoglobin. Aqueous solutions of hemoglobin and cisplatin were mixed at a molar ratio of 1:5 and incubated at 37 °C for 24 h.

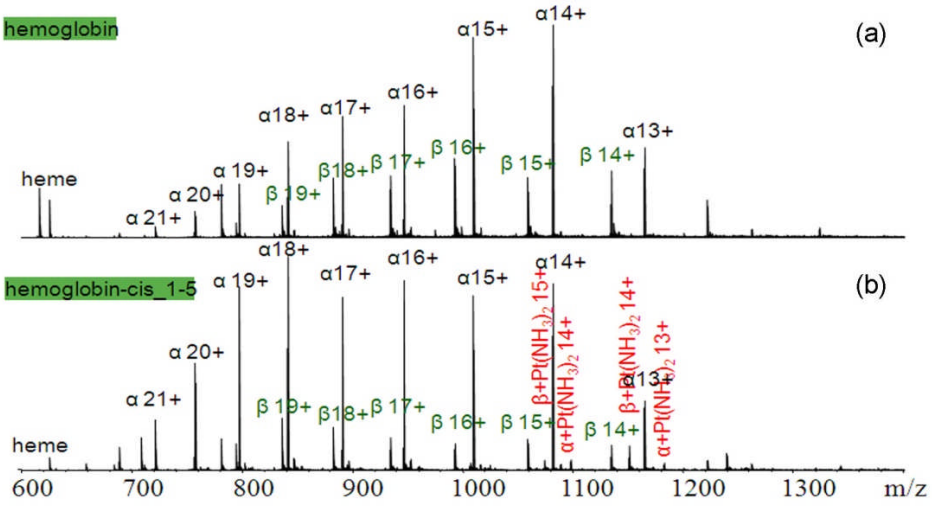

Table A.1 Isotopic distribution peaks of $[A + Pt(NH_3) + B + 2H]^{4+}$ and ions. The isotopic distributions of $[A + Pt(NH_3) + B + 2H]^{4+}$ and $[B + Pt + B + 2H]^{4+}$ ions are highlighted in bold. Assigned peaks labeled with "▲" are the ions used as internal calibrants.

Assignments	Exp. mass (Da)	Theo. mass (Da)	Error (ppm)
▲$[A+2H]^{2+}$	523.77464	523.77453	0.21
▲$[B+3H]^{3+}$	540.61232	540.61230	0.04
$[A+Pt(NH_3)+B+3H]^{5+}$	576.07273	576.07290	-0.30
$[B+Pt(NH_3)+H]^{3+}$	610.93808	610.93856	-0.79
$[B+Pt(NH_3)_2+H]^{3+}$	616.61349	616.61408	-0.96
$[A+Pt(NH_3)_2]^{2+}$	637.27559	637.27587	-0.44
$[A+Pt(NH_3)+B+2H]^{4+}$	**719.33830**	**719.33806**	**0.33**
	719.58876	**719.58875**	**0.01**
	719.83924	**719.83931**	**-0.10**
	720.08972	**720.08995**	**-0.32**
	720.34043	**720.34067**	**-0.33**
	720.59078	**720.59064**	**0.19**
▲$[B+2H]^{2+}$	810.41479	810.41481	-0.02
$[B+Pt+B+2H]^{4+}$	**858.40087**	**858.40156**	**-0.80**
	858.65212	**858.65229**	**-0.20**
	858.90300	**858.90285**	**0.17**
	859.15375	**859.15351**	**0.28**
	859.40350	**859.40421**	**-0.83**
	859.65423	**859.65418**	**0.58**
	859.90553	**859.90491**	**0.72**
	860.15573	**860.15545**	**0.33**
$[B+Pt(NH_3)+B+2H]^{4+}$	863.15910	863.15949	-0.45
$[B+Pt(NH_3)]^{2+}$	915.40228	915.40293	-0.71
$[B+Pt(NH_3)Cl+H]^{2+}$	933.39047	933.39127	-0.86
$[A+Pt(NH_3)+B+H]^{3+}$	959.44958	959.44998	-0.42
▲$[A+H]^{+}$	1046.54180	1046.54179	0.01
Mean absolute deviation (ppm)			0.40

Table A.2 CAD Fragments of [A + Pt(NH_3) + B + 2H]$^{4+}$ ion. Assigned peaks labeled with "▲" are the ions used as internal calibrants.

Assignments	Exp. mass (Da)	Theo. mass (Da)	Error (ppm)
B_b_3	396.19898	396.19899	-0.03
B_b_7 $^{2+}$	404.70642	404.70665	-0.58
B_b_8 $^{2+}$	497.74620	497.74631	-0.22
▲B_b_4	509.28303	509.28306	-0.06
[A+2H] $^{2+}$	523.77451	523.77453	-0.04
B_b_9 $^{2+}$	533.26492	533.26486	0.10
B_b_5	566.30447	566.30452	-0.09
B_b_{10} $^{2+}$	582.79899	582.79907	-0.15
[B+Pt-CH_4S+H] $^{3+}$	589.26206	589.26192	0.24
[B+Pt-NH_3+H] $^{3+}$	599.58775	599.58753	0.37
[B+Pt+H] $^{3+}$	605.26338	605.26305	0.55
[B+Pt(NH_3)+H] $^{3+}$	610.93818	610.93856	-0.62
B_b_{11} $^{2+}$	611.30991	611.30980	0.18
[A+Pt+B_a_{12}+2H] $^{4+}$	643.29632	643.29614	0.28
[B+Pt+A_b_6+2H] $^{4+}$	650.04961	650.04970	-0.14
[A+Pt+B_b_{12}+2H] $^{4+}$	650.29448	650.29487	-0.60
[A+Pt(NH_3)+B_b_{12}+2H] $^{4+}$	654.05513	654.05565	-0.80
▲B_b_6	680.34750	680.34745	0.07
[B+Pt(NH_3)+A_y_7+2H] $^{4+}$	690.83163	690.83060	1.49
[A+Pt+B-NH_3+2H] $^{4+}$	711.32591	711.32603	-0.17
[A+Pt+B+2H] $^{4+}$	715.58215	715.58267	-0.73
[A+Pt(NH_3)+B+2H] $^{4+}$	719.83932	719.83931	0.01
[B_a_{12}+Pt] $^{2+}$	762.31672	762.31662	0.13
[B_b_{12}+Pt] $^{2+}$	776.31416	776.31408	0.10
A_b_6	784.41018	784.41005	0.17
[B-CH_4S+2H] $^{2+}$	786.41310	786.41312	-0.03
[B-NH_3+2H] $^{2+}$	801.90140	801.90153	-0.16
B_b_7	808.40603	808.40603	0.00
[B+2H] $^{2+}$	810.41499	810.41481	0.22
[B_b_{13}+Pt] $^{2+}$	832.85608	832.85612	-0.05
[B+Pt+A_b_6+H] $^{3+}$	866.39669	866.39717	-0.55
[B+Pt-CH_4S-NH_3] $^{2+}$	874.37526	874.37469	0.65
[B+Pt-CH_4S] $^{2+}$	882.88780	882.88796	-0.18
[B+Pt-CO-NH_3] $^{2+}$	884.37900	884.37892	0.09
[B+Pt-NH_3] $^{2+}$	898.37644	898.37638	0.07
[B+Pt] $^{2+}$	906.88946	906.88965	-0.21

$[B+Pt+NH_3]^{2+}$	915.40277	915.40293	-0.17
▲B_b_8	994.48488	994.48534	-0.46
$[A+H]^{1+}$	1046.54125	1046.54179	-0.52
▲B_b_9	1065.52207	1065.52245	-0.36
▲B_b_{10}	1164.5913	1164.59087	0.37
Mean absolute deviation (ppm)			0.29

Table A.3 ECD Fragments of the $[A + Pt(NH_3) + B + 2H]^{4+}$ ion

Assignments	Exp. mass (Da)	Theo. mass (Da)	Error (ppm)
A_c_2	289.16167	289.16188	-0.73
$A\text{-}c_3$	388.23012	388.23029	-0.44
B_c_3	413.22533	413.22554	-0.51
▲$[A+2H]^{2+}$	523.77453	523.77453	0.00
$B\text{-}c_4$	526.30956	526.30961	-0.10
A_c_5	551.29393	551.29362	0.56
B_c_5	583.33100	583.33107	-0.12
$[B+Pt(NH_3)+H]^{3+}$	610.60457	610.60438	0.31
A_c_6	664.37750	664.37769	-0.29
B_c_6	697.37418	697.37400	0.26
▲$[A+Pt(NH_3)+B+2H]^{4+}$	719.83929	719.83931	-0.03
$[B+2H\text{-}CH_4S]^{2+}$	786.41359	786.41312	0.03
▲$[B+2H]^{2+}$	810.41481	810.41481	0.00
B_c_7	825.43279	825.43258	0.25
$A+Pt+B_z_{12}^{3+}$	874.41373	874.41406	-0.38
$B+Pt\text{-}CH_4S^{2+\cdot}$	883.39248	883.39243	0.06
$[B+Pt+H]^{2+\cdot}$	907.39370	907.39411	-0.45
$A+Pt(NH_3)+B_z_{13}^{3+\cdot}$	917.09947	917.10027	-0.87
$A+Pt(NH_3)+B_z_6^{2+\cdot}$	933.42222	933.42235	-0.14
$[A+Pt+B+2H]^{3+\cdot}$	954.11063	954.11096	-0.35
$[A+Pt(NH_3)+B+2H]^{3+\cdot}$	959.78588	959.78647	-0.61
B_c_8	1011.51202	1011.51189	0.13
$A+Pt(NH_3)+B_z_7^{2+\cdot}$	1026.96238	1026.9633	-0.90
▲$[A+H]^{+}$	1046.54183	1046.54179	0.04
B_c_9	1082.54917	1082.54900	0.16
$A+Pt(NH_3)+B_z_8^{2+\cdot}$	1090.99337	1090.99229	0.99
$A+Pt(NH_3)+B_z_9^{2+\cdot}$	1148.01292	1148.01377	-0.74
$A+Pt(NH_3)+B_z_{10}^{2+\cdot}$	1176.52437	1176.52451	-0.12
B_c_{10}	1181.62000	1181.61742	2.18
$A+Pt(NH_3)+B_z_{11}^{2+\cdot}$	1233.06608	1233.06658	-0.41
B_c_{11}	1238.63910	1238.63888	0.18
$A+Pt(NH_3)+B_z_{12}^{2+\cdot}$	1303.10696	1303.10781	-0.65
$[A+Pt+B+2H]^{2+\cdot\cdot}$	1422.65622	1422.65371	1.76
$[A+Pt(NH_3)+B+2H]^{2+\cdot\cdot}$	1431.16535	1431.16644	-0.76
$[B\text{-}CH_4S\text{-}H]^{+}$	1571.81968	1571.81897	0.45
▲$[B+H]^{+}$	1619.82230	1619.82234	-0.02
$[B+Pt\text{-}CH_4S]^{+\cdot}$	1765.77947	1765.77703	1.38

$[B+Pt-NH_3-H]^+$	1795.74635	1795.74548	0.48
$[B+Pt-NH_3]^{+\cdot}$	1796.75430	1796.75385	0.25
$[B+Pt-H]^+$	1812.77370	1812.77203	0.92
$[B+Pt]^{+\cdot}$	1813.78271	1813.78040	1.27
Mean absolute deviation (ppm)			0.46

Table A.4 CAD Fragments of $[B + Pt + B + 2H]^{4+}$ ion

Assignments	Exp. mass (Da)	Theo. mass (Da)	Error (ppm)
$B_b_8^{2+}$	497.74635	497.74631	0.08
$B_b_9^{2+}$	533.26470	533.26486	-0.30
$B_b_{12}^{2+}$	679.83967	679.83926	0.60
$B_b_{13}^{2+}$	736.38119	736.38129	-0.14
$[B_a_{12}+Pt]^{2+}$	762.31685	762.31662	0.30
$[B_b_{12}+Pt]^{2+}$	776.31406	776.31408	-0.03
$[B-CH_4S+2H]^{2+}$	786.41306	786.41312	-0.08
$[B+Pt+B_b_{12}+2H]^{4+}$	793.61489	793.61505	-0.20
$[B-NH_3+2H]^{2+}$	801.90177	801.90153	0.30
B_b_7	808.40614	808.40603	0.14
$[B+2H]^{2+}$	810.41486	810.41481	0.06
$[B+Pt+B_b_{13}+2H]^{4+}$	821.88599	821.88608	-0.11
$[B+Pt+B-CH_4S-NH_3+2H]^{4+}$	842.64562	842.64537	0.30
$[B+Pt+B-CH_4S+2H]^{4+}$	847.15125	847.15250	-1.48
$[B+Pt+B-NH_3+2H]^{4+}$	854.6458	854.64622	-0.49
$[B+Pt+B+2H]^{4+}$	858.90294	858.90285	0.10
$[B+Pt-CH_4S]^{2+}$	882.88828	882.88796	0.36
$[B+Pt-CO-NH_3]^{2+}$	884.37925	884.37892	0.37
$[B+Pt-NH_3]^{2+}$	898.37651	898.37638	0.14
$[B+Pt]^{2+}$	906.89000	906.88965	0.39
B_b_8	994.48579	994.48534	0.45
B_b_9	1065.52184	1065.52245	-0.57
B_b_{10}	1164.59126	1164.59087	0.33
B_b_{11}	1221.61296	1221.61233	0.52
Mean absolute deviation (ppm)			0.31

Table A.5 ECD Fragments of $[B + Pt + B + 2H]^{4+}$ ion

Assignments	Exp. mass (Da)	Theo. mass (Da)	Error (ppm)
B_c_3	413.22554	413.22555	0.02
B_c_4	526.30961	526.30956	-0.10
B_c_5	583.33107	583.33096	-0.19
B_c_6	697.37400	697.37396	-0.06
$[B+2H-CH_4S]^{2+}$	786.41312	786.41236	-0.97
▲$[B+2H]^{2+}$	810.41481	810.41466	-0.19
B_c_7	825.43258	825.43259	0.01
▲$[B+Pt+B+2H]^{4+}$	858.90285	858.90206	-0.92
$[B+Pt-CH_4S+H]^{2+\cdot}$	883.39243	883.39136	-1.21
$[B+Pt+H]^{2+}$	906.88965	906.89265	3.31
$[B+Pt+H]^{2+\cdot}$	907.39411	907.39326	-0.94
B_c_8	1011.51180	1011.51206	0.26
$B+Pt+B_z_{12}^{3+\cdot}$	1059.83333	1059.83032	-2.84
B_c^9	1082.54900	1082.54903	0.03
$B+Pt+B_z_{13}^{3+\cdot}$	1102.51833	1102.51711	-1.11
$[B+Pt+B+2H-CH_4S]^{3+\cdot}$	1129.20578	1129.20360	-1.93
$[B+Pt+B+2H]^{3+\cdot}$	1145.20261	1145.20454	-1.69
B_c_{10}	1181.61921	1181.61802	-1.01
B_c_{11}	1238.63888	1238.63883	-0.04
$B+Pt+B_z_7^{2+\cdot}$	1305.09008	1305.09119	0.85
$B+Pt+B_z_8^{2+\cdot}$	1369.11940	1369.11862	-0.57
$B+Pt+B_z_9^{2+\cdot}$	1426.14088	1426.14080	-0.06
$B+Pt+B_z_{10}^{2+\cdot}$	1454.65162	1454.65848	4.72
$B+Pt+B_z_{11}^{2+\cdot}$	1511.19368	1511.19288	-0.53
$B+Pt+B_z_{12}^{2+\cdot}$	1589.24427	1589.24379	-0.30
▲$[B+H]^{+}$	1619.82234	1619.82155	-0.49
$B+Pt+B_z_{13}^{2+\cdot}$	1653.27358	1653.27487	0.78
$[B+Pt+B+2H-CH_4S]^{2+\cdot\cdot}$	1693.80567	1693.80253	-1.85
$[B+Pt+B+2H]^{2+\cdot\cdot}$	1717.80736	1717.80382	-2.06
$[B+Pt-CH_4S]^{+\cdot}$	1765.77703	1765.7783	0.72
▲$[B+Pt-H]^{+}$	1812.77203	1812.76993	-1.16
$[B+Pt]^{+\cdot}$	1813.78040	1813.77545	-2.73
$[B+Pt+CH_4S-H]^{+}$	1860.77651	1860.77303	-1.87
Mean absolute deviation (ppm)			1.07

Table A.6 CAD Fragments of [CaM(107~126) + Pt + CaM(127-148) + 3H]$^{5+}$ and [CaM(37-74) + 4H]$^{4+}$ ions

Assignments	Exp. mass (Da)	Theo. mass (Da)	Error (ppm)
▲Z_y_3	377.19655	377.19655	0.00
Y_b_4-H_2O	411.18735	411.18743	-0.19
X_y_3	419.24339	419.24350	-0.26
Y_b_4	429.19818	429.19799	0.44
Z_b_5	500.24635	500.24634	0.02
Z_y_4	508.23699	508.23704	-0.10
Y_b_5-H_2O	526.21437	526.21437	0.00
X_y_4	548.28614	548.28609	0.09
▲Z_y_5	609.28479	609.28471	0.13
Z_y_{10} $^{2+}$	621.80411	621.80412	-0.02
X_y_5	663.31324	663.31304	0.30
Z_b_{13} $^{2+}$	692.32302	692.32297	0.07
Y_b_7-H_2O	698.262574	698.26278	-0.30
Y_b_7	716.27328	716.27334	-0.08
X_y_6	762.3815	762.38145	0.07
Z_b_8	827.389468	827.38937	0.12
▲Z_y_7	869.4368	869.43719	-0.45
Z_b_9	898.42689	898.42649	0.45
Z_b_{17} $^{2+}$	935.92776	935.92800	-0.26
Y_b_{10}-H_2O	982.41083	982.41124	-0.42
X_y_8	1020.46705	1020.46664	0.40
[X+Pt+Y+3H] $^{5+}$	1017.84696	1017.84615	0.80
[X+Pt+Y_y_{12}+2H] $^{4+}$	1021.70039	1021.70072	-0.52
Z_b_{10}	1027.46927	1027.46908	0.18
[X+Pt+Y_y_{13}+2H] $^{4+}$	1046.46790	1046.46782	-0.12
[X+Pt+Y_y_{14}+2H] $^{4+}$	1078.48085	1078.48246	-1.70
[X+Pt+Y_y_{15}+2H] $^{4+}$	1092.73828	1092.73783	0.22
▲Z_y_9	1095.53291	1095.53255	0.33
[X+Pt+Y_y_{16}+2H] $^{4+}$	1121.49361	1121.49457	-1.04
[X+Pt+Y_y_{17}-NH_3] $^{4+}$	1131.49982	1131.49329	5.58
[X+Pt+Y_y_{17}+2H] $^{4+}$	1135.75068	1135.74993	0.47
Z_b_{11}	1140.55422	1140.55314	0.95
[X+Pt+Y_y_{18}+2H-NH_3] $^{4+}$	1160.25409	1160.25003	3.31
[X+Pt+Y_y_{18}+2H] $^{4+}$	1164.50763	1164.50667	0.64
[X+Pt+Y_y_{19}+2H] $^{4+}$	1192.77443	1192.77768	-2.91
[X+Pt+Y_y_{20}+2H] $^{4+}$	1221.53422	1221.53442	-0.33

Z_y_{10}	1242.60061	1242.60096	-0.28
Z_b_{12}	1268.61149	1268.61172	-0.18
▲Z_y_{11}	1357.62757	1357.62791	-0.25
Z_b_{13}	1383.63898	1383.63866	0.23
Z_y_{12}	1470.71256	1470.71197	0.40
Z_b_{14}	1514.67913	1514.67915	-0.01
Z_b_{15}	1627.76619	1627.76321	1.83
Mean absolute deviation (ppm)			0.59

Appendix B (Supporting Information for Chapter 3)

Figure B.1 ESI-FTMS analyses of anti-cancer platinum drug-CaM mixtures after different reaction times. CaM:Pt_1 (1:2) at (a) 60min, (b) 90min, and (c) 120min; CaM:Pt_3 (1:1) at (a') 60min, (b') 90min, and (c') 120min.

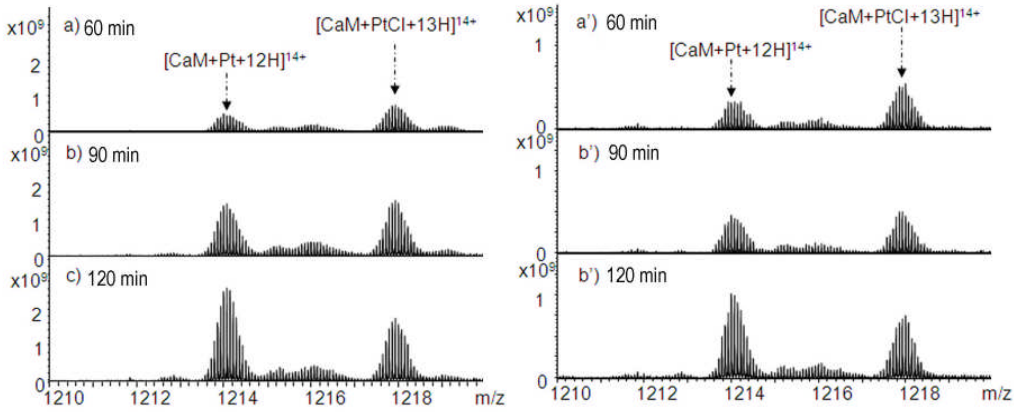

Figure B.2 ESI-FTMS analyses of trypsin-digested CaM-cisplatin (Pt_1) samples at different molar ratios. (a) CaM:Pt_1 (1:1); (b) CaM:Pt_1 (1:2); (c) CaM:Pt_1 (1:8).

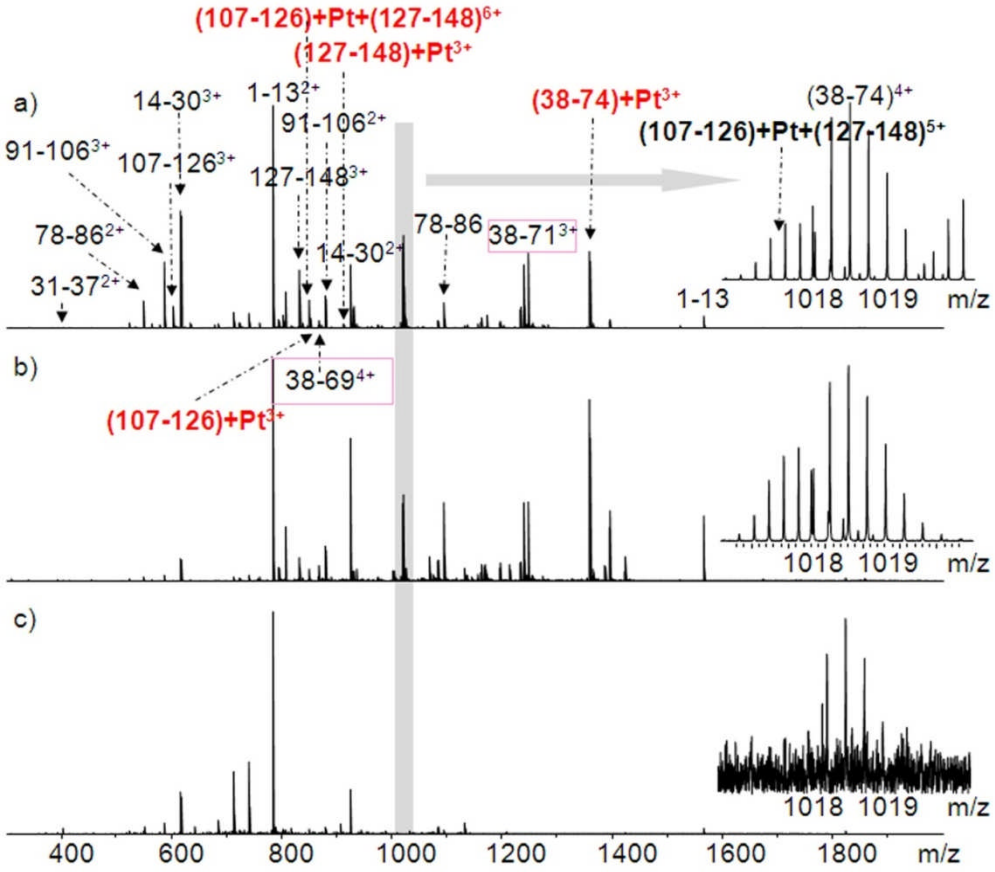

Figure B.3 ECD spectra of $[CaM+16H]^{16+}$ ions at *m/z* 1050 in a CaM sample. The insert is shown to compare with Figure 2b, which indicates that the intra-chain cross-linking of Pt between CaM(109) and CaM(144) contributes to repressed detections of cleavages in the region of CaM(106-148) in the top-down analyses. 91% backbone cleavage efficiency was achieved.

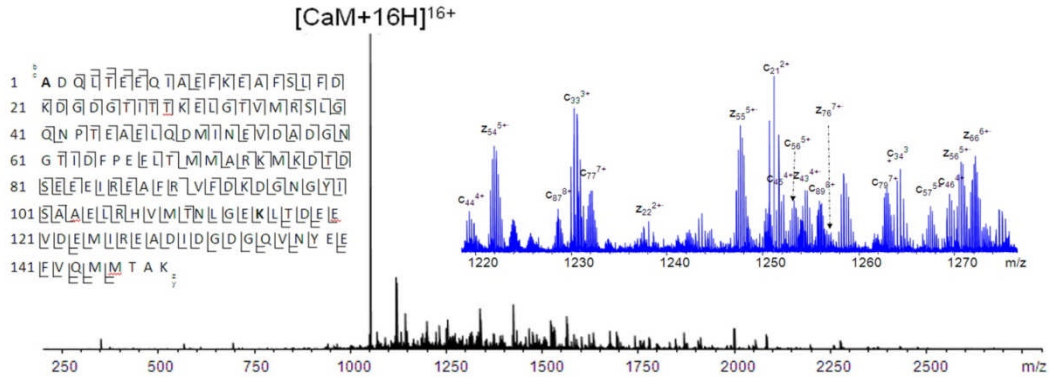

Figure B.4 Bottom-up MS/MS spectra of the CaM:Pt(dien) (1:8). (a) CAD spectrum of $[CaM(38\text{-}74)+3Pt(dien)+H]^{7+}$ ion at *m/z* 709; (b) CAD (b-1) & ECD (b-2) spectra of $[CaM(107\text{-}126)+2Pt(dien)+H]^{5+}$ ion at *m/z* 600; (c) CAD spectrum of $[CaM(127\text{-}148)+Pt(dien)+2H]^{4+}$ ion at *m/z* 697. Single stars represent singly Pt(dien)-modified fragments; double stars represent doubly Pt(dien)-modified fragments.

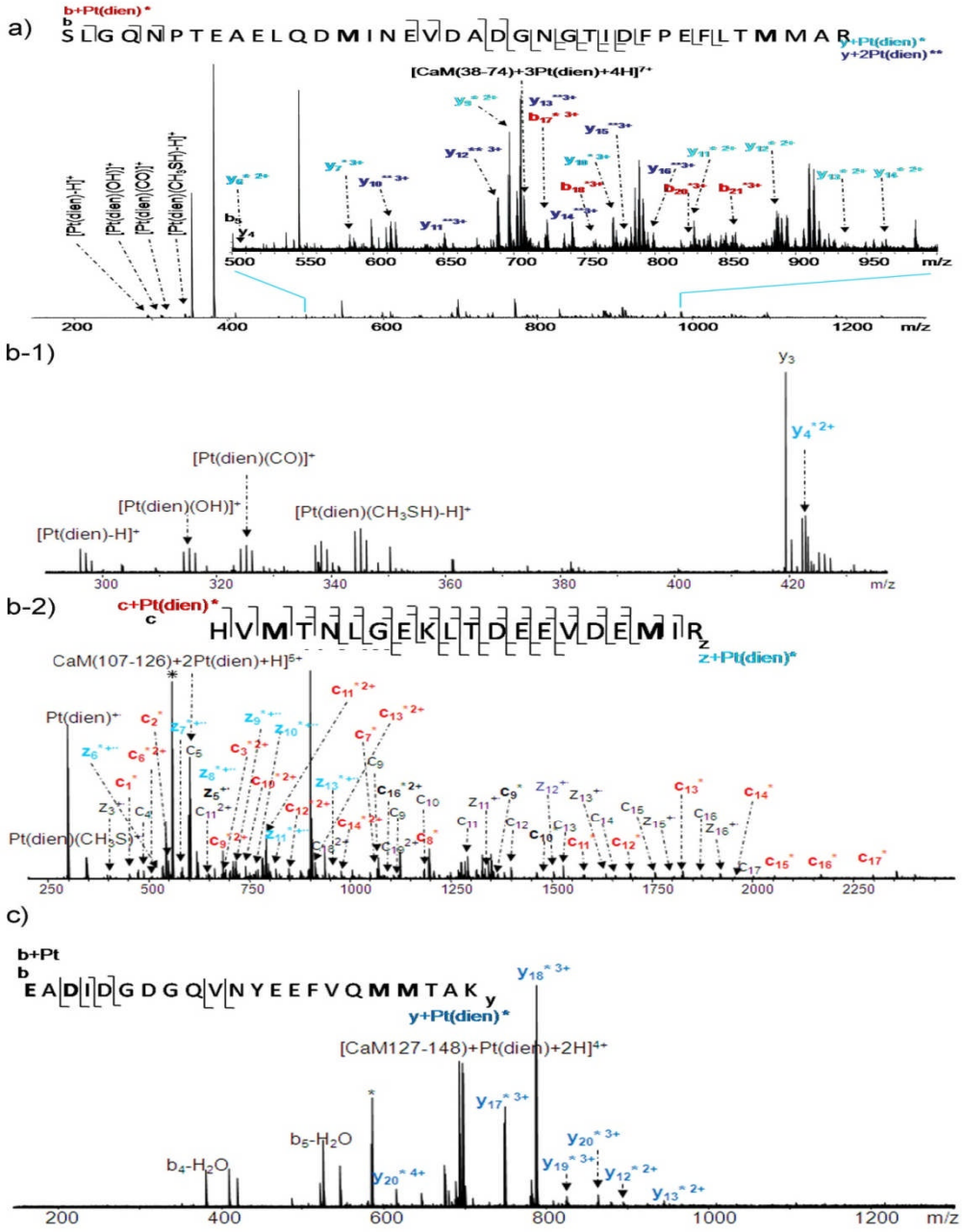

Table B.1 Peak-list table for Figure 3.2 b'.

Assignments	Exp. mass (Da)	Theo. mass (Da)	Error (ppm)
$[CaM+Pt_6(NH_3)_4+H]^{13+}$	1386.677006	1386.673225	2.73
$[CaM+Pt_7(NH_3)_6-H]^{13+}$	1404.131852	1404.134884	-2.16
$[CaM+Pt_8(NH_3)_8-3H]^{13+}$	1421.673874	1421.673598	0.19
$[CaM+Pt_9(NH_3)10-5H]^{13+}$	1439.059673	1439.058202	1.02
$[CaM+Pt^{10}(NH3)12-7H]^{13+}$	1456.595243	1456.596912	-1.15
Mean absolute deviation (ppm)			1.45

Table B.2 ECD Fragments of the $[CaM+2Pt+12H]^{16+}$ ions

No.	Assignments	Exp. mass (Da)	Theo. mass (Da)	Error (ppm)
1	c_4	487.251185	487.251089	0.20
2	c_5-NH_3	571.272554	571.272066	0.85
3	c_5	588.299110	588.298615	0.84
4	c6	717.341071	717.341228	-0.22
5	c_{13}^{2+}	781.888567	781.888477	0.12
6	c_{21}^{3+}	834.413684	834.414059	-0.45
7	c_7	846.384520	846.383953	0.67
8	c_{14}	846.910394	846.911461	-1.26
9	c_{23}^{3+}	891.429248	891.429057	0.21
10	c_{49}^{6+}	908.450501	908.449960	0.60
11	c_{41}^{5+}	913.256014	913.256163	-0.16
12	c_{33}^{4+}	923.205572	923.204933	0.69
13	c_{24}^{4+}	930.106823	930.105842	1.05
14	$?^{2+}$	933.959746		
15	c_{25}^{3+}	949.112602	949.112996	-0.42
16	c_{16}^{2+}	955.463113	955.462538	0.60
17	$?^{3+}$	961.785910		
18	c_{94}^{11+}	972.469758	972.468904	0.88
19	c_{79}^{9+}	982.249595	982.250077	-0.49
20	c_{26}^{3+}	982.796265	982.795556	0.72
21	c_{53}^{6+}	987.315973	987.315676	0.30
22	c_{96}^{11+}	988.202801	988.200869	1.96
23	c_{80}^{9+}	995.366295	995.365239	1.06
24	c_{97}^{11+}	998.384463	998.386015	-1.55
25	c_{17}^{2+}	998.978543	998.978552	-0.01
26	$c^{45\ 5+}$	1001.493617	1001.493358	0.26
27	$?^{5+}$	1006.899099		
28	c_{46}^{5+}	1015.700577	1015.700781	-0.20
29	c_{82}^{9+}	1019.261988	1019.262073	-0.08
30	c_{27}^{3+}	1020.491172	1020.490244	0.91
31	c_{90}^{10+}	1020.589788	1020.588878	0.89
32	c_{100}^{11+}	1028.858151	1028.856488	1.62
33	c_{91}^{10+}	1030.495724	1030.495721	0.00
34	$?^{3+}$	1033.498990		
35	c_{101}^{11+}	1036.676848	1036.677290	-0.43
36	c_{102}^{11+}	1043.044905	1043.044017	0.85

37	c_{37}^{4+}	1045.019694	1045.019357	0.32
38	c_{92}^{10+}	1045.201623	1045.202563	-0.90
39	c_{103}^{11+}	1049.500306	1049.501937	-1.55
40	c_{28}^{3+}	1054.173714	1054.172804	0.86
41	c_{67}^{7+}	1055.074252	1055.073554	0.66
42	c_{93}^{10+}	1056.706278	1056.705258	0.97
43	c_{76}^{8+}	1062.133808	1062.135027	-1.15
44	c_{48}^{5+}	1064.127351	1064.126113	1.16
45	c_{38}^{4+}	1066.776957	1066.777364	-0.38
46	$?^{3+}$	1067.181663		
47	c_{94}^{10+}	1069.514904	1069.514755	0.14
48	$[CaM+2Pt-H_2O+12H]^{16+}$	1073.368652	1073.367424	1.14
49	$[CaM+2Pt+12H]^{16+}$	1074.494353	1074.493084	1.18
50	$[CaM+2Pt(NH_3)+12H]^{16+}$	1075.558402	1075.557242	1.08
51	$[CaM+2Pt(NH_3)_2+12H]^{16+}$	1076.620720	1076.621401	-0.63
52	c_{86}^{9+}	1077.847853	1077.847672	0.17
53	c_{95}^{10+}	1081.019396	1081.017449	1.80
54	c_{59}^{6+}	1085.018357	1085.019890	-1.41
55	c_{96}^{10+}	1086.719723	1086.719596	0.12
56	c_{29}^{3+}	1087.856033	1087.855363	0.62
57	c_{49}^{5+}	1089.938816	1089.938497	0.29
58	c_{87}^{9+}	1092.186173	1092.185738	0.40
59	c_{78}^{8+}	1092.650223	1092.650656	-0.40
60	c_{39}^{4+}	1095.048661	1095.048374	0.26
61	$?^{8+}$	1097.152540		
62	c_{97}^{10+}	1098.225201	1098.224200	0.91
63	c_{88}^{9+}	1100.078004	1100.078751	-0.68
64	c_{60}^{6+}	1104.027280	1104.026745	0.48
65	c_{79}^{8+}	1105.156919	1105.156227	0.63
66	c_{70}^{7+}	1106.673577	1106.673581	0.00
67	c_{40}^{4+}	1108.802640	1108.802070	0.51
68	c_{50}^{5+}	1112.943886	1112.944782	-0.81
69	$?^{8+}$	1113.906926		
70	$?^{3+}$	1115.883442		
71	c_{89}^{9+}	1116.531223	1116.531154	0.06
72	c_{80}^{8+}	1119.534174	1119.534595	-0.38
73	$z_{74}+2Pt^{8+}$	1119.747419	1119.748572	-1.03
74	b_{19}^{2+}	1121.042682	1121.043222	-0.48
75	$?^{8+}$	1122.533770		
76	$z_{65}+2Pt-H_2O^{7+}$	1124.785837	1124.784931	0.81
77	$z_{65}+2Pt\ 7^{+}$	1127.072093	1127.071608	0.43
78	c_{19}^{2+}	1129.556824	1129.556496	0.29

79	c_{81}^{8+}	1130.413850	1130.413598	0.22
80	c_{30}^{3+}	1130.554111	1130.553684	0.38
81	$?^{10+}$	1135.541130		
82	$c^{41\ 4+}$	1140.817080	1140.816715	0.32
83	$[CaM+2Pt+12H-H_2O-CH_3S]^{15+\cdot}$	1141.791667	1141.792273	-0.53
84	$[CaM+2Pt+12H-CH_3S]^{15+\cdot}$			
85	$[CaM+2Pt+12H-H_2O]^{15+\cdot}$	1144.926094	1144.925288	0.70
86	$[CaM+2Pt+12H]^{15+\cdot}$	1146.126927	1146.125993	0.81
87	$z_{107}+2Pt^{11+}$	1147.780157	1147.783193	-2.65
88	$?^{9+}$	1156.222090		
89	c_{92}^{9+}	1161.223933	1161.224262	-0.28
90	c_{52}^{5+}	1161.763879	1161.768796	-4.23
91	c_{83}^{8+}	1162.675131	1162.674247	0.76
92	$z_{67}+2Pt^{7+}$	1163.940663	1163.940926	-0.23
93	$?^{7+}$	1165.942120		
94	c_{31}^{3+}	1173.234130	1173.233411	0.61
95	c_{93}^{9+}	1174.004376	1174.005033	-0.56
96	$?^{5+}$	1175.574590		
97	$z_{68}+2Pt^{7+}$	1176.372827	1176.373992	-0.99
98	c_{74}^{7+}	1176.419026	1176.420805	-1.51
99	$z_{121}+2Pt^{12+}$	1177.537619	1177.537189	0.37
100	$?^{7+}$	1178.377140		
101	$?^{8+}$	1180.399070		
102	$?^{9+}$	1183.016110		
103	c_{53}^{5+}	1184.577415	1184.577356	0.05
104	c_{20}^{2+}	1187.071101	1187.069968	0.95
105	c_{94}^{9+}	1188.238722	1188.237808	0.77
106	$z_{59}+2Pt^{6+}$	1190.352377	1190.352448	-0.06
107	$z_{69}+2Pt-H_2O^{7+}$	1190.377452	1190.376543	0.76
108	$z_{69}+2Pt^{7+}$	1192.804719	1192.806414	-1.42
109	c_{85}^{8+}	1192.938986	1192.940081	-0.92
110	c_{43}^{4+}	1194.093265	1194.092309	0.80
111	c_{75}^{7+}	1195.147411	1195.145872	1.29
112	$?^{7+}$	1194.808800		
113	$?^{9+}$	1202.240420		
114	$z_{91}+2Pt^{9+}$	1205.870621	1205.869506	0.92
115	$z_{70}+2Pt^{7+}$	1207.242180	1207.241798	0.32
116	c_{96}^{9+}	1207.353931	1207.354298	-0.30
117	c_{32}^{3+}	1211.262424	1211.262570	-0.12
118	c_{86}^{8+}	1212.453502	1212.452721	0.64
119	c_{76}^{7+}	1213.725382	1213.724705	0.56
120	$z_{60}+2Pt^{6+}$	1215.032755	1215.031015	1.43

121	c_{44}^{4+}	1219.355010	1219.354229	0.64
122	$[CaM+2Pt+12H-CH_3S]^{14+\cdot\cdot}$	1224.634869	1224.635372	-0.41
123	$[CaM+2Pt+12H-CO]^{14+\cdot\cdot}$	1225.992780	1225.992537	0.20
124	$[CaM+2Pt+12H-H_2O]^{14+\cdot\cdot}$	1226.706234	1226.705705	0.43
125	$[CaM+2Pt+12H]^{14+\cdot\cdot}$	1227.992732	1227.992174	0.45
126	c_{33}^{3+}	1229.935720	1229.935254	0.38
127	c_{67}^{6+}	1230.751932	1230.751267	0.54
128	c_{77}^{7+}	1232.023615	1232.023988	-0.30
129	c_{88}^{8+}	1237.461981	1237.462685	-0.57
130	$?^{7+}$	1242.000000		
131	$z_{72}+2Pt^{7+}$	1242.687540	1242.691819	-3.44
132	$?^{6+}$	1242.943100		
133	$?^{3+}$	1243.000000		
134	$?^{5+}$	1244.201300		
135	$z_{62}+2Pt^{6+}$	1248.375161	1248.377637	-1.98
136	c_{78}^{7+}	1248.456738	1248.456408	0.26
137	$?^{3+}$	1249.610000		
138	$?^{8+}$	1250.000000		
139	c_{21}^{2+}	1250.615870	1250.615744	0.10
140	$?^{2+}$	1251.364150		
141	c_{45}^{4+}	1251.865868	1251.865714	0.12
142	$z_{95}+2Pt^{9+}$	1251.888717	1251.888961	
143	c_{56}^{5+}	1253.204806	1253.204948	-0.11
144	$?^{7+}$	1253.888000		
145	c_{89}^{8+}	1255.971803	1255.971638	0.13
146	$?^{7+}$	1256.000000		
147	$?^{4+}$	1258.371706		
148	$?^{10+}$	1260.359460		
149	$z_{107}+2Pt-H_2O^{5+}$	1260.656613	1260.659728	-2.47
150	$z_{73}+2Pt^{7+}$	1260.837659	1260.836639	0.81
151	$z_{107}+2Pt^{5+}$	1262.561551	1262.561119	0.34
152	c_{79}^{7+}	1262.892100	1262.891791	0.24
153	c_{34}^{3+}	1263.618710	1263.617813	0.71
154	$z_{52}+2Pt^{5+}$	1264.739565	1264.739841	-0.22
155	$z_{131}+2Pt^{12+}$	1265.994248	1265.993547	0.55
156	$_{?}^{11+}$	1265.000000		
157	$?^{12+}$	1266.000000		
158	c_{57}^{5+}	1267.412701	1267.412372	0.26
159	$?^{5+}$	1268.000000		
160	c_{46}^{4+}	1268.873590	1268.872484	0.87
161	$?^{7+}$	1272.606500		
162	$z_{132}+2Pt^{12+}$	1273.246333	1273.246219	0.09

163	$?^{12+}$	1274.000000		
164	z_{53}+2Pt-H_2O $^{5+}$	1272.942707	1272.942630	0.06
165	? $^{9+}$	1274.495550		
166	z_{53}+2Pt $^{5+}$	1275.944404	1275.943558	0.66
167	z_{74}+2Pt $^{7+}$	1279.710457	1279.711822	-1.07
168	c_{80} $^{7+}$	1279.323742	1279.324212	-0.37
169	$?^{8+}$	1280.000000		
170	? $^{7+}$	1282.491800		
171	c_{58} $^{5+}$	1290.418417	1290.417760	0.51
172	c_{70} $^{6+}$	1290.951358	1290.951298	0.05
173	c_{81} $^{7+}$	1291.756077	1291.757359	-0.99
174	z_{64}+2Pt $^{6+}$	1293.408162	1293.408711	-0.42
175	z_{122}+2Pt $^{11+}$	1294.864144	1294.865979	-1.42
176	$?^{5+}$	1295.000000		
177	c_{35} $^{3+}$	1297.309026	1297.309517	-0.38
178	z_{54}+2Pt $^{5+}$	1299.148906	1299.149528	-0.48
179	? $^{5+}$	1301.000000		
180	c_{47} $^{4+}$	1301.885028	1301.885641	-0.47
181	c_{59} $^{5+}$	1301.420330	1301.420750	-0.32
182	? $^{7+}$	1303.474260		
183	c_{92} $^{8+}$	1306.251575	1306.251385	0.15
184	c_{22} $^{2+}$	1308.631393	1308.630910	0.37
185	c_{82} $^{7+}$	1310.191838	1310.192015	-0.14
186	z_{76}+2Pt $^{7+}$	1311.441480		
187	z_{65}+2Pt $^{6+}$	1314.748303	1314.748996	-0.53
188	[CaM+2Pt+12H-CH_3S] $^{13+\cdots}$	1318.836070	1318.838135	-1.57
189	[CaM+2Pt+12H-H_2O] $^{13+\cdots}$	1321.067250	1321.067725	-0.36
190	[CaM+2Pt+12H] $^{13+\cdots}$	1322.453906	1322.453153	0.57
191	c_{60} $^{5+}$	1324.630509	1324.630639	-0.10
192	z_{55}+2Pt $^{5+}$	1324.770001	1324.768528	1.11
193	$?^{5+}$	1328.000000		
194	c_{83} $^{7+}$	1328.626544	1328.626667	-0.09
195	z_{77}+2Pt $^{7+}$	1330.304938	1330.304636	0.23
196	z_{66}+2Pt-H_2O $^{6+}$	1333.422287	1333.421153	0.85
197	c_{72} $^{6+}$	1334.631125	1334.631462	-0.25
198	c_{61} $^{5+}$	1336.034546	1336.034932	-0.29
199	z_{66}+2Pt $^{6+}$	1336.088729	1336.088891	-0.12
200	c_{94} $^{8+}$	1336.640563	1336.641625	-0.79
201	c_{23} $^{2+}$	1337.142104	1337.141653	0.34
202	? $^{6+}$	1338.759470		
203	c_{36} $^{3+}$	1340.321720	1340.320779	0.70
204	z_{90}+2Pt $^{8+}$	1342.349572	1342.349504	0.05

205	? $^{9+}$	1345.376740		
206	z_{56}+2Pt $^{5+}$	1347.774205	1347.773920	0.21
207	? $^{7+}$	1348.884500		
208	? $^{10+}$	1349.706570		
209	z_{43}+2Pt $^{4+}$	1351.311122	1351.311961	-0.62
210	? $^{8+}$	1352.773000		
211	z_{102}+2Pt $^{9+}$	1353.712654	1353.713556	-0.67
212	z_{91}+2Pt $^{8+}$	1356.477797	1356.477285	0.38
213	z_{67}+2Pt $^{6+}$	1357.931567	1357.930016	1.14
214	? $^{6+}$	1360.099190		
215	c_{49} $^{4+}$	1362.171530	1362.171302	0.17
216	c_{85} $^{7+}$	1363.214732	1363.216196	-1.07
217	z_{92}+2Pt $^{8+}$	1365.357533	1365.356925	0.45
218	c_{74} $^{6+}$	1372.153591	1372.155863	-1.66
219	z_{68}+2Pt $^{6+}$	1372.435848	1372.435355	0.36
220	? $^{6+}$	1374.771600		
221	z_{57}+2Pt $^{5+}$	1377.388759	1377.387797	0.70
222	c_{63} $^{5+}$	1378.861357	1378.861283	0.05
223	z_{44}+2Pt $^{4+}$	1379.334074	1379.333964	0.08
224	z_{131}+2Pt $^{11+}$	1380.994694	1380.992299	1.73
225	z_{69}+2Pt-H_2O $^{6+}$	1388.770549	1388.771907	-0.98
226	z_{132}+2Pt $^{11+}$	1388.996875	1388.995386	1.07
227	z_{69}+2Pt $^{6+}$	1391.440236	1391.439604	0.45
228	c_{37} $^{3+}$	1393.023301	1393.023384	-0.06
229	c_{75} $^{6+}$	1394.171361	1394.168971	1.71
230	c_{24} $^{2+}$	1394.655297	1394.655124	0.12
231	z_{58}+2Pt $^{5+}$	1397.202516	1397.201483	0.74
232	z_{107}+2Pt-H_2O $^{9+}$	1400.732706	1400.732594	0.08
233	z_{81}+2Pt $^{7+}$	1400.621241	1400.624647	-2.43
234	c_{64} $^{5+}$	1401.866275	1401.866672	-0.28
235	z_{107}+2Pt $^{9+}$	1402.736261	1402.733768	1.78
236	z_{120}+2Pt $^{10+}$	1403.139980	1403.139043	0.67
237	?$^{5+}$	1403.000000		
238	z_{70}+2Pt $^{6+}$	1408.280181	1408.280886	-0.50
239	z_{95}+2Pt $^{8+}$	1408.375197	1408.374366	0.59
240	z_{45}+2Pt $^{4+}$	1411.593647	1411.593364	0.20
241	z_{121}+2Pt $^{10+}$	1412.844525	1412.840680	2.72
242	c_{25} $^{2+}$	1422.664410	1422.664151	0.18
243	z_{71}+2Pt $^{6+}$	1427.617419	1427.618955	-1.08
244	z_{59}+2Pt $^{5+}$	1428.423507	1428.421708	1.26
245	z_{46}+2Pt $^{4+}$	1429.354651	1429.353902	0.52
246	c_{89} $^{7+}$	1435.110340	1435.108949	0.97

247	c_{77}^{6+}	1437.362678	1437.360625	1.43
248	$?^{2+}$	1442.176230		
249	z_{47}+2Pt $^{4+}$	1447.112014	1447.111927	0.06
250	z_{72}+2Pt $^{6+}$	1449.135856	1449.135271	0.40
251	c_{52}^{4+}	1451.959839	1451.959176	0.46
252	z_{60}+2Pt $^{5+}$	1457.837282	1457.835763	1.04
253	c_{39}^{3+}	1459.728326	1459.728739	-0.28
254	z_{48}+2Pt $^{4+}$	1468.871743	1468.869937	1.23
255	z_{73}+2Pt $^{6+}$	1470.978176	1470.975354	1.92
256	z_{61}+2Pt $^{5+}$	1472.045369	1472.043187	1.48
257	c_{26}^{2+}	1473.188130	1473.187990	0.10
258	c_{40}^{3+}	1478.734907	1478.735894	-0.67
259	c_{53}^{4+}	1479.969370	1479.968251	0.76
260	$?^{6+}$	1484.872660		
261	z_{74}+2Pt $^{6+}$	1492.990490	1492.990454	0.02
262	$?^{5+}$	1494.048690		
263	z_{62}+2Pt $^{5+}$	1497.851964	1497.851709	0.17
264	z_{49}+2Pt $^{4+}$	1497.141856	1497.140959	0.60
265	? $^{9+}$	1500.956880		
266	$?^{3+}$	1506.416720		
267	$?^{3+}$	1507.722080		
268	? $^{8+}$	1513.000000		
269	$?^{10+}$	1519.190850		
270	c_{41}^{3+}	1520.753210	1520.753194	0.01
271	$?^{3+}$	1521.000000		
272	z_{131}+2Pt $^{6+}$	1519.191184	1519.191177	0.00
273	z_{89}+2Pt $^{7+}$	1525.539479	1525.537512	1.29
274	c_{27}^{2+}	1529.728950	1529.730022	-0.70
275	$?^{4+}$	1532.436430		
276	z_{50}+2Pt $^{4+}$	1537.908816	1537.906876	1.26
277	c_{55} 4+	1537.497254	1537.497630	-0.24
278	$?^{6+}$	1542.393240		
279	$?^{11+}$	1546.254890		
280	z_{51}+2Pt $^{4+}$	1552.162874	1552.162244	0.41
281	c_{13}	1562.769610	1562.769676	-0.04
282	c_{56}^{4+}	1566.254010	1566.254366	-0.23
283	$?^{2+}$	1571.000000		
284	$?^{4+}$	1570.000000		
285	$?^{8+}$	1572.698870		
286	$?^{2+}$	1573.000000		
287	$?^{4+}$	1575.000000		
288	z_{107}+2Pt-H_2O $^{8+}$	1575.575603	1575.572841	1.75

289	z_{52}+2Pt-H_2O $^{4+}$	1576.420604	1576.420580	0.02
290	z_{107}+2Pt $^{8+}$	1577.826316	1577.824162	1.37
291	z_{65}+2Pt $^{5+}$	1577.497207	1577.497340	-0.08
292	z_{107}+2Pt $^{8+}$	1577.826316	1577.824162	1.37
293	z_{52}+2Pt $^{4+}$	1580.673981	1580.672982	0.63
294	c_{28} $^{2+}$	1580.253960	1580.253861	0.06
295	c_{57} $^{4+}$	1584.012975	1584.013645	-0.42
296	?$^{4+}$	1584.000000		
297	z_{53}+2Pt-H_2O $^{4+}$	1590.425749	1590.425709	0.03
298	z_{74}+2Pt $^{6+}$	1492.826775	1492.829246	-1.66
299	z_{53}+2Pt $^{4+}$	1594.929601	1594.928350	0.78
300	z_{66}+2Pt-H_2O $^{5+}$	1599.703907	1599.703750	0.10
301	? $^{2+}$	1599.765710		
302	z_{66}+2Pt $^{5+}$	1603.307168	1603.305863	0.81
303	z_{95}+2Pt-H_2O $^{7+}$	1607.142333	1607.140258	1.29
304	z_{95}+2Pt $^{7+}$	1609.427300	1609.426807	0.31
305	?$^{2+}$	1609.000000		
306	c_{58} $^{4+}$	1612.772433	1612.770381	1.27
307	z_{54}+2Pt-H_2O $^{4+}$	1619.185653	1619.182450	1.98
308	z_{54}+2Pt $^{4+}$	1623.685857	1623.685091	0.47
309	c_{59} $^{4+}$	1627.026720	1627.025747	0.60
310	z_{67}+2Pt $^{5+}$	1629.116270	1629.114386	1.16
311	c_{29} $^{2+}$	1630.778140	1630.777701	0.27
312	?$^{5+}$	1632.000000		
313	?$^{5+}$	1643.121810		
314	?$^{4+}$	1644.532710		
315	c_{74} $^{5+}$	1646.786809	1646.786838	-0.02
316	z_{68}+2Pt $^{5+}$	1646.522168	1646.520679	0.90
317	?$^{5+}$	1649.725560		
318	z_{55}+2Pt-H_2O $^{4+}$	1651.205504	1651.206199	-0.42
319	z_{55}+2Pt $^{4+}$	1655.710480	1655.708840	0.99
320	z_{69}+2Pt-H_2O $^{5+}$	1665.921878	1665.923956	-1.25
321	c_{45} $^{3+}$	1668.149810	1668.149636	0.10
322	z_{69}+2Pt $^{5+}$	1669.729148	1669.726362	1.67
323	?$^{2+}$	1672.819560		
324	?$^{5+}$	1673.132130		
325	?$^{3+}$	1677.156700		
326	z_{56}+2Pt-H_2O $^{4+}$	1680.967309	1680.970765	-2.06
327	z_{56}+2Pt $^{4+}$	1684.466917	1684.465581	0.79
328	z_{70}+2Pt $^{5+}$	1689.743351	1689.735607	4.58
329	c_{14}	1691.811880	1691.812272	-0.23
330	c_{30} $^{2+}$	1695.327219	1695.326888	0.20

331	z_{71}+2Pt-H_2O $^{5+}$	1709.142049	1709.138885	1.85
332	z_{71}+2Pt $^{5+}$	1712.941327	1712.941291	0.02
333	z_{57}+2Pt $^{4+}$	1721.235009	1721.232639	1.38
334	z_{72}+2Pt-H_2O $^{5+}$	1735.354705	1735.359285	-2.64
335	z_{72}+2Pt $^{5+}$	1738.157874	1738.159519	-0.95
336	z_{58}+2Pt $^{4+}$	1746.252348	1746.250034	1.33
337	c_{31} $^{2+}$	1759.346870	1759.346479	0.22
338	c_{15}	1762.849260	1762.849385	-0.07
339	z_{73}+2Pt $^{5+}$	1764.764988	1764.768385	-1.92
340	z_{59}+2Pt $^{4+}$	1785.277174	1785.275316	1.04
341	z_{74}+2Pt $^{5+}$	1790.992326	1790.993349	-0.57
342	z_{43}+2Pt $^{3+}$	1801.081185	1801.079272	1.06
343	c_{32} $^{2+}$	1815.892540	1815.888511	2.22
344	z_{60}+2Pt $^{4+}$	1822.297847	1822.293192	2.55
345	z_{44}+2Pt $^{3+}$	1838.776308	1838.776193	0.06
346	z_{61}+2Pt $^{4+}$	1840.054836	1840.052473	1.28
347	c_{33} $^{2+}$	1844.900046	1844.900949	-0.49
348	? $^{1+}$	1865.902360		
349	z_{62}+2Pt $^{4+}$	1872.065837	1872.062817	1.61
350	z_{45}+2Pt $^{3+}$	1881.790292	1881.788727	0.83
351	c_{34} $^{2+}$	1895.423669	1895.424788	-0.59
352	z_{46}+2Pt $^{3+}$	1905.802417	1905.803710	-0.68
353	c_{16}	1909.915852	1909.917799	-1.02
354	z_{47}+2Pt $^{3+}$	1929.147132	1929.146811	0.17
355	? $^{3+}$	1934.153340		
356	z_{48}+2Pt $^{3+}$	1958.160290	1958.157491	1.43
357	z_{65}+2Pt $^{4+}$	1972.125225	1972.120812	2.24
358	z_{49}+2Pt $^{3+}$	1995.513694	1995.517982	-2.15
359	c_{17}	1996.948989	1996.949828	-0.42
360	z_{66}+2Pt $^{4+}$	2003.879279	2003.880510	-0.61
361	c_{36} $^{2+}$	2010.979895	2010.980881	-0.49
362	z_{50}+2Pt $^{3+}$	2050.203770	2050.206842	-1.50
363	z_{51}+2Pt $^{3+}$	2069.215140	2069.213900	0.60
364	z_{69}+2Pt-H_2O $^{4+}$	2082.901128	2082.904951	-1.84
365	z_{69}+2Pt $^{4+}$	2087.408001	2087.407592	0.20
366	z_{52}+2Pt $^{3+}$	2107.230315	2107.228217	1.00
367	z_{53}+2Pt $^{3+}$	2127.241860	2127.244845	-1.40
368	z_{54}+2Pt-H_2O $^{3+}$	2158.906854	2158.907824	-0.45
369	z_{54}+2Pt $^{3+}$	2164.579285	2164.577696	0.73
370	z_{55}+2Pt-H_2O $^{3+}$	2201.933232	2201.940444	-3.28
371	z_{55}+2Pt $^{3+}$	2207.274491	2207.276028	-0.70
372	z_{56}+2Pt $^{3+}$	2245.617465	2245.618350	-0.39

373	c_{19}	2257.101740	2257.102306	-0.25
374	c_{41}^{2+}	2281.633082	2281.629493	1.57
375	c_{20}	2372.129920	2372.129249	0.28
	Mean absolute deviation (ppm)			0.59

Table B.3 ECD Fragments of the $[CaM+5Pt(dien)+10H]^{20+}$ ions

No.	Assignments	Exp. mass (Da)	Theo. mass (Da)	Error (ppm)
1	$[Pt(dien)-2H]^{+\cdot}$	296.060078	296.060123	-0.15
2	$[Pt(dien)]^{+\cdot}$	298.075730	298.075773	-0.14
3	$[Pt(dien)+H\cdot]^{+}$	299.083250	299.083598	-1.16
4	$[Pt(dien)(CO)-H\cdot]^{+}$	325.062743	325.062325	1.29
5	$[Pt(dien)(CH_3S)-H\cdot]^{+}$	344.063334	344.063506	-0.50
6	$Pt(dien)(CH_3S)^{+\cdot}$	345.071224	345.071331	-0.03
7	c_3	374.167161	374.167025	0.36
8	b_4	470.224588	470.22454	0.10
9	c_4	487.251057	487.251089	-0.07
10	b_5	571.272025	571.272218	-0.34
11	c_5	588.298704	588.298767	-0.11
12	$z_{12}+2Pt(dien)^{3+\cdot}$	689.927521	689.927823	-0.44
13	b_6	700.314677	700.314811	-0.19
14	$z_{20}+2Pt(dien)^{4+\cdot}$	717.530829	717.531519	-0.96
15	c_6	717.341075	717.34136	-0.40
16	$?^{3+}$	727.286910		
17	$z_{21}+2Pt(dien)^{4+\cdot}$	735.290662	735.290806	-0.20
18	$z_{48}+4Pt(dien)^{9+\cdot}$	741.206532	741.206553	-0.03
19	$z_{31}+3Pt(dien)^{6+\cdot}$	747.458561	747.459470	-1.22
20	$z_{14}+2Pt(dien)^{3+\cdot}$	765.636456	765.636859	-0.53
21	$z_{22}+2Pt(dien)^{4+\cdot}$	767.550330	767.551468	-1.48
22	$z_{57}+4Pt(dien)^{10+\cdot}$	769.032138	769.031759	0.49
23	$z_{51}+4Pt(dien)^{9+\cdot}$	779.225319	779.225741	-0.54
24	c_{13}^{2+}	781.888045	781.88847	-0.55
25	$z_{15}+2Pt(dien)^{3+\cdot}$	784.643353	784.644022	-0.85
26	$z_{65}+4Pt(dien)^{11+\cdot}$	790.259691	790.261517	-2.31
27	$z_{52}+4Pt(dien)^{9+\cdot}$	791.897174	791.897178	-0.01
28	$z_{59}+4Pt(dien)^{10+\cdot}$	794.548943	794.548718	0.28
29	$z_{66}+4Pt(dien)^{11+\cdot}$	801.990407	801.992662	-2.81
30	$?^{9+}$	808.900450		
31	$z_{60}+4Pt(dien)^{10+\cdot}$	809.355453	809.355804	-0.43
32	$z_{54}+4Pt(dien)^{9+\cdot}$	811.013047	811.013315	-0.33
33	$z_{46}+4Pt(dien)^{8+\cdot}$	815.097114	815.097816	-0.86
34	$?^{3+}$	816.314700		
35	$z_{16}+2Pt(dien)^{3+\cdot}$	822.985996	822.986351	-0.43
36	$z_{55}+4Pt(dien)^{9+\cdot}$	825.357039	825.357484	-0.54
37	$?^{5+}$	825.328810		

38	z_{69}+4Pt(dien)$^{11+\cdot}$	832.091926	832.092520	-0.71
39	z_{35}+3Pt(dien)$^{6+\cdot}$	833.343887	833.346139	-2.70
40	z_{48}+4Pt(dien)$^{8+\cdot}$	834.856114	834.856462	-0.42
41	z_{56}+4Pt(dien)$^{9+\cdot}$	838.025275	838.026872	-1.91
42	z_{17}+2Pt(dien)$^{3+\cdot}$	841.992622	841.993513	-1.06
43	c_7	846.383316	846.383953	-0.75
44	z_{29}+3Pt(dien)$^{5+\cdot}$	848.135954	848.136442	-0.58
45	z_{57}+4Pt(dien)$^{9+\cdot}$	854.367353	854.3678131	-0.54
46	z_{65}+4Pt(dien)$^{10+\cdot}$	869.185226	869.186941	-1.97
47	z_{30}+3Pt(dien)$^{5+\cdot}$	873.943514	873.944980	-1.68
48	z_{51}+4Pt(dien)$^{8+\cdot}$	876.502434	876.503049	-0.70
49	z_{18}+2Pt(dien)$^{3+\cdot}$	880.335063	880.3358423	-0.89
50	z_{66}+4Pt(dien)$^{10+\cdot}$	882.090974	882.091200	-0.26
51	c_{15}^{2+}	881.928653	881.928331	0.37
52	c_{23}^{3+}	891.429015	891.429057	-0.05
53	z_{31}+3Pt(dien)$^{5+\cdot}$	896.949295	896.950374	-1.20
54	z_{68}+4Pt(dien)$^{10+\cdot}$	903.597184	903.598053	-0.96
55	[CaM+5Pt(dien)-H2O+10H]$^{20+}$	913.665494	913.665499	-0.01
56	[CaM+5Pt(dien)+10H]$^{20+}$	914.566326	914.566027	0.33
57	z_{19}+2Pt(dien)$^{3+\cdot}$	918.030147	918.030603	-0.50
58	z_{55}+4Pt(dien)$^{8+\cdot}$	928.526216	928.526327	-0.12
59	z_{65}+3Pt(dien)$^{9+\cdot}$	932.64424	932.644262	-0.02
60	z_{33}+3Pt(dien)$^{5+\cdot}$	939.775017	939.776735	-1.83
61	?$^{5+}$	942.579640		
62	?$^{9+}$	946.761680		
63	c_{25}^{3+}	948.777807	948.778526	-0.76
64	z_{48}+4Pt(dien)$^{7+\cdot}$	953.978085	953.977774	0.33
65	c_{16}^{2+}	955.461835	955.462538	-0.74
66	z_{20}+2Pt(dien)$^{3+\cdot}$	956.372235	956.372933	-0.73
67	[CaM+5Pt(dien)-CH_3S-H2O+10H] $^{19+\cdot}$	959.278132	959.280302	-2.26
68	[CaM+5Pt(dien)-CH_3S+10H]$^{19+\cdot}$	960.226745	960.228227	-1.54
69	[CaM+5Pt(dien)-H_2O+10H]$^{19+\cdot}$	961.753196	961.753735	-0.56
70	[CaM+5Pt(dien)+10H]$^{19+\cdot}$	962.700602	962.701660	-1.10
71	z_{65}+4Pt(dien)$^{9+\cdot}$	965.539523	965.539553	-0.03
72	?$^{9+}$	970.988670		
73	z_{58}+4Pt(dien)$^{8+\cdot}$	973.545398	973.546739	-1.38
74	?$^{7+}$	975.140160		
75	z_{11}+2Pt(dien)$^{2+\cdot}$	976.866016	976.865640	0.38
76	z_{21}+2Pt(dien)$^{3+\cdot}$	980.052277	980.051983	0.30
77	c_{26}^{3+}	982.460682	982.461086	-0.41
78	c_{17}^{2+}	998.978327	998.978552	-0.23
79	[CaM+4Pt(dien)-CH_3S-H_2O+10H]$^{18+}$	995.958021	995.957715	0.31

80	[CaM+4Pt(dien)-CH_3S+10H]$^{18+}$	996.958369	996.958303	0.07
81	[CaM+4Pt(dien)-H_2O+10H]$^{18+}$	998.624525	998.624222	0.30
82	[CaM+4Pt(dien)+10H]$^{18+}$	999.624754	999.624809	-0.06
83	[CaM+5Pt(dien)-CH_3S-H_2O+10H]$^{18+\cdot\cdot}$	1012.517103	1012.517504	-0.40
84	[CaM+5Pt(dien)-CH_3S+10H]$^{18+\cdot\cdot}$	1013.571719	1013.573751	-2.00
85	[CaM+5Pt(dien)-H_2O+10H]$^{18+\cdot\cdot}$	1015.182782	1015.184009	-1.21
86	[CaM+5Pt(dien)+10H]$^{18+\cdot\cdot}$	1016.183387	1016.184596	-1.19
87	[CaM+4Pt(dien)-CH_3S-H_2O+10H]$^{17+\cdot}$	1054.601115	1054.602528	-1.34
88	[CaM+4Pt(dien)-CH_3S+10H]$^{17+\cdot}$	1055.602001	1055.603038	-0.98
89	[CaM+4Pt(dien)-H2O+10H]$^{17+\cdot}$	1057.365952	1057.366953	-0.95
90	[CaM+4Pt(dien)+10H]$^{17+\cdot}$	1058.425060	1058.426398	-1.26
91	c_{117}+2Pt(dien)$^{13+}$	1061.812279	1061.812756	-0.45
92	c_{38}^{4+}	1066.526508	1066.526542	-0.03
93	b_9	1070.499605	1070.500046	-0.41
94	[CaM+5Pt(dien)-CH_3S-H_2O+10H]$^{17+\cdots}$	1072.135116	1072.136355	-1.16
95	[CaM+5Pt(dien)-CH_3S+10H]$^{17+\cdots}$	1073.192642	1073.195801	-2.94
96	[CaM+5Pt(dien)-H_2O+10H]$^{17+\cdots}$	1074.959298	1074.959711	-0.38
97	c_{93}+Pt(dien)$^{10+}$	1086.310822	1086.311212	-0.36
98	c_{49}^{5+}	1089.536692	1089.537162	-0.43
99	z_{30}+3Pt(dien)$^{4+\cdot}$	1092.179897	1092.179818	0.07
100	c_{94}+Pt(dien)$^{10+}$	1099.119676	1099.120709	-0.94
101	c_{40}^{4+}	1108.802188	1108.802070	0.11
102	c_{86}+Pt(dien)$^{9+}$	1110.852945	1110.854621	-1.51
103	c_{77}+Pt(dien)$^{8+}$	1115.153248	1115.154333	-0.97
104	c_{96}+Pt(dien)$^{10+}$	1116.324985	1116.325551	-0.51
105	[CaM+4Pt(dien)-CH_3S-H_2O+10H]$^{16+\cdot\cdot}$	1120.513669	1120.515187	-1.35
106	[CaM+4Pt(dien)-CH_3S+10H]$^{16+\cdot\cdot}$	1121.575870	1121.578228	-2.10
107	[CaM+4Pt(dien)-H2O+10H]$^{16+\cdot\cdot}$	1123.389994	1123.389771	0.20
108	[CaM+4Pt(dien)+10H]$^{16+\cdot\cdot}$	1124.515018	1124.515431	-0.37
109	c_{97}+Pt(dien)$^{10+}$	1127.727591	1127.729845	-2.00
110	c_{19}^{2+}	1129.053648	1129.054791	-1.01
111	c_{78}+Pt(dien)$^{8+}$	1129.408078	1129.407317	0.67
112	c_{30}^{3+}	1130.218559	1130.219214	-0.58
113	c_{41}^{4+}	1140.816085	1140.816715	-0.55
114	c_{79}+Pt(dien)$^{8+}$	1142.161889	1142.163663	-1.55
115	c_{80}+Pt(dien)$^{8+}$	1156.540502	1156.542032	-1.32
116	c_{10}	1158.563786	1158.563708	0.07
117	c_{100}+Pt(dien)$^{10+}$	1161.046132	1161.046734	-0.52
118	c_{81}+Pt(dien)$^{8+}$	1167.420970	1167.421036	-0.06
119	c_{101}+Pt(dien)$^{10+}$	1169.747148	1169.749938	-2.39
120	c_{31}^{3+}	1173.233902	1173.233411	0.42
121	c_{82}+Pt(dien)$^{8+}$	1183.550084	1183.551362	-1.08

122	c_{53}^{5+}	1184.176463	1184.176056	0.34
123	c_{20}^{2+}	1186.568598	1186.568263	0.28
124	$[CaM+4Pt(dien)-CH_3S-H_2O+10H]^{15+\cdots}$	1195.214402	1195.216345	-1.63
125	$[CaM+4Pt(dien)-CH_3S+10H]^{15+\cdots}$	1196.415953	1196.417050	-0.92
126	$c_{83}+Pt(dien)^{8+}$	1199.680959	1199.681688	-0.61
127	$c_{93}+Pt(dien)^{9+}$	1206.899263	1206.900538	-1.06
128	c_{32}^{3+}	1210.927075	1210.928099	-0.85
129	c_{44}^{4+}	1218.851827	1218.852557	-0.60
130	$c_{94}+Pt(dien)^{9+}$	1221.132951	1221.133313	-0.30
131	$c_{85}+Pt(dien)^{8+}$	1230.073049	1230.072898	0.12
132	c_{33}^{3+}	1229.934715	1229.935254	-0.44
133	$c_{96}+Pt(dien)^{9+}$	1240.24939	1240.249804	-0.33
134	$c_{86}+Pt(dien)^{8+}$	1249.459456	1249.460165	-0.57
135	c_{21}^{2+}	1250.615729	1250.615744	-0.01
136	c_{45}^{4+}	1251.865782	1251.865714	0.05
137	c_{56}^{4+}	1253.204701	1253.204948	-0.20
138	$?^{16+}$	1255.796560		
139	$?^{4+}$	1257.869450		
140	c_{34}^{3+}	1263.617647	1263.617813	-0.13
141	$c_{87}+Pt(dien)^{8+}$	1265.590347	1265.590490	-0.11
142	$?^{5+}$	1267.211670		
143	c_{46}^{4+}	1268.871561	1268.872484	-0.73
144	$c_{77}+Pt(dien)^{7+}$	1274.173891	1274.174901	-0.79
145	$?^{9+}$	1284.938490		
146	c_{11}	1287.601493	1287.606302	-3.73
147	$c_{100}+Pt(dien)^{9+}$	1289.940532	1289.940007	0.41
148	$c_{55}+Pt(dien)^{5+}$	1290.015016	1290.012598	1.87
149	$c_{89}+Pt(dien)^{8+}$	1292.853160	1292.853686	-0.41
150	c_{35}^{3+}	1296.640610	1296.640618	-0.01
151	$?^{7+}$	1298.468630		
152	c_{47}^{4+}	1301.133767	1301.133132	0.49
153	c_{59}^{5+}	1301.419784	1301.42075	-0.74
154	$c_{79}+Pt(dien)^{7+}$	1305.184872	1305.186004	-0.87
155	c_{22}^{2+}	1308.128919	1308.129216	-0.23
156	$c_{90}+Pt(dien)^{8+}$	1312.618001	1312.61709	0.69
157	$?^{7+}$	1314.899920		
158	$c_{80}+Pt(dien)^{7+}$	1321.618669	1321.618426	0.18
159	$c_{81}+Pt(dien)^{7+}$	1334.051096	1334.051574	-0.36
160	c_{23}^{2+}	1336.639751	1336.639947	-0.15
161	c_{36}^{3+}	1340.319966	1340.320779	-0.61
162	$c_{92}+Pt(dien)^{8+}$	1343.258450	1343.258826	-0.28
163	$?^{7+}$	1345.910930		

164	c_{82}+Pt(dien)$^{7+}$	1352.486454	1352.486231	0.16
165	c_{49}^{4+}	1361.669998	1361.669633	0.27
166	?$^{7+}$	1364.348310		
167	c_{83}+Pt(dien)$^{7+}$	1370.920160	1370.920890	-0.53
168	c_{94}+Pt(dien)$^{8+}$	1373.647589	1373.649068	-1.08
169	c_{63}^{5+}	1378.456444	1378.459977	-2.56
170	?$^{7+}$	1382.925310		
171	c_{50}^{4+}	1390.677257	1390.677203	0.04
172	c_{37}^{3+}	1392.353599	1392.354483	-0.63
173	c_{24}^{2+}	1394.153161	1394.153419	-0.19
174	c_{96}+Pt(dien)$^{8+}$	1394.281455	1394.280491	0.69
175	?$^{2+}$	1401.159230		
176	c_{64}^{5+}	1401.867273	1401.866672	0.43
177	c_{85}+Pt(dien)$^{7+}$	1405.509923	1405.510416	-0.35
178	c_{25}-H_2O^{2+}	1414.160925	1414.160574	0.25
179	?$^{1+}$	1417.646743		
180	c_{38}^{3+}	1421.698617	1421.699630	-0.71
181	c_{25}^{2+}	1422.663974	1422.664151	-0.12
182	c_{86}+Pt(dien)$^{7+}$	1427.667162	1427.667273	-0.08
183	?$^{12+}$	1442.175260		
184	c_{87}+Pt(dien)$^{7+}$	1446.244955	1446.245235	-0.19
185	c_{52}^{4+}	1451.456024	1451.457506	-1.02
186	c_{39}^{3+}	1459.395113	1459.394030	0.74
187	?$^{3+}$	1471.608450		
188	c_{26}^{2+}	1473.187500	1473.187990	-0.33
189	c_{89}+Pt(dien)$^{7+}$	1477.549534	1477.546458	2.08
190	c_{40}^{3+}	1478.401710	1478.401457	0.17
191	c_{53}^{4+}	1479.967559	1479.968251	-0.47
192	?$^{3+}$	1493.915950		
193	?$^{3+}$	1506.415980		
194	?$^{2+}$	1507.705720		
195	c_{41}^{3+}	1520.753519	1520.753194	0.21
196	c_{27}^{2+}	1529.730215	1529.730022	0.13
197	c_{92}+Pt(dien)$^{7+}$	1534.05336		
198	c_{55}^{4+}	1536.996711	1536.996003	0.46
199	?$^{2+}$	1549.242880		
200	c_{13}	1562.770080	1562.769676	0.26
201	c_{56}^{4+}	1566.253023	1566.254366	-0.85
202	?$^{6+}$	1570.072130		
203	c_{82}+Pt(dien)$^{6+}$	1577.565060	1577.565535	-0.30
204	c_{28}^{2+}	1580.253955	1580.253861	0.06
205	c_{57}^{4+}	1583.510552	1583.512017	-0.93

206	$?^{6+}$	1591.735880		
207	c_{83}+Pt(dien)$^{6+}$	1598.238236	1598.239825	-0.99
208	$?^{2+}$	1599.765740		
209	$?^{2+}$	1608.769190		
210	c_{58}^{4+}	1612.266469	1612.268753	-1.42
211	c_{44}^{3+}	1625.135842	1625.135439	0.25
212	c_{59}^{4+}	1626.776576	1626.774944	1.00
212	c_{29}^{2+}	1630.778168	1630.777701	0.29
213	c_{45}^{3+}	1668.150143	1668.149636	0.30
214	c_{61}^{4+}	1669.793779	1669.791846	1.16
215	$?^{2+}$	1672.818790		
216	$?^{3+}$	1677.161210		
217	c_{14}	1691.812455	1691.812272	0.11
218	c_{30}^{2+}	1694.825403	1694.825182	0.13
219	c_{31}^{2+}	1759.347762	1759.346479	0.73
220	c_{15}	1762.850828	1762.849385	0.82
221	c_{32}^{2+}	1815.893164	1815.888511	2.56
222	c_{33}^{2+}	1844.397857	1844.399242	-0.75
223	$?^{1+}$	1865.904520		
224	$?^{2+}$	1873.420190		
225	c_{34}^{2+}	1894.924541	1894.923082	0.77
226	c_{16}	1909.918207	1909.917780	0.22
227	c_{17}	1996.950698	1996.949828	0.44
228	$?^{2+}$	2010.477840		
229	c_{18}	2110.036609	2110.033892	1.29
230	c_{19}	2257.105508	2257.102306	1.42
231	$?^{1+}$	2281.622640		
232	c_{20}	2372.127611	2372.129249	-0.69
233	c_{21}	2500.226977	2500.224212	1.11
	Mean absolute deviation (ppm)			0.60
	Standard deviation (ppm)			0.88

Appendix C (Supporting information for Chapter 4)

Table C.1 Distance constraints between sulfur atoms of Met residues obtained from NMR structures of CaM

Residue	Residue	d(1—2) for 30 conformations (Å)																												
1	2	C1	C2	C3	C4	C5	C6	C7	C8	C9	C10	C11	C12	C13	C14	C15	C16	C17	C18	C19	C20	C21	C22	C23	C24	C25	C26	C27	C28	C29	C30
51	71	7.1	5.0	5.3	2.9	5.5	5.8	4.9	5.9	5.5	5.7	4.5	5.3	4.4	6.3	2.9	4.8	3.0	4.3	4.0	4.8	4.5	6.0	4.0	4.6	4.3	4.4	3.2	5.6	5.4	3.7
51	72	8.7	5.5	6.8	7.5	5.8	5.7	8.4	7.3	8.2	8.6	8.0	6.6	8.3	6.5	8.5	5.7	7.2	8.4	7.1	7.2	7.7	6.4	7.9	8.6	5.8	7.2	6.9	8.3	7.5	6.4
109	124	8.4	8.2	8.3	8.8	7.2	6.8	8.6	8.8	8.2	7.4	8.9	7.5	8.2	8.0	7.8	8.4	8.3	8.8	8.1	9.0	8.2	8.2	9.2	8.0	9.1	8.6	7.6	9.2	6.8	8.9
109	144	11.3	10.5	10.5	12.4	11.2	11.4	12.0	12.2	11.2	11.4	12.1	11.3	12.1	11.8	11.7	11.8	12.1	12.4	9.7	12.2	9.3	11.7	11.4	9.9	12.7	11.7	12.2	11.8	10.5	10.9
144	145	7.1	6.7	5.6	9.6	9.1	7.8	7.9	8.3	7.4	8.1	8.1	9.0	8.3	7.3	9.3	7.7	7.2	8.1	5.5	9.4	5.2	8.9	9.4	7.4	9.9	8.1	7.9	8.1	9.0	6.4

Table C.2 Predicted cross-linking sites as obtained from rigidity and flexibility analysis at energy cutoffs (A) -2 kcal/mol and (B) -1 kcal/mol. The first two columns give the potential cross-linking Met residues, the third shows the sulfur-surfur distance d(1—2) obtained from the crystal structure of Ca_4–CaM (1CCL). The remaining columns show the modes in both +Ca and –Ca structures that can bring Met residues close to within 5 Å, and the corresponding d(1—2) distances, and the MS results wherever available. (kcal/mol is used as a default unit in FIRST software, which can be converted to SI unit according to 1 kcal/mol=4.2 kJ/mol).

(A)

Rigidity cutoff -2 kcal/mol.			+Ca structure (1CLL)		-Ca structure (calcium-deleted structure of 1CLL)	
Residue 1	Residue 2	d(1—2), (Å) native	Mode of close	d(1—2), (Å) simulated	Mode of close	d(1—2), (Å) simulated
36	71	10.9			m_{13}+	4.9
36	72	11.6			m_{13}+	4.2
51	71	9.9				
51	72	12.5				
109	124	5.2	Many modes	<5	Many modes	<5
109	144	12.3	m_{14}-	4.4	m_{14}-	4.8
109	145	10.3				
124	144	9.6	m_{18}+	4.5	m_{14}+	4.6
124	145	11.0				

(B)

Rigidity cutoff -1 kcal/mol.			+Ca structure (1CLL)		-Ca structure (calcium-deleted structure of 1CLL)	
Residue 1	Residue 2	d(1—2), (Å) native	Mode of close	d(1—2), (Å) simulated	Mode of close	d(1—2), (Å) simulated
36	71	10.9				
36	72	11.6				
51	71	9.9				
51	72	12.5				
109	124	5.2	Many modes	<5	Many modes	<5
109	144	12.3				
109	145	10.3				
124	144	9.6			m^{+}_{18}	4.7
124	145	11.0				

Appendix D (Supporting information for Chapter 5)

Figure D.1 ECD spectra of peptide-cisplatin adduct at different pH values. (a) ECD spectrum of $[Sp_{(2\text{-}11)}+Pt(NH_3)+H]^{3+}$ ions at pH 3; (b) ECD spectrum of $[Sp_{(2\text{-}11)}+Pt(NH_3)+H]^{3+}$ ions at pH 7; (c) ECD spectrum of $[Sp_{(2\text{-}11)}+Pt(NH_3)+H]^{3+}$ ions at pH 10.

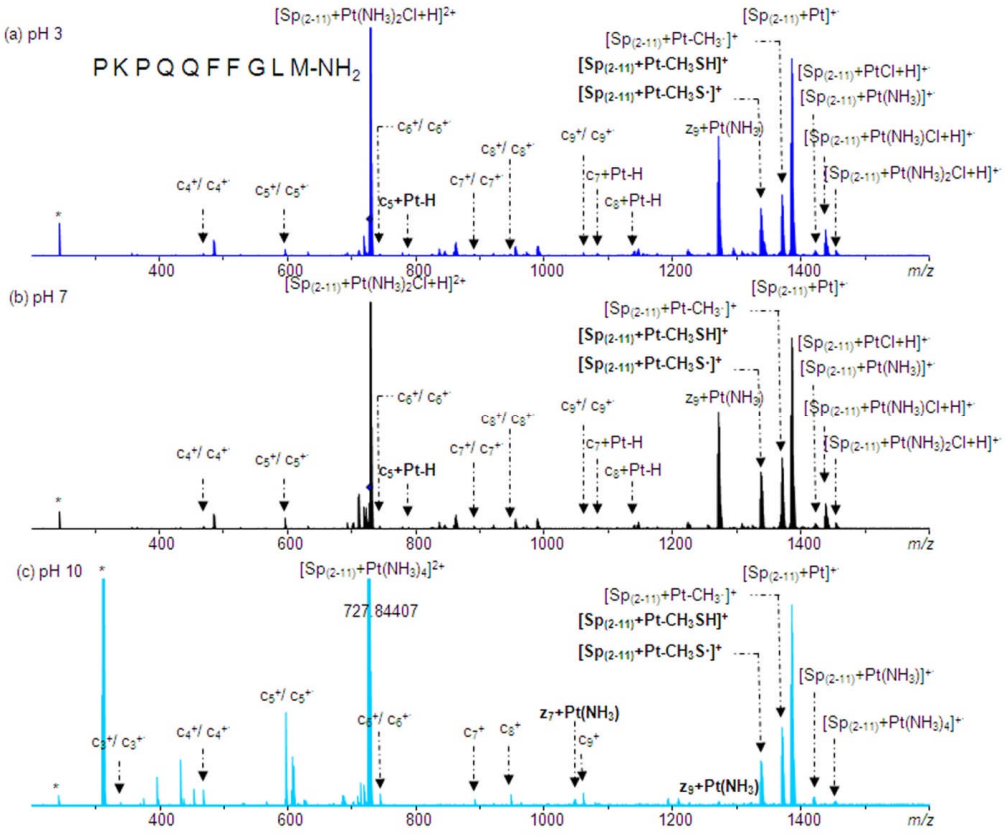

Figure D.2 ECD spectra of peptide-cisplatin adduct at different pH values. (a) ECD spectrum of $[Sp+Pt(NH_3)+H]^{3+}$ ions at pH 3; (b) ECD spectrum of $[Sp+Pt(NH_3)+H]^{3+}$ ions at pH 7.

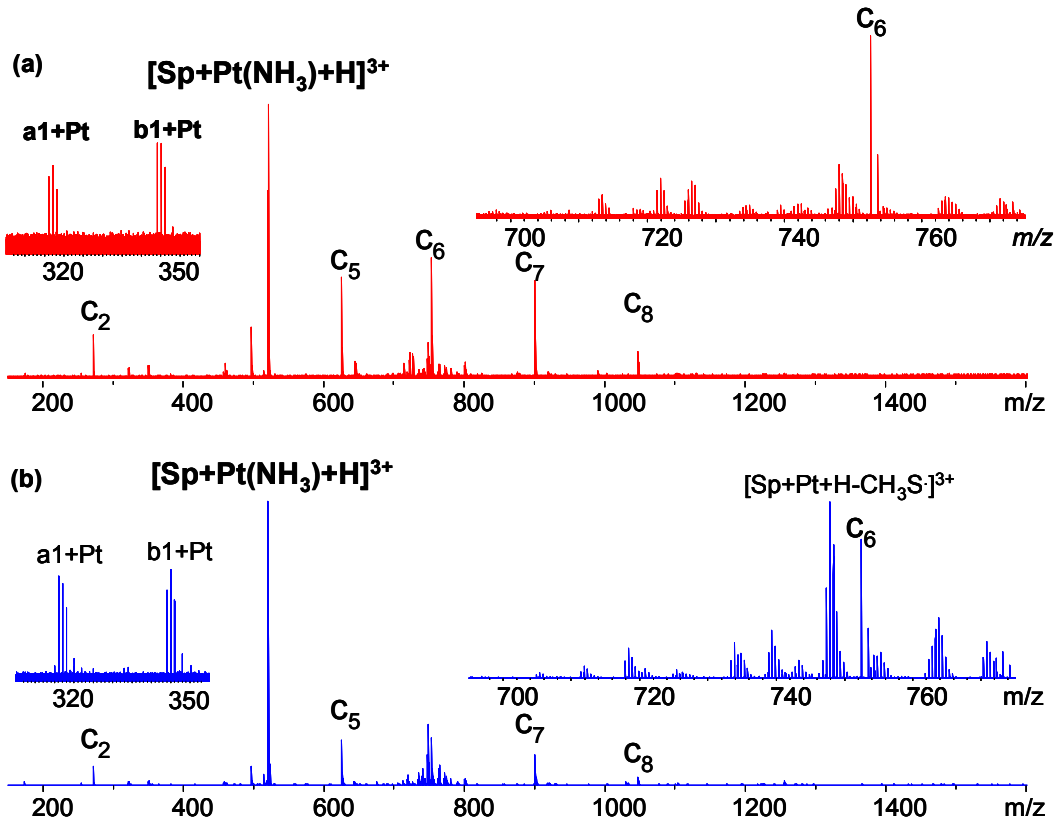

Figure D.3 (a) Full MS spectra of insulin-cisplatin adducts with in source dissociation voltage of 70 V, (b) Full MS spectra of the insulin-cisplatin reaction sample, and (c) CAD spectra of the [insulin + $Pt(NH_3)_2$ + insulin + 7H]$^{9+}$ ion at *m/z* 1300. The insets of Figure a and b show that the intensity of the [insulin + $Pt(NH_3)_2$ + insulin + 7H]$^{9+}$ species is the same with or without ion source dissociation.

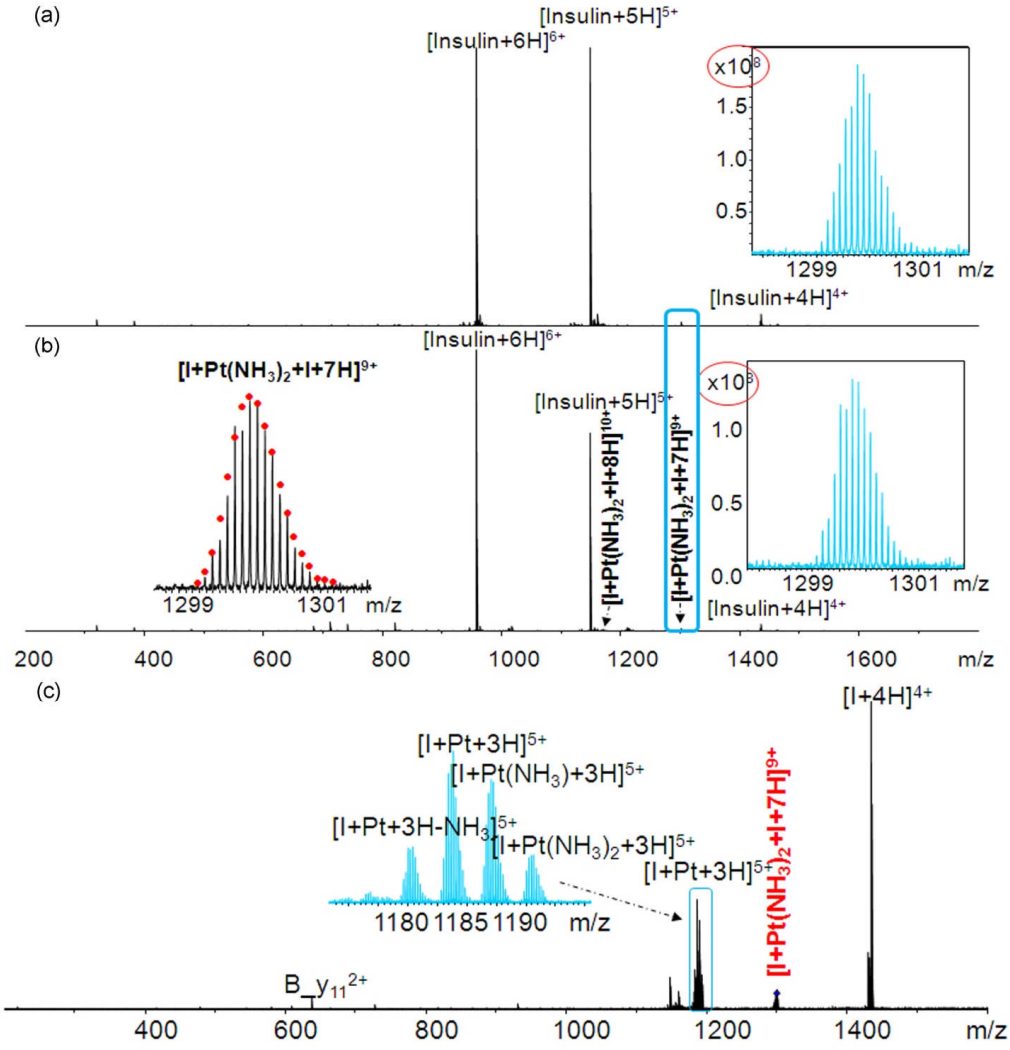

Appendix E (Supporting information for Chapter 6)

Table E.1 Complete peak list table for the ECD spectrum of $[P1+P1+3H]^{3+}$ at *m/z* 841.42281. The spectrum was internal calibrated by ions (c_5, $[P1+P1+3H]^{3+}$, $(z_6+P1)^{+\cdot}$, $(z_7+P1)^{+\cdot}$, and $(z_8+P1)^{+\cdot}$) which are not involved in cleaving of the disulfide bond. For ions at *m/z* 1228 to 1232 Da region, the isotope peaks of each ion were listed as highlighted in grey. For rest of the peaks, the mass errors were calculated based on the *m/z* values of the monoisotopic peak ions unless stated otherwise.

Assignments	**Isotopic number**	**Experimental *m/z* (Da)**	**Theoretical *m/z* (Da)**	**Mass error (ppm)**
$z_4^{+\cdot}$		506.27274	506.27350	-1.50
z_4^{+}		507.28114	507.28133	-0.37
–		655.37117		
$c_5^{+\cdot}$		583.32591	583.32589	0.03
c_5^{+}		584.33371	584.33371	0.00
$[P1-SH]^{2+}$		614.82863	614.82898	-0.57
$P1(S)^{2+\cdot}$		630.81490	630.81502	-0.19
$P1(SH)^{2+}$		631.31801	631.31893	-1.46
$P1(SSH)^{2+}$	A+1	647.80783	647.80888	-1.62
$[P1+P1+3H]^{3+}$		841.42281	841.42282	-0.01
$c_8(S)^{+}$		856.44147	856.44060	1.02
$c_8(SH)^{+}$		857.44943	857.44842	1.18
$z_8(S)^{+}$		929.45605	929.45495	1.18
–		952.50459		
$c_9(S)^{+\cdot}$		984.47664	984.47537	1.29
$c_9(S)^{+}$		985.48445	985.48319	1.28
$z_9(S)^{+}$		986.47762	986.47641	1.23
$c_9(SH)^{+}$		986.49229	986.49102	1.29
–		1003.50478		
–		1017.45653		
$(c_8+P1)^{2+}$		1058.53312	1058.53168	1.36
$(z_8+P1)^{2+\cdot}$		1095.54424	1095.54277	1.34
–		1101.5517		
–		1117.51829		

$(c_9+P1-H)^{2+}$		1123.05474	1123.05298	1.57
$(c_9+P1)^{2+}$		1123.5558	1123.55689	-0.97
$(z_9+P1)^{2+\cdot}$	A	1124.05715	1124.05405	3.25
$(z_9+P1)^{2+\cdot}$	A+1	1124.55606	1124.55520	1.00
2+		1132.0649		
2+		1175.08563		
$(z_{10}+P1)^{2+\cdot}$		1189.57539	1189.57374	1.38
$(c_{10}+P1)^{2+}$		1197.08932	1197.09110	-1.49
1+	A	1228.58695		
$[P1-SH+H]^{+}$	A	1228.65234	1228.65069	1.34
1+	A+1	1229.59002		
$[P1-SH+H]^{+}$	A+1	1229.65528	1229.65406	0.99
$[P1-S+H]^{+\cdot}$	A	1229.66047	1229.65851	1.59
1+	A+2	1230.59302		
$[P1-SH+H]^{+}$	A+2	1230.65809	1230.65738	0.58
$[P1-S+H]^{+\cdot}$	A+1	1230.66275	1230.66189	0.70
$[P1-S+2H]^{+}$	A	1230.66772	1230.66634	1.12
$[P1-S+H]^{+\cdot}$	A+2	1231.664	1231.66520	-0.97
$[P1-S+2H]^{+}$	A+1	1231.6714	1231.66971	1.37
$[P1-S+2H]^{+}$	A+2	1232.67502	1232.67303	1.61
1+		1233.63717		
1+		1234.64577		
2+		1239.12829		
2+		1239.13407		
1+		1245.61336		
$P1(S\cdot)^{+\cdot}$		1261.63058	1261.63059	-0.01
$[P1+P1+3H]^{2+\cdot}$		1262.13359	1262.13450	-0.72
$P1(SH)^{+}$		1262.63589	1262.63841	-2.00
1+		1276.57802		
1+		1277.58589		
$[P1+S\cdot+H]^{+}$		1293.60407	1293.60266	1.09
$(z_2+P1-H)^{+}$		1537.77905	1537.77798	0.70
$(z_2+P1)^{+\cdot}$		1538.78743	1538.78580	1.06
$(z_3+P1)^{+\cdot}$-H		1666.82204	1666.82057	0.88
$(z_3+P1)^{+\cdot}$		1667.82629	1667.82840	-1.27
$(z_4+P1-H)^{+\cdot}$		1765.89030	1765.88899	0.74
$(z_4+P1)^{+\cdot}$	A	1766.89341	1766.89681	-1.92
$(z_4+P1)^{+\cdot}$	A+1	1767.90079	1767.90018	0.35
$(z_5+P1)^{+\cdot}$		1868.89818	1868.89817	0.01
$(z_6+P1)^{+\cdot}$		1939.93591	1939.93528	0.32
$(c_7+P1-H)^{+}$		2016.98593	2016.98767	-0.86

$(z_7+P1)^{+\cdot}$		2076.99501	2076.99420	0.39
$(z_7+P1)^{+}$		2077.99789	2078.00202	-1.99
$(c_8+P1-H)^{+}$		2116.05207	2116.055608	-1.67
$(c_8+P1)^{+}$		2117.06156	2117.06391	-1.11
$(z_8+P1)^{+\cdot}$		2190.07844	2190.07826	0.08
$(z_8+P1)^{+}$	A	2191.08169	2191.08608	-2.00
$(z_8+P1)^{+}$	A+1	2192.08789	2192.08949	-0.73
$(c_9+P1)^{+}$		2247.11096	2247.10991	0.47
Mean				0.77

Table E.2 Fragment ions assignments and mass error of the ECD spectrum of $[P1+P2+3H]^{3+}$ at *m/z* 857.73795.

Assignments	Experimental *m/z* (Da)	Theoretical *m/z* (Da)	Mass error (ppm)
$z_4^{+\cdot}$ P1/P2	506.27328	506.27350	-0.43
z_4^{+} P1/P2	507.28126	507.28133	-0.14
$c_5^{+\cdot}$	583.32575	583.32589	-0.24
c_5^{+} P1	584.33368	584.33371	-0.05
$[P2\text{-}SeH]^{2+}/[P1\text{-}SH]^{2+}$	614.82881	614.82898	-0.28
2+	622.30167		
2+	622.82643		
$[P1(S)\text{-}H+2H]^{2+\cdot}$	630.81509	630.81502	0.11
$[P1(S.)+2H]^{2+}$	631.32076	631.31893	2.90
2+	631.32816		
$[P1(SH)+2H]^{2+}$	631.82288	631.82284	0.06
2+	639.82041		
2+	647.81791		
$[P2(Se.)\text{-}H+2H]^{2+}$	654.78869	654.78723	2.23
$[P2(Se.)+2H]^{2+}$	655.29051	655.29114	-0.96
c_6 P1/P2	655.37088	655.37083	0.08
2+	659.78280		
$[P1+Se.+2H]^{2+}$	671.27698	671.27715	-0.25
1+	721.39214		
2+	723.82066	723.82060	0.08
2+	731.31445		
2+	740.31966		
c_7(S.) P1	757.37265	757.37219	0.61
c_7(SH) P1	758.37983	758.38001	-0.24
$^{2+}$	764.77607		
1+	805.31698		
1+	840.35173		
3+	857.73795		
c_8(SH) P1	857.44798	857.44842	-0.51
1+	880.33451		
1+	886.34236		
c_8(Se.) P2	904.38528	904.38500	0.31
1+	929.45523		
1+	946.47409		
1+	977.40001		
1+	985.48352		

1+	986.47663		
1+	986.49151		
1+	1003.50407		
c_9(Se.) P2	1051.45381	1051.45342	0.37
$(P1+c_8)^{2+}$ / $(P2+c_8)^{2+}$	1083.00912	1083.00779	1.23
1+	1088.53841		
z_9(Se.) P2	1108.44016	1108.43984	0.29
1+	1117.51737		
2+	1126.02499		
2+	1135.03661		
$(P2+c_9)^{2+}$	1148.03166	1148.03085	0.71
$(P2+z_9)^{2+}$	1148.52901	1148.52746	1.35
$(P1+c_9)^{2+}$	1157.04471	1157.04377	0.81
z_{10}(Se.) P2	1165.46149	1165.46131	0.15
$(P1+z_9)^{2+}$	1185.53608	1185.53698	-0.76
2+	1199.05665		
1+	1212.61945		
1+	1216.63224		
$(P1+z_{10})^{2+}$/ $(P2+z_{10})^{2+}$	1214.04864	1214.04771	0.77
$(P1+c_{10})^{2+}$/ $(P2+c_{10})^{2+}$	1221.56444	1221.56506	-0.51
1+	1228.58555		
$[P1\text{-}SH+H]^{+}$/	1228.65141	1228.65069	0.59
$[P1\text{-}S+H]^{+\cdot}$/ $[P2\text{-}Se+H]^{+\cdot}$	1229.66063	1229.65851	1.72
$[P1\text{-}S+2H]^{+}$ /	1230.66660	1230.66634	0.21
1+	1234.64408		
1+	1245.61193		
$P1(S\cdot)^{+\cdot}$	1261.63071	1261.63059	0.10
$P1(SH)^{+}$	1262.63825	1262.63841	-0.13
1+	1278.63387		
$[P1+P2+3H]^{2+\cdot}$	1286.60526	1286.60847	-2.49
$P2(Se.)^{+}$	1309.57402	1309.57500	-0.75
1+	1318.53889		
$(P2+S.)^{+}$	1341.54684	1341.54702	-0.13
1+	1446.63403		
$P1+z_2$	1520.75964	1520.75998	-0.22
$P2+c_2$	1585.73537	1585.73696	-1.00
$P2+z_3$	1586.72969	1586.73023	-0.34
$P1+z_3$	1667.82780	1667.82840	-0.36
?	1715.77067		
$P1+z_4$	1766.89642	1766.89681	-0.22
$P1+z_5$	1917.84667	1917.84599	0.35
$P1+z_6$	1987.87874	1987.87969	-0.48

P1+z_7/ P2+z_7	2124.93666	2124.93864	-0.93
P1+z_8/ P2+z_8	2239.02012	2239.02617	-2.70
$[P2+P1-HSH]^{+\cdot}$	2539.22941	2539.22975	-0.13

Table E.3 Fragment ions assignments and mass error of the ECD spectrum of $[P2+P2+3H]^{3+}$ at *m/z* 873.38609.

Assignments	Experimental *m/z* (Da)	Theoretical *m/z* (Da)	Mass error (ppm)
c_5^+	584.33368	584.33371	-0.05
2+	597.86076		
$[P2\text{-}SeH]^{2+}$	614.82874	614.82898	-0.39
2+	622.82653		
$P2(Se.)^{2+}$	655.29051	655.29114	-0.96
c_6	655.37088	655.37083	0.08
2+	723.81819	723.82060	-3.33
1+	794.43050		
c_7 (Se.)	805.31698	805.31658	0.50
c_8(Se.)	904.38500	904.38500	0.00
z8(Se.)	977.39910	977.39941	-0.32
c_9(Se.)	1051.45345	1051.45342	0.03
z_9(Se.)	1108.44002	1108.43984	0.16
1+	1136.48245		
z_{10}(Se.)	1165.46142	1165.46131	0.09
1+	1181.48029		
2+	1223.02810		
$[P2\text{-}SeH+H]^{+\cdot}$	1228.65102	1228.65069	0.27
$[P2\text{-}Se+2H]^+$	1230.66626	1230.66634	-0.07
$P2+c_{10}$ (Se)	1245.53744	1245.53737	0.06
$[P2+P2\text{-}SeH+3H]^{2+\cdot}$	1270.11735	1270.11851	-0.91
1+	1276.53003		
1+	1293.55640		
P2(Se.)	1309.57489	1309.57500	-0.08
$[P2+P2+3H]^{2+\cdot}$	1310.07699	1310.07901	-1.54
P2+Se.	1389.49139	1389.49163	-0.17
1+	1446.63414		
$P2+z_2$	1568.70442	1568.70441	0.01
$P2+z_3$	1715.77306	1715.77283	0.13
$P2+z_4$	1814.84202	1814.84125	0.42
$P2+z_7$	2172.88834	2172.88324	2.35

Appendix F (Supporting information for Chapter 7)

IR-ECD pulse program:

```
# ECD_KEY:

ECD.lines = 7

ECD.1 = "; Custom IR-ECD event using pulse-train definition"

ECD.2 = "; ECD; start delay=d3, event time=d12, IRMPD: start delay=d4,
event time=d13"

ECD.3 = " (d13 setnmr3|12 1u setnmr3^12)"

ECD.4 = "   DT_LOW, d7 setnmr3|20"

ECD.5 = "   1u setnmr3^20"

ECD.6 = "   lo to DT_LOW times l24"

ECD.7 = " (d12 setnmr3|26 1u setnmr3^26) "

;--------------------------------------

;Dynamic Trap Plate Block (lower)

;--------------------------------------

;DT_LOW, d7 setnmr3|20   ; lower dynamic trap voltage with voltage ramp

;   1u setnmr3^20

;   lo to DT_LOW times l24 ; L[24] steps in voltage ramp
```

Shots-ECD pulse program:

```
# CORRELATED_SHOTS_KEY:

CORRELATED_SHOTS.lines = 4

CORRELATED_SHOTS.1 = "; Custom DR-ECD event using pulse-train
definition"

CORRELATED_SHOTS.2 = "; ECD and CORR_SHOT start at same time:
ECD event time=d12, CORR_SHOT event time=p7"

CORRELATED_SHOTS.3 = " 10u pl7:f1; set attenuation for correlated
shots (FCtrl-1)"

CORRELATED_SHOTS.4 = " ((d12 setnmr3|26 1u setnmr3^26) (p7 ph2
<CORR_SHOTS_LIST>^):f1)"
```

Figure F.1 (a) ESI spectrum of insulin, (b) ESI spectrum of the reaction products of insulin with acetic anhydride, and (c) ECD spectrum of the reaction products of insulin with acetic anhydride.

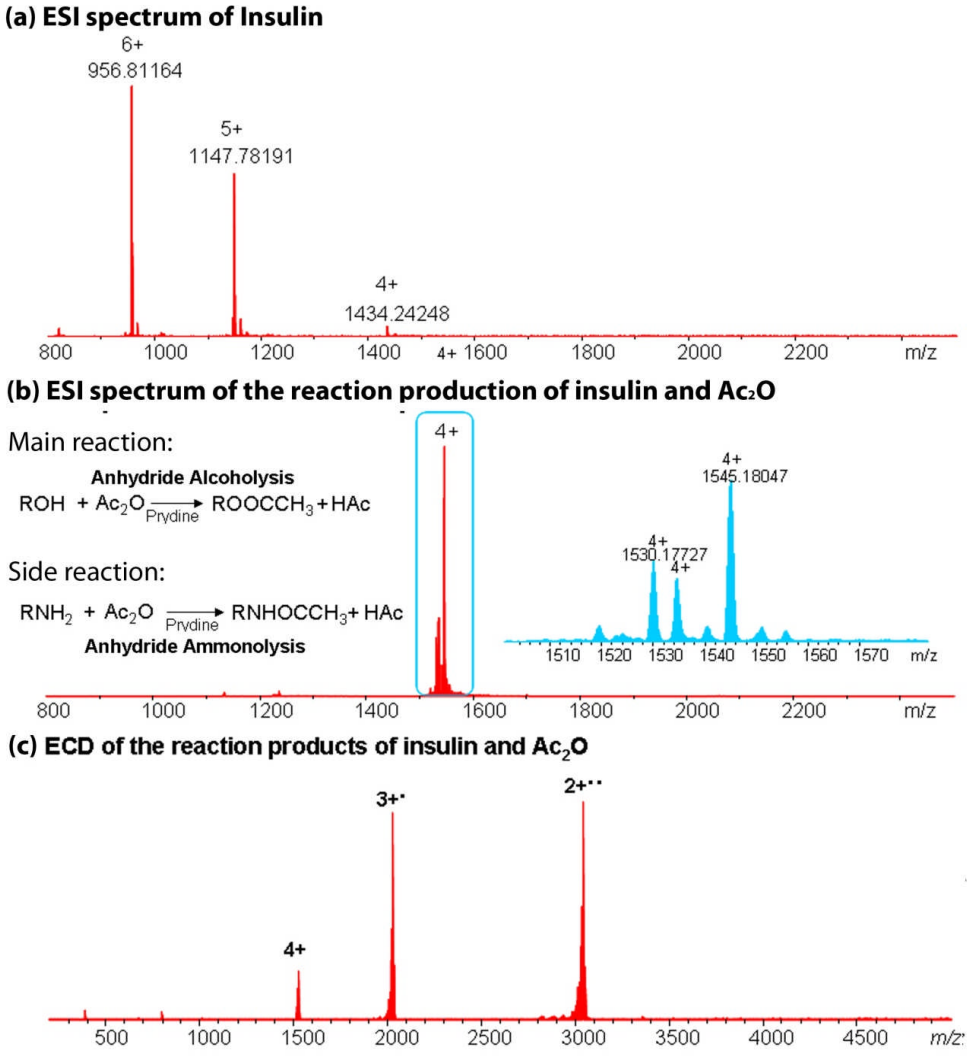

Figure F.2 IR-ECD spectra of the [Rnase A+13H]$^{13+}$ ion at *m/z* 1053. (a) IR laser pulse length 420 ms, laser power 10%; (b) IR laser pulse length 420 ms, laser power 15%.

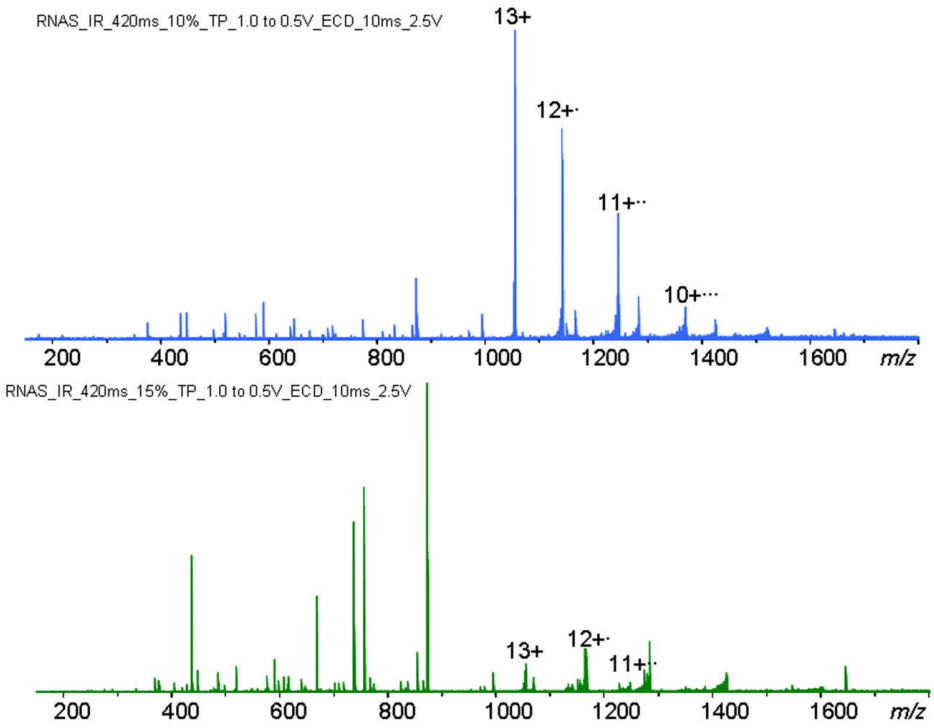

Scheme F.1 Possible ECD fragmentation pathways of the $[insulin+6H]^{6+}$ ion.

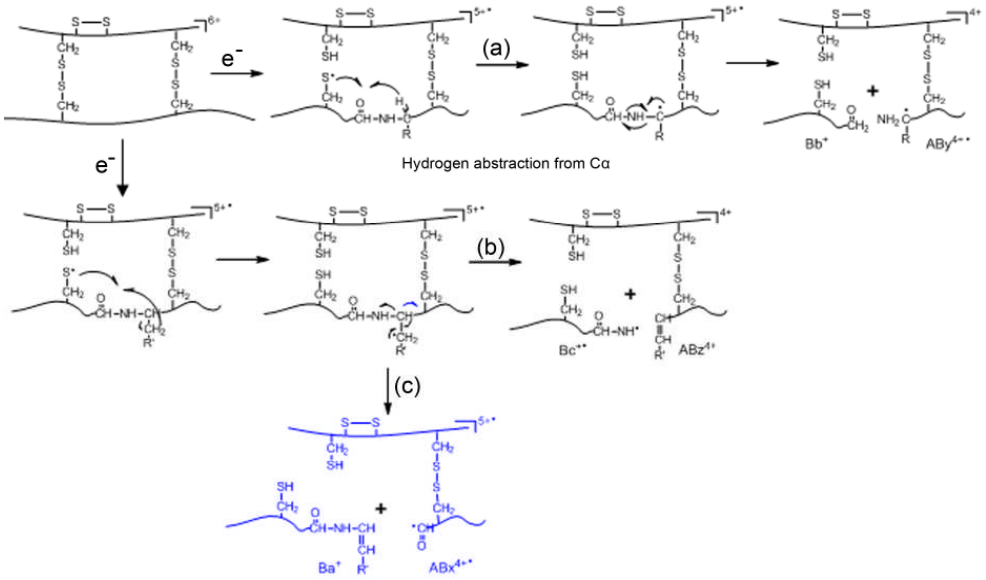

Curriculum vitae

Huilin Li

Email: Huilin.li@warwick.ac.uk

Education:

Ph.D. Chemistry

University of Warwick, Department of Chemistry, Coventry, UK 2009.10 – 2012.11

Thesis title: Studies of protein posttranslational modifications using high resolution tandem mass spectrometry

Supervisor: Professor Peter B. O'Connor

M.Sc. Physical Chemistry

Changchun Institute of Applied Chemistry, Chinese Academy of Sciences, Changchun, China 2005.9 – 2008.12

Thesis title: Ultrafiltration LC-MS approach to investigate the interaction of protein targets with natural products

Supervisor: Professor Zhiqiang Liu

B.Sc. Pharmacy

Shandong University, Jinan, China 1998.9 – 2002.7

Research and Professional Experience:

2007—2009, Assistant Professor, Changchun Institute of Applied

Chemistry, Chinese Academy of Sciences

2002—2007, Research Assistant, Changchun Institute of Applied Chemistry, Chinese Academy of Sciences

Awards:

- Travel Award for the 25th Lake Louise Tandem Mass Spectrometry Workshop, Lake Louise, Alberta, Canada. Nov. 28 – Dec. 1, 2012.
- Warwick Postgraduate Research Scholarship (WPRS). 2009 – 2012
- University of Warwick Departmental Studentships. 2009 – 2012
- IMSF Travel Grant for the 19th International Mass Spectrometry Conference. Kyoto, Japan, Sep. 15 – 21, 2012.
- BMSS Travel Award for the 59th ASMS Conference on Mass Spectrometry. Denver, CO, USA. Jun. 5 – 9, 2011.
- Travel Award for the 8th UppCon Conference on Electron Capture and Transfer Dissociation. Villars-sur-Ollon, Switzerland, Feb. 6-10, 2011.

Publications:

1. **Huilin Li**, Yulin Qi, Tzu-Yung Lin, Steve L. Van Orden, Mark P. Barrow, Peter B. O'Connor. Top-down Electron Capture Dissociation of Disulfide Bonded Proteins. In preparation.
2. **Huilin Li**, Jonathon R. Snelling, James H. Scrivens, Peter J. Sadler, Peter B. O'Connor. Mass Spectrometric Strategies to Improve the Identification of Pt(II)-modification Sites on Peptides and proteins. *Anal. Chem*. **2012**. Submitted.
3. Juan Wei, **Huilin Li**, Peter B. O'Connor. Structural Characterization of Chlorophyll a by High Resolution Tandem Mass Spectrometry. *J. Am. Soc. Mass Spectrom*. **2012**. Under revision.

4. **Huilin Li**, Peter B. O'Connor. Electron Capture Dissociation of Disulfide, Sulfur-Selenium, and Diselenide Bound Peptides. *J. Am. Soc. Mass Spectrom.* **2012**, 23, 2001-2010.

5. **Huilin Li**, Stephen A. Wells, J. Emilio Jimenez-Roldan, Rudolf A. Römer, Yao Zhao, Peter J. Sadler, Peter B. O'Connor. Protein Flexibility is Key to Cisplatin Cross-linking in Calmodulin. *Protein Sci*. **2012**. 21, 1269-1279.

6. Yulin Qi, Mark P. Barrow, **Huilin Li**, Joseph E Meier, Steve L. Van Orden, Christpher J. Thompson, and Peter B O'Connor. Absorption-mode: The Next Generation of Fourier Transform Mass Spectra. *Anal. Chem.* **2012**. 84, 2923–2929.

7. Hui Zhou, **Huilin Li**, Zhong Zheng, Fengrui Song, Junpeng Xing, Zhiqiang Liu, Shuying Liu. Screening for α-Glucosidase Inhibitors from Coptidis-rehmanniae Herb Couple by Using Ultrafiltration Liquid Chromatography/Mass Spectrometry. *J. Liq. Chromatogr. Related Technol.* **2012**, 35, 1-14.

8. **Huilin Li**, Tzu-Yung Lin, Steve L. Van Orden, Yao Zhao, Mark P. Barrow, Ana M. Pizarro, Yulin Qi, Peter J. Sadler, Peter B. O'Connor. Use of Top-down and Bottom-up Fourier Transform Ion Cyclotron Resonance Mass Spectrometry for Mapping Calmodulin Sites Modified by Platinum Anticancer Drugs. *Anal. Chem.,* **2011**, 83, 9507-9515.

9. **Huilin Li**, Yao Zhao, Hazel I. A. Phillips, Yulin Qi, Tzu-Yung Lin, Peter J. Sadler, Peter B. O'Connor. Mass Spectrometry Evidence for Cisplatin as a Protein Cross-linking Reagent. *Anal. Chem.* **2011**, 83, 5369-5376.

10. Yulin. Qi, Steve L. Van Orden, Christopher J. Thompson, Mark P. Barrow, **Huilin. Li**, Pilar. Perez-Hurtado,and Peter B O'Connor. Variation of the Fourier Transform Mass Spectra Phase Function with Experimental Parameters. *Anal. Chem.,* **2011**, 83, 8477-8483.

11. Wenlong Liu, Shu Liu, **Huilin Li**, Fengrui Song, Zhiqiang Liu, Shuying Liu. Binding of Alpha 1-acid Glycoprotein with Aconitum Alkaloids: an Investigation by IF-MALDI-FT-MS. *Rapid Commun. Mass Spectrom.* **2011**, 25, 973-978.

12. Shu Liu, Jun Yan, **Huilin Li**, Fengrui Song, Zhongying Liu, Zhiqiang Liu, Shuying Liu. Studies on Chemical Constituents of Compound Indigowoad Root Granule by Mass Spectrometry. *Chem. J. Chinese U.* **2010**, 31, 1137-1142.

13. **Huilin Li**, Fengrui Song, Junpeng Xing, Zhiqiang Liu, Shuying Liu. Screening and Structures Characterization of α-Glucosidase Inhibitors from Hawthorn Leaves Flavonoids Extract by Ultrafiltration LC-DAD-MS^n and SORI-CID FT ICR MS. *J. Am. Soc. Mass Spectrom.* **2009**, 20, 1496-1503.

14. Xiangyu Meng, **Huilin Li,** Fengrui Song, Chunming Liu, Zhiqiang Liu, Shuying Liu. Studies on Triterpenoids and Flavones in *Glycyrrhiza uralensis Fisch*. by HPLC-ESI-MS^n and FT-ICR-MS^n. *Chinese J. Chem*. **2009**, 27, 299-305.

15. **Huilin Li**, Fengrui Song, Zhong Zheng, Zhiqiang Liu, Shuying Liu. Characterization of Oligsaccharides and Phenolid Acids in the Cinese Herb Tanshen by ESI-FT ICR MS. *J. Mass Spectrom.* **2008**; 43, 1545-1552.

16. Hao Yue, Zifeng Pi, **Huilin Li**, Fengrui Song, Zhiqiang Liu and Shuying Liu. Studies on the Stability of Diester-diterpenoid Alkaloids from the *Genus Aconitum L.* by High Performance Liquid Chromatography Combined with Electrospray Ionisation Tandem Mass Spectrometry (HPLC/ESI/MS^n). *Phytochem. Anal.* **2008**, 19, 141-147.

17. Yue Liu, Zhiqiang Liu, **Huilin Li**, Fengrui Song, Shuying Liu. Studies on Diterpenoids Constituents from Euphorbia Kansui by Electrospray Ionization Multi-stage Tandem Mass Spectrometry. *Chem. J. Chinese U.* **2008**, 29, 1727-1735.

18. Xiaoyan Qiu, Meng Cui, **Huilin Li**, Zhiqiang Liu and Shuying Liu. Prompt Disulfide Fragmentations of Disulfide-containing Proteins in a Matrix-Assisted Laser Desorption/ Ionization Source. *Rapid Commun. Mass Spectrom*. **2007**, 21, 3520-3525.

19. Yufeng Zhao, Fengrui Song, Hao Yue, Xinhua Guo, **Huilin Li**, Zhiqiang Liu, Shuying Liu. Deoxyaconitine of Metabolite of Aconitine by Human Intestinal Bacteria and Electrospray Ionization Tandem Mass Spectrometry. *Chem. J. Chinese U.* **2007**, 28, 2051-2055.

20. Hongjuan Dong, Zhiqiang Liu, Fengrui Song, Zhan Yu, **Huilin Li**, Shuying Liu. Structural Analysis of Monoterpene Glycosides Extracted from *Paeonia lactiflora Pall.* using Electrospray Ionization Fourier Transform Ion Cyclotron Resonance Mass Spectrometry and High-performance Liquid Chromatography/ Electrospray Ionization Tandem Mass Spectrometry. *Rapid Commun. Mass Spectrom*. **2007**, 21, 3193-3199.

21. Shumin Wang, **Huilin Li**, Zhiqiang Liu, Shuying Liu, Bemlian Cui. Studies on the Contents of Catechin and Epicatechin in Catechu by HPLC, *Lishizhen Medicine and Materia Medica Research.* **2006**, 17, 490-491.

22. Hongjuan Dong, Zhiqiang Liu, Fengrui Song, Zhan Yu, **Huilin Li**, Shuying Liu. Studies on Paeoniflorin by Electrospray Ionization Tandem Mass Spectrometry. *Chem. J. Chinese U.* **2006**, 27, 2066-2069.

23. **Huilin Li**, Junpeng Xing, Zhiqiang Liu, Shuying Liu. Analysis of Cephalosporins by Electrospray Ionization Multi-stage Tandem

Mass Spectrometry. *J. Chinese Mass Spec. Soc.* **2005**, 26, 198-202.

Presentations:

1. **Huilin Li**, Stephen A. Wells, J. Emilio Jimenez-Roldan, Rudolf A. Römer, Yao Zhao, Peter J. Sadler, Peter B. O'Connor. Protein Flexibility is Key to Cisplatin Cross-linking in Calmodulin. (Poster) 19th International Mass Spectrometry Conference, Kyoto, Japan, Sep. 15-21, 2012.

2. **Huilin Li**, Stephen A. Wells, J. Emilio Jimenez-Roldan, Rudolf A. Römer, Yao Zhao, Peter J. Sadler, Peter B. O'Connor. Protein Flexibility is Key to Cisplatin Cross-linking in Calmodulin. (Talk) 10th European FTMS Conference, Warwick, UK, April 1-5, 2012.

3. **Huilin Li**, Tzu-Yung Lin, Steve L. Van Orden, Yao Zhao, Ana M. Pizarro, Peter J. Sadler, Peter B. O'Connor. Mapping the Binding Sites of Platinum Anticancer Drug-Cisplatin to Calmodulin (Poster). 32nd BMSS Conference, Cardiff, UK, Sep. 11-14, 2011.

4. **Huilin Li,** Tzu-yung Lin, Ana Pizarro, Peter J. Sadler, Peter B. O'Connor. Mapping the binding Sites of Platinum Anticancer drugs to Calmodulin (Poster). *59th ASMS Conference on Mass Spectrometry and Allied Topics.* Denver, CO, June 5-9, 2011.

5. **Huilin Li**, Yao Zhao, Hazel I. A. Phillips, Yulin Qi, Peter J. Sadler, and Peter B. O'Connor. Mass spectrometry evidence for cisplatin as a cross-linking reagent (Poster). 8th UppCon Conference on Electron Capture and Transfer Dissociation. Villars-sur-Ollon, Switerland, Feb. 6-10, 2011

6. Zhiqiang Liu, **Huilin Li**, Zhaofu Wang, Shuying Liu. Non-covalent interactions of herbal compounds with biomacromolecules by Mass Spectrometry. 2nd World Chinese Conference on Mass Spectrometry. Jun. 26-27, 2008.

7. **Huilin Li**, Fengrui Song, Zhiqiang Liu, Shuying Liu. Characterization of Oligsaccharides and Phenolid Acids in the Cinese Herb Tanshen by ESI-FT ICR MS. (Oral Presentation). The 12th International Beijing Conference and Exhibition on Instrumental Analysis (12th BCEIA). Oct. 18-21, 2007

8. **Huilin Li**, Junpeng Xing, Fengrui Song, Zhiqiang Liu, Shuying Liu. Characterization of tanshinones extracted from Salvia miltiorrhiza bunge by supercritical fluid extraction with HPLC/PDA/ESI-MS, HPLC-MS^n and FT-ICR MS (Poster). 16th National Symposium and Exhibition on Chromatography &1st Dalian International Symposium and Exhibition on Chromatography (NISEC). June 4 - 6, 2007

9. **Huilin Li**, Junpeng Xing, Fengrui Song, Zhiqiang Liu and Shuying Liu Fragmentation pathways of Tanshinones by ESI-FT-ICR-MS (Poster). The 11th International Beijing Conference and Exhibition on Instrumental Analysis (11th BCEIA). Oct. 20-23, 2005